ATO

CEET2005
Scientific Report

April 2001 – January 2002

OPD 01/350 april 2002
Rapportnummer: B569

Confidential

Consortium:
ATO
Carrier Transicold
P&O Nedlloyd
Ecofys
The Greenery International
Shell Solar Energy B.V.

WAGENINGEN UR

ATO

CEET2005
Scientific Report

April 2001 – January 2002

OPD 01/350 april 2002
Rapportnummer: B569

Confidential

Consortium:
ATO
Carrier Transicold
P&O Nedlloyd
Ecofys
The Greenery International
Shell Solar Energy B.V.

ATO B.V.
Agrotechnological Research Institute
Bornsesteeg 59
P.O. Box 17
6700 AA Wageningen
The Netherlands
Tel: +31.317.475024
Fax: +31.317.475347

Contents

page

Full-scale container experiment

Details of energy consumption in full-scale container experiment

Introduction

The experiment was performed in the months November and December 2001. Between end of CA-storage and end of container experiment were 33 days. From the discussion at the last CEET-meeting on 10 January 2001 some questions arose about the energy consumption during the experiment. In this document we try to answer these questions in more detail.

In the experiment separate phases can be recognised:

A:	Cooling full speed	~90-250 hrs
B:	Cooling half speed	~250-350 hrs
C:	Transport period with cycling	~350-800 hrs

In Figure 1 the return air temperature measured with the ATO measurement system is shown in which the separate phases are indicated. Typical (fixed) transport temperature for apples sensitive for chilling injury is around 4.4-5.6ºC depending on condition. The transport period with cycling (cycling is on-off control of compressor) is divided in three parts:

CI:	Irregular cycling
CII:	High frequent cycling
CIII:	medium frequent cycling

In the not-cooling mode during the cycling the supply air temperature follows the return air temperature up to a limit. In the cooling mode during the cycling the supply air temperature is 0.5ºC (freezing temperature for these apples around –1.5ºC).

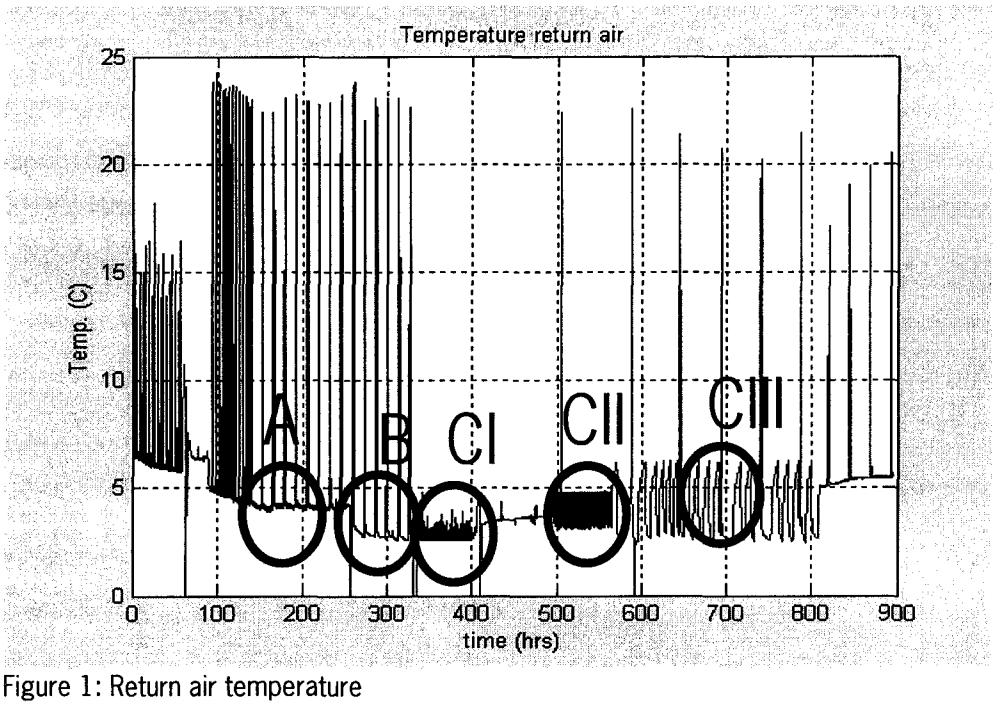

Figure 1: Return air temperature

In this document the focus will be on phase A, B and CIII. These correspond with transport in full speed, half speed and half speed with cycling. Next, the topic of energy efficiency will be discussed. This will be followed by comments on product quality during the experiment.

Energy efficiency

In Table 1 the measurements and values for energy consumption in the different phases are given. During the periods in which energy consumption is measured the unit was in steady state. The sudden change in return air temperature between phase A and B is most likely due to a change in airflow pattern as fan speed was reduced from full to half speed. The irregular cycling in phase CI is caused by problems reading supply and return air temperatures of the unit into the external PC. For the cycling in phases CII and CIII a work around has been programmed to prevent further problems. The results shown in Table 1 were taken with a fresh air intake of 15 m^3/hr.

Table 1: Information of the different phases

Phase	Time [hrs]	Energy consumption value [kWh]	Average setpoint temp.	Bandwidth	Information	Number of defrosts in time interval (column 2)
A	145	0	3 ºC	-	Fans full speed Defrost Interval 12 hrs.	5
	215.25	335.2				
B	249.333	0	3 ºC	-	Fans half speed, Defrost interval 12 hrs.	4
	311.667	179.3				
CIII	721.233	0	-	2 ºC (lower limit) – 6 ºC (upper limit)	Fans half speed, Cycling (on-off) of unit, Defrost interval 48 hrs.	1
	776.5	100.5				

The (uncorrected) averaged levels of energy consumption as calculated from Table 1 (ΔEnergy in 3rd column Table 1 divided by Δtime of period in 2nd column Table 1) for the different phases are shown in Table 2.

Table 2: Uncorrected levels of energy consumption

Phase	Characteristics	Average energy consumption [kW]
A	Cooling full speed	4.772
B	Cooling half speed	2.876
CIII	Transport period with medium frequent cycling	1.818

The intervals of the different phases are chosen such that all (uncontrolled) parameters (e.g. settings for cycling) stay fixed between both measurement values. Common climate conditions for such transport would be a RH of 90-95%, an O_2 of 21% and a CO_2 of 0-4%. The figures presented at the meeting on 10 January 2002 were the result of averaging over the whole phase period. To enable the comparison between the different phases one should correct this results with the number of defrost actions. Defrost termination temperature in all these phases was 25ºC. The relatively long defrost interval of 48 hours in phase CIII is due to the interaction between the additional ATO software and the software of the Carrier unit.

As the Carrier unit available at ATO is equipped with 4 heaters of each 0.75 kW a defrost will require 3.0 kW. In Figure 2 the defrost peaks are shown for phase A, B and CIII. The duration of the defrost period in phases A and B is approximately 1 hour, and in phase CIII this duration is approximately 0.5 hour.

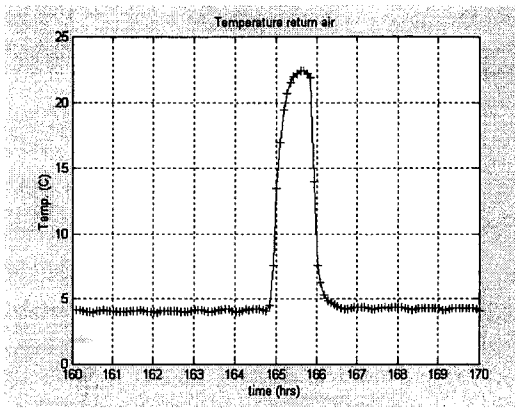

Figure 2a: Defrost in phase A

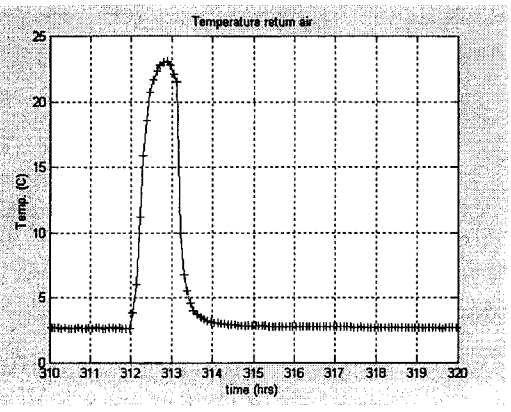

Figure 2b: Defrost in phase B

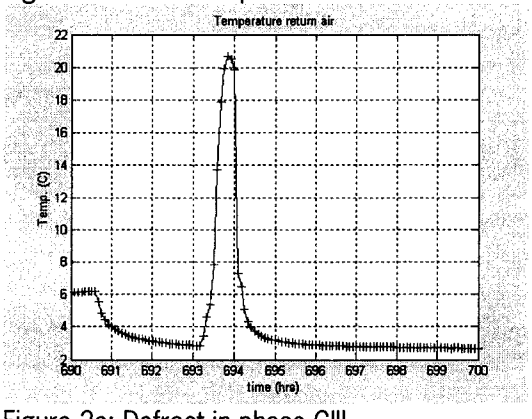

Figure 2c: Defrost in phase CIII

The information about the defrost (frequency and duration) the energy consumption in the different phases can be corrected to enable a comparison. This correction is for each separate phase defined as follows:

*Energy consumption of period (column 3 in Table 1)[kW]- Number of defrosts (column 7 in Table 1)[-/hrs] * duration of one defrost[hrs] * energy consumption of one defrost[kW]*

divided by

*duration of period (column 2 in Table 1) [hrs]-Number of defrosts (column 7 in Table 1)[-/hrs] * duration of one defrost[hrs]*

With this correction the corrected figures for energy consumption in the different phases are shown in Table 3.

Table 3: Corrected levels of energy consumption

Phase	Characteristics	Average energy consumption [kW]
A	Cooling full speed	4.907
B	Cooling half speed	2.896
CIII	Transport period with medium frequent cycling	1.806

This results in energy savings between phase A and CIII of 63%, of which 40% between phase A and B, and 23% between phase B and CIII.

Product Quality

Product quality of apples from the container experiment was similar to quality in the control treatment. Product quality was determined as firmness (most important quality parameter for apples), measured at the end of the transport period in the centre and in the upper layer of 10 pallets from different positions in the container as illustrated in Figure 3.

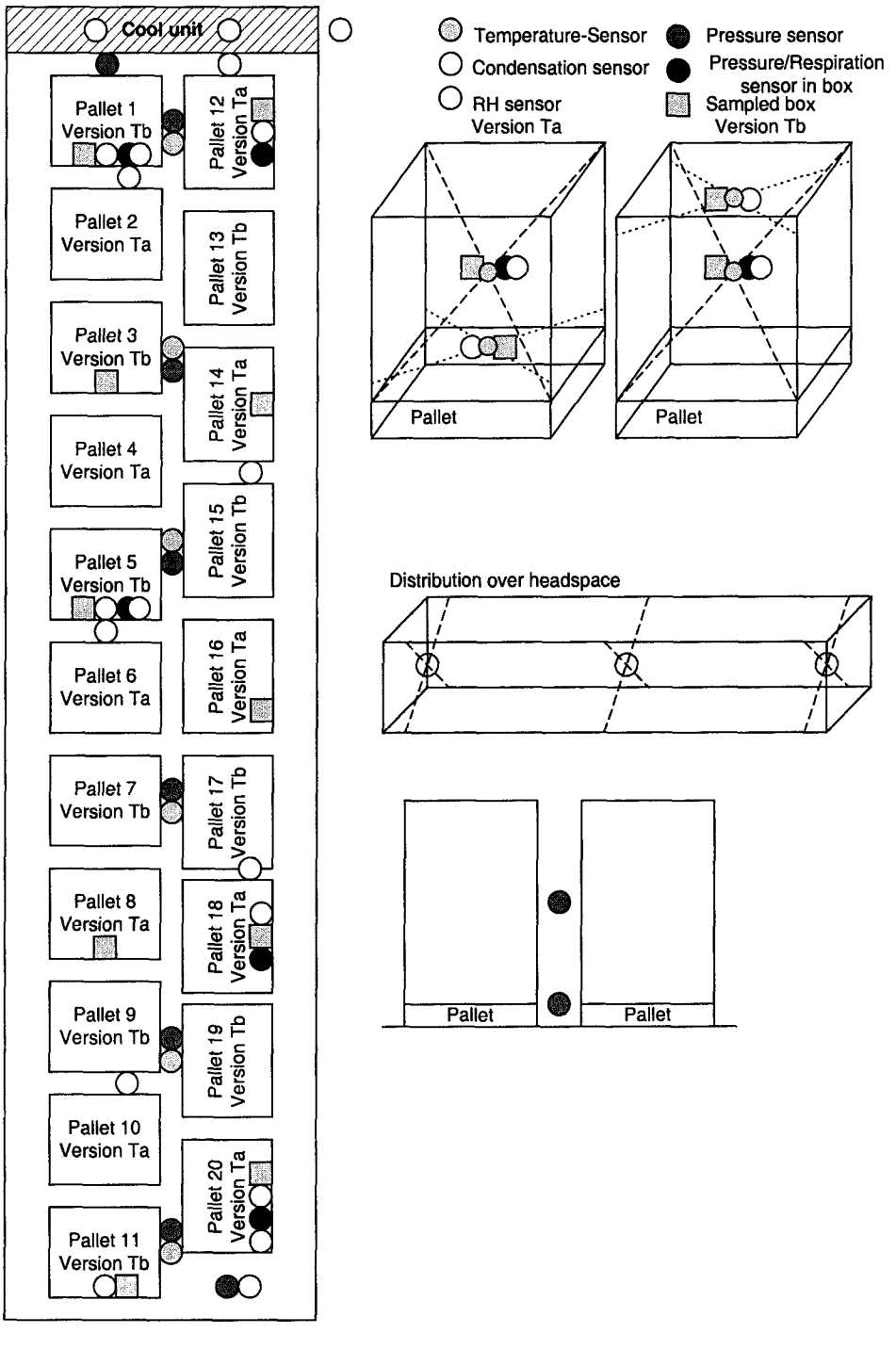

Figure 3: Locations of sensors and sampled boxes

The firmness of the apples from the container experiment was compared with firmness of apples from a control treatment that were kept at a constant temperature of 5°C (RH > 95%). No significant difference in firmness was found between apples from the control and apples from the container treatment.

Initial product quality

Apples (cv Elstar; 2nd harvest) form a local grower (Province Zeeland, The Netherlands) were stored for 1 month under CA conditions. During 2 days apples (20 tons) were transferred from bulk storage to standard transport boxes (LxBxH 40 x 30 x 24 cm). Apples with external disorders were sorted out, but no selection was made on size. Boxes were placed on pallets (9 layers x 10 boxes).
The quality parameters, firmness, sugar content and internal disorders from 5 boxes of each center pallet (5th layer; n=20) were measured. The initial average firmness at the center of each pallet is shown in figure 18.

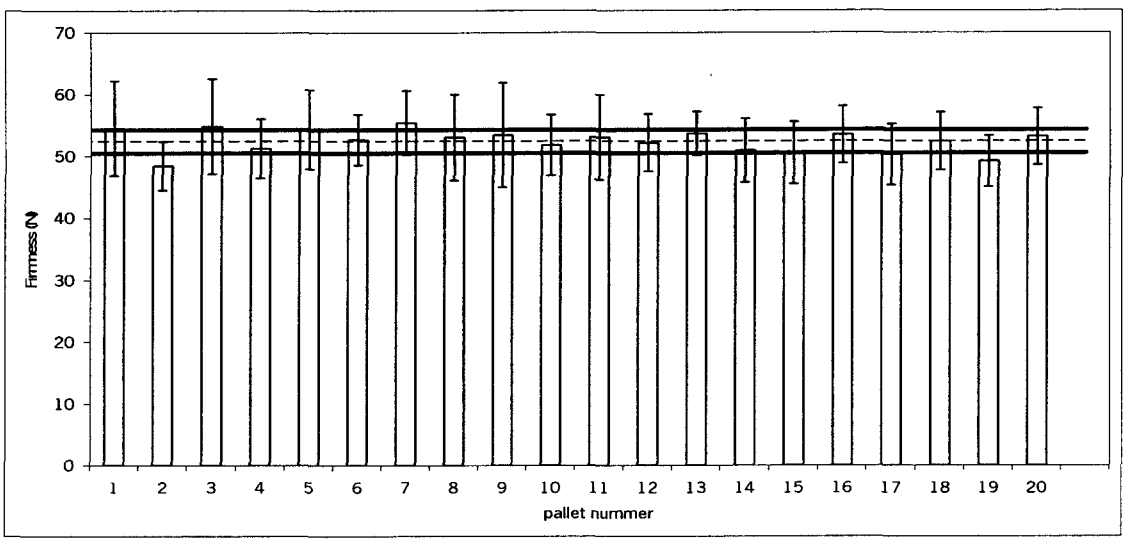

Figure 18. Firmness of Elstar apples at the center (layer 5) of each pallet before transport.

Average initial firmness of all apples (direct after CA storage) from the center was below (52.4 ± 5.8) the required firmness of 60 N. The average sugar content of all apples (14.4% ± 0.5%) was not significant different compared to harvested apples (13.4% ± 1.0). No internal or external disorders could be observed.

Products were kept at ambient air (5 - 10°C) before refrigerated transport to ATO. As reference for the full scale container experiment, two pallets were stored at constant temperature 5°C ± 0.3°C and 90% RH. Firmness of this reference was monitored during and after the experiment (figure 19).

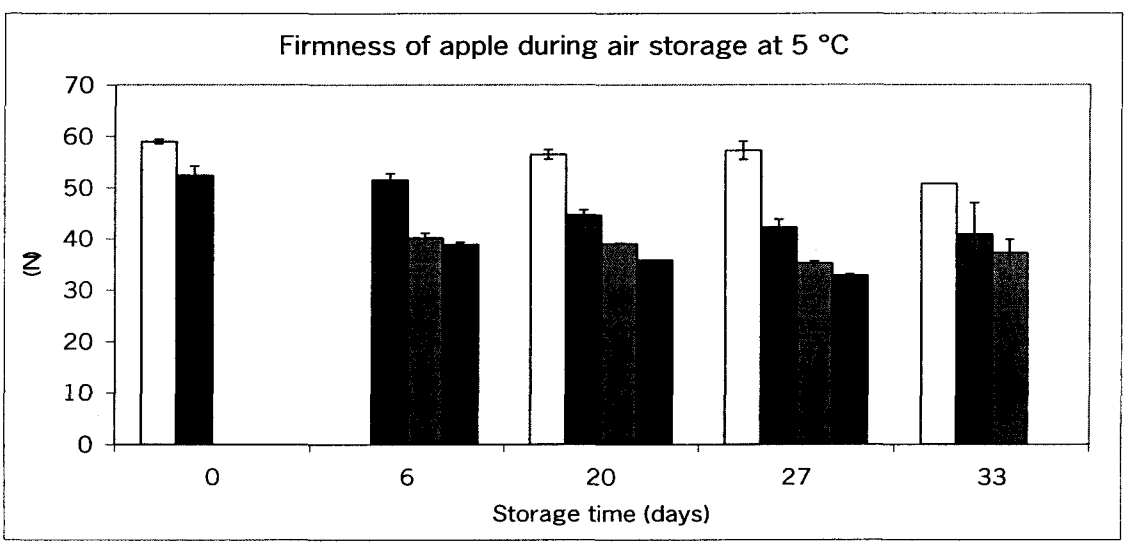

Figure 19. Firmness of the reference batch during storage at 5 °C (□ = 0; □ = 7; □ = 14 days shelf-life) and a small scale experiment at ATO (□ = 0 days shelf-life).

Firmness of apples 6 days after CA storage (at the start of the experiment), rapidly declined during shelf life. The values are below the market limit (45 N) and are not acceptable. After 33 days air storage the firmness decay at the center position of the reference pallet is 9.1 N (43.3 N ± 7.4 N; n=25). This is comparable to the level of firmness decay in all small scale experiments carried out at ATO (figure 19).

Firmness after large scale experiment.

After the large scale container experiment, firmness and storage disorders at 3 different positions (lower = layer 3; center = layer 5 and upper = layer 7) were measured. All boxes containing sensors were evaluated on external disorders (fig 20).

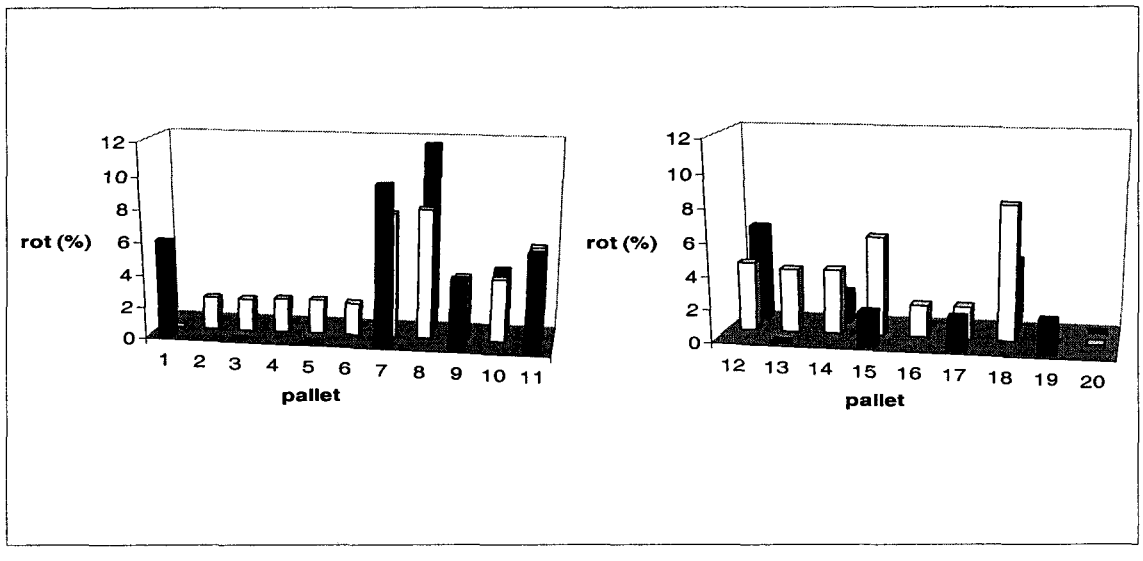

Figure 20. Storage disorders (% rot) at different pallets and positions in the container (= upper layer ; = center layer; = lower layer).

Larger % of rot were found in pallets 7 and 8, but no significant difference was found between the row 1 (pallet 1-11) and row 2 (pallet 12-20). No clear pattern could be observed between % of rot and the position within the container. No difference in % rot was found between the reference and the sensor boxes. Apples with external disorders were situated along the wall or the bottom of the package. This indicates that these disorders are probably due to handling during packaging, transport, loading and unloading.

The average firmness values at the 3 positions of the reference were compared to average firmness values of the container pallets (figure 19 and table 13). No differences were found between the reference and the container pallets.

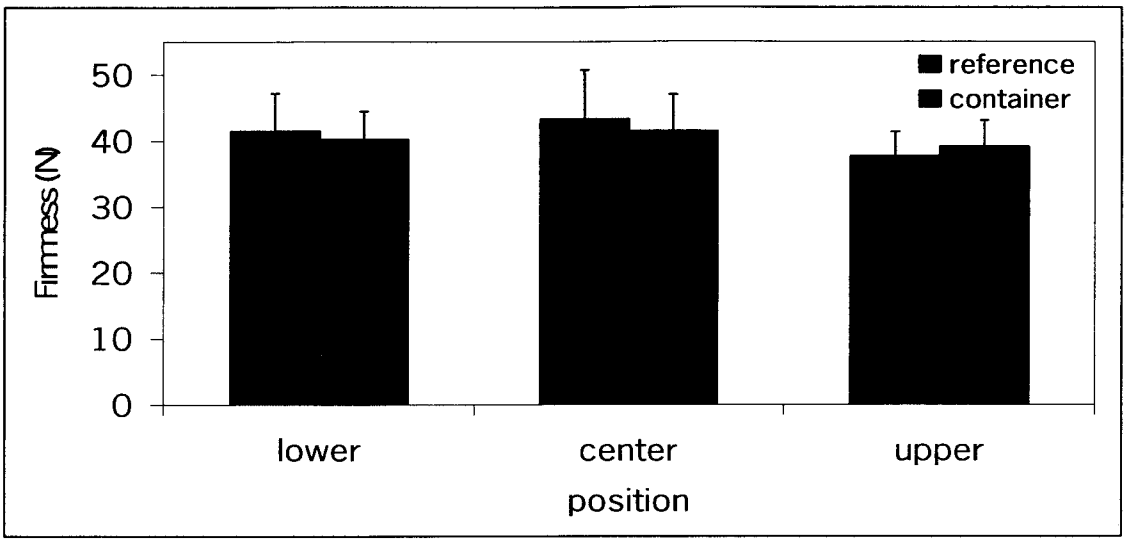

Figure 19. Average firmness of all Elstar apples (N) at different positions on the pallets (lower, center and upper) after 33 days storage.

The firmness decay of all apples in center pallets is 10.9 N (41.5 N ± 5.5 N; n= 400), which is comparable to firmness loss of the reference and of all small scale experiments carried out at ATO.

Table 13 Average firmness of reference pallet and container pallets at different positions.

position [1]	initial [2]		reference [3]		container [4]	
	avg	se	avg	se	avg	se
lower	-	-	41.5	5.7	40.3	4.2
center	52.4	5.8	43.3	7.4	41.5	5.5
upper	-	-	37.7	3.7	39.1	4.0

[1] Each pallet consists of 9 layers; lower = layer 3; center = layer 5; upper layer 7
[2] Average value of all data (n=400)
[3] Average values of 25 apples after 33 days storage.
[4] Average value of all data (n= 200 for lower and upper; n=400 for center) after 33 days storage.

Conclusions

- The initial firmness (52.4 N ± 1.9 N) was below the standard firmness after 1 month CA storage.
- The average firmness of apples stored in the container were not significant lower compared to firmness of apples stored at constant temperature.
- The decay in firmness of both reference and container is in the same order compared to all small scale experiments performed at ATO.

Task 1 Optimisation of product quality under varying conditions

I Gas exchange rates in response to temperature and CA conditions

After harvest fruits and vegetables stay metabolically active, which is expressed in high respiration rates. Respiration provides the energy and metabolites for maturation and ripening. A reduction of respiration (low temperature, low O_2 concentration) results in lower energy supply and delays ripening processes. Measurements of O_2 and CO_2 gas exchange give a general indication of the metabolic activity, whereas ethylene gas exchange measurement give an indication of the ripening stage.

The main focus of task 1 is to assess quality of fresh products as dependent on product environment. Fresh products nowadays are transported under static storage conditions (constant temperature, O_2, CO_2 and relative humidity) with minimal fluctuations. To maintain these conditions a large energy input is required. When less strict climate conditions can be used without reduction of product quality, it might be possible to reduce energy consumption during transport.

To be able to compare fresh products in a changing climate it is necessary to know how products behave in a well-defined static climate. In the next paragraph relations between "steady state" climate conditions (temperature and O_2) and gas exchange rates (O_2, CO_2 and ethylene) of apples and tomato are described.

The effect of temperature on gas exchange rates

Apple

In figure 1 O_2 gas exchange rates of 'Elstar' apples (from a local grower, province Gelderland, The Netherlands) stored under air and CA conditions (1.2 % O_2 and 2.5 % CO_2) are plotted against the product temperature (average temperature during measurement). In this experiment the temperature was increased each day directly after the gas exchange (O_2, CO_2 and ethylene) measurements.

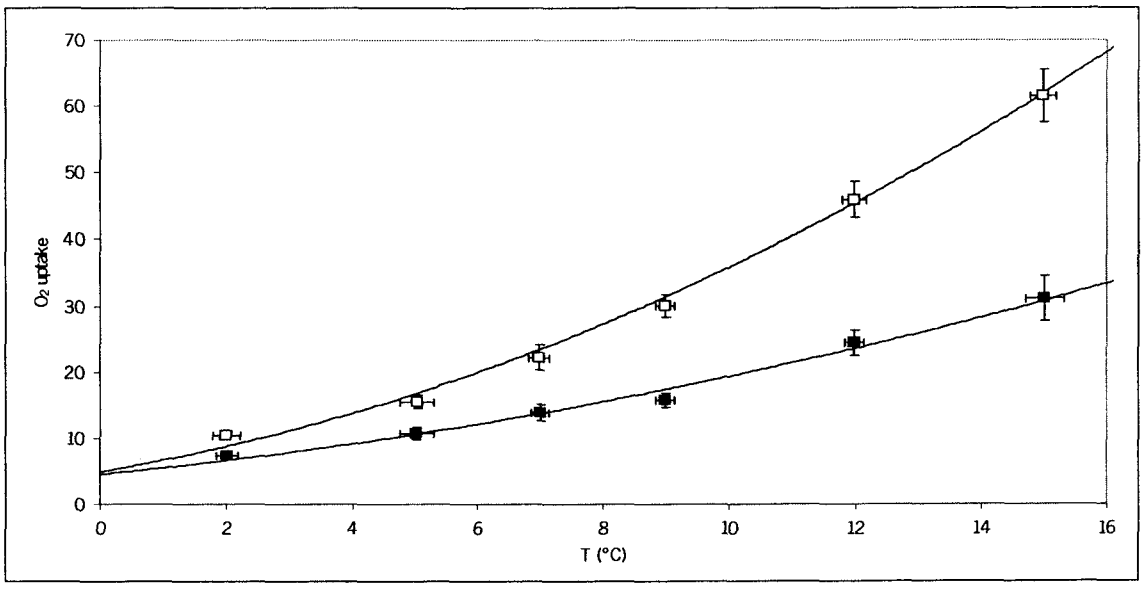

Figure 1. O_2 gas exchange rates (nmol/kg.s; n=10) of apple vs product temperature. □ = CA stored; □ = Air stored.

The highest O_2 gas exchange rates were measured at the air stored apples. The lowest O_2 gas exchange rates were reached at standard CA conditions. O_2 and CO_2 gas exchange rates were fitted with different models (table 1) according to Zwietering et al (1991). Two models gave good correlations between temperature and O_2 gas exchange rates / CO_2 gas exchange rates. One of the models to describe gas exchange rates as function of temperature is the model of Ratkowsky. It is based on the observation that at lower temperatures (below 15 °C) the square root of processes change linear with temperature:

$$(1) \quad \upsilon_x = [b\,x\,(T\,x\,a)]^2$$

where υ_x = gas exchange rate (nmol/kg.s); b= Ratkowsky parameter ($K^{-1}.s^{-0.5}$); a = the minimum temperature for gas exchange (K).

Another model which can be used to describe the relationship between temperature and O_2 or CO_2 gas exchange rates, is based on Arrhenius equation:

$$(2) \quad \upsilon_x = (a\,x\,EXP(-b/(8.314\,x\,T)))$$

Where υ_x = gas exchange rate (nmol/kg.s); a = reaction rate constant; b = energy of activation (J/mol).

This model is based on enzyme kinetics, but is only valid for a limited temperature range. It does not describe freezing and denaturation properly.

Table 1. Model parameters for O_2 and CO_2 gas exchange rates (nmol/kg.s) of apple vs temperature (K).

		Ratkowsky		Arrhenius	
O_2 gas exchange		Value	se	Value	se
Air	r^2	94.8		94.8	
	se fit	1.91		1.91	
	F-stat	1280		1278	
	a	2.63 E+02	5.86 E-01	2.338 E+11	2.172 E+14
	b	2.29 E-01	6.70 E-03	7.097 E+05	2.200 E+03
CA	r^2	98.0		97.5	
	se fit	2.52		2.81	
	F-stat	4394		3525	
	a	2.67 E+02	2.71 E-01	2.15 E+17	1.49 E+17
	b	3.77 E–01	6.08 E-03	8.56 E+04	1.64 E+03
CO_2 gas exchange					
Air	r^2	95.0		94.4	
	se fit	3.87		4.09	
	F-stat	1773		1589	
	a	2.70 E+02	3.99 E-01	4.92 E+19	6.28 E+19
	b	4.01 E-01	1.06 E-02	9.89 E+04	3.03 E+03
CA	r^2	98.1		98.6	
	se fit	1.42		1.21	
	F-stat	3620		4971	
	a	2.69 E+02	2.83 E-01	1.30 E+19	9.04 E+18
	b	3.06 E-01	5.59 E-03	9.69 E+04	1.65 E+03

Ratkowsky's empirical equation seems to describe the relation between temperature and O_2 / CO_2 gas exchange rates better (smaller standard deviation in parameters). Within small temperature ranges linear relations between temperature and gas exchange can be used.

The effect of temperature on ethylene production during Air and CA storage was quantified (figure 2). Large deviations in ethylene production were found in air stored apples, standard deviation increased with temperature. During CA storage ethylene production were lower. This was expected since the enzyme involved in ethylene production requires O_2.

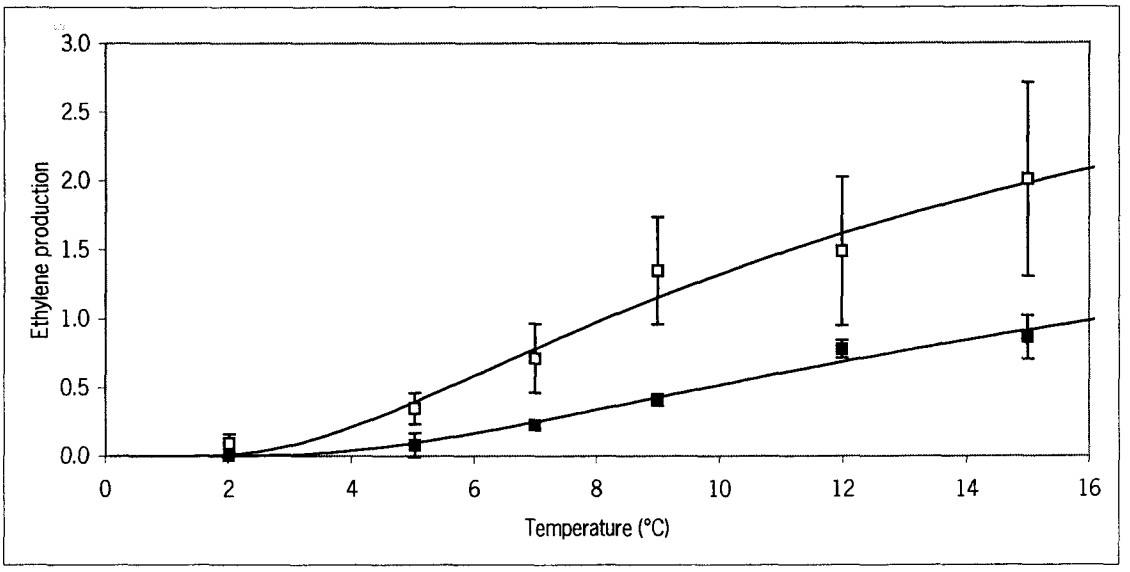

Figure 2. Ethylene production (pmol/kg.s) of apples (cv. Elstar) at different storage temperatures (°C). □ = CA stored; □ = Air stored.

Tomato

Tomatoes (™ Prominent) from a local grower (Province Zuid Holland, The Netherlands) were stored under optimal CA conditions: 5 % O_2 and 1.5 % CO_2. First gas exchange measurements at 10 °C were carried out after 3 days acclimatisation. The temperature was increased daily directly after the last gas exchange measurements. Linear relations were observed between O_2 and CO_2 gas exchange rates and temperature (table 2).

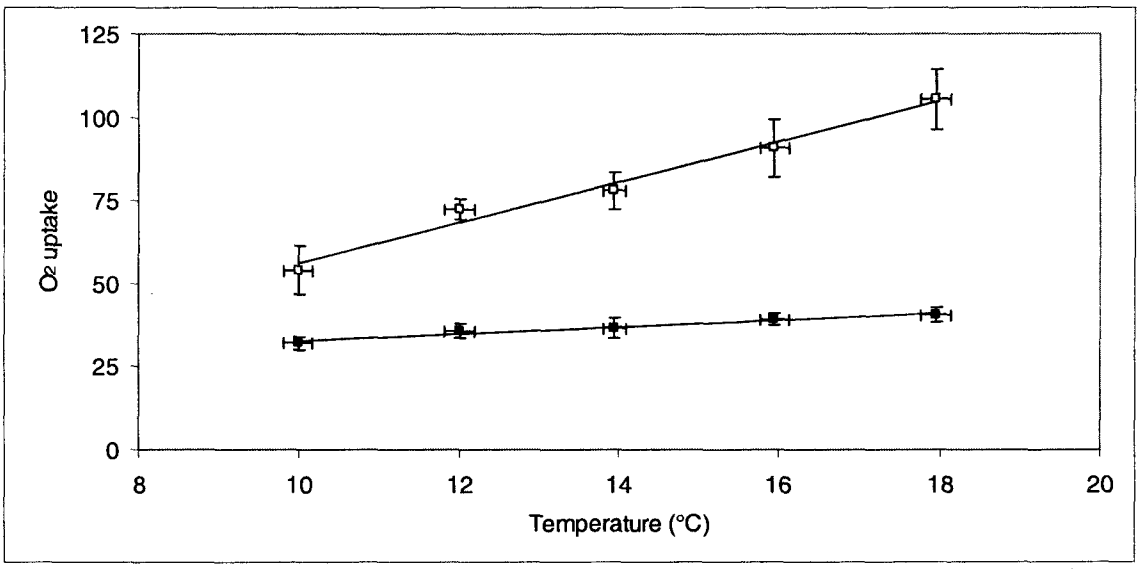

Figure 3. O_2 gas exchange rates (nmol/kg.s; n=...10) of tomato (™ Prominent) vs product temperature. □ = CA stored □= Air stored.

Table 2. Linear regression parameters for O_2 and CO_2 gas exchange rates (nmol/kg.s) of tomato (™ Prominent) vs temperature (°C).

		O_2 gas exchange	CO_2 gas exchange
Air	r^2	98.1	99.8
	slope	6.11	6.69
	constant	-5.13	-12.3
CA	r^2	96.4	94.7
	slope	1.05	1.20
	constant	22.3	19.6

No clear relation was found between storage temperature and ethylene production. This was the case for both Air and CA stored tomatoes. Although large differences were found between gas exchange rates (O_2 and ethylene) of CA and Air stored tomatoes, no difference in quality parameters (firmness, colour, skin disorder, rot) were observed. The benefit of CA storage for tomato (™ Prominent) is minimal.

The effect of gas concentration on gas exchange rates

The relation between oxygen concentration (pO_2) and O_2 gas exchange rates can be described using Michaelis Menten kinetics. Although this description is a simplification, based on one enzymatic reaction (were O_2 is assumed to be rate limiting) instead of all the enzymes involved, the relation fits well with experimental data. The relation between pO_2 and O_2 gas exchange rates is described as:

$$(3)\quad \upsilon O_2 = \frac{\upsilon m O_2 \times pO_2}{KmO_2 + pO_2}$$

where $\upsilon O2$ = O_2 gas exchange rate (nmol/kg.s); pO_2 = O_2 concentration (kPa); υmO_2 = maximum O_2 gas exchange rate (nmol/kg.s); KmO_2 = oxygen concentration at half maximum oxygen uptake (kPa).

CO_2 gas exchange rates are a result of 2 metabolic processes: oxidative CO_2 production and fermentative CO_2 production. The relation between O_2 concentration and CO_2 gas exchange is the sum of both processes (Peppelenbos et al., 1993) :

$$(4)\quad \upsilon CO_2 = RQ_{ox} \times \upsilon O_2 + \frac{\upsilon m_f CO_2}{1 + (pO_2 / Km_f O2)}$$

where $\upsilon CO2$ = CO_2 gas exchange rate (nmol/kg.s); RQ_{ox} = ratio between oxidative CO_2 gas exchange and O_2 gas exchange; pO_2 = O_2 concentration (kPa); $\upsilon m_f CO_2$ = maximum fermentative CO_2 gas exchange rate (nmol/kg.s); $Km_f O_2$ = Michaelis Menten constant for the inhibition of fermentative CO_2 production by O_2 (kPa).

Apple

Effects of gas conditions on O_2 gas exchange rates (figure 4) and CO_2 gas exchange rates (figure 5) of apple (cv Elstar) were measured at various storage temperatures. Apples used in these experiments were stored for 7 months under optimum CA storage conditions (1.2 % O_2 and 2.5 % CO_2 at 1.8 °C). The apples were placed for 3 days at 2 °C under various gas conditions (40 kPa O_2 was applied to verify how the model fitted at high oxygen concentrations). After the last gas exchange measurements the temperature was increased. The acclimatisation time between the subsequent temperatures was approximately 40 hours.

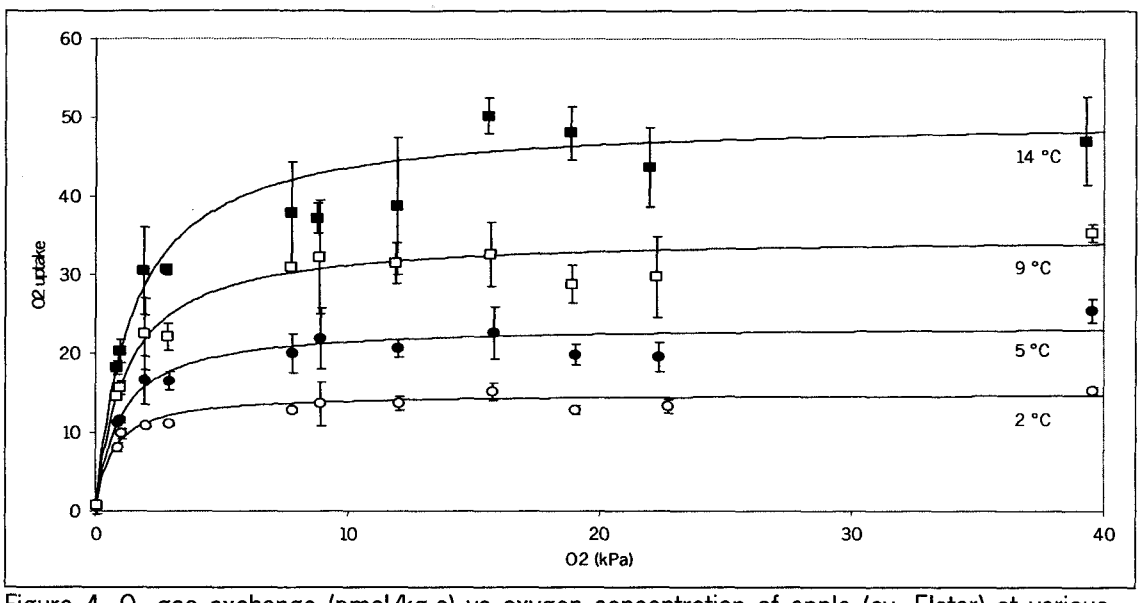

Figure 4. O_2 gas exchange (pmol/kg.s) vs oxygen concentration of apple (cv. Elstar) at various storage temperatures. □= 2 °C ; □= 5 °C; □= 9 °C; □ = 14 °C.

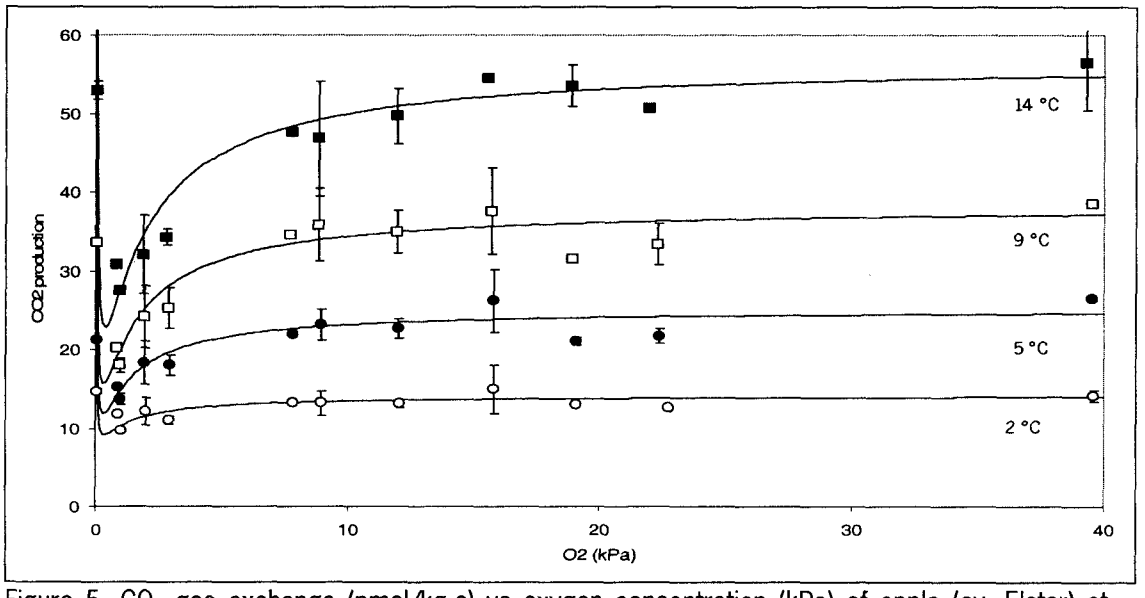

Figure 5. CO_2 gas exchange (pmol/kg.s) vs oxygen concentration (kPa) of apple (cv. Elstar) at various storage temperatures. □= 2 °C ; □= 5 °C; □= 9 °C; □ = 14 °C.

Linear relations (figure 6. and table 3) were found between the O_2 model parameters (VmO_2 and KmO_2) and storage temperature. As a result O_2 gas exchange rates of apple (cv. Elstar) can be calculated at storage temperatures between 2 °C and 14 °C.

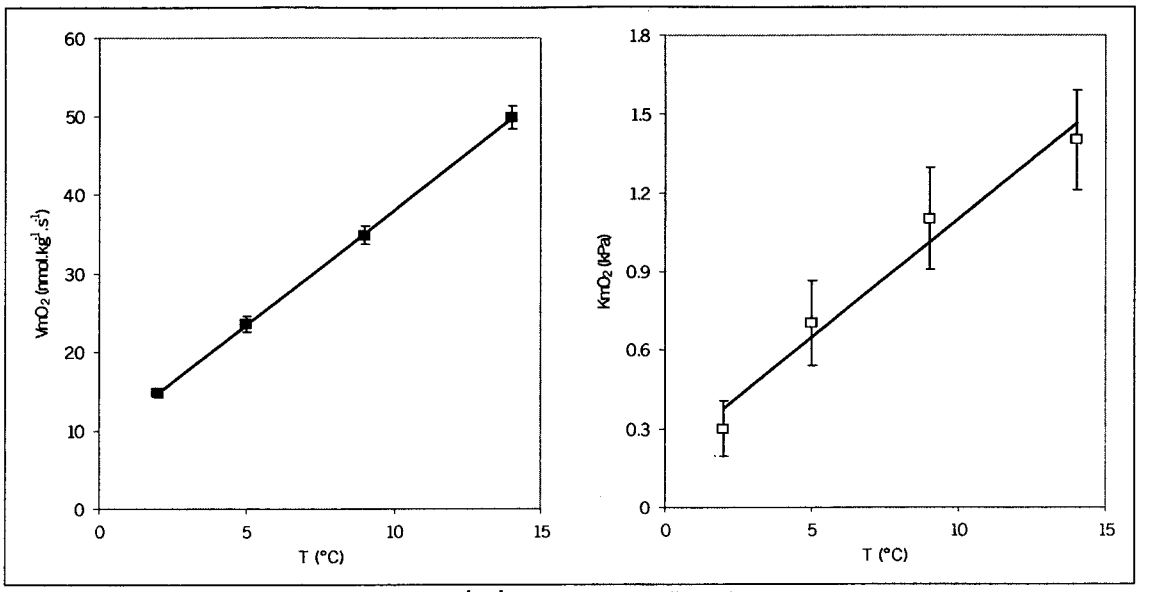

Figure 6. KmO_2 (kPa) and VmO_2 (nmol.kg^{-1}.s^{-1}) of apple (cv. Elstar) vs temperature.

For CO_2 gas exchange the Michaelis Menten parameter $\upsilon mfCO_2$ and $\upsilon m_{ox}CO_2$ are temperature dependent, whereas RQ_{ox} and $KmfCO_2$ are temperature independent.

Table 3. Model parameters for O_2 and CO_2 gas exchange rates of apple (cv. Elstar) at various storage temperatures.

parameter	2 °C		5 °C		9 °C		14 °C	
	avg	se	avg	se	avg	se	avg	se
r^2	87.4		83.2		83.2		89.7	
υmO_2	14.8	0.3	23.5	0.7	34.9	1.1	49.9	1.4
KmO_2	0.654	0.105	0.965	0.162	1.180	0.194	1.442	0.189
r^2	62.8		83.8		91.2		81.4	
$\upsilon mfCO_2$	22.1	4.6	35.8	9.8	67.0	21.2	86.8	24.9
RQ_{ox}	0.953	0.019	1.070	0.016	1.095	0.014	1.135	0.023
$KmfCO_2$	0.0835	0.0441	0.0599	0.0370	0.0404	0.0246	0.0553	0.0391
$\upsilon m_{ox}CO_2$	14.0		24.6		37.2		48.2	

Tomato

Tomatoes (™ Evident) were stored for 3 days at 10 °C. After the last measurement the temperature was increased by 5 °C. Gas exchange rates were shown to be stable within a 40 hour acclimatisation period.

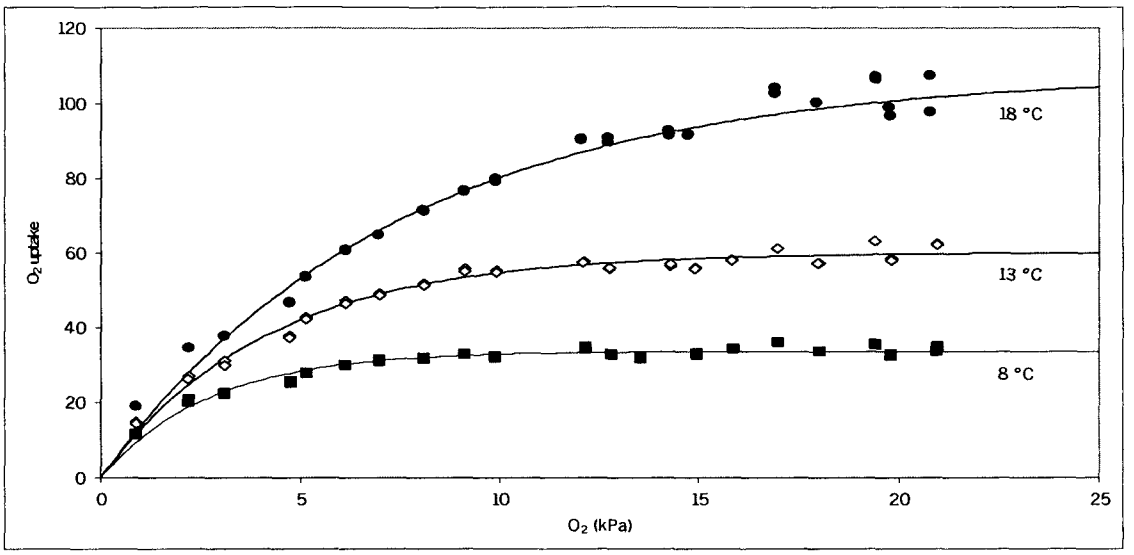

Figure 7. O_2 gas exchange (nmol/kg.s) of tomato (™ Evident) vs oxygen concentration (kPa) at different storage temperatures (°C). □= 18 °C; □= 13 °C; □ = 8 °C.

O_2 gas exchange rates (figure 6) and CO_2 gas exchange (figure 7) rate follow normal Michaelis Menten kinetics. Model parameters are shown in table 4.

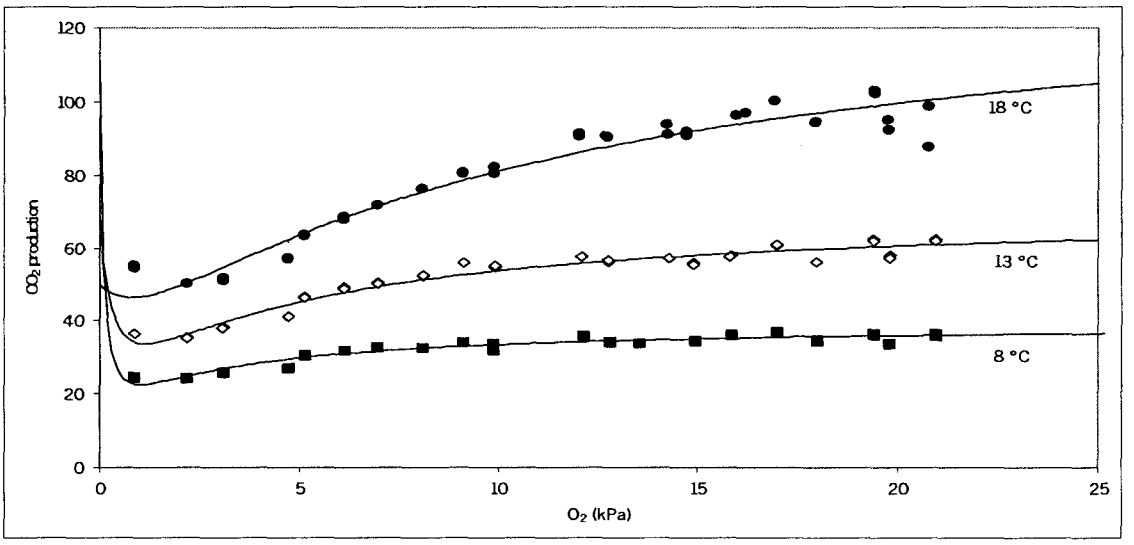

Figure 8. CO_2 gas exchange rates (nmol/kg.s) of tomato (™ Evident) vs oxygen concentration (kPa) at different storage temperatures (°C). □= 18 °C; □= 13 °C; □ = 8 °C.

Table 4. Model parameters for O_2 and CO_2 gas exchange rates of tomato (™ Evident) at various storage temperatures.

parameter	8 °C		13 °C		18 °C	
	avg	se	avg	se	avg	se
r^2	97.4		98.2		98.5	
υmO_2	38.4	0.5	72.8	1.1	148.2	3.9
KmO_2	2.05	0.12	3.71	0.20	8.57	0.54
r^2	96.8		99.3		98.4	
$\upsilon mfCO_2$	107.5		68.5	12.7	50.0	
RQ_{ox}	1.015		0.965	0.004	0.91972	0.009
$KmfCO_2$	0.0994		0.379	0.098	1.814	0.357
$\upsilon m_{ox}CO2$	37.4		65.0		144.4	

High regression coefficients (r^2 > 96.8) were found for all gas exchange models, indicating that the data fitted well to the models. An exception was found for CO_2 gas exchange rates at 18 °C were the fermentative production did not fit well. As for apple linear relations existed for O_2 and CO_2 model parameters (except for RQ_{ox} and $VmfCO_2$) and storage temperature. This allows us to calculate O_2 gas exchange rates of tomato (™ Evident) at storage temperatures between 8 and 18 °C.

Ethylene production

Ethylene production was measured after O_2 and CO_2 gas exchange measurements. The enzyme which is involved in ethylene production is an "ordered bi-substrate" (ACC and O_2) enzyme. These type of enzymes do not follow normal Michaelis Menten kinetics (figure 9). Ethylene production can be modelled with a so-called co-operative Michaelis Menten model:

$$(5) \quad \upsilon C_2H_4 = \frac{\upsilon mC_2H_4 \times pO_2^{\,h}}{(KmC_2H_4)^h + pO_2^{\,h}}$$

where υC_2H_4 = C_2H_4 gas exchange rate (pmol/kg.s); υmC_2H_4 = maximum C_2H_4 gas exchange rate (pmol/kg.s); pO_2 = O_2 concentration (kPa); h = Hill coefficient; KmC_2H_4 = oxygen concentration at half maximum ethylene production.

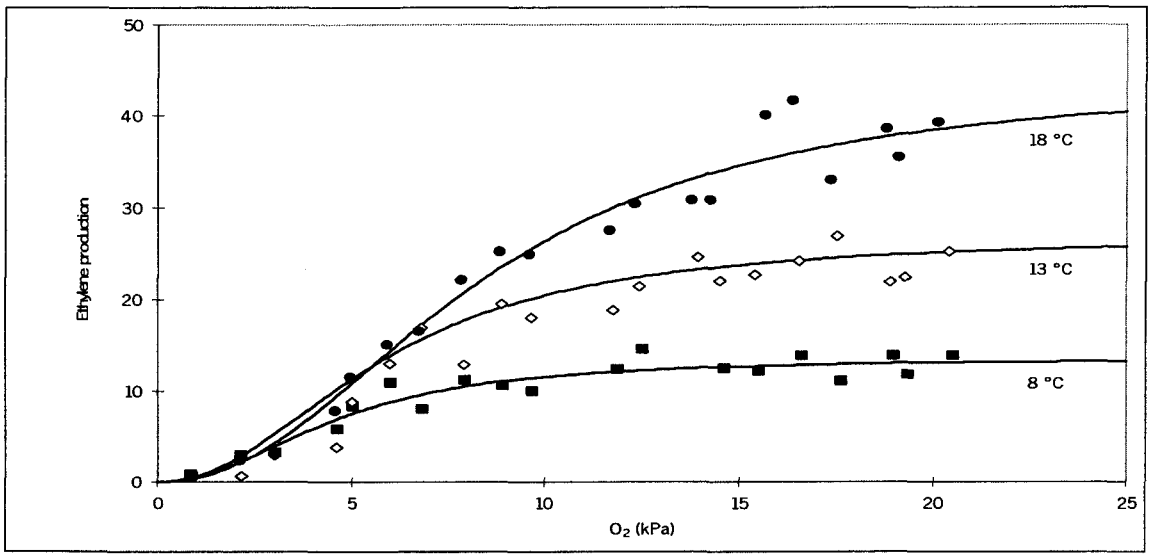

Figure 9. Ethylene production (nmol/kg.s) of tomato (™ Evident) as function of O_2 concentration (kPa) at various temperatures.

The co-operative Michaelis Menten model fitted well to the experimental data (table 5), whereas the normal Michaelis Menten model showed large deviations between the model and the experimental data. Also υmC_2H_4 and KmC_2H_4 had larger standard deviations.

Table 5. Model parameters for ethylene production of tomato (™ Evident) at various storage temperatures.

parameter	8 °C		13 °C		18 °C	
	avg	se	avg	se	avg	se
r^2	92.3		95.1		96.9	
se fit	1.23		1.95		2.46	
υmC2H4	13.6	0.8	26.8	1.9	44.0	4.1
KmC2H4	4.55	0.46	5.81	0.56	8.32	0.93
h	2.19	0.50	2.15	0.42	2.20	0.37

(1) Apples from both harvests were from a l
The Netherlands.
(2) Experiment were repeated after 3 and 6
Elstar apples (1.2 % O_2, 2.5 % CO_2 and 1
(3) Optimal CA conditions (1.2 % O_2 and 2.5

All gas exchange rates (O_2, CO_2 and ethy
Firmness of 25 apples was measured with
shelf-life at 18 °C and 90 % RH.

Gas exchange rates

O_2 gas exchange rates decrease after h
(temperature and gas conditions). The respc
5 days after harvest (figure 10). O_2 gas e
storage at 9 °C (after the climacteric rise in

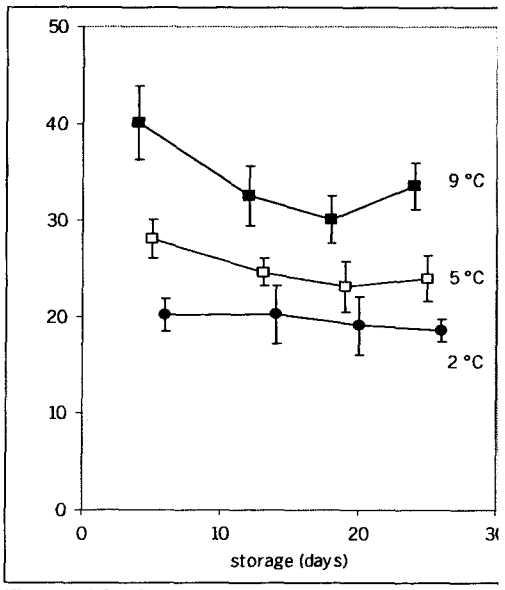

Figure 10. O_2 gas exchange rates (nmol/kg
various temperatures, directly after harvest.

O_2 gas exchange rates during CA storage v
gas exchange rates of air stored apples te
clear differences in O_2 gas exchange rates v
After 3 and 6 months CA storage significa
between the applied temperatures.

CEET2005 Report – January 2002

Conclusions

- Gas exchange rates of apple (cv. Elstar) and tomato (™ Pr
quantified as function of oxygen concentration and temperat
best fits to experimental data.
- Although large differences were found between gas exchang
and Air stored tomatoes (™ Prominent), no difference in quali
skin disorder, rot) were observed.
- Linear relations were found between the O_2 gas exchange pa
temperature. This makes it possible to calculate O_2 gas excha
at different transport temperatures and gas conditions.
- The O_2 gas exchange model and CO_2 gas exchange model fitt
- Ethylene production of tomato (™ Evident) can be described v
cooperative Michaelis Menten.

II Effect of temperature, storage conditions (Air and storage time on firmness of apples

Transport conditions for fruit and vegetables are often based c
storage. These climate conditions are stricter than needed given
30 days). Therefore conditioning may be less strict, when this
quality decay. Less strict climate conditions may lead to redu
conditioning, since the amount of energy used for cooling or m
reduced.

Knowledge is required, which describes quality decay during trans
In transport simulations the effect of storage conditions, transpor
exchange rates (O_2, CO_2 and ethylene) and firmness of Elstar a
paragraph results of harvest 2000 are shown.

Experimental set-up

Simulation experiments with Elstar apples were performed in
containers were connected to a flow-through system, in which
using mass flow controllers. A 500-ml gas flow was led throug
connected with two cuvets and the 65-L container (placed in serie
used at each condition.

Table 6. Experimental conditions.

harvest (1)	temperature (°C)	gas conditions	storage ti (months)
2000	2	Air	0, 3, 6
2000	5	Air	0, 3, 6
2000	9	Air	0, 3, 6
2000	2	CA (3)	0, 3, 6
2000	5	CA	0, 3, 6
2000	9	CA	0, 3, 6
2001	5	Air	0, 6
2001	9	Air	0, 6
2001	14	Air	0, 6
2001	5	CA	0, 6
2001	9	CA	0, 6
2001	14	CA	0, 6

		Transport time (days)		
	T (°C)	7	14	28
CA	2	0.054	0.045	0.044
	5	0.055	0.071	0.046
	9	0.144	0.143	0.117
AIR	2	0.205	0.174	1.4
	5	0.215	0.350	13.8
	9	0.358	0.361	

Figure 13. Firmness of apples (cv. Elstar) and ethylene production (pmol/kg.s) after transport (days) at various storage temperatures (°C), directly after harvest. ▩ = > 50 N; = 45 – 50 N; ■= < 45 N.

Firmness decline directly after transport is very low (figure 13). Firmness of apples stored for 28 days under normal air was not acceptable (minimum firmness for Elstar is 45 N). No internal storage disorders were observed during CA storage at 5 °C and 9 °C. Firmness of air stored products declines faster during at elevated temperatures during shelf-life (figure 14).

		Transport time (days)		
	T (°C)	7	14	28
CA	2	0.054	0.045	0.044
	5	0.055	0.071	
	9	0.144	0.143	0.117
AIR	2	0.205	0.174	
	5	0.215		
	9			

Figure 14. Firmness of apples (cv. Elstar) after 7 days shelf life and transport (days) at various storage temperatures (°C), directly after harvest. Ethylene production (pmol/kg.s) during transport. ▩ = > 50 N; = 45 – 50 N; ■= < 45 N.

During shelf-life large differences in firmness occurred for the air stored apples. CO_2 gas exchange rates were significant different between the applied temperatures for both CA and Air storage. No significant differences in O_2 gas exchange rates were observed between the temperatures in CA storage. Only slight changes in O_2 and CO_2 gas exchange rates were found (figure 10 and 11), during firmness decay. Therefore it is unlikely that either O_2 or CO_2 gas exchange rates can be used to predict quality during shelf-life nor can be used for dynamic control of climate conditions. However a threshold value for ethylene production might be used (figure 14). Above this value unacceptable firmness decay occurs during shelf-life.

Conclusions

- Gas exchange rates (O_2, CO_2 and ethylene) and firmness of apples have been quantified in relation to transport temperature, transport conditions (air and optimal CA), transport time and transport period.
- Based on logistic data (transport time and transport period) it is possible to choose transport conditions in which firmness will be maintained and energy costs for climate conditioning reduced.
- Firmness is retained during CA storage at elevated temperatures (5 °C and 9 °C) and decreases slower during shelf-life compared to air storage.
- O_2 and CO_2 gas exchange rates during transport do not predict quality decay during shelf-life.
- Ethylene production seems to be predictive for firmness decline during shelf-life.

III Effect of temperature fluctuations on product quality

In practice fluctuations in climate conditions (T, O_2, CO_2 and relative humidity) are minimised for long-term storage, which often leads to over dimensioning of cooling capacity and ventilation capacity. Until now energy consumption has never been a constraint during transport. In general it is assumed that product quality benefits from a stable environment. We hypothesised that when fresh products can be stored with larger fluctuations in climate conditions and without quality loss, it will decrease the energy demands during transport.
However, little or no knowledge is available how fresh products behave under changing climate conditions. To quantify the effect of temperature fluctuations (bandwidth and frequency) several fresh products (apple, tomato and bell pepper) were stored at temperatures close to optimal. Product quality and gas exchange rates of products stored under changing climate conditions were compared to product stored at constant temperature.

Apple

Two experiments were performed (table 7) at different temperature setpoint (Ts) and storage duration (days). In the first experiment larger temperature fluctuations at a higher setpoint (to minimise defrost frequency) were applied to quantify the effect on product quality. In the second experiment a storage period of 30 days was applied (normal transport period for New Zealand – The Netherlands).

Table 7. Experimental settings

experiment	Ts (°C)	bandwith ± (°C)	frequency (hrs)	Storage time (days)
I [1]	4.0	< 0.3	-	2 x 5
I	4.0	3.0	12	2 x 5
I	4.0	3.0	6	2 x 5
I	4.0	1.5	12	2 x 5
II [2]	2.5	2.0	24	30

[1] apples were stored under optimal CA conditions (1.2 % O_2 and 2.5 % CO_2)
[2] apples were stored at 21 % O_2

In the figure 15 the air and product temperature patterns for experiment (I) are shown. The average product temperature for all fluctuations was 4°C ± 0.2. Only at high frequency fluctuations the product temperature does not reach the minimum and maximum bandwidth.

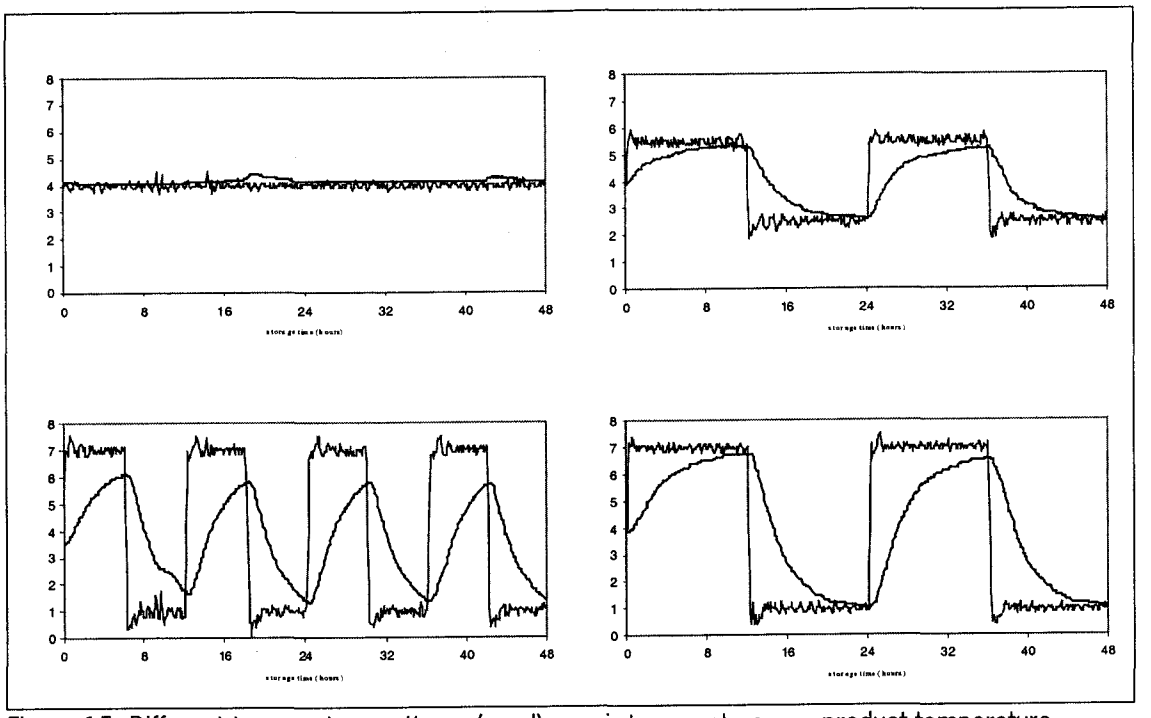

Figure 15. Different temperature patterns (exp I). — air temperature, — product temperature.

No negative effect on apple firmness was observed after 2 periods of 5 days with various temperature fluctuations (fig 16.).

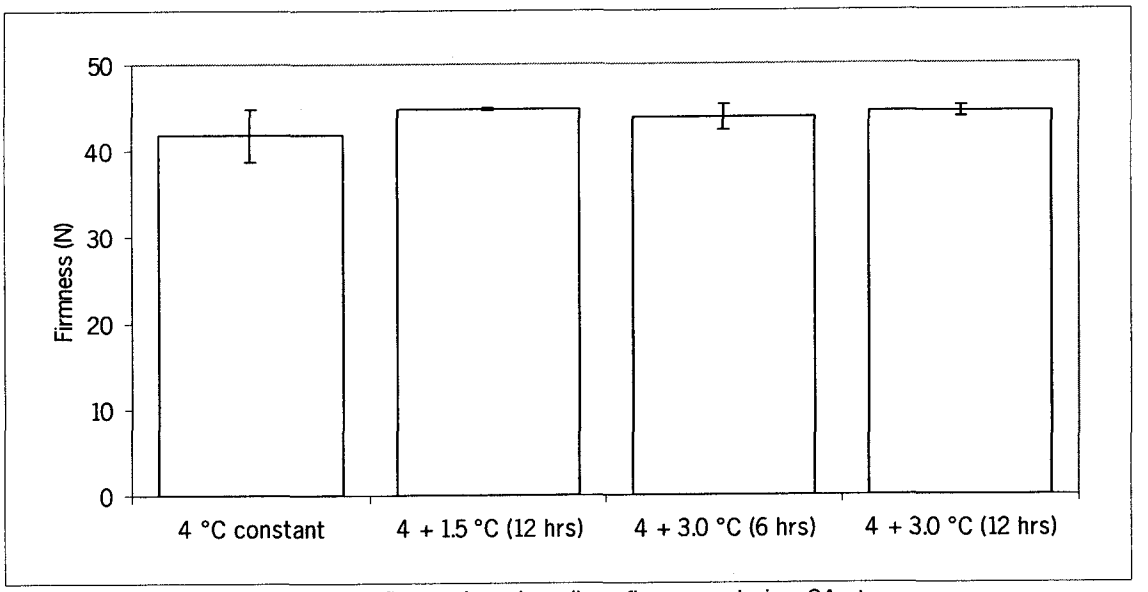

Figure 16. Effect of temperature fluctuations (exp I) on firmness during CA storage.

In the second experiment effects of long-term fluctuations on product quality determined. Apples from harvest 2001 were stored for 3 days at 2.5°C before temperature fluctuations (bandwidth 2.5°C; 24 hr frequency) were applied.

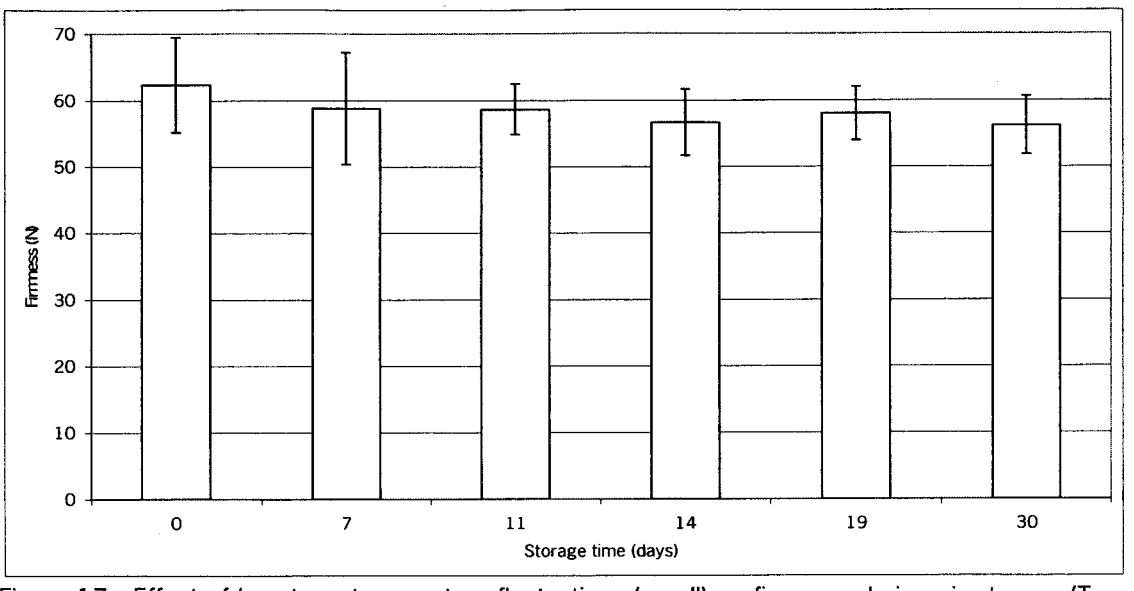

Figure 17. Effect of long-term temperature fluctuations (exp II) on firmness during air storage (Ts = 2.5°C ± 2.0°C – 24 hr frequency).

Although there is a tendency that the average firmness declines (figure 17), it was not significant within the storage period ($p<0.05$). The decline in firmness was comparable to air storage at a constant temperature.

Tomato and Bell Pepper

To measure the effect of temperature fluctuations on tomato (™ Evident) , green bell pepper (™ Special) and red bell pepper (™ Prego) all products were stored under conditions described in table 8. Products were stored under ambient air in standard transport boxes. For tomato and bell pepper the quality parameters colour development, firmness, weight loss, spots and rot were measured. Gas exchange rates of tomato and red bell pepper were measured after 5 and 10 days temperature fluctuations.

Table 8. Experimental settings for tomato and bell pepper

Ts (°C)	bandwith ± (°C)	frequency (hrs)	Storage time (days)
10.0	< 0.3	-	2 x 5
10.0	3.0	12	2 x 5
10.0	3.0	6	2 x 5
10.0	1.5	12	2 x 5

Tomato

Quality of tomato (™ Evident) was measured directly after 10 days temperature fluctuation and monitored during shelf life at 18°C and 85% RH (table 9). No significant ($p<0.05$) differences in firmness, weight loss, colour development, rot and spots were observed during shelf life.

Table 9. Firmness of tomato (™ Evident) stored at various temperature patterns, during shelf life at 18°C and 85% RH.

Fluctuation pattern	shelf life (days)							
	1		3		5		8	
	avg	se	avg	se	avg	se	avg	se
10 ± 3.0°C – 12 hr	6.98	0.03	6.78	0.03	6.64	0.06	5.45	0.01
10 ± 3.0°C - 6 hr	7.02	0.03	6.68	0.06	6.58	0.08	5.40	0.14
10 ± 1.5°C –12 hr	6.98	0.03	6.70	0.03	6.66	0.08	5.43	0.10
10 °C – constant	7.02	0.03	6.84	0.06	6.50	0.14	5.33	0.07

Gas exchange rates after a period of 5 days temperature fluctuations were at a higher level compared to 10 days temperature fluctuations (table 10). No differences in O_2 and CO_2 gas exchange rates were measured between the various temperature fluctuation patterns (both after 5 and 10 days).

Table 10. Gas exchange rates of tomato at 10 C, after 5 and 10 days with various temperature fluctuations.

	gas conditions		gas exchange rates			
	O_2	CO_2	O_2 (nmol/kg.s)		CO_2 (nmol/kg.s)	
	(kPa)	(kPa)	avg	se	avg	se
5 days						
10 ± 3.0°C – 12 hr	20.5	0.53	47.0	1.6	44.7	2.7
10 ± 3.0°C - 6 hr	20.5	0.53	48.5	10.5	46.8	8.4
10 ± 1.5°C – 12 hr	20.5	0.51	51.0	9.6	49.5	7.8
10 °C – constant	20.4	0.54	47.9	1.5	45.7	1.1
10 days						
10 ± 3.0°C – 12 hr	20.6	0.60	40.5	0.7	36.5	1.2
10 ± 3.0°C - 6 hr	20.6	0.60	41.9	6.5	37.5	5.9
10 ± 1.5°C – 12 hr	20.6	0.61	43.3	5.9	39.9	5.3
10°C – constant	20.6	0.61	40.6	2.7	36.4	1.3

Bell pepper

Quality of bell pepper was assessed after 10 days with various temperature fluctuation patterns. For bell peppers weight loss was closely correlated with loss in firmness. No significant differences ($p<0.05$) in firmness (table 11) and weight loss were observed between the applied temperature fluctuation patterns for green and red bell pepper. This indicates that the applied temperature fluctuation patterns do no alter the product quality.

Table 11. Firmness of green and red bell pepper stored at various temperature patterns, during shelf life at 18 °C and 85 % RH.

	shelf life (days)							
	1		3		5		8	
	avg	se	avg	se	avg	se	avg	se
bell pepper (green)								
10 ± 3.0°C – 12 hr	1.92	0.06	2.26	0.08	2.52	0.06	2.98	0.25
10 ± 3.0°C - 6 hr	1.94	0.03	2.33	0.08	2.62	0.05	3.10	0.14
10 ± 1.5°C – 12 hr	2.08	0.17	2.18	0.14	2.60	0.17	3.08	0.11
10°C – constant	2.08	0.06	2.29	0.12	2.43	0.19	2.98	0.09
bell pepper (red)								
10 ± 3.0°C – 12 hr	2.38	0.03	2.64	0.23	2.94	0.14	3.76	0.17
10 ± 3.0°C - 6 hr	2.48	0.11	2.66	0.03	3.04	0.00	3.92	0.06
10 ± 1.5°C – 12 hr	2.34	0.08	2.60	0.23	2.98	0.03	3.70	0.25
10°C – constant	2.44	0.11	2.56	0.11	2.88	0.06	3.84	0.11

Gas exchange rates after a period of 5 days temperature fluctuations were at a higher level compared to 10 days (table 12). When bell peppers were stored at 10.0 ± 3.0°C (frequency 12 hr) gas exchange rates were significant higher compared to products stored at constant 10°C. No effects on product quality were observed.

Table 12. Gas exchange rates of red bell peppers at 10°C, after 5 and 10 days with various temperature fluctuations.

	gas conditions		gas exchange rates			
	O_2	CO_2	O_2 (nmol/kg.s)		CO_2 (nmol/kg.s)	
	(kPa)	(kPa)	avg	se	avg	se
5 days						
10 ± 3.0°C – 12 hr	20.8	0.32	48.8	3.8	45.8	3.3
10 ± 3.0°C - 6 hr	20.8	0.29	42.2	1.0	40.2	1.8
10 ± 1.5°C – 12 hr	20.7	0.35	46.1	2.0	41.4	1.4
10°C – constant	20.7	0.37	44.4	1.2	39.4	0.4
10 days						
10 ± 3.0°C – 12 hr	20.7	0.42	43.6	2.4	35.3	1.7
10 ± 3.0°C - 6 hr	20.7	0.39	34.4	1.0	28.4	0.8
10 ± 1.5°C – 12 hr	20.7	0.43	39.0	0.8	32.4	0.7
10°C – constant	20.8	0.42	37.9	1.8	29.8	1.1

Conclusions

- The various temperature fluctuation patterns did not influence the firmness of apple, nor the firmness, colour development and weight loss of tomato and bell pepper (green and red).
- Red bell pepper stored for 5 and 10 days at 10.0 ± 3.0°C (frequency 12 hr) have higher O_2 and CO_2 gas exchange rates compared to storage at constant 10°C. However this was not reflected in additional quality loss.
- O_2 and CO_2 gas exchange rates can not be used to predict quality of red bell peppers.

Suggestions for further research

Based on observations of TASK 1 further research is recommended, which will be necessary for successful implementation of new transport strategies. This research should focus on:

- the response of fresh products to changes in climate conditions (temperature and gas conditions),
- the possibility to preserve quality by changing climate conditions after threshold value has been reached,
- defining save threshold values for model products,
- the possibility to monitor product response under static conditions and variable climate conditions,
- the perspective to use product response for a dynamic control of transport (storage) conditions.

Product response might be monitored by ethylene production or gas exchange rates, differences in storage temperature (T_{in} vs T_{out}). Although ethylene production seems to be a powerful tool to monitor product response, other on-line measurements or a combination might even provide more accurate way to control product quality.

Task 2 Optimisation of climate control under energetic and quality constraints

Model predictions of conditions in a ca-reefer container

Introduction

In the CEET research project we are developing novel ways to control the climate conditions inside a refrigerated sea-container (reefer), possibly equipped with a Controlled Atmosphere (CA) unit. The objective of this new control method is to minimise energy consumption, while retaining a certain (minimal) level of product quality. The control algorithm achieves this objective by making model predictions during shipment. The predictions are based on in-transit measurements of climatic conditions, and available physical models on the energy consumption, climatic conditions, and the product physiology. In order to reach the objective the controller will dynamically change the set points of the container.

In this chapter we will summarise the modelling approach used in this project, and show the predictive power of these models by comparing it with data obtained by validation experiments. With further simulation for a transport with apples we will give an indication of the impact on energy consumption and product quality of the novel control method. Details on the models are not given in this summary, but are given in an separate accompanying report.

Model-Predictive Control

A schematic diagram visualising the concept of the Model-Predictive Control is shown in figure 1. Based on predictions of future energy consumption and product quality change, the controller dynamically adjusts the set points of the cooling unit of the refrigerated container. The models take the control actions as input, and predict subsequently the climatic conditions of supply air, the air flowing around the pallets with packaged produce, the conditions of the air inside the package, the product quality change, and also the energy consumption of the cooling unit.

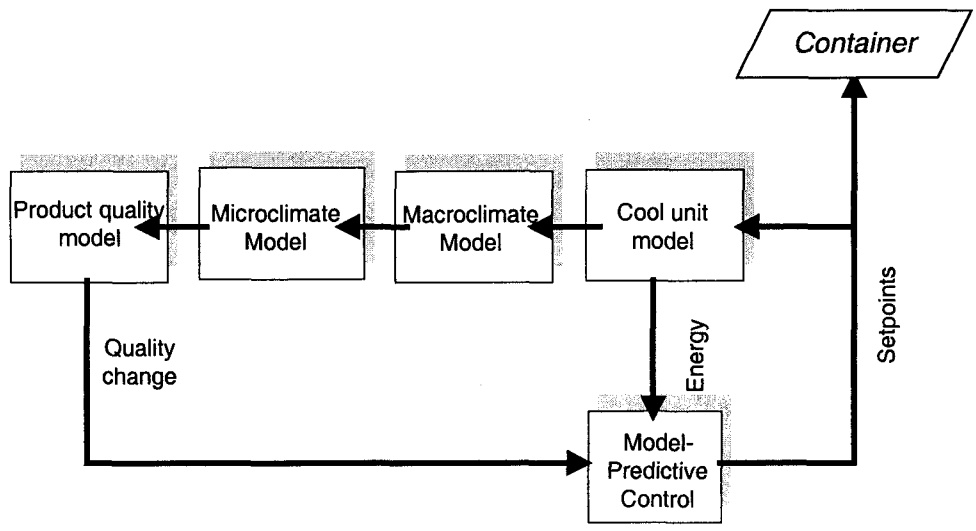

Figure 1. Schematic diagram of Model-Predictive Controller driving the set points of a refrigerated container. Controller accepts input on energy consumption and product quality change from models.

Cooling unit model

Given the set points this model computes the energy consumption, and also the conditions of the supply air, i.e. its temperature, humidity, and respiratory gas concentrations. Following Jolly et al. (2000), we have built a detailed model of the cooling unit, with modelled components shown in figure 2a. In co-operation with Carrier Transicold we have built a network model of the steady state heat flows, which are shown in figure 2b.

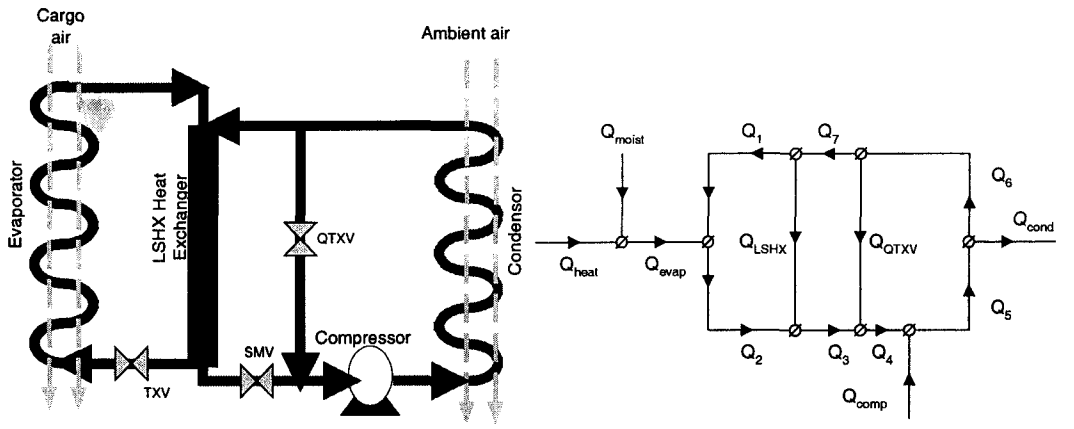

a) **b)**

Figure 2a) Schematic diagram of components in the model of the refrigeration unit, and b) Network diagram of heat flows in model of refrigeration unit. (Q)TXV are thermostatic expansion valves, and SMV modulates the refrigerant flow.

This detailed model is part of a larger network model, encompassing other components in the cooling unit, namely the evaporator fan, the heaters, the fresh air intake, and the Controlled Atmosphere unit. The heat flow network representation of the model is depicted in figure 3, where it is shown that it is coupled to the climate models by the heat flow of the supply and return air. Next to the heat flows, a similar network model is used for the flow of water vapour, O_2, CO_2, and N_2. Due to the slow dynamics of the control of respiratory gases, the model also includes the logic for this control. A more detailed description of the cool unit model, you will find in the special report on modelling.

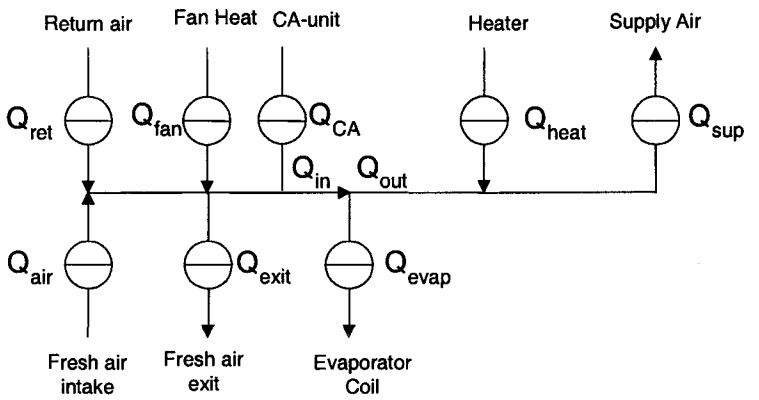

Figure 3. Network model of heat flows inside the cooling unit, with Q_{evap} given by the model depicted in figure 2.

We have tested the prediction of energy consumption of this model by comparing it to experimental data obtained at ATO and at the lab of Carrier Transicold. As shown in figure 4, the model has reasonable accuracy. The tests at Carrier Transicold are according industry standard, performed at specific temperatures given in Fahrenheit. Hence, the test conditions are given in those units in figure 4b.

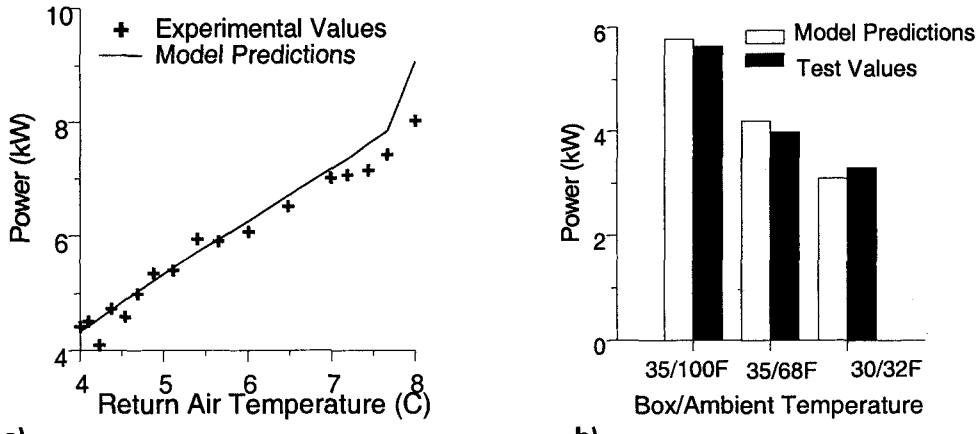

a) b)

Figure 4. Comparison of results from the energy model with a) experimental data from our lab, and b) standard test data from the manufacturer.

Climate model

As a function of the conditions of the supply air, the climate model predicts the change in product temperature, humidity and gas conditions in the packaging. The heat flow network is shown in figure 5. Similar models have been built for the mass flows of water vapour and the respiratory gases. The model for the respiratory gas conditions is somewhat simpler, because experiments have shown that there are no gradients in gas concentrations inside the container. The mass flow models are coupled to the heat flow model, due to the heat produced by respiration (P_{resp}) and extracted by evaporation (P_{evap}).

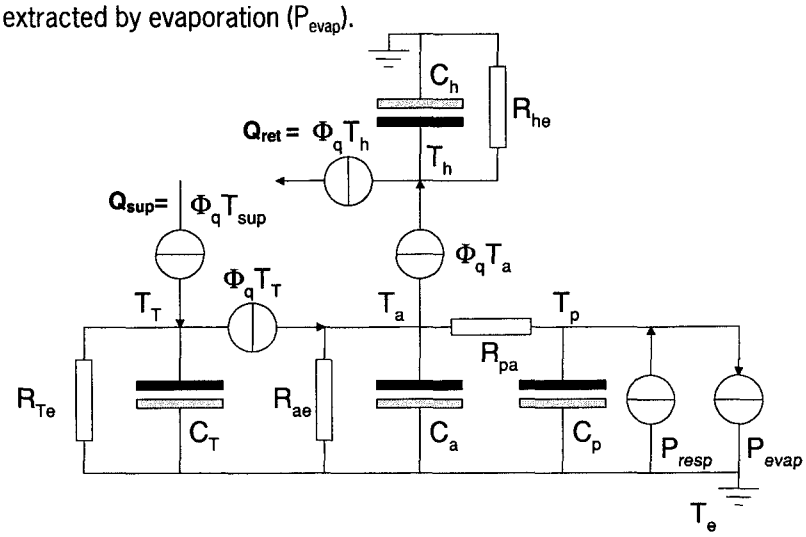

Figure 5. Network of heat flows inside the cargo space. Coupling to energy model is by Q_{sup} and Q_{ret}. Heat current sources are driven by the airflow forced by the evaporator fan, with $\Phi_q = \rho_a c_{p,a} \Phi_v$, and Φ_v the volumetric flow rate of the fan.

For the production/consumption of the respiratory gases we take a simple respiration model given by Peppelenbos (1996). The aerobic respiration follows a Michaelis-Menten kinetic without inhibition by CO_2, and fermentative CO_2 production does have inhibition by O_2. The model is valid only for low CO_2 levels, a condition valid for refrigerated container transport.

A more detailed description of the climate model, you will find also in the special report.

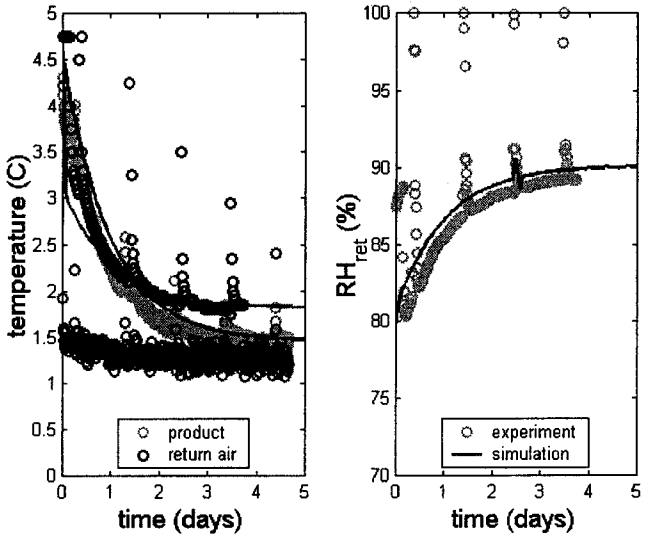

Figure 6. Comparison of climate model with lab experiment of cooling 15 tons of apples from 5°C to 1°C, packed in open trays. Shown are the average product temperature, temperature and relative humidity of return air.

The output of the climate model is fed to the cooling unit model, and the product quality model. We have tested the heat flow network model by comparing it to cooling experiments with a container loaded with 15 tons of apples. From the results in shown figure 6 follows that we can predict quite accurately the average product temperature, which is an important parameter for the product quality. Furthermore, we have tested the mass flow network model for the respiratory gases with CA-experiments on the same container with apples. From the results in figure 7 follows that we are able to predict accurately the change in oxygen.

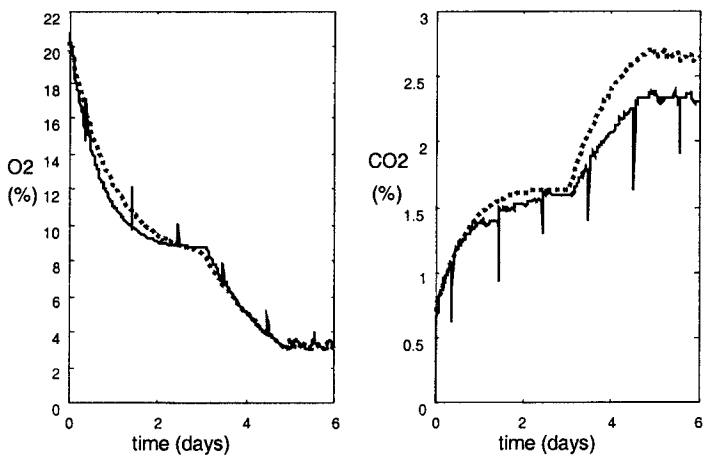

Figure 7. Comparison of results from the model (dashed line) and CA-experiment (solid line).

However, the prediction of CO_2 is a bit off for low oxygen levels, which is probably due to inaccuracy in the parameters for anaerobic respiration. For the purpose of this project this inaccuracy is not very significant, as the product quality is more influenced by temperature, moisture loss, and oxygen consumption (see below). The aim of this paper is to show the potential of the reduction of energy consumption with model predictive control, and hence the improvement of the accuracy of the CO_2 production will be dealt with in the follow-up research project.

At this stage the climate model only predicts the average climate conditions inside the container. As observed in experiments performed at ATO there is some slight temperature variation between front and backside of the cargo space. In the models to be developed in the follow-up project we like to extend the model with this temperature variation inside the container. In order to do this prediction of the air distribution inside the container and the airflow through the packages have to

be known. The latter models have been developed (van der Sman,2002) (Vollebregt,2001), but the former model is currently still under development. A preprint of the study by van der Sman (2002) and a summary of the report by Vollebregt has been included in the special report.

Product quality change model

Coupling of product temperature, and oxygen consumption to product quality. For apples, which we use in simulations below, the most important quality parameter is firmness. We modelled the firmness of apples by extended the model postulated by Tijskens et al. (1997, 1998). A description of this model you will find in a subsequent chapter. This model has been validated against experimental data obtained with Elstar apples.

In the quality change model we state that firmness of apples, its most important quality aspect, is related to the decay of they cell walls – which are made of pectins. During ripening pectin is broken down by the action of so-called pectolytic enzymes. The production of these enzymes is triggered by the ripening hormone ethylene. The production of ethylene is regulated by temperature, respiratory gases, and by ethylene itself by autocatalysis.

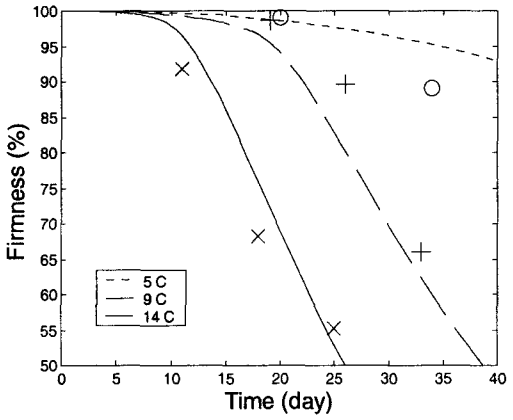

Figure 8. Firmness of Elstar apples stored at atmospheric conditions and various temperatures. Symbols indicate experimental values, and the lines indicate the values predicted with the product quality change model.

We have compared the product quality change model with experiments performed on Elstar apples, which are stored under different temperatures and CA-conditions. In figure 8 and 9 the model predictions are compared with experimental values. We have obtained reasonable agreement with experiment.

As shown in figure 8 both the model and experiments indicate that firmness shows an initial slow decay rate, and subsequently a fast decay rate. The change in decay rate is linked to the autocatalytic production of ethylene – which must be avoided in practice. As also found by Hertog et al. (2001), the initial slow rate of decay is proportional to the metabolic rate, which can be derived from the respiration model employed in the climate model.
Hence, by monitoring the respiratory rate, and linking it to the firmness of apples we can monitor the main quality aspect of apples. We envision that in the final CEET-concept ethylene sensors – being developed in this project - can be used, and hence the occurrence of the fast ripening can be detected and subsequent actions can be taken by the control algorithm (such as extensive ventilation, low temperatures or high carbon dioxide levels).

For other product it is expected that product quality change models can be linked to the respiratory rate (Tijskens and Polderdijk, 1996) (Hertog et al.,2001).

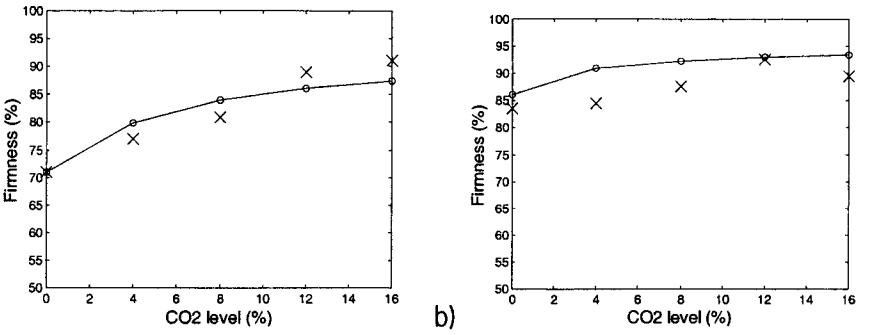

Figure 9. Firmness of Elstar apples after 21 days of storage at 18°C, and a) 21% O_2 and b) 3% O_2 and various CO_2 levels.
Symbols indicate experimental values, and the lines indicate model predictions.

Table I Ambient conditions during transport from New Zealand to Rotterdam

Days of travel	Temperature	RH
16	20	85
24	21	95
28	13	85
32	6	85

Energy reduction

After having validated that the various models have sufficient accuracy, with respect to our project goals, we test the total concept by coupling all models and compute the energy consumption for different scenarios. We apply the model calculation to a 32-day transport of 15 tons of apples from New Zealand to Rotterdam, the main port of Western Europe. The ambient temperature and humidity we take equal to the month-averaged values from the period January to March, which are shown in Table I.

We assume that the MPC control algorithm can change the following set points:

- supply air temperature
- gas conditions (O_2)
- fresh air intake
- air circulation rate

The CA-system of the container operates with a nitrogen membrane system, where the control of CO_2 is indirect. Hence, only the O_2 is taken as a set point. Initial product temperature is 7°C, and its set point is 4°C. Under standard conditions, we take fresh air intake is 75 m^3/h, and air circulation is 1 m^3/s.

In figure 10 and 11 we show the results of the simulations using different control algorithms. The graphs indicate 1) the energy consumption, 2) change in firmness, 3) product temperature, 4) gas conditions, 5) moisture loss from product, and 6) R.H. of the air surrounding the product. Moisture loss and R.H. of air around product are also indicative for the product quality. If moisture loss is more than 5%, the peel of apples shrivels, and is unacceptable for sale. If R.H. is 100% condensation occurs, which promotes mould growth.

For the simulation the change of set points is generated by simple rules. In the latter stage of the project the scenarios will be generated an actual MPC Controller. First we have performed calculations for two practical scenarios: 1) transport with constant temperature set point, without CA, and 2) transport with constant temperature, but now with CA. Subsequently, we have calculated two scenarios which allow variations in product temperature and/or gas conditions. These results are shown in figure 10 and 11.

The average power consumption in the various scenarios described above, is listed in Table II. One can observe from the results in figure 10 and 11 that short time variations in product temperature and gas conditions does not have much influence on quality parameters as firmness, weight loss, and risk of condensation (leading to spoilage). This finding has been confirmed by experiments performed at ATO by Boogaard et al. (2001).

But allowing temperature variation means that energy consuming compressors in cooling unit and CA system can be periodically be shut down, leading to significant energy reduction (See Table II).

Table II Energy consumption according to various control algorithms

Control Algorithm	Average Consumed Power (kW)
Standard Temperature Control – No CA	4.6
Standard Temperature Control with CA	7.6
Cooling unit compressor cycling , No CA	1.8
Standard Temperature Control, CA cycling	6.1

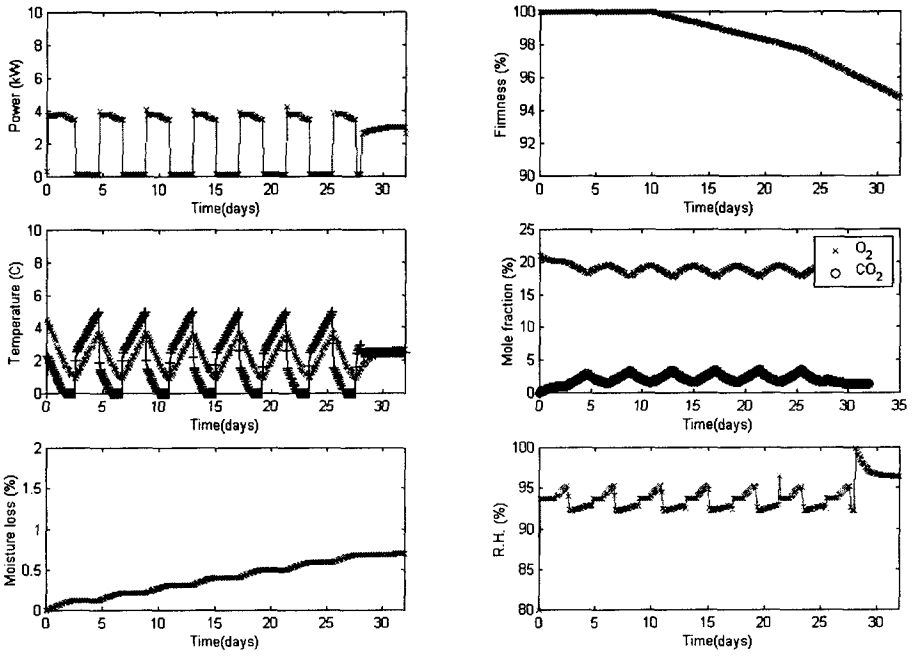

Figure 10 Simulation with control where compressor is cycled on and off, and furthermore Temperature set point and fresh air intake are changed dynamically. CA-system is off and air circulation is 0.5 m^3/s.

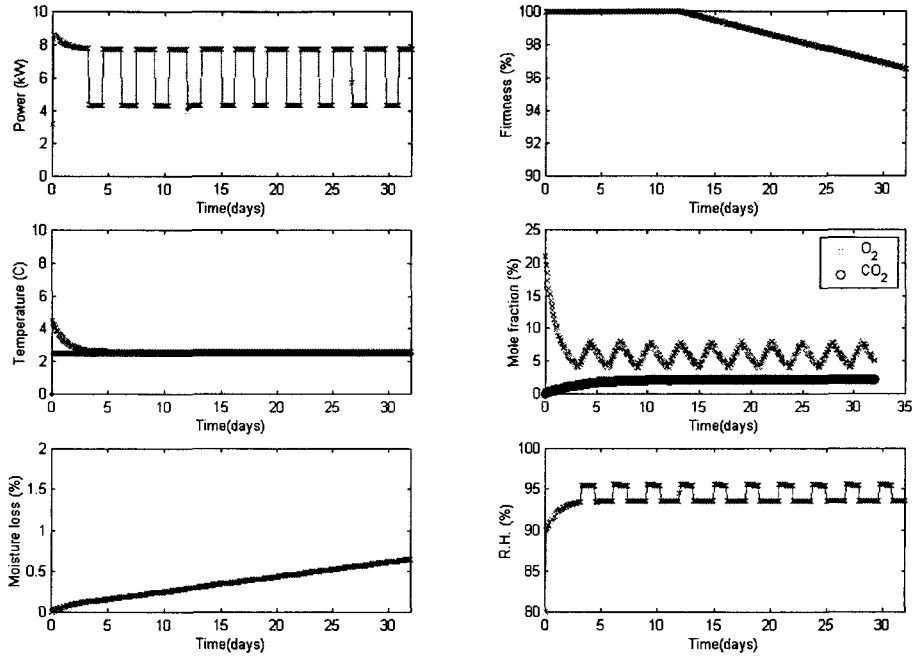

Figure 11. Constant temperature set point (4°C), but with variable O_2 – set point and fresh air intake control. Average O_2 set point is taken 6%. CO_2 is at about 2%. Air circulation is 0.5 m^3/s.

Conclusions

We have shown that by means of a new control algorithm, which dynamically changes set points, significant energy reduction in refrigerated container transport of perishables can be obtained without unacceptable loss of product quality. In the coming period we continue the research by coupling the model to a MPC-controller. Furthermore, we think our approach has potentials for incorporation of post-harvest treatments during transport, such as delayed storage (for prevention of chilling injury) or fruit ripening.

Further research

Crucial to the final success of the new method for energy reduction by dynamically changing set points is that no condensation occurs on the packed product. This aspect has not yet been investigated fully. Condensation may limit the amount of cycling of the cool unit. Hence, interaction between fluctuation of the supply air temperature and condensation has to be investigated. In container experiments using open trays as packaging for the product, we have observed that condensation has occurred very locally, namely mainly in the top layer of the pallets. For a reliable prediction of condensation, a more detailed description of the macro- and micro-climate inside the cargo space is needed.

The model describing the energy consumption of the cool unit, assumes that no ice frost occurs on the evaporator coil. During transport of produce requiring low temperatures, such as apples, this is not a valid assumption. Frost formation is known to have a significant impact on the cooling efficiency of the cool unit. Hence, for optimal operation of the supervisory control algorithm this effect has to be incorporated in the cool unit model.

During several container experiments we have observed a temperature gradient between front and backside of the cargo space. This is due to a quite non-uniform distribution of the airflow in the cargo-space. Preliminary calculations have shown that the airflow mainly flows between the first rows of pallets. We imagine better airflow distribution can be obtained by a 'false ceiling' in the headspace of the container. By extension and improvement of the preliminary model on the airflow distribution we can obtain a good design of this 'false ceiling'. Other benefits can be obtained by this false ceiling. By directing the airflow in the headspace directly above the pallets, to flow from front to back, also the risk of condensation can be reduced significantly, because now this airflow

will not be cooled, and therefore will not give condensation. Furthermore, redirection of the airflow will mean that during cycling of the cool unit, temperature fluctuations in the return air will be less pronounced than in the system nowadays. Hence, this also may lead some extra energy reduction.

In several container experiments we have observed a very significant effect of the type of packaging. The amount of time needed to cool the packed product is considerably less for open trays than that for more closed boxes, as used in the last container experiment. Hence, in open trays the product will experience much more the temperature fluctuations in the supply air during cool unit cycling. Hence, the effect of packaging has to be taken into account in the control algorithm. More research (model and experimental study) is needed on the humidity conditions in the packaging, as a function of packaging design and external conditions as airflow velocity, temperature and relative humidity. This research is an extension of the work by Vollebregt (2001).

Special designed boxes (measuring 30 x 40 x 15 cm) for container transport have been developed at ATO in other research projects, such as a modified humidity packaging for bell peppers, and modified atmosphere packaging for broccoli. These new packaging designs have a large impact on the product quality compared to existing packaging designs. We view that optimizing the packaging design will proof another way to reduce energy consumption.

The product quality change model needs to be validated using subsequent experiments. Also, similar models will be developed for other produce such as tomatoes, bell peppers etc. The focus of these models will be the link with respiration of the produce. If this link can be established, monitoring quality during transport can give an indication of the quality change of the product. Hence, in further research we will cooperate closely with the people in the project working on the experiments on respiration.

References

- Boogaard H.A.G.M., et al., 2001., lecture CA2001, Rotterdam.
- Jolly P.G., et al. 2000. Simulation and measurement on the full-load performance of a refrigeration system in a shipping container. *Int. J. Refr.* 23(2): 112-126.
- Hertog, M.L.A.T.M., Nicholson, S.E., and Banks N.H. (2001). The effect of modified atmospheres on the rate of firmness change in 'Braeburn' apples. *Postharvest Bio. Techn.* 23: 175-184.
- Peppelenbos, H.W. 1996. The use of gas exchange characteristic to optimize CA storage and MA packaging of fruits and vegetables. *Ph.D. Thesis* Univ. Wageningen, the Netherlands.
- van der Sman, R.G.M. 2002. Prediction of airflow through a vented box by the Darcy-Forchheimer equation. *J. Food Eng.*, in press.
- Tijskens L.M.M. and Polderdijk J.J. (1996) . A generic model for keeping quality of vegetable produce during storage and distribution. *Agric. Syst.* 51: 431-452.
- Tijskens L.W. et al. 1997. Modelling the firmness of 'Elstar' apples during storage and transport. *Acta Hort.* 485: 363-.
- Tijskens L.M.M. et.al. (1998) Kinetics of polygalacturonase activity and firmness of peaches during storage. *J. Food Eng.* 35: 111-126.
- Verdijck, G.J.C., Lukasse, L.J.S., and Sillekens J.J.M. 2000. Aspects of Control Structure Selection in Post-Harvest Processes. *Proc. Agri-Control 2000*, Wageningen, the Netherlands.
- Vollebregt H.M. 2001. Modelling the effect of cross-flow on the climate in transport containers for perishable goods. *Final report of the post-graduate program* Mathematics for Industry, Stan Ackermans Institute, Eindhoven University of Technology

List of publications related to the research of the modeling work in this project

- R.G.M. van der Sman, and H.S. Yun, Modelling air flow in vented box packed with produce. *Refr. Sci. Techn.* Proc. Improving Postharvest Techn. Fruits, Vegetables and Ornamentals. Murcia, Spain: 866-871. (2001).
- Lukasse, L., R.G.M. van der Sman, et.al. Reefer containers, status quo and new developments. *Koude & Luchtbehandeling* 94(6):22-27 (2001).

- R.G.M. van der Sman, G.J.C. Verdijck. Model predictions and control of conditions in a CA-reefer container. *Acta Horticulturea* Proc. CA2001, Rotterdam, the Netherlands, in press (2002).
- R.G.M. van der Sman. Prediction of airflow through a vented box by the Darcy-Forchheimer equation. *J. Food Eng.*, in press (2002).
- H.M. Vollebregt. Modelling the effect of cross-flow on the climate in transport containers for perishable goods. *Final report of the post-graduate program* Mathematics for Industry, Stan Ackermans Institute, Eindhoven University of Technology (2001).

Contribution of Carrier Transicold

Introduction

The focus of this project is to optimize product quality & minimize energy consumption during a containerized reefer transport of fresh produce. In order to formulate the optimization logic, inputs such as product quality (initial & ongoing), metabolic rate, transportation route, and product tolerance to temperature & gas composition are required. The use of green chemical may further aid in energy consumption reductions, without compromising product quality.

Aim

- ► Assist in the development of a refrigeration system model that predicts the energy consumption of a perishable product at varying cargo & ambient temperature conditions.
- ► Improve efficiency of refrigeration system components to achieve lower energy consumption during transportation of product. Integrate new concepts within the refrigeration unit hardware.
- ► Assist ATO in container testing of apples. Trouble shoot and maintain the EverFRESH controlled atmosphere unit being used for full container tests.

Results

For the last period, Carrier's participation has been focused on the three areas noted above. When necessary, Carrier engineers have worked with the engineers and technicians at ATO to support the development of the energy models.
Further progress has been made in the development of automatic fresh air venting system, a more efficient CA air compressor, and advanced atomizers for humidity control.
Carrier has provided support for the full-scale container testing that has been completed to demonstrate the power savings realizable with alternate climate conditioning requirements (i.e. greater temperature fluctuation).

Conclusions

Container scale testing has demonstrated a control approach for apples that allows for 60% energy savings without loss in product quality.

Further research and development

The work planned for early 2002 consists of:

- ► Final review of container test data and assist in developing a complete report on the full scale container test
- ► Continue development of moisture (& green chemical) delivery system using improved water atomizers.

Contribution of P&O Nedlloyd

The aim of this project is to develop a Container with a much better Insulation factor then the present Reefer Containers. In this way we need less power to keep the cargo temperature controlled which is contributing to the total power saving.

At the moment we have no concrete results regarding actual testing however some calculations proved that the K-value could be reduced by some 25% of the present value when we decide for a new foam technique.

We are discussing with a Chinese Container manufacturer and a European foam manufacturer's the possibilities for a new special vacuum foam technique. According to the foam manufacturer it is possible to have the vacuum foam panels according to the sizes suggested by the Container Manufacturer and P&ONedlloyd. These small size panels are used to avoid the loss in heat-leakage value in case of damaged panels. The only problem we have now to overcome is the total investment for the company as this new type of insulating panels are approx. three times more expensive then the present foaming technique.

The Manufacturer prepared new drawings, which we discussed during a visit to this manufacturer in November 2001. Together with the container manufacturer we made some computer calculations for the new heat-leakage value for the possible new container. According to the calculations we can achieve a reduction of 25%.

Also we were looking to a different option to have a better K-value for the container and that is to increase the thickness of the present foam panels. In order to get the same K-values as we are able to get when using vacuum panels we will have a severe reduction of cargo space which will be unacceptable for the industry.

As the total investment for this new type reefer with vacuum foam-panels is far beyond the possibilities we have at hand at the moment we will not build a prototype container. In case there will be done some test shipments it is easy to calculate the extra savings we can have during a test transport for which test we can use a normal reefer container.

Task 3 Development of a robust integrated sustainable energy system

Introduction

Aim of the project

'The agro-container concept of the 21st century' is an extensive project aiming at the development of a reefer container concept that reduces the environmental pressure of climate controlled agro-transport. This is achieved by means of energy reduction and integration of sustainable energy sources in stand-alone containers [CEET2005-1]. The project concerns a refrigerated container without Controlled Atmosphere (CA). A consortium consisting of ATO, P&O Nedlloyd, Carrier Transicold, Ecofys, Shell Solar and The Greenery International conducts research for this project on the grounds of the Resolution on subsidies for Economy, Ecology and Technology from the Ministries of Economic Affairs and of Education, Culture and Science.

The goal of energy reduction is achieved by means of both reducing the energy demand and improving the efficiency of the cooling unit and the energy supply system. The energy demand can be reduced by optimising the product climate, the climate control and improving the isolation of the container. Reducing the energy demand and optimising the container's hardware is done in task 2. Optimising the container's software is part of task 7. The energy supply system is designed in task 3. ATO, P&O Nedlloyd and Carrier Transicold work together in task 2. Ecofys and Shell Solar carry out task 3. At the same time means of cost and energy reduction in the product chain are studied in task 6 by ATO and P&O Nedlloyd. This report focuses on Task 3.

In the beginning of 2002 three system configurations of the container where described [CEET2005-6] that could be realised by the project:

1. The energy optimised system
2. The product optimised system
3. The chain optimised system

In a later stage it was concluded that configuration 2 is the system that will be realised within this project.

Current reefer transport (reference technology)

As a reference technology the 40ft HC integral reefer was used within this project. The 40ft HC reefer makes up the majority of the current reefer fleet (1999) and its market share is still growing [Uytendaal 1999]. In 1997 1.7% of the reefer container fleet had the possibility of applying Controlled Atmosphere (CA) [CEET2005-1].

Inside the reefer the temperature can be kept between -25 and 25°C at ambient temperatures of -20 and 50°C. This is normally done with a built-in compressor refrigerator unit. In this project the container refrigeration technology of Carrier Transicold is used, since they are part of the consortium. They are one of the two major suppliers of container refrigeration equipment. Carrier supplied a 69NT40-489 refrigeration unit with Everfresh Controlled Atmosphere for the climate/product interaction and energy optimisation research performed in task 2. The technical specifications of this model are the bases for the estimations of the energy use of the container [Carrier, 1998].

Choice of products

The CEET2005 project is restricted to agricultural products which quality (shelf life) profits from cooling and controlled atmosphere. Although this is only a small part of the total seaborn reefer trade, further narrowing down is necessary to be able to perform a detailed climatological and logistical analysis. Together with ATO (task 6) it was decided to focus on apples which are transported from New-Zealand to the Netherlands and bell pepper from the Netherlands to the United States of America (USA). Their so-called cold chain (overview of the places, duration and

transport mode in which the product is kept cold) is discussed below, a more elaborate report in presented in Task 6.

The Cold chain of apples and bell pepper
Fruit and vegetables are transported all over the world by ship, train, truck and plane. To lower the handling costs the same container is used in several transport modes (intermodality).

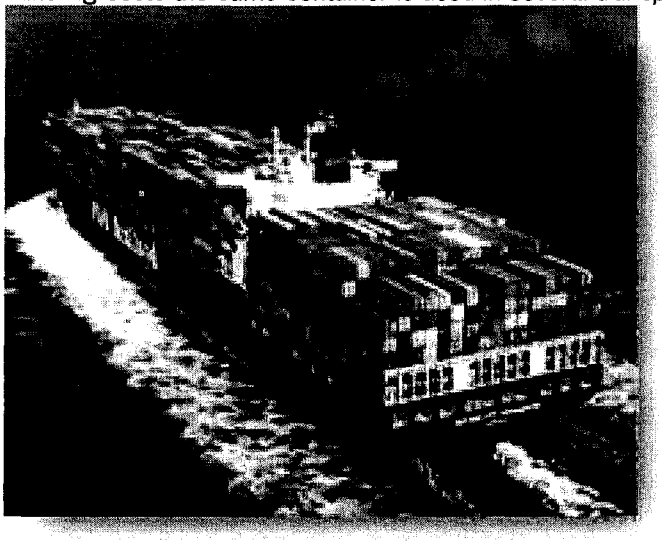

Figure 1 Container ship P&O Sutton [ponlweb]

Apples can be kept in good condition for about a year when applying climate (temperature, humidity and gas) control. The transport from producer to consumer is generally the following[1].

Apples are transported from the producer to a packinghouse by truck in about a day from the moment of harvesting. They are stored less than a week in the packinghouse. From there they are transported in a cooling truck to a cold store in the port of Wellington (New Zealand). Apples can stay for about a week at the cold store. In the harbour either a reefer ship (during the season) or a reefer container (when the supply is not enough to fill a complete ship) is stuffed. After about 3-4 weeks the ship arrives in the harbour of Rotterdam (the Netherlands). Here the container is stripped most off the time. The apples are put in a cold store for 3 weeks at most. From the cold store they are transported to the cold store of the importer in a cooling truck or reefer container. Apples can be stored for a year at the importer. From the importer transport goes mainly by cooling truck to a distribution centre and from there to the supermarkets (the Netherlands).

Bell peppers are much more vulnerable than apples and can be kept in good condition for about 30 days depending on the season. Bell peppers are only transported over sea to the USA during the summer when the peppers are strong enough to sustain the long trip. During the rest of the year they are transported by plane. In this project it is investigated whether an improved reefer can extend the shelf life in such way that marine transport is economically favourable. The transport of bell peppers via the sea is generally the following[2].

The bell peppers are transported from the producers (the Netherlands) to the cold store of the exporter by truck within a few hours from harvesting. At the exporter a reefer container is stuffed and transported in one hour by truck to the port of Rotterdam. At the port the reefer is stored in a reefer stack for a day at most. The sea trip to the East Coast of the USA (New York) takes about 8 days. At the port of New York the reefer container is stored in a reefer stack for 1-2 days, from which it is transported within a day on a truck to the importer. There the reefer is stripped and the bell peppers are put in a cold store for a day at most. From the importer they are transported in a cooling truck to the cold store of a distribution centre and on to the supermarket within two days.

[1] Source: P.Schreurs (task 6 - Eteca)
[2] Source: S.Tromp (task 6 – ATO-DLO)

Work carried out by Ecofys

Reduction of the pressure of the reefer transport sector on the environment is within this project achieved by means of both reducing the energy demand and improving the efficiency of the cooling unit and the energy supply system. Possibilities for a sustainable/more efficient energy supply system for the reefer container are investigated in this report.

The report starts with an evaluation of the criteria the energy supply system should meet (0). Those where established by discussions with the project partners. The main criteria the system should meet are: deliver enough power, be autonomous, have an available – over whole world - fuel source, be sustainable and compatible with intermodality of the reefer containers. Cost aspects of the concepts are also considered. In the next paragraph (0) different possible energy supply systems are discussed. The conventional ones - diesel gensets, electricity on the ship – are compared to new option, such as photo voltaic cells, fuel cells, electric buffers, bio-diesel genset, H_2/LPG/NG and an absorption heat pump.

In order to increase the number of optional supply systems the energy demand of the reefer container needs to be reduced. Therefore Ecofys has also been investigating ways to reduce the energy consumption of the refrigeration unit. In this last respect the focus is on the hardware of the unit (since software is tackled in task 7). This is discussed in 0.

Results: energy supply system

Criteria for an energy supply system

The cold chain of the products transported and the configuration chosen for the CEET2005 reefer concept define a specific set of criteria for the design of the energy supply system. The main criteria the system should meet are as said: deliver enough power, be autonomous, have an available – over whole world - fuel source, be sustainable and compatible with the intermodality of the reefer containers, they will be discussed in more detail below. Apart from these criteria the power supply should be compatible with the total cold chain.

Power

The current CA reefer has a power demand of ~7-10 kW. This depends on the product transported, the demanded inside temperature and the outside temperature. To estimate the power demand of the current CA reefer we devised a simple model reckoning with several heat sources and losses as is shown in Figure 2. The numbers used for internal heat losses from transmission and ventilation; and internal sources such as from circulation, product activity and machinery are listed in Table 1. The numbers given in the column CEET2005 are estimates from the partners given during the project.

External heat sources and losses such as radiation, solar irradiation and heat transport by the wind depend strongly on the climatological circumstances at the location of the container. To estimate the temperature rise of the container shell due to solar radiation we looked at a day in the Netherlands with maximum sunshine. In that case the temperature of the shell can rise 50 to 60 degrees above the outside air temperature when there is no heat transport by wind. With a little bit of wind the temperature rise decreases rapidly, but even at 10 Beaufort the temperature rise is still 7 to 9 degrees. The shell temperature should be used when calculating transmission losses for the temperature extremes.

40ft High Cube reefer filled with 12/15 tons of bell pepper/apples

		current reefer	source	Ceet2005 reefer	source	Diff.
transmission	W/K	44.1	P&O	26.0	P&O	-42%
leakage	W/K	3.5	P&O	2.3	Ecofys	-35%
product activity	W	300-540	ATO	300-540	ATO	-
circulation	W/K	1320.0	ATO	396.0	ATO	-70%
compressor	W	3300.0	ATO	2805.0	Carrier	-15%
COP		2.0	ATO	2.2	Ecofys	-10%
heating	W	1800.0	ATO	1620.0	Ecofys	-10%
CA	W	1717.5	Carrier	1545.8	Ecofys	-10%

Table 1 Estimated losses and sources of heat, and cooling performance of 40ft HC reefer in current situation and estimated for CEET2005 reefer.

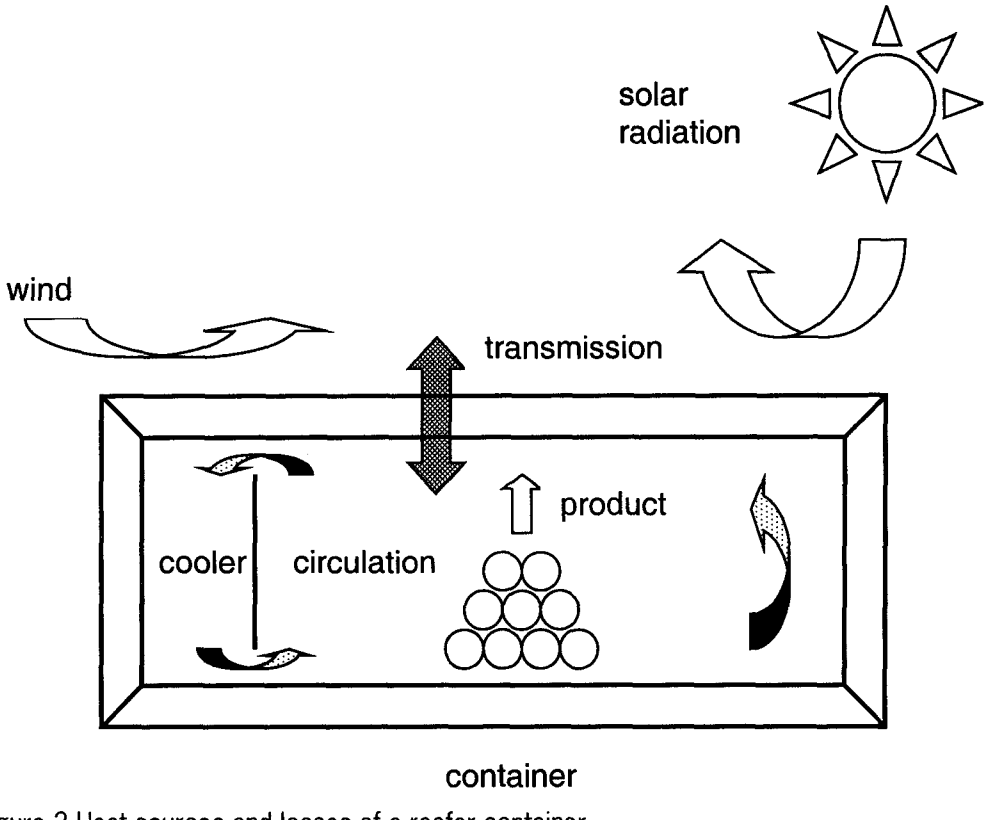

Figure 2 Heat sources and losses of a reefer container

In Table 2 the average power demand in different climatological scenarios for bell pepper and apples are shown for a current non-CA reefer and for the CEET2005 non CA-reefer. To give an indication of the variation in energy demand the outside temperatures were varied between –10 and +40°C. The heaters – used for defrosting the cooling coils - are not used the whole time but only about 10% of the time. The energy supply system should be able to deliver the total power of the heaters, therefore the peak power an energy supply system should be able to deliver is ~2 kW higher than the average power. From the table it can be seen that in both a cold and a warm climate the container needs to be cooled. Given these outside temperatures the average power demand for the CEET2005 is ~2 kW. If the sun heats the container, an extra temperature rise of the container outer shell of 50 to 60 degrees should be included as extreme. This leads to an extra energy demand of maximal 0.9 kW, which makes the total average power demand ~3 kW. The energy supply system should be able to deliver a peak power of ~5 kW.

Temperature (°C) outside	inside	product	Current average Power (kW)	CEET2005 average power (kW)
-10	4	apple	3.8	1.4
0	4	apple	4.0	1.5
10	4	apple	4.3	1.7
20	4	apple	4.5	1.8
30	4	apple	4.7	2.0
40	4	apple	5.0	2.1
-10	10	bell pepper	3.8	1.4
0	10	bell pepper	4.0	1.6
10	10	bell pepper	4.2	1.7
20	10	bell pepper	4.5	1.9
30	10	bell pepper	4.7	2.0
40	10	bell pepper	5.0	2.2

Table 2 Energy demand of current and CEET2005 reefer container for apples and bell pepper in different climatological circumstances

Autonomy
Since the CEET2005 reefer container should be able to 'survive' a foreseeable stand-alone or power off period" [CEET2005-5], the energy supply system needs to have a certain autonomy in maintaining the climate inside the container. From the description of the cold chain of apples and bell pepper it is known that the duration of both continental transport and storage outside of a cold store (at producer or in harbour) is relatively short (24 hours or less). The energy supply system should be able to supply this energy without the need for refilling. With the power demand calculated above the current reefer container needs 90-120 kWh/day and the CEET2005 needs 40-50 kWh/day and it should be able to supply a peak power of ~5 kW.

It should be noted that when other uses of the container are considered this could lead to a different stand-alone energy demand. For instance, if one wishes to use the container as a stand-alone storage facility at a remote area, a much larger stand-alone energy demand is expected (several days or weeks instead of one day). This is not the situation this report deals with in the first place.

Availability of the fuel
The reefer container is transported from a cold store near the producer or harbour in New Zealand or the Netherlands to the harbour (in New Zealand or the Netherlands) and from that harbour to the cold store of the importer (the Netherlands or USA). The fuel for the CEET2005 reefer container should be readily available at all these locations. When an extension of the use of the reefer is considered, fuel availability should be investigated.

Reliability
The reefer is on the way for several weeks. Reliability is an important criterion since maintenance engineers are not always available. Because of the remoteness of some locations in the cold chain high cost are involved when repairs are necessary during a voyage.

Costs (investment, maintenance and fuel)
Costs are subdivided into investment, maintenance and fuel costs. They are indicated to be able to compare the systems mutually and with respect to the current situation.

Dimensions and weight
Ideally the energy supply system should be built-in for a stand-alone container. Especially in the case of marine transport, changes in the capacity of the ship are not desirable. Existing large container ships have the ability to transport 700 reefer containers [Ponlweb]. At the same time the storage space of the container should not decrease. A clip-on power supply is satisfactory in

continental transport as can be seen from the current use of clip-on diesel gensets. Its dimensions are limited by the space available between the driver's cabin and the reefer.

In some circumstances the total weight of the reefer plus payload can be limiting its use. For instance in some countries the reefers are not allowed at inland roads because of their high weight. It must be emphasised that the payload is currently 85% of the total maximum weight of the reefer. Lowering the weight of the box and cooling equipment will probably benefit the energy efficiency of the reefer, but it will not solve the problem of inland accessibility.

Sustainability
Sustainability was the original requirement for the CEET2005 reefer. This idea was abandoned in April 2000 since the prospects for the application of renewable energy were estimated to be low [CEET2000-5].

Energy supply systems for reefer containers
In the following sections potential energy supply systems will be discussed. In the first section conventional power supply systems are briefly discussed to be able to compare them with new systems discussed later on. In the last section some other cooling concepts that could also reduce the energy use of the reefer container are shown.

Conventional power supply systems

Diesel genset
During over-land transport or a longer storage period a diesel genset is currently used to supply power to the container (see). The genset is not built in, but can be attached to the upper front of the reefer container (Carrier and Maersk) or under the chassis of the truck for permanent usage (Maersk). A tank with 390 l (8 days) or 490 l (10 days) (Carrier) or 150 (36 hours) or 455 l (5 days) diesel is taken along (Maersk)[3]. Since power is available as long as there is fuel, the genset is a semi stand-alone power supply.
This system has several drawbacks. First of all it is unreliable because the motor gets contaminated with exhaust gases. This results in high maintenance costs. Overall costs were estimated to be 0.54 $/kWh[4].

Electricity
On the ship electricity is readily available at low costs, since the fuel price for fuelling the ship's diesel generators is low. This system is not stand-alone. On the ship a limited amount of connection points is available, on new ships this is about 700[5]. This makes up for 10-20% (for respectively 20 or 40ft boxes) of the total amount of containers transported on such a ship. The overall costs of energy for a reefer on the ship are 0.032 $/kWh[6].

New energy supply systems
The new energy supply systems investigated are photo voltaic cells, fuel cells, electric buffer, thermal buffer, bio-diesel genset, H_2/LPG/NG and an absorption heat pump.

Photo-voltaic cells
Photo-voltaic cells (PV) on top of the container could – in theory - provide endless energy. In this respect PV provides true stand-alone power. The main advantage of solar energy is that it is a fully renewable energy source. Per kWh 0.37 kg of CO_2 emission is avoided. However, the efficiency of PV is still low (10-15%) and the investment costs are high.

[3] personal communication R.de Mul (Carrier) and Mearskweb
[4] including: investment cost of a Carrier genset, fuel and maintenance.
[5] On the P&O Nedlloyd Kobe (build in1998) 700 reefers can be powered [Ponlweb]
[6] confidential information from P&O Nedlloyd (P.Eekel)

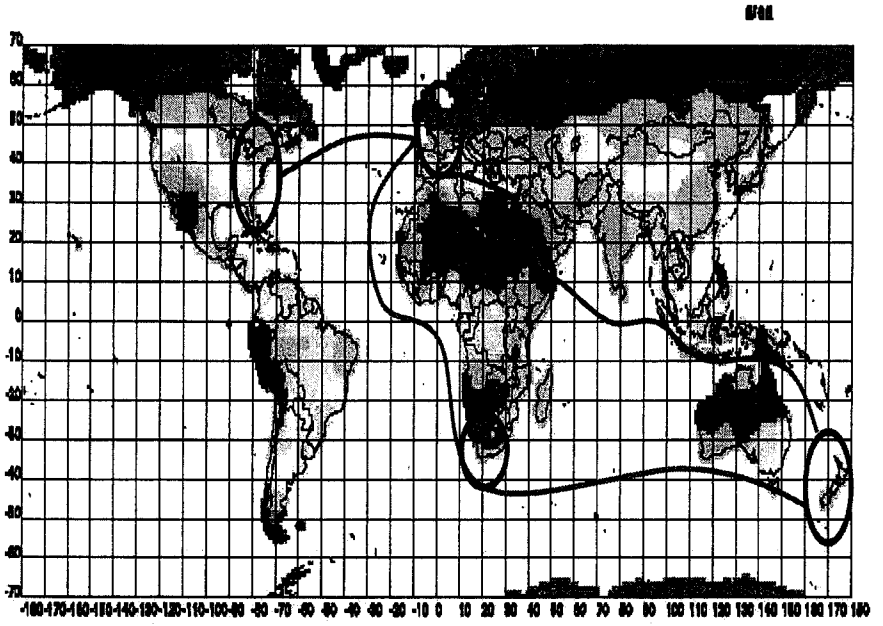

Figure 3 Annual irradiation chart of the world with selected routes: Apples from New Zealand or South Africa to Holland and bell pepper from The Netherlands to the United States

When thinking of global transport applications it should be considered that the energy, which can be supplied by the sun, is not constant over the world, because the sun's irradiation is not the same everywhere. This is depicted in Figure 3. The energy demanded by the container is also not constant over the world, because the outside temperature varies. In Figure 4 the energy demanded by the current reefer (see 0) is compared to the energy which can be supplied with PV at several locations. The calculation was performed with an PV area of 30 m^2 (completely covering the roof of the container) and an efficiency of 10%. It is clear from this figure that even at locations with a lot of sun (South Africa) the energy supplied by PV does not come near to the current energy demand. Even for the CEET2005 reefer PV can only supply a factor 2 less energy than the demand.
At a fixed location (harbour, distribution centre) solar cells (on the roof of a building for instance) could always make a contribution to the energy supply.

Another important drawback for the use of solar cells is their fragility and handling of containers on ships and in the harbour is very rough on the containers outer construction. This can probably be overcome by applying hard coatings for this application.

It should also be born in mind that on ships and in the harbour the containers are stacked 6 high on the ship's deck. This would mean that only the top containers could be covered with PV. If PV could supply the container with stand-alone energy it is feasible that all reefers would be placed at the top position. This is however difficult for logistic reasons. In that case a ship could carry ~450 stand-alone 40ft HC reefers, compared to 700 nowadays[7].

Costs for PV are dominated by investment costs of both PV and batteries, since maintenance is low and there are no fuel costs. The electricity price from a PV covered container roof is calculated without taking into account installation costs or frame costs. Since the energy demand is much higher than the supply, buffering is not useful. In this case energy from a PV covered container roof would cost 0.63 $/kWh. When half of the maximum day yield is stored in a battery (lead-acid battery), the price would be ~0.84 $/kWh.

[7] This is only possible when inspection of inside climate would not involve the physical presence of the engineer.

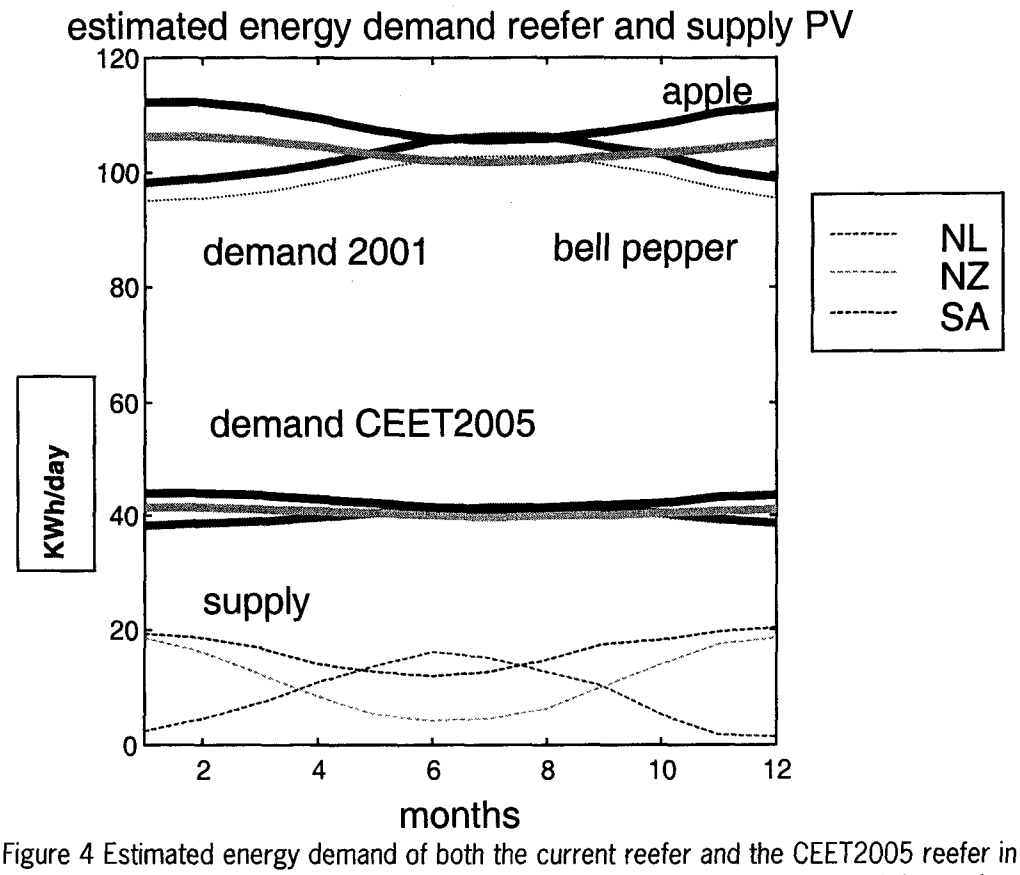

Figure 4 Estimated energy demand of both the current reefer and the CEET2005 reefer in several climates (bold line) and energy supply of solar panels mounted on the top of the reefer (dashed line) during the year. Bell pepper is kept at a temperature of 10°C and apples at 4°C.

Both because of the lack in energy supply and their fragility PV can not be applied on top of reefer containers for intermodal use. When containers are stationary, PV can contribute to the energy supply when not integrated with the container.

Fuel cell

The fuel cell is an electrochemical device in which a fuel and an oxidant reacts directly to produce electricity. Apart from being very efficient, fuel cells have the advantage of being silent and non-polluting. The waste product is the burnt fuel. Normally the fuel is hydrogen and as a consequence, the product is water. CO_2 may be present as well, if a hydrocarbon - such as methanol or gasoline - is used. The operating temperature of all fuel cells is too low to produce NO_x. Since a fuel is required for operating the fuel cell, this is a semi stand-alone power supply.

At the moment a lot of research is done for the development of fuel cells for automotive and stationary applications [Padro, 1999]. For cars 50-100 kW Proton Exchange Membrane (PEM) type of fuel cells are developed by several fuel cell developers in collaboration with the car industry. Other types of fuel cells are still in an earlier phase of research than the PEM type. Either methanol or gasoline in combination with a reformer will fuel the fuel cells. Fuel cell powered cars are expected to enter the US market around 2003-2005 and the European market around 2005-2010[8].

For stationary applications PEM fuel cells from 1 kW to 2 MW are developed. These fuel cells could enter the market some years earlier (2001-2003)[9]. Up till now demonstration projects showed that

[8] The US market will be the first, due to the Californian legislation on zero-emission vehicles, which will be enforced in 2003. Personal communications R.Mallant,ECN and Snieder, Shell Hydrogen.

[9] Fuel cell developer Plug Power expects to introduce a 7kW fuel cell for stationary applications in 2003 [PlugPowerweb]

the technique is reliable [Padro, 1999]. The dimensions of a PEM stack are around 1 kW/l or kg [ECNweb].

Costs of the fuel cells are expected to drop as soon as larger numbers can be produced, but it is difficult to predict to which level exactly. Plug Power expects to be able to introduce a 7 kW fuel cell for stationary applications for $4000,- in 2003, with an overall power cost of 0.07-0.10 $/kWh when running on methanol [PlugPowerweb]. Maintenance costs are expected to be much lower than for instance diesel gensets, since fuel cells have no moving parts. The costs of fuels are discussed in 0.

For application of fuel cells in the CEET2005 reefer container we need to look at the developments for both the stationary and automotive applications. The first for low power fuel cells, and the second for its robustness. In view of this, application in a container is promising for its efficiency, reliability and low emission of pollutants. However, the development of the technique is expected not before 2003-2005.

Electrical buffer
A battery is an electrochemical device to store energy. Batteries are used to provide backup energy or store the energy generated at a time when demand is lower than the supply, as is often the case with for instance PV. Since the buffer needs refilling this is a semi stand-alone energy supply system. There are several different battery types. The most commonly used is the lead-acid battery, followed by the Ni-Cd battery, but the last one is much more expensive per kWh. A relatively new battery type is the Ni-MeH (Nickel-Metal Hydride) battery, which has the advantage that it has no heavy metals components. In general it can be said that batteries are heavy and expensive. One kWh from a battery weighs 15 – 27 kg (for lead-acid or Ni-MeH battery) and has a volume of 15 or 5.5 l. The costs of a kWh for these batteries are $ 85,- or 200,- . [Burges, 1996]

Alternative fuels for internal combustion engines
Different fuels can fuel internal combustion engines. Normally the engine is only suited for one type of fuel. Some engines can be fuelled by different fuels at the same time, as for instance a LPG/gasoline engine in a car. Some of these fuels have less impact on the environment than diesel. In the next sections alternative fuels will be discussed.

Bio-diesel
Bio-diesel is a fuel produced from vegetable oil. Bio-diesel can be used directly in an existing, unmodified diesel engine. Because it has similar properties to petroleum diesel fuel, bio-diesel can be blended in any ratio with petroleum diesel fuel [IEA, 1994]. The main advantage of bio-diesel is that emission reductions can be considerable compared to the use of diesel fuel. Especially there is no SO_2 emission. NO_x emissions are about the same or higher [Handboek, IEA 1994].

Sources for producing bio-diesel are for instance rapeseed (rapeseed oil methyl ester, or RME), soybean, sunflower, or waste vegetable oil. The availability of the fuel depends heavily on the country, for instance in Germany about 1000 petrol stations supply bio-diesel [Handboek].
The price of bio-diesel depends on the country due to different taxes, subsidies and costs of the feedstock (import or own production). For instance in the USA fuel costs are estimated to be $0.50-0.66/l higher than for diesel [IEA, 1994], and in Germany bio-diesel is $0.10/l cheaper than diesel, because there is no oil tax on bio-diesel for consumers [March, 2000 Biodeweb]. Efficiency of the engine when running on bio-diesel is 1% lower then when running on diesel [Jager, 1998]. Bio-diesel is already used in bus fleets all over Europe with good results regarding efficiency and maintenance [Ademe, 1999]

LNG/CNG/LPG
Liquid Natural Gas (LNG) or Compressed Natural Gas (CNG) are the liquefied or compressed gaseous state of methane which can be produced from underground gas reserves. The use of LNG or CNG requires some modification to a normal internal combustion engine as well as a strong fuel tank. The availability of LNG and CNG depends on the country. For instance in Argentina, GOS, Italy and New Zealand a lot of gasoline fuelling stations are equipped for CNG

fuelling. LNG is much less available due to the high costs of low temperature storage. The advantage of using LNG or CNG is its lower emission of greenhouse gasses. The CO_2 emission is 20% less compared to gasoline. The larger amount of space needed for the storage tanks can be a problem in the case of CNG [Handboek]. The energy density of pressurized natural gas (200 bar) is 20% of that of diesel. That of LNG is 66%. Investment costs of LNG and CNG are high, but fuel price is low.

Liquefied Petroleum Gas (LPG) is a by-product of petroleum refining or natural gas processing and consists mainly of propane. A normal gasoline engine can run on LPG without large modifications to the engine. The CO_2 emission is comparable to gasoline.

Ethanol
Ethanol can be used in internal combustion engine or as fuel additive to gasoline. In the first case the engine needs to be adapted to ethanol use. Ethanol can be produced from corn or sugar beet. As with all bio-fuels the CO_2 emission from burning is equal to the amount of CO_2 taken up by the crop. However, during production of the fuel some CO_2 is produced. Emission of NO_x is about 50% less compared to diesel and there is no SO_2 emission. [Handboek]

In the USA and Brazil ethanol plays a relatively large role as an alternative fuel for cars. Brazil has had a large ethanol program since the 1970s[10]. In both cases stimulation of the agricultural sector via subsidies played a mayor role in the programs [SER, 1993]. The availability of ethanol outside Brazil and the USA is low. The costs of fuel depend on the taxes and subsidies given in a specific country for the production of corn or sugar beet. Both the techniques of production and use in engines are well developed.

Methanol
Methanol can be used in internal combustion engine, as fuel additive to gasoline, or as a fuel for fuel cells. In the first case the engine needs to be adapted to methanol use. Currently, methanol is made in large quantities from natural gas as feed stock for the chemical industry. Its CO_2 emission during burning is comparable to that of gasoline, but there is no SO_2 emission [Handboek]. The CO_2 emission during production depends on the production process used, but in the case of steam reforming it can be somewhat lower than gasoline production. In the future methanol may be produced from bio-mass, making it a renewable motor fuel. In that case the CO_2 emission from burning is equal to the amount of CO_2 taken up by the crop. Methanol as a fuel for internal combustion engines is a proven technique, which has been tested in a lot of field experiments in the USA, Germany, China and New Zealand [Handboek]. Methanol can also be reformed to a gas, which can be used in a diesel motor or fuel cell. As was discussed in 0 the fuel cell has a much higher efficiency than an internal combustion engine. This technique is still under development. Methanol can be produced with the same costs as gasoline. Investment costs are comparable to diesel engines when an internal combustion engine is used, but much higher for use with fuel cells. The availability of methanol as a fuel is low.

H_2
Internal combustion engines can also be fuelled by H_2 instead of gasoline or diesel. The engine needs to be adapted to this fuel. Fuelling with H_2 would have several advantages over diesel fuel. First of all there would be no SO_2 and NO_x emission. Secondly, this engine would have lower maintenance costs since exhaust gases do not pollute the engine. The technique is already available in demonstration projects of busses and cars[11]. The investment costs are a factor 1.1 higher than a normal combustion engine [Stromen 14-04-2000]. H_2 can also be used to fuel a fuel cell. In both cases storage of H_2 is a problem which has to be solved. As can be seen in the appendix the energy density per unit volume of H_2 is much less compared to other fuels, therefore it has to be stored under high pressure, at low temperatures or in special storage materials. Most of these techniques are not fully developed yet [Padro,1999]. The availability of H_2 is not good at moment, but this could be much better in 10 years time due to the development of the fuel cell car (see 0). The total CO_2 emission depends on the way of production. The cheapest way is to produce

[10] 24% of the cars ran on a mixture of ethanol and gasoline in 1985
[11] Nuon bus developed together with Hydrogen Systems; and BMW cars.

H_2 from fossil fuels. To have zero CO_2 emission electrolysis could be used, but this is much more expensive [Padro, 1999].

Gas turbine
On the ship or in the harbour, the energy of several containers together could also be supplied by a small gas turbine. For instance on a container ship with 700 containers a power of 700 x 3-5 kW = 2.1 – 3.5 MW is probably required for the CEET2005 containers. One or two OPRA gas turbines of 1.5 MW each could provide this power. The advantage over a diesel engine is that the OPRA gas turbine is smaller (2.2 x 1 x 1.6 m) and 10 times lighter. The efficiency is however lower, 26 – 37% depending on if a recuperation cycle is used. This last model is still under development.

Energy density of pressurised natural gas (200 bar) is 20% of that of diesel, that of LNG is 66%, so more space is needed for the fuel.
The advantage of using gas over diesel was already discussed in 0 and lies in lower NOx and CO emissions.

Absorption heat pump
An absorption heat pump can be used as a cooling machine. It converts heat of a certain temperature to heat of a lower temperature. Instead of a mechanical compressor an absorption medium is used. The supply heat can be waste heat from exhaust gasses or an engine. It is not an energy supply system as such, but a complete cooling machine. Since it can only function when heat from the outside is available, this system is not a stand-alone system.

The replacement of a compressor cooling unit with an absorption cooling unit could lead to an energy reduction of 75% [Schiphouwer, 1997]. In comparison with a compressor refrigerator other advantages of an absorption refrigerator are that it produces no noise or vibrations and needs less maintenance [Schiphouwer, 1997]. A huge disadvantage is that when no heat is available an energy buffer is necessary. This could be done with an additional heater working on diesel, but this works with low efficiency. Besides the cooling unit itself, also the other elements of the unit (ventilators for air circulation, heaters for defrosting etc.) need energy. The waste heat cannot supply this and therefore an additional energy source is necessary.
Other disadvantages are that the technology is not used for transport cooling yet and that compatibility with different modalities is difficult since the energy supply would be integrated with the truck or ship. For each modality a separate heat supply system should be designed. In a ship this would mean that all reefers should be placed next to the engine, or the diesel generators for heat supply to prevent heat transmission losses.
Costs of the system are difficult to estimate since integration of an absorption heat pump refrigerator in the transport sector is not a standard technology.

Energy saving options in cooling units hardware
To further reduce energy consumption the hardware of the cooling unit is investigated. From the measurements on the test reefer by ATO it became clear that the high power consumption is caused by the compressor, the heater and the evaporator fans. The following power reduction options considered are targeted to tackle these problem components:

Heat recovery after condenser
The installation dehumidifies the container air by compressing and cooling the air so vapour can be removed. An electrically powered resistance heater re-heats the air to obtain the desired temperature in the container. A modification to this configuration would be to use the heat of the condenser to reheat the air (see Figure 5). This can be done by placing a heat exchanger in the outside airflow that cools the condenser. This could reduce the power needed to cool the condenser and reduce the power consumed by the heater.

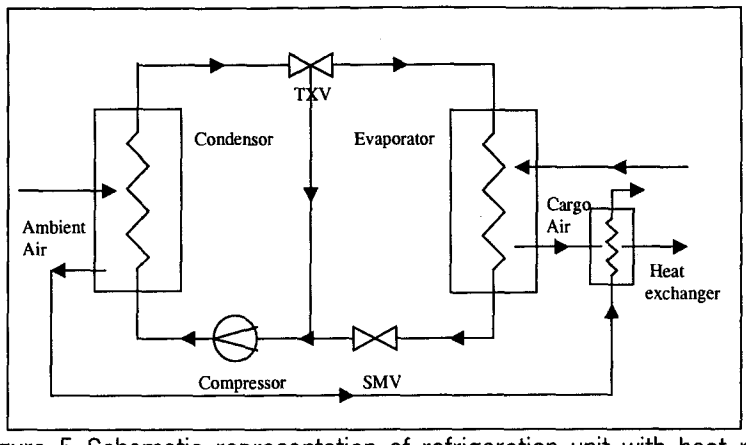

Figure 5 Schematic representation of refrigeration unit with heat recovery (TXV = thermostatic expansion valve, SMV = suction modulation valve)

Dehumidification with desiccant wheel

Dehumidification could also be done by means of a desiccant wheel (see Figure 6). This could make the heater redundant and also reduce the demand for cooling. The temperature increase caused by the compressor would reduce the demand for heating the air before it is supplied to the filter. Possibly the heater would be redundant too. Warm air from the main condenser fan can be used to dry the desiccant wheel.

At ATO there is an EU project called DRY COMFORT that investigates possibilities to use membrane technology in desiccant dehumidification for stationary and mobile applications in food storage. There could be possibilities to work together in a later stadium of the project, when more is known about the applicability of membranes.

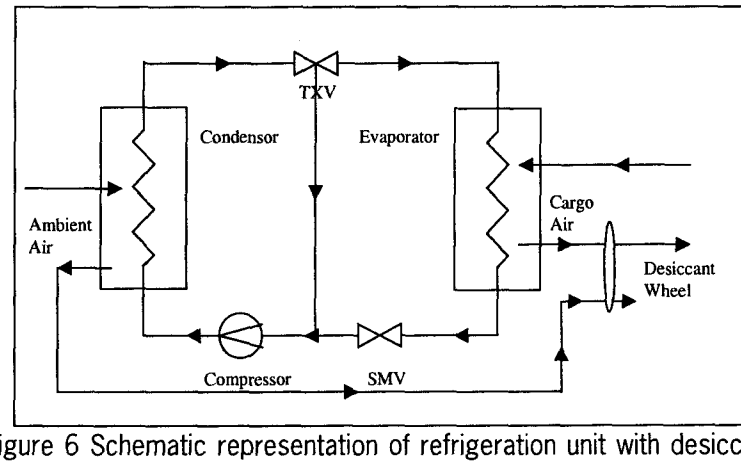

Figure 6 Schematic representation of refrigeration unit with desiccant wheel (TXV = thermostatic expansion valve, SMV = suction modulation valve)

Air recycling

In the right (cold) climate, the outside air can be used to condition the container. This air can be mixed with container air directly, or its cold can be used to cool the container via a heat exchanger (see Figure 7). In order to do this, outside temperature and humidity need to be monitored. This is not envisioned in the current configuration of the system, but it would be an option in which a considerable amount of energy can be saved. From simulations with air recycling in the Dutch climate it was concluded that energy reduction of 5-10% is feasible.

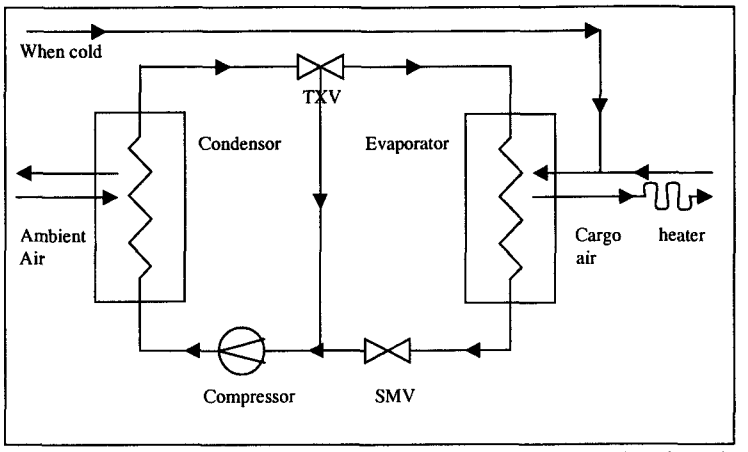

Figure 7 Schematic representation of refrigeration unit with air recycling (TXV = thermostatic expansion valve, SMV = suction modulation valve)

Conclusions on energy supply

Current CA-containers and container infrastructure are highly optimised to meet actual market demands. Developing an energy supply system that is more efficient, more reliable or based on renewable sources is therefore challenging. In the previous section several energy supply systems where discussed. In order to be able to compare these systems, the criteria given in 0 are applied to several systems in Table 2. To give an indication of the prospect of the technology for this project also a criterion 'availability of the technology' is included.

Table 2 Criteria applied to energy systems. ++: suitable/cheap, - -: unsuitable/expensive, 0: not applicable, ?: unknown

	Diesel genset	Electricity (ship)	PV	Fuel Cells	Electric buffer	Bio-diesel genset	H2/LPG/NG	Absorption heat pump
Power	++	++	< 2.2 kW	++	-	++	++	+
Autonomy	+/-	- -	++	+/-	+	+/-	+/-	-
Availability (fuel source)	+	ship ++	+	-/+	++	some regions -	Some regions -/+	transport ++
Reliability	+	++	++	?	++	+	+	+
Sustainability	-	-	+	-/+	-/+	+	-/+	+
Investment cost	-	++	- -	-	- -	-	-	- -
Maintenance cost	-	++	++	+	+	-	-	?
Fuel cost	+	++	0	-/+	0	+	-/+	+
Built-in	-	- -	-	+	+	-	-	++
Availability technology	++	++	++	- - >2005	++	+	-/++	-

From this table it can be seen that when the criterion of 'power' is applied, PV, electrical buffers and absorption heat pumps should be dropped. The alternative fuels that remain interesting - bio-diesel, H_2, LPG and NG - have the serious drawback that they are only available in some regions. Fuels cells are highly interesting, but the technology is not developed far enough to be incorporated in a reefer container in 2005. From the cost perspective it seems that the conventional electricity on the ship is cheapest option. The conventional genset for over land transport is not necessarily the cheapest option - especially the maintenance costs are high - however other options have other major drawbacks that are not solved within the coming 2-5 years.

From the survey it can be concluded that in the case of marine transport, efforts to improve the efficiency can turn out favourable, but will not take effect on the containers installation. Transportation on trains or trucks involves a per-container energy supply, which offers possibilities for photo voltaic cells, fuel cells or absorption heat pumps. However all of them have serious drawbacks. There is no alternative energy supply system available within 2-5 years that meets all criteria for the total cold chain.

Relationship with ecological and technological aims

The aim of this part of the project 'The agro-container concept of the 21st century' was to develop a reefer container concept that reduces the environmental pressure of climate controlled agro-transport by means of energy reduction in the energy supply system and integration of sustainable energy sources in stand-alone containers.

In this report several supply systems where investigated and compared to the conventional systems. Most promising systems where photo voltaic cells, fuel cells, bio-diesel or absorption heat pumps. From an environmental point of view photo voltaic cells are the most interesting system. Since the energy is sustainable and no CO_2-emmisions are generated. However, with the energy demand currently achievable for the CEET2005 container only about half of the energy demand can be supplied with a roof full of photo voltaic cells. An alternative could be to use bio-diesel on routes where there can be sufficient supply of bio-diesel. The potential in the near future lies in these dedicated routes. Fuel cells also offer perspective since they are ~50% more efficient as a diesel engine. Depending on the fuel used to power the fuel cell – H_2 or gasoline - even more CO_2-reduction can be achieved. However this scenario is only feasible after 2010.

From the research on energy reduction options it can be concluded that there are still possibilities in the hardware of the cooling unit to reduce the energy demand of the container. When these are applied further reduction in the order of 5-10% seems achievable.

It can be concluded that for the near future (before 2005) no emission reduction can be expected from the application of alternative supply systems for a sea container. However, there are possibilities to be investigated in continental transport, and dedicated transport. These are discussed in chapter 0.

Conclusions

'The agro-container concept of the 21st century' is an extensive project aiming at the development of a reefer container concept that reduces the environmental pressure of climate controlled agro-transport. This is achieved by means of energy reduction and integration of sustainable energy sources in stand-alone containers. In this report alternative energy supply systems are discussed. The energy supply systems investigated are diesel gensets, electricity, photo voltaic cells, fuel cells, electric buffer, thermal buffer, bio-diesel genset, H_2/LPG/NG and an absorption heat pump. The main criteria the system should meet are: deliver enough power, be autonomous, have an available – over whole world - fuel source, be sustainable and compatible with intermodality of the reefer containers.

Current containers and container infrastructure are highly optimised to meet actual market demands. Developing an energy supply system that is more efficient, more reliable or based on renewable sources is therefore challenging. During sea transport, containers will usually be supplied with electricity from the ship. Efforts to improve the efficiency or apply renewable sources can turn out favourable, but will not take effect on the containers installation. On the ship there is no cost-effective alternative for use of diesel generators available now.

Transportation on trains or trucks usually involves a per-container energy supply. This offers possibilities to apply renewable, cleaner or more efficient sources, such as:

- photo-voltaic cells on the roof of the container: with the current energy demand achieved for the CEET2005 container it does not generate enough power. Photo-voltaic cells are also too fragile for handling the containers in the harbour. It could be an option to put cells on the roof of the distribution centre.
- fuel cells: cost-effective, small cells are not available yet, but after 2010 it is an applicable technology which has the potential to reduce the energy demand of containers with another 50%.
- the use of bio-diesel in conventional gensets: could be interesting depending on the location (fuel should be available at any point in the cold chain).
- absorption heat pump: still too fragile for transport application and the heat source is only available when the vehicle is driving.

It can be concluded that compatibility with the intermodality of the reefer containers is the most important problem. Beside that techniques as the fuel cell, the absorption heat pump or bio-diesel are not developed into a cost-effective alternative yet. There is no alternative energy supply system available within 2-5 years that meets all criteria for the total cold chain.

Scope for further research and development

It is shown in this report that sustainable or more efficient alternative energy supply systems, such as photo voltaic cells, fuel cells, bio-diesel or absorption heat pumps all have their drawbacks compared to the conventional systems. Not one of them can be integrated in the total cold chain within 2-5 years. This does not mean that no alternative for parts of the cold chain can be developed. Especially transportation on trains or trucks involves a per-container energy supply, which offers more possibilities for photo voltaic cells, fuel cells or absorption heat pumps than transport on ships. Still, research should be done to improve the now available techniques. Also dedicated transport from one place to the other gives more opportunities for especially for bio-diesel because the supply problem is more easily to handle when only one rout has to by supplied.

Summarised, the recommended research is to investigate the feasibility of the implementation of the techniques developed in this project in combination with:

- photo-voltaic cells for continental transport and distribution centres
- bio-diesel for dedicated routes
- fuel cells for continental transport
- absorption heat pumps for continental transport

References

Ademe, Non technical barriers to the development of liquid biofuels in Europe; phase 3, march 1999.
Biodeweb: www.uni-muenster.de/Energie/bio/markt/bioindex.html
Burges, K., K.J. Hoekstra, A. Kil, T.C.J van der Weiden, F. Wouters, Handboek accu's in PV-systemen – deel 1, Ecofys, E243, 1996.
Burges, K., R. Zischke, G. Loois, and T.C.J. van der Weiden, Market Potential and introduction of hybrid stand-alone power supply in Europe, Ecofys, 1999.
Carrier Transicold, Operation and service manual container refrigeration unit model 69NT40-489 with Everfresh controlled atmosphere, Syracuse, 1998.
CEET2005-1: The agro-container concept of the 21st century, research work plan, March 25 1998.
CEET2005-2: CEET2005; Management report of the period of 1-10-98 to 1-4-99.
CEET2005-3: CEET2005; Half-year report 1-4-1999 to 1-10-1999
CEET2005-4: CEET2005; Appendix half-year report of CEET2005
CEET2005-5: CEET2005; minutes of meeting 3-4-2000

CEET2005-6: CEET2005; Management report june 2000.
CEET2005-7: CEET2005; Half-year report December 2000
CEET2005-8: CEET2005; Management report October 2000 - April 2001
ECNweb: www.ecn.nl/fossil/spfcsys/
Handboek energie en milieu, Dossier: Energiegegevens, Samson Bedrijfsinformatie, Alphen aan den Rijn / Zaventhem.
IEA, Biofuels, 1994.
Jager, de, D. and A.P.C.Faaij and W.P. Troelstra, Kosten–effectiviteit van transport brandstoffen uit biomassa, Utrecht, Novem 1998.
Kok, J.P.B., Reefer-containers in maritieme ketens, Wageningen, maart 2000.
Mearskweb: www.mearsksealand.dk/mearsksealand
Padró, C.E.G. and V. Putsche, Survey of the economics of hydrogen technologies, NREL/TP-570-27079, NREL, Golden (Colorodo), 1999.
PlugPowerweb www.plugpower.com
Ponlweb: www.ponl.com
Schiphouwer, H. and R.J.M. van Gerwen and H. van der Stoel and M.J.E. Verschoor, Technische haalbaarheidsstudie energiezuinige transportkoelunits, TNO-MEP, Apeldoorn, 1997.
Uytendaal, A. High cube reefers versus traditional reefer boxes, Reefer conference 29-9-1999, London.
Welby, E.M., McGregor, B, Agricultural Export Transportation Handbook, USDA, 1997 (http://www.ams.usda.gov/tmd/export/index.htm)

APPENDIX: Comparison of energy densities of fuels and buffers

	Gravimetric (kg/kWh)	Volumetric (l/kWh)
FUEL[12]		
Diesel	0.086	0.10
Bio-diesel		
H_2	0.03 gas at 300 bar 0.03 liquid 1.7 in MeH[13]	1.33 0.42 0.31
Ethanol		0.17
Methanol		0.23
BUFFER		
Electrical buffer[14]	15 Pb-S 27 Ni-MeH	15 5.5

[12] Fuel: without tank
[13] MeH: metal hydirde with 2 wt% H_2 stored
[14] [Burges 1996]

Task 4 Development of slow-release systems for green chemicals

Introduction

From an agro-industrial point of view, plants are a very obvious source natural antimicrobial and are known to contain antimicrobial or medicinal metabolites. In many instances, these compounds play a role in the natural resistance or defense against microbial or other diseases. A wealth of literature exists describing their favourable properties and identifying the active components. In general, herbs and spices and several of their active ingredients have been Generally Recognised As Safe (GRAS), either because of their traditional use without any documented detrimental impact or because of dedicated toxicological studies. Their application in postharvest crop protection may be facilitated by this feature although appropriate toxicological evaluations cannot be passed-by in any legislation.

The aim of task 4 is to implement the use of green chemicals in the climate control system of the container. In principle this is an energy efficient means of preventing deterioration of the perishable product, since the requirements for temperature and humidity control can become less strict.

Results

Selection of products, postharvest pathogens and volatile plant oils

In the phase of this tasks, green chemicals derived from plant sources have been selected for post-harvest protection of container stored apples, tomatoes and chicory. The post-harvest pathogens which are most commonly associated with the selected products are *Pseudomonas marginalis*, *Botrytis cinerea*, *Penicillium expansum*, *Alternaria alternata*, and *Rhizopus stolonifer*.

On basis of an extensive literature screening and experience, 8 volatile plant oils with antimicrobial activity were selected (Table 1). The selection criteria applied were the following:

- **Reported antimicrobial activity;**
- Presence in the selected products;
- Reported safe use as flavour (GRAS-status);
- Delivery via gasphase possible;
- Obtainable in large quantities.

Table 1. The selected volatile plant oils and their presence in chicory, tomato, and apple

Volatile plant oil	Present in		
	Chicory	Tomato	Apple
Carvacrol	+	+	
Thymol	+		
Trans-2-hexenal	+	+	+
Decanal			+
Hexyl acetate			+
Ethyl hexanoate			+
Geraniol			+
Trans-2-pentenal		+	+

In vitro screening of volatile plant oils for antimicrobial activity
In the second phase of this task, the screening programme including 8 volatile plant oils was completed for *Botrytis cinerea*, *Rhizopus stolonifer* and *Penicillium expansum*. We investigated the inhibition of germination of conidia and the delay in linear growth of the mycelial mat at different doses of the selected compounds. Decanal and trans-2-hexenal were found to be the most potent antifungal agents towards *B. cinerea* and *P. expansum*. Trans-2-hexenal was also the most active inhibitor of *R. stolonifer*. However, the latter fungus was relatively insensitive towards decanal. Microscopic analysis revealed that *R. stolonifer* forms special survival structures in response to exposure to decanal. Trans-2-hexenal was selected for further research.

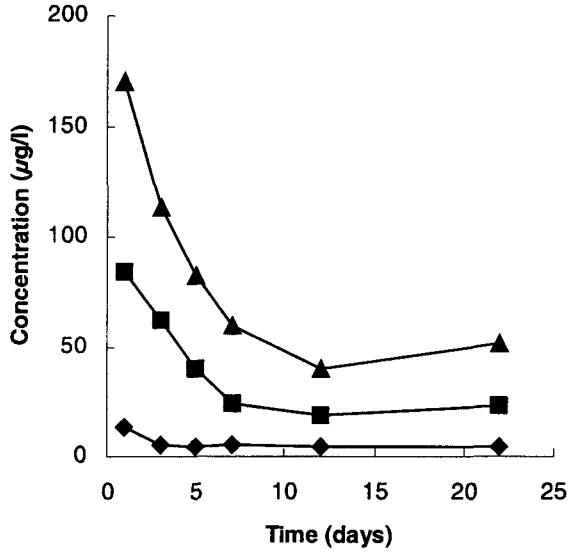

Fig. 1. Concentration profiles of trans-2-hexenal during in vitro studies.

Development of a test system for continuous administration of volatile plant oils
In the *in vitro* system the headspace concentration of the oils was varied by varying the amount of oil added to the petridishes but the actual headspace concentrations were not determined. In the reporting period the corresponding headspace concentrations of three dosages of trans-2-hexenal in similar petridishes were analysed by gaschromatography. Headspace concentrations were linearly proportional to the volumes added and decreased in time according to first order kinetics (Fig. 1). Since no organisms were present, this decrease must be caused by chemical oxidation or leakage. As a consequence, *in vitro* efficacy could only be related to a broad concentration range.

For evaluation of *in situ* efficacy and phytotoxicity a test system was required in which the headspace concentration could be kept constant. Also, this system would have to allow combined application of volatile plant oils with conventional modified gas atmospheres. A system was developed in which a constant headspace concentration was obtained by passing gas of the desired composition in a washing bottle over trans-2-hexenal into a stainless steel container (Fig. 2). Lower concentrations were achieved by changing the flow over the oil and by dilution with a second inlet flow into the container.

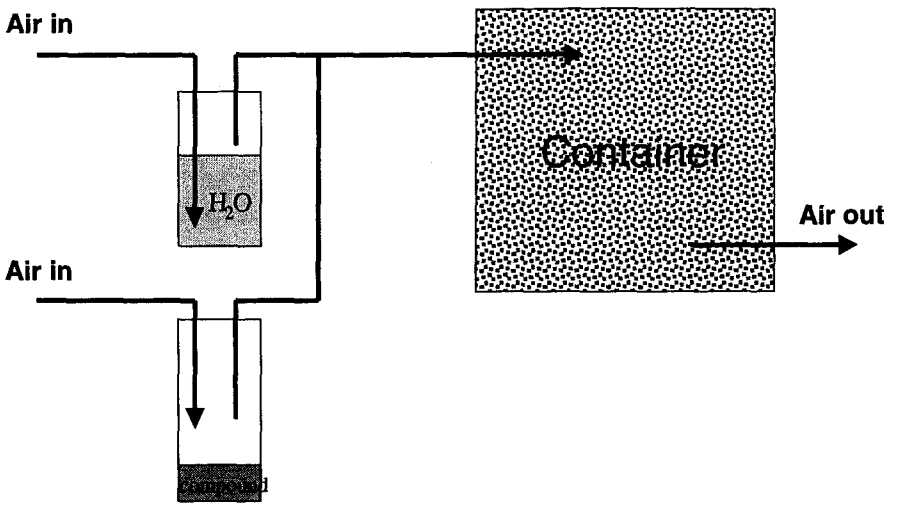

Fig 2. Test system for continuous administration of a constant head space concentration of volatile plant oils.

Potential causes of the variation of the headspace concentration of trans-2-hexenal and the gradual decrease of the steady state concentration of trans-2-hexenal that were observed initially have been identified and adaptations have been introduced to minimize variation:
Temperature variation of the liquid trans-2-hexenal (which affects the evaporation and hence the concentration in the container) has been minimized by insulated the washing bottle by a water jacket.

The procedure for taking gas samples for analyzing the concentration of the plant volatiles and the gaschromatographical analysis have been reviewed, adapted and protocolized. These adaptations have resulted in a decrease of the analytical variance.

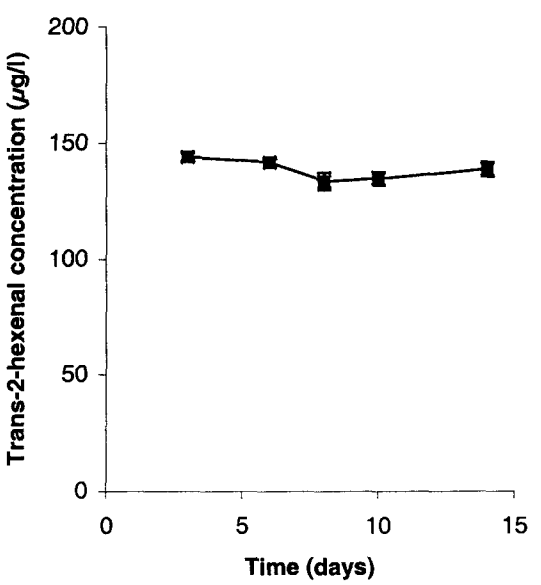

Fig. 3. With the newly developed test system, constant headspace concentration of volatile plant oils are achieved.

The gradual decrease of the trans-2-hexenal headspace concentration has been eliminated by replacing the airflow through the washing bottle by nitrogen (Fig 3).

Application of volatile plant oils for postharvest protection of apples against fungal decay

Using the developed system, the effect of three concentrations of trans-2-hexenal on apples was studied at 5°C which is well above the regular storage temperature (0 – 1°C). At all concentrations, a considerable part of the trans-2-hexenal (50-90%) was metabolized by the apples. No fungal development nor product damage occurred during storage. However, when the apples were subsequently stored at 18°C, damage was observed of apples that had been exposed to the highest concentration. Since no fungal development was observed on control apples, no conclusions can be made about the antifungal efficacy. When apples were artificially infected with *Penicillium expansum* spores, development of this fungus was observed irrespective of the presence of trans-2-hexenal. It should be noted that these apples had been severely infected.

In a second storage experiment, which was conducted as described previously (2 weeks storage at 5°C, followed by 7 days exposure to ambient conditions at 18°C), the procedure for damaging and infecting the apples (in this case with *Penicillium expansum*) was refined and recorded in a protocol. Storage in the presence of trans-2-hexenal decreased the number of infected apples by up to 70% (Fig. 4A) and decreased the rate of *Penicillium* development by up to 60% (Fig. 4B). Typically, these effects were not visible immediately after storage but became evident in the week after. The applied concentration of trans-2-hexenal (140 µg/L) did not induce damage of the product.

A cost estimation of the use of trans-2-hexenal has been made. In the experiment described above, the costs of trans-2-hexenal were 0.11 €/m^3/day.

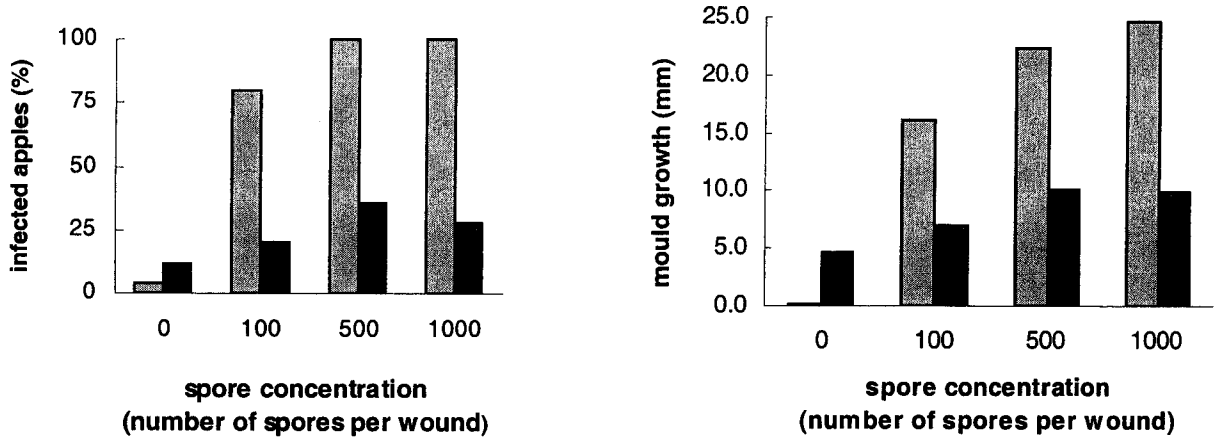

Fig 4. Development of *Penicillium expansum* on apples after storage in the presence of trans-2-hexenal. A, effect on the number of infected apples; B, effect on the radial growth of *P. expansum* on apples.

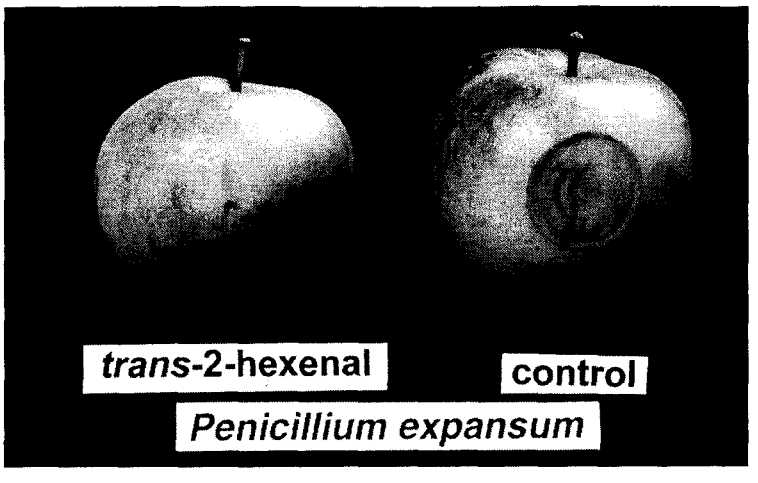

Fig. 5. Effect of the presence of trans-2-hexenal during storage on development of *Penicillium expansum* on apples.

Conclusion

A system has been developed for the postharvest storage of fresh products under a constant overflow of volatile plant oils. With trans-2-hexenal as an example, it has been shown that a concentration range can be identified where the oil suppresses fungal development on apples without causing damage to the apples. Since the storage experiments were conducted at 5°C while apples are normally stored at 0 – 1°C, this technology could lead to a reduction of energy required for cooling of the container during transport. This technology may also be used in other sectors where fungal decay of fresh products results in significant product losses.

Scope for further research

In this research, one variety of apple has been studied and the apples were mechanically damaged and artificially infected with spores of *Penicillium expansum*. In future research, the efficacy of trans-2-hexenal as natural antifungal agent should be confirmed with other apple varieties, apples of various ages, apples infected with spores of other postharvest pathogenic fungi, and with uninoculated apples. Also other products and volatile plant oils should be considered.

Task 5 Monitoring the surrounding environment and the product respons

Aim

The objective of task 5 within CEET 2005 is to develop sensors that can monitor product traits and the product environment such that these measurements provide the required information to be able to control product quality. The sensors to be developed should detect warning signals of product deterioration, due to excessive respiratory activity, ripening, or attacks by pests and pathogens. Such signals can subsequently be used to control the product environment and thus prevent further quality loss.

Work carried out

To be able to decide on the nature of the sensors to be developed within the project, we have made an inventory of the current knowledge on product quality, quality deterioration and maintenance of product quality, and on the available technology to monitor the product and its environment. In order to measure product quality and product environment under container circumstances, the utilised sensors must be tested for sensitivity, durability, reliability, robustness, low energy consumption and must be low-cost. Further boundaries for the sensors to be used in a container system developed are set by the fact that direct measurements on products in a container are hard to realise, as products in a container are packed in boxes and a container should be able to function stand-alone. Thus, the implementation of sensors that need to be in contact with or close to the product is physically limited. In contrast, measurements of the volatiles in the air surrounding the product in a container seem much more attractive and feasible.

The types of sensors that we have investigated in the course of the project are firstly a particulates detector to detect the presence of fungal spores. Secondly, the use of a volatile detection system to measure signs of product deterioration, such as anaerobiosis, ripening or damage due to pathogens has been investigated. Secondly, the use of a particulates detector has been investigated. In addition, the product environment needs to be monitored to ensure the proper conditions for maintenance of product quality. Therefore, we have chosen to develop a combined CO_2/O_2 sensor, since manipulations of the CO_2 and O_2 concentration in the air are an important means of controlling product respiration and ripening.

Results

Particulates Detector
Detectors for airborne particles are commercially available, so no specific development of this kind of sensor will take place until their usefulness has been demonstrated in a model container containing decomposing, sporulating products. If commercial sensors prove effective at detecting fungal infections of products by means of their released spores, we will proceed with tests and development of this sensor system

Volatiles
For the measurement of volatiles in the product environment we have investigated the use of an array of gas sensors. In common terminology such an array is denoted as an electronic nose, in short e-nose.

The aim of the conducted research was twofold, namely to:
(1) gather insight in the volatiles profile (flavour and off-flavour) emitted by the most important model product, i.e., apples and
(2) determine the best candidate among the currently commercially available e-noses.

These aims have been achieved through an extensive search in the scientific literature and the internet. It turns out that the most promising e-noses have become available during the last year.

Volatiles profile

It is well known that ethylene is the volatile that supplies most information on the stadium of ripeness, hence ethylene is the selected target analyte. The current research has focused on testing a promising e-nose, the so-called zNose (EEV Chemical Sensor Systems, 1077 Business Center Circle, Newbury Park, CA 91320, USA; http://www.estcal.com), with respect to its capability of detecting sufficiently small differences of level of the target analyte (low ppm range). Other e-noses were not considered because they did not meet requirements such as sufficient stability and robustness or limited size (hand-held). Headspace samples were collected from apples, which is an important model product. One sample contains apple aroma only. Three samples were taken of apple aroma spiked with various levels of ethylene. Finally, a reference sample was prepared that contained ethylene only (in N_2). These samples were send to EEV Chemical Sensor Systems for analysis.

Analysis using the zNose yields the following results:

1. the spiked samples yield different results for the interferents, which implies that the zNose is not sufficiently quantitative for the current application,
2. the number of detected components depends on subsequent data analysis,
3. ethylene could not be detected.

Candidates for prototype e-nose

An overview of commercially available e-noses is given in Table 1. The 'best' instruments (especially in terms of stability) are based on existing analytical instrumentation, i.e., GC (zNose) and MS (HP 4440A and Smart Nose-300). Their applicability is limited here because of size restrictions (as well as price). The most promising e-noses are both hand-held sized. One is based on conducting polymers (Cyranose 320), while the other works with metal oxyde semiconductors (KAMINA). The manufacturers claim a high stability as well as reproducibility between sensors. These claims need to be tested. It is likely that software must be developed to handle drift.

Table 1. Overview of commercially available electronic noses

Manufacturer	Product	Technology
WMA Airsense Analysentechnik GmbH	PEN	10×MOS
Alpha M.O.S.	FOX 2/3/4/5000	6/12/18/24×MOS, CP, QCM
Bloodhound Sensors Ltd.	BH114	14×CP, DLC
Cyrano Sciences Inc.	Cyranose 320	32×CP
Element Ltd.	FreshSense	MOS
Environics Industry Oy	MGD-1	Imcell™ (IMS)
Electronic Sensor Technology	zNose	GC-SAW
Forschungszentrum Karlsruhe	KAMINA	40×MOS
	SAGAS	8×SAW+1 reference
HKR Sensorsysteme GmbH	QMB6/HS40XL	QCM, MS
	HS40/MS	QCM, MS
Hewlett Packard	HP 4440A	MS
Lennartz Electronic	MOSES II	8×QCM, 8×MOS, calorimetric, electrochemical

EEV Chemical Sensor Systems	e-Nose 5000	CP, MOS, QCM
Microsensor Systems, Inc.	Vaporlab	SAW
Motech Sensorik, Netzwerke und Consulting GmbH	VOCmeter	QCM, MOS, electrochemical
Nordic Sensor Technologies AB	NST 3210/20/20A	MOSFET, MOS
Osmetech plc	Multisampler-SP (A32S)	32×CP
	Core sensor module	48×CP
Daimler Chrysler Aerospace RST Rostock	Sam	QCM, SAW, MOS
Smart Nose	Smart Nose-300	MS

CP = conductive polymer, DLC = discotic liquid crystal, GC = gas chromatography, MS = mass spectrometry, IMS = ion mobility spectrometry, MOS = metal oxide semiconductor, FET = field effective transistor, QCM = quartz crystal microbalance, SAW = surface acoustic wave.

O_2 and CO_2

For fruit and vegetable storage conditions under controlled atmosphere, a reliable and sensitive oxygen sensor is needed to accurately measure oxygen at concentrations of around one percent (v/v). Most existing sensor designs are expensive or require regular maintenance, calibration or replacement. The principle of fluorescence and luminescence quenching of some dyes by molecular oxygen has been known for many years, but low-cost, stable and accurate commercial sensors are not available. We have developed a sensor, based on luminescence lifetime measurements, that uses low-cost, off-the-shelf components.

Prototype 1: O2 sensor

In the first prototype the dye used was a palladium porphyrin with a very long luminescence half-life. The dye was custom synthesized and thus expensive, but with one gram of the dye is sufficient for thousands of sensors. The total cost for materials per sensor is estimated to be around $100. The innovative aspects of this development are the construction of the sensing layer and the method of measuring the half-life, so that the sensor output without the addition of linearization circuitry is nearly a perfectly linear function of O_2 concentration. The luminescence lifetime measurement is based on a so-called 'Phase Locked Loop' (PLL), which is a common circuit in high frequency electronics. This circuit comprises a voltage controlled oscillator (VCO), a

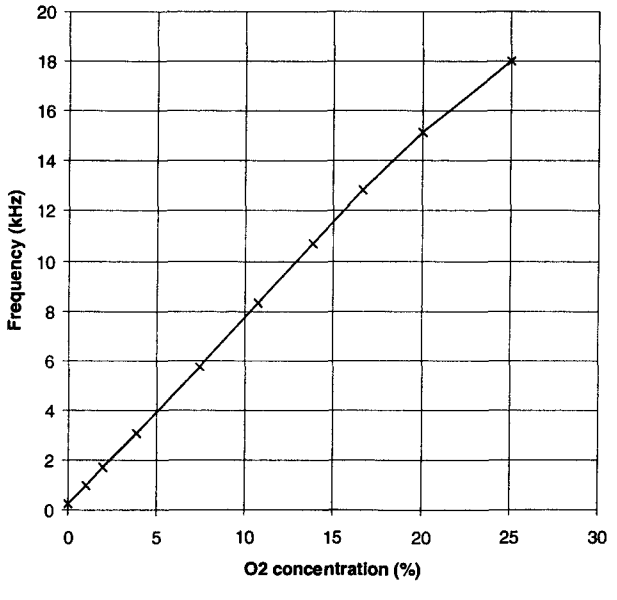

phase comparator and an integrator. A blue light source, used to generate the luminescent state in the dye, is driven from the output of the VCO and, and the red luminescent signal from the dye is amplified and input to the phase comparator. The circuit forms a loop that maintains a constant phase shift between these signals, by varying the frequency. Changes in the O_2 concentration produce changes in the lifetime of the luminescent state and thus the frequency output of the phase-locked –loop.

The first prototype sensor was capable of measuring at normal air conditions with 21% oxygen, while maintaining excellent sensitivity and accuracy at low oxygen levels. Because the intensity of the luminescence signal decreases with increasing oxygen concentration because of quenching, the measurement is most accurate and stable at low O_2 concentrations.
The effect of changing the humidity of the air being measured was very small, about one percent of the signal output from dry to saturated air. There was a bigger effect of changing temperature on the response of the sensor; a one percent signal change is produced per degree Celsius, but this can be compensated for by simultaneous temperature measurement. As the sensor measures oxygen partial pressure, an atmospheric pressure dependent correction must be applied to get a volume percent O_2 value (if this is required). For this, a small monolithic absolute pressure sensor is included in the design. All compensation and linearization will be done by a simple microprocessor system included in the sensor housing.

For the oxygen sensor a circuit board was developed with an integrated optical detection system. Signal processing software has been integrated for linearization and temperature and air pressure correction. Tests have shown that sensitivity and accuracy of the device is good, but the stability of the sensing layer needs to be improved.

Prototype 2: Integrated O2 and CO2 sensor
For the oxygen and CO_2 sensor development, we joined forces with a small external company specialised in analytical chemistry. They already developed a prototype carbon dioxide sensor and are helping us now to solve the stability problems with our oxygen sensor. We agreed to bundle our products into one cheap device for measuring both oxygen and carbon dioxide. To stabilise the chemical probe for oxygen detection we already made some improvement by encapsulating the dye in another polymer.

Prototype 3: Improved O2 sensor
For stabilising the optical oxygen sensor, we have looked look for and screened other, more stable probes. Besides that we can optimise the measurement system to reduce average light exposure of the probe and therefore extend sensor lifetime. First, we tried to stabilise the oxygen-sensitive dye we were using in the oxygen sensor. As stabilisation was not satisfactory, we have decided to use another dye. This dye poses other requirements on the optical and electronic parts of the sensor. We are currently working on re-designing the sensor to make it suitable for use with the new dye.

Relationship with ecological and technological aims of the project

We are working towards a commercial sensor product for simultaneous oxygen and carbon dioxide measurements. This sensor consumes a tiny amount of power. An accurate measurement of climate and product status allows for larger variations in climate regulation, which saves on energy for the cooling system. Besides that, proper climate control during storage and transport minimises the risk of product loss.

The oxygen sensor is a good alternative for the accurate but heavy, fragile and expensive paramagnetic oxygen analysers. Competing technologies deploying the same photochemical effect for oxygen detection, use remote fiberoptic sensing and are more complex and much more expensive. The combination of both O_2 and CO_2 sensors in one cheap device is a major advantage compared to using separate sensors.

The sensor knowledge and experience gained by the CEET project greatly accelerated other sensor developments in our institute. For example, we have developed a prototype ethanol sensor with a detection limit of 50ppb for use in fruit storage, controlled by the ATO patented DCS system. This system regulates the oxygen concentration by measuring the ethanol production of the fruit. The system is designed to increase storage time and preserve fruit quality.

Conclusions

The currently commercially available e-nose systems seem not to be suitable for the measurement of important volatiles in the product atmosphere in a container. However, technological developments in this area is progressing at a high rate. It seems feasible that in future cheaper sensors with a higher specificity, stability and reproducibility become available.

With the combined O_2 and CO_2 sensor developed within this project accurate measurement of O_2 and CO_2 seems possible. The device offers a good alternative for the currently available equipment. Further work is needed on the stability of the O_2 sensor.

Scope for further research and development

There seems to be plenty of scope to develop product monitoring during transport or storage further. In order to avoid unnecessary climate conditioning and energy use, input from sensors giving information about product status seems very useful.

Measurements that should be investigated further are firstly the measurement of ethanol and ethylene. These compounds give important information about unwanted ripening of the product. ATO has recently developed an ethanol sensor for use in commercial fruit storage. First tests have shown that with modifications this sensor may also be suitable for the measurement of ethylene.

Other measurements that should be investigated further are the (two- or three- dimensional) measurement of temperature in the container, the monitoring of water loss by the product and the measurement of condensation on the product. Technological advances in these areas are fast and implicate that further development of these techniques for application during storage or transport seems feasible.

Task 6 Chain optimisation and marketing opportunities

Introduction

This document describes the activities and results of the period April 2001 – December 2001 of task 6 of the CEET2005 project. During this period both the maritime market research part as the continental market research part were finished. A short summary of the final results of the market analysis are given below, followed by a view on the scope for further research and development.

Aim of the task

The aim of task 6 is to determine the potential market and set the logistics and commercial boundaries for the new agro-container. Task 6 is divided into a maritime/intercontinental and continental part, as supply chains differ significantly.

Results of last phase

The results of this phase of task 6 are:

- completion of the maritime part of the market and logistics analysis including conclusions about feasibility of new reefer concept and commercial plan for implementation of new concept
- completion of the continental part.

The overall results of the study are written down in a report comprising the maritime part of the market analysis and a separate report comprising the continental part of the market analysis. These reports comprise the headlines of the complete market analysis and will be available both at ATO as project coordinator and P&ONedlloyd Erasmus University / ERBS bv as responsible for task 6. The conclusions of both reports cover all findings and are summarized below.

Conclusions maritime part

Starting point for study

The focus of the market research is put on the European import flows of fresh produce from the Southern Hemisphere. Main reasons are:

- Dutch export function for fresh produce is declining because of stronger positions of South Europe, North Africa and South America
- Dutch export of fresh produce is not a significant market segment for maritime reefer carriers.
- For maritime reefer carriers European import flows of fresh produce from the Southern Hemisphere are relevant.

Capabilities of new reefer container

Benefits of the potential capabilities of the new reefer container can be divided into benefits for the market and benefits for the policy makers (see table**). In order to prove viable both market actors and policy makers should benefit from the innovations.**

Capabilities	Benefits for market actors	Benefits for policy makers
Energy reduction	Logistics costs savings	Pressure on world energy consumption Economic strengthening of agro-logistics sector
Improved product maintenance	Reduction in loss Shift air to sea Extension of import/export markets Higher product value	Economic strengthening of agro-logistics sector
Intermodal use	Reduction in damage loss (uninterrupted cold chain) Alternative for road transport	Reduction in road transport
Monitoring	Increased market flexibility	Increased traceability

Supply chain analysis

To get an insight in the dimensions of the benefits for the different market actors that are involved with a reefer container, a supply chain analysis is needed. Results of the supply chain analysis are:

- For various product – trade – period combinations different supply chain configurations exists.
- Order processes within a particular supply chain can be complex processes, with different actors having different interests.
- Power in the supply chains of fresh produce is increasingly with the supermarket organisations.
- Supermarket organisations focuses both on quality control as on cost control.
- Importers have changed their role and position in the supply chain under influence of the retailers' taking control over the supply chains.
- Container carriers are logistics actors in the supply chain and have a corporate focus on volume (scale) and cost minimisation. This corporate focus does not completely match the requirements related with the specific reefer segment.
- Supermarket organisations will probably outsource supply chain activities to one dedicated partner combining product knowledge, logistics knowledge, trading capabilities, IT knowledge. This partner, probably a partnership between actual actors in the supply chains, will translate market requirements into transport requirements:
  - quality is no point of discussion: there is no willingness to pay for additional quality by supermarket organisations
  - cost control is very important
  - year round supply and availability of variety is important.

Requirements for capabilities of new reefer container

- Energy savings have proven to be the most interesting improvements. The most promising strategy for container carriers for the coming years is to break further into the conventional reefer market with standard equipment with a volume and cost driven mind.
- There is no real requirement for the improvement of product quality, for which the actors are willing to pay the additional costs. Supermarkets would force the other actors in the supply chain to absorb additional costs, as quality is not seen as an additional service but as a standard.
- Diminishing the level of damage and loss by improving the product maintenance function of the reefer machine is not very much an issue as only a fraction of claims (not more than 10%) is related with the working of the reefer machine.
- Analysis has shown that there is certainly an interest with European exporters of products that are transported by air in the actual situation for a shift from air to sea. For a container

carrier this would only mean a small volume, for which high investment risks in specific equipment should be made.
- Thorough analysis of the position and strategy of a container carrier in the reefer market has shown that as long as the reefer segment is integrated in the corporate strategy of the container carrier, which aims at cost minimisation and volume maximisation, focus should not be put on development of a variety of special equipment for small market niches[15].
- At the moment and also within the time horizon of five years, intermodal modalities are not offering a viable alternative to climate controlled road transport. Both on the demand side as on the supply side things should be changed to make a match eventually possible.
- Additional requirements that the market imposes for a new to develop reefer container are:
  - on-line monitoring
  - relative humidity control.

Quantitative results

(The figures calculated here are by no means validated results of the study project, but give indication about potential results under certain assumptions!!!).

- Based on a rough calculation with assumptions about fuel needed per energy use, fuel price, amount of trips per year, the operation of one CEET2005 container on the stretch between Europe and New Zealand could result in a cost saving of $60 per trip and $240 a year.
- At the moment there is no real information about investment costs for the new technology and assumption is that no additional maintenance and repair costs will arise.
- Based on a lifetime of a reefer container of 10 years a present value of the cost savings of $1850 can be counted, based on which the investment decision can be based.
- The total energy and fuel savings a year by complete implementation of the new technology on the stretch between New Zealand and Europe for apples, is respectively 8.65 million kW and 1.6 million kg.

Remark: Container carriers operate in alliances. This means that containers of one carrier are many times transported by the vessel of another carrier. Energy savings will therefore not automatically benefit the investor in the energy saving technology.

Commercial plan

- For successful introduction of a new product, this product must offer an acceptable technology, an acceptable profit and an acceptable financial risk.
- Five attributes that affect the rate of adoption of a new technology are:
  - Relative advantage: for the new reefer technology this will be perceived as positive for energy reductions, resulting in reduced logistics costs, and a shift form air to sea whereby market expansion is expected.
  - Compatibility: the way of thinking about product maintenance during transport changes with the new technology. Together with the relative conservative character of shippers in the industry, this leads to barriers for the acceptance of the new technology.
  - Complexity: complexity of the new reefer technology should not be the bottleneck for introduction.
  - Trialability: the new technology is not easy to try out: investments must be done, the market actors should be informed about the development and time effort is needed to smoothen the introduction and operation of the new technology.
  - Observability: the new technology should be implemented on a particular trade, for a particular product, for a particular client and on a particular vessel to be able to observe the positive and negative results of the new technology. This does not suit

[15] We would advice a container carrier to separate its reefer segment from the dry cargo segment within the organisation. This allows a better service towards the market and a higher flexibility in adapting the organisation and activities towards supply chain requirements. However as this implies radical changes in organisational structure which will not be executed within a short time frame, our starting-point is the integrated situation

the structure and working of the container carriers that use their equipment in a flexible way on their networks.

- The ownership question should be related to the complexity and level of speciality of the new reefer container:
  - As long as the main technological improvement is energy use reduction, whereby the complexity of the container is not changed very much, the container carrier should be the investor in the new technology.
  - As soon as additional features are considered that make the performance of the container more specific, co-operation with the shipper should be considered, either in the form of a joined investment, either in the form of firmed long term contracts for use of the specific equipment.
- Two target market segments can be identified: The first and seemingly most potential target market is the market for which energy saving would be main benefit. This is the market of standard fruit types that are transported in large volumes from the Southern Hemisphere to Europe: apples, pears, grapes and citrus. On the longer run the logistics for this market will be dictated from the import region, either by the retail organisations, or by their dedicated logistics partners. The second target market is the market of fresh produce that with the actual technology cannot be transported by sea. Improved product maintenance capabilities of the new technology should make this possible. This target market comprises the more delicate products like exotics and vegetables. There are two potential markets to be captured:
  - Fresh produce that at the moment is transported by air to and from Europe.
  - Fresh produce that is consumed in Europe, that at the moment is sourced in Europe, but that is available (can be produced) in overseas countries.
- Implementation of the new reefer technology will certainly be faced with reluctance. To help customers adopt the new technology the following rules for client approach should be taken into account:
  - Identifying and filling a small market need with the new product before entering the market of the dominant technology. This means selection of a particular product – trade – period combination, for example apples from New Zealand to Europe in a pre-season period
  - Involvement of well-established firms in the use of the product. We propose a player like Enza, which is the export board for apples from New Zealand.
  - Providing information to users. Users must be convinced of the working of the new technology, that it doesn't harm the products transported and that there are benefits.
  - Offering training to users. In case the new technology requires new handling procedures, training should be given to the operational personnel of the operating company.
  - Consider small but significant modifications that increase the perceived compatibility with previous practice. For this technology, this means that the new way of handling the reefer machine should not deviate very much from the old way.
  - Offering pricing and financing options that share investment risk, of user risk. User risk is with the maintenance of product quality. Financial options could be offered to compensate shippers in case anything happens to product quality.
  - Bundling of the new hardware product with a supporting service product. The market analysis has shown that monitoring product conditions is an issue for the market actors. The new technology provides possibilities to build in a monitoring function for the shippers. This could be the service product that is offered to the first adopters of the new technology.

Conclusions continental part

Starting point for the study

The EET study focuses on the design of a new (container) unit that improves the actual technology available for the transport of fresh products. However, the performance of the multimodal alternative is merely determined by the performance of the modality itself (responsiveness, transit

time, costs, etc.) rather than by the performance of the loading unit. An integral approach is required, where both the modality itself as the loading unit are considered. Key aspect for the analysis of the market potential for a multimodal logistic concept for fresh products, is to find a match between the transport requirements, as imposed by commercial actors, and the performance of a multimodal logistics concept using a newly developed loading unit.

Competitive position intermodal transport
One should expect that with increasing congestion and increasing costs for road transport on one hand and continuous attention for development of a sustainable European transport system on the other hand, intermodal transport for fresh products could be feasible. However, almost all individual initiatives that were analysed in this study have not proven to be successful. And in general the competitive position of intermodal transport has weakened over recent years, mainly caused by performance not reaching requirements. This has resulted in a significant decrease of continental perishable cargo transported by shortsea vessel, inland barge or train.

Expectation is that for the next five years intermodal transport will not be a competitive alternative for the transport of fresh product and that no real potential exists for the development of a continental intermodal unit for the transport of fresh products:

- the intermodal modalities (rail, barge short sea shipping) will not meet transport requirements as imposed by market actors:
  - high responsiveness and flexibility;
  - reliable product maintenance;
  - acceptable and reliable transit time;
  - acceptable costs.
- although performance of road transport is declining due to congestion and increase in costs - mainly caused by internalization of external costs-, the competitive position of road transport will remain firm for this specific market segment the coming decade. Reason for this is that in particular for the main transport requirements that are imposed by market actors in the fresh product market road transport scores highest.
- Only on very specific trade routes intermodal transport for fresh products can be a competitive alternative. Development of such trades/routes is very much depending on the initiatives of individual companies.

Potential for development of innovative reefer unit
As long as the intermodal modalities do not meet logistical requirements as imposed by market actors in the fresh product segment. development of an innovative reefer unit is not viable. Such a technological development will not solve logistical mismatch that in the actual situation exists between transport requirements and performance of intermodal transport.
Technological requirements that could be met by development of a new loading unit for continental intermodal transport are:

- reliable product maintenance, by self-sustaining reefer machine
- reliable product maintenance by monitoring and remote control possibilities
- RDC-order fitting combinations of small parcel sizes possible by developments of compartments in loading unit

Scope for further research and development

Continuation of the project into real market implementation is only viable if both market actors and policy makers will have a benefit. If only market actors will benefit, financial involvement of the policy makers is not needed. If only policy makers will benefit, market incentives will not be present and market implementation will not be viable.

Maritime reefer container
Only if test results are positive and significant energy savings can be realised, while guaranteeing product quality, continuation of the project could be viable. A pilot project based on the starting

points as described in the commercial plan of the market analysis (task 6) should be started. Main arguments for a pilot project are:

- initial investments risks should be shared both by private as policy making actors
- market acceptance should be tested
- innovation should be adapted based on registered results of pilot project

Crucial for the set up of a pilot project is the participation of the market actors (P&ONedlloyd, Carrier Transicold, Greenery) in the pilot project.

Continental reefer container

Market analysis has shown that development of a continental reefer unit is not viable (at least for the next five years). Result of the analysis is that for the coming five to ten years road transport will remain the main mode of transport for fresh products. Application of the technology as developed by ATO to the road transport sector in order to gain energy savings in road transport of fresh products should be considered.

Both technological as market and logistical research is needed in order to come to market implementation.

Evaluation parameters

Results of Task 6 give more insight in the parameters 'economy' and 'ecology' as defined by EET.

Task 7 Development of integrated dynamic control strategies

Introduction

In the CEET 2005 project Supervisory Optimizing Control algorithms (SOC-system) will be developed. These algorithms take product dynamics into account in the optimization of a specific transport. This additional layer will improve the transport of agro-material by conditions to guarantee optimal quality against lowest possible cost.

The current control system of the container receives setpoints not from a SOC-system but directly from the user. In current operation the setpoints are determined only once in the beginning of the transport and often are not even optimal for purposes of transport, but for storage of agro-materials. The additional layer that will be developed in this project will improve the transport of agro-material by conditions to guarantee optimal quality against lowest possible cost. The system is illustrated in Figure 1.

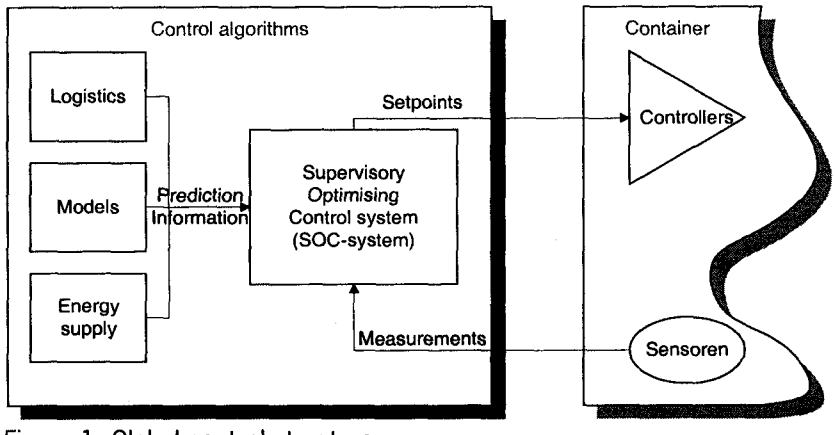

Figure 1: Global control structure

The SOC-system uses:
- monitoring information about product quality and product behaviour (Task 1, 4 and 5),
- information on energy supplies (Task 3),
- information about the trajectory of the container (Task 6).

The information is used to determine the optimal container settings. The main difference between the existing and the new structure is the direct use of product, logistic and energy information in determining the optimal setpoints for the hardware controllers. The existing hardware controllers try to reach and maintain these setpoints in the container.

Aim

The aim of Task 7 of the project is the "Development of a model-based Product Quality Control algorithm for container transport of agro-material".
As specified in the report of April 2000 as configuration 2, the supervisory controller uses:
- fixed setpoints for climate parameters and product activity (e.g. respiration, humidity loss, heat production)
- on-line interactive climate control by optimizing between energy use and product activity
- no fixed tolerances (R = f(T,RH,O2,CO2))
- an estimation filter that estimates from CO2 and/or O2 measurements the actual product activity,

The development of integrated dynamic control strategies is performed with the objective in mind that energy consumption is reduced with 50 % as compared to the current practice of refrigeration

at full air speed. The control unit will try to reduce energy use on climate control (eg. less ventilation, less cooling) without increasing product activity dramatically. This is realized by on-line measuring product activity and controlling climate conditions.

Results

Essential for Task 7 in the entire project was the co-operation with the other tasks in the project as will be mentioned in one of the next sections.
First the theoretical and technical results of Task 7 will be discussed followed by the meaning these results have and may have on container transport of agro-material.
The theoretical and technical results of Task 7 can be outlined according to the following steps in the design of an integrated dynamic control strategy to improving process control:

1. the formulation of the control objective,
2. building the necessary models,
3. selection of the control structure,
4. design of the selected controllers,
5. validation of the control system and
6. implementation of the controller.

Summarising the results for each step:

1. Estabilishing relation between climate conditions and product quality (firmness) together with the relation between climate condition and energy consumption of the climate unit,
2. Necessary models for the different components of the entire container such as product, micro-climate, macro-climate, cool-unit are established and discussed in the corresponding sections of this report. Furthermore, models for measurement and estimation of product response to changes in climate settings have been established. This involves the mechanisms of respiration and fermentation that take place inside the product.
3. A control structure is selected that captures the main characteristics of the transport operation on the different time scales. Details are discussed in the corresponding sections of this report.
4. A new local control algorithm has been design, implemented and tested on a full-scale container. This local control algorithm cycles the refrigeration unit to fit the energy consumption to the actual requirements by the product. A non-linear climate controller has been designed and is being tested in simulation studies. An estimation filter has been designed to estimate product response to changes in climate conditions.
5. The control system is being validated for each control component separately. The estimation filter has been validated performing small-scale and medium-scale experiments with apples.
6. The new local control algorithm is being implemented. Results with this new local control algorithm are discussed in the corresponding sections of this report. The estimation filter is being implemented on a medium scale.

From these results it may be concluded that with the use of the predictive capacities of the different model components it is possible to determine the most accurate and optimal settings for the container transport of agro-material. This means that energy consumption is largely reduced as it is directed towards the actual needs of the product. Through the measurement and estimation of product response it will be possible not only to monitor, but also to control the product and its quality directly.

Deliverables

- The aim is to deliver a Supervisory Optimal Controller that consists of three different levels of control each operation at their own characteristic time scale.
  - On the slow time scale the algorithm will optimize the CA/refrigerator setpoint trajectories. This optimization will take into account both product quality preservation and energy consumption.
  - On the intermediate time scale a non-linear MPC-algorithm will be utilised correcting the desired trajectories calculated on the slow time scale.

- With the new cycling local control algorithms that operate on the fast time scale the (refrigeration) unit is controlled more efficiently, thereby largely reducing energy consumption.
- An estimation filter will be delivered that estimates product responses to changes in climate settings have been established. This involves the mechanisms of respiration and fermentation that take place inside the product.

Resources

The resources used in this task are:
- Modelling and control software (Matlab)
- Experimental facilities such as climate rooms, a full-scale container (P&O Nedlloyd), a refrigeration unit (Carrier Transicold), product (The Greenery)
- Measurement facilities
- Communication software (Labview)

Requirements from / interactions with other tasks

The SOC will be the part that performs the overall optimization. Therefore it combines inputs from all other tasks, but especially with.
Task 1: integration of product behaviour/dynamics in the control components,
Task 2 and 3: use of extended models for simulation studies and simplified control models includinding climate and energy models,
Task 6: use of logistic information.

Evaluation parameters

Economy
The SOC-algorithm will allow for better product quality preservation, by improved control of the climatic conditions *around the product*. Control of climatic conditions *around the product* comes natural in the SOC-algorithm by computation of setpoints for supply air on the basis of measurements in both supply and return air, and possibly in the cargo-hold's headspace. An effect is that more mature harvesting becomes possible, which will allow higher yields for farmers and improved flavor for consumers.

Putting the algorithm to the market can be quick, as it just concerns a piece of software. Parts of the SOC-algorithm will be applicable to any refrigerated storage facility. The developed methodology is ready to explore opportunities for such transfer.

First impression is that more efficient operation of the CA/refrigerating-units will result in significant energy savings, by just exploiting favorable ambient conditions. The experimental results discussed in the chapter about the Full-scale container experiment in this report, show a 50-60 % reduction, as compared to full power refrigeration, in energy consumption using the new cyling control algorithms on the fast time scale (local controllers).

Ecology
As may be concluded from the experimental results more efficient operation of the CA/refrigerating-units will result in significant energy savings, by just exploiting favorable ambient conditions directly fullfilling the needs of the products, but not more.

Technology
On the slow time scale the intended SOC-algorithm will use weather-forecasts (and when not available weather averages), an estimate of the remaining duration of the trip and shelf-file, market-prices of the transported product. To feed this information to the container requires communication of the container's microprocessor with the outside world. This communication is technically feasible, but not available in current reefer transport.

As energy consumption is largely reduced (up to 50-60 %) new hardware components may be developed that operate more efficiently at these new operating points. Furthermore, as cycling of the refrigeration unit largely contributes to the realised reduction in energy consumption this cycling behaviour should be taken into consideration in the design of these new hardware components.

Time schedule

In the oncoming half-year the nonlinear control algorithms will be further developed and transferred to enable real-time testing. Special attention will be drawn at the identification of mass flows of air inside the container and the upscaling of the on-line measurement/estimation procedure of the level of respiration by the product. Furthermore, product models developed and adapted using the results of Task 1, need to be incorporated at the corresponding locations in the control components.

Below a time schedule is shown that could be achieved and fullfills all requirements of the project:
Table 7.1: Time schedule of task 7

Subtask	Finished
Upscaling respiration procedure (incl. Different products)	April 2002
Installing additional equipment for the experiment	February 2002
Integrating product models (including an approach for different products)	April 2002
Finish simulation studies control nonaffine algorithms	February 2002
Perform experiment	March 2001
Development first approach to long-term control component	June 2002

Appendix 1: Details on the research

On-line estimation of respiration and fermentation rates

Introduction

Respiration and fermentation rates primarily depend on product commodity, ripeness, temperature and gas conditions. On-line monitoring of respiration/fermentation rates in CA-storage facilities can be used for

- Monitoring the product state
- Control of respiration/fermentation rates (ripening)
- Detection of anaerobic conditions

The development of a (recursive) estimator for respiration/fermentation that does not require any specific experimental conditions is presented. This estimator is expected to be suitable for usage in full-scale storage/transport facilities.

Respiration and fermentation

Respiration and fermentation is the amount of sugars consumed in respectively abundance and absence of oxygen. The reactions are given by:

$$C_6H_{12}O_6 + 6O_2 \xrightarrow{r_{O2}/6} 6CO_2 + 6H_2O + E_r$$

$$C_6H_{12}O_6 \xrightarrow{r_f/2} 2CO_2 + 2C_2H_3OH + E_f$$

The amount of oxygen available gives, depending on the product, the rate at which both reactions take place (see figure 1). The metabolism for respiration and fermentation can be described by Michaelis Menten kinetics.

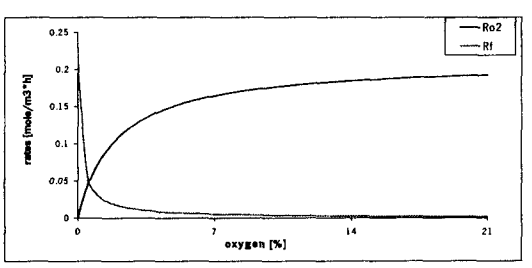

Figure 1: Respiration and fermentation rate in relation to the amount of oxygen concentration (Peppelenbos, 1996)

On-line estimation

On-line estimation of respiration and fermentation rate is possible from the gas balances. The total amount of oxygen consumed gives the amount of respiration and from the ratio between O_2 and CO_2 the amount of fermentation can be calculated, given the amount of respiration. A major problem for application in practice is the unknown amount of leakage of the store/container. Due to this unknown leakage errors occur in the estimated respiration/fermentation rates, regardless which estimation procedure is used.

Mathematical Simulations

A model is accomplished for the estimation of respiration and fermentation rate using a Kalman Filter (KF), example given for fermentation rate. The knowledge about the (Michaelis Menten) respiration and fermentation kinetics were introduced in the model, resulting in a good correlation between calculated and model based values of the respiration and fermentation rates (see figure 2).

$$\hat{r_f}(t+1) = r_{f\max} * \frac{k_f}{k_f + n_{O2}(t)}$$ KF Michaelis Menten

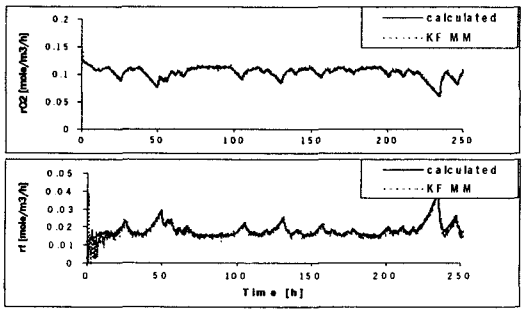

Figure 2 Model based respiration and fermentation rates compared to calculated respiration and fermentation rates

Conclusions and future research

1. The rates of respiration and fermentation estimated from the O2 and CO2-balances converge to their true values (in absence of leakage).
2. An x% error in estimated dilution rate of the CA-store will result in a x% error in the estimates of both respiration and fermentation rate, but no error in estimated respiration quotient.

In the near future the (im)-possibilities of the estimation method will be investigated by means of dynamic pilotscale experiments in a special-purpose experimental setup.

Literature

Peppelenbos, H.W. and Rabbinge R. (1996). Respiratory characteristics and calculated ATP production of apple fruit in relation to tolerance of low O-2. Journal-of-Horticultural-Science 71 (6): 985-993.

A Modelling and Control Structure for Product Quality Control in Climate Controlled Processing of Agro-material

Abstract

In this chapter a modelling and control structure for product quality control is presented for a class of operations that process agro-material. This class can be characterised as climate controlled operations, such as transport. The basic model consists of three parts. These are the quality and behaviour of the product, and its direct and indirect environment. This decomposition is reflected in the proposed control structure. The significance of the explicit inclusion of product behaviour is that the control is much more geared to the demands of the product. The applicability and potential advantages of the proposed structure are illustrated in different industrial cases, such as the storage of potatoes and the transport of apples in reefer-containers.

Introduction

In transport of agro-materials two important objectives can be recognised. One is energy consumption and the other is product quality. Tighter demands on the efficiency of post-harvest processes as well as quality requirements require a dynamical operation that directly includes the relevant product characteristics. Present process controllers aim at keeping climate variables, such as temperature, as close as possible to setpoints. These setpoints are determined *a priori* and are constant, or, at best, adjusted according to pre-set blueprints (which are often aimed at long term storage of products). The dynamical aspects of product behaviour with its quality attributes are not directly controlled in processing agro-material. Model-based (supervisory) controllers allow for connecting sub-systems and incorporating constraints. These developments enhance the opportunity for a new controller methodology for processing agro-material, as is also stated e.g.in Galara (1999) and for drying operations in Achanta (1996). Using models of the process and product in the controller (e.g. in Model Predictive Controllers) enables the use of prediction and optimisation techniques to determine the most appropriate control action. The goal of the new controller methodology is the use of the maximum knowledge about process and product quality to design controllers that are safe, energy efficient, reduce quality variation and maximise product quality. The first step in the development of such controllers is to define a generic modelling and control structure.

In this paper such a structure will be presented that is fit to a special class of climate controlled post-harvest processes. This class is characterised by different time scales (as in most post-harvest processes involving agro-material), and disturbance and control inputs that only drive the product environment and not the product directly. The model and control structure must be dedicated to product and product quality. Furthermore, it should be sufficiently generic in order to shorten development time and reduce cost of the controllers for a range of processes.

Modelling

First principle based modelling starts with the conservation laws for the extensive variables energy, mass and momentum. The model in extensive variables is reformulated in terms of intensive variables, such as temperature and concentration, resulting in a set of differential equations for the process state. From this set the following (physically oriented) separation of the process state in sub-states can be deduced,

- pimary product states, x_p, that are subject to reactions of biological and/or chemical components n the product representative for the product quality attributes, Q, such as colour, shape, taste and smell,
- secondary product states, x^p_d, that are not directly involved in the reactions, but indirectly through the reaction constants, such as temperature and moisture content of the product,
- direct climate states, x^c_d, that are directly in contact with the product, such as temperature and humidity of the air directly surrounding the product, and
- indirect climate states, x_i, that are not directly in contact with the product, such as temperature and humidity of the air in air channels, air rooms etc.

The sub-states for the secondary product states and the direct climate states can be considered together as one environment. This is motivated by the observation that the time scales for these state variables are of the same order of magnitude. The fast equilibrium between these state variables makes them behave as one entity. Consequently, the system can be separated into three sub-states

- primary sub-state (x_p),
- direct environment sub-state (x_d) that directly interacts with the primary state variables,
- indirect environment sub-state (x_i) that does not affect the directly, but only through the direct environment.

This separation in the process model is particularly suited for control purposes as aimed at here. The relations between the
different classifications into sub-states are illustrated in Figure 1.

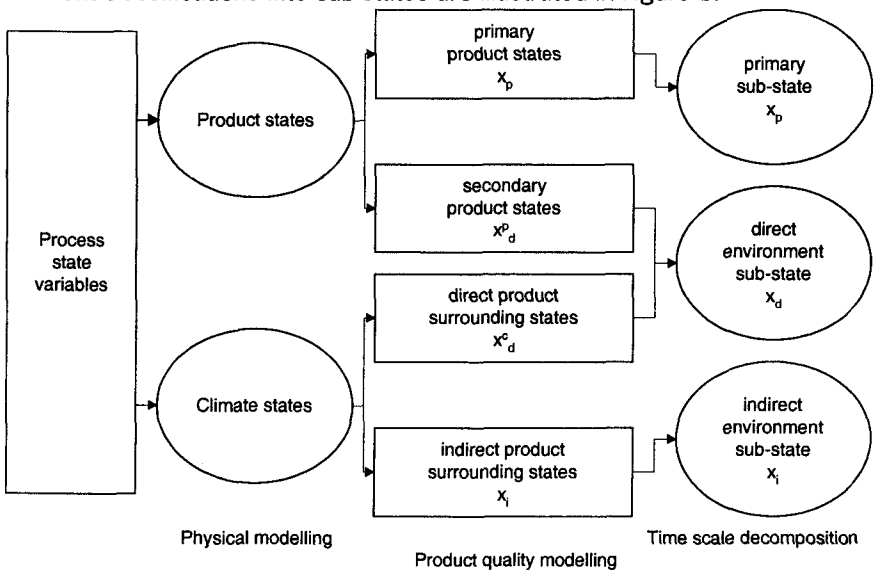

Figure 1: Relations between the different classifications of sub-states

In Figure 2 the relations between the different components of the model structure are shown. The structure of the process is strictly hierarchical whereby the primary state variables are in the centre, capsulated by the direct environment state variables of the containing unit. The indirect state variables form yet another outer shell enclosing the unit completely. As it is, the plant input, that can be manipulated only, is sequentially linked together with the primary state variables, which are the target, with the environments in between.

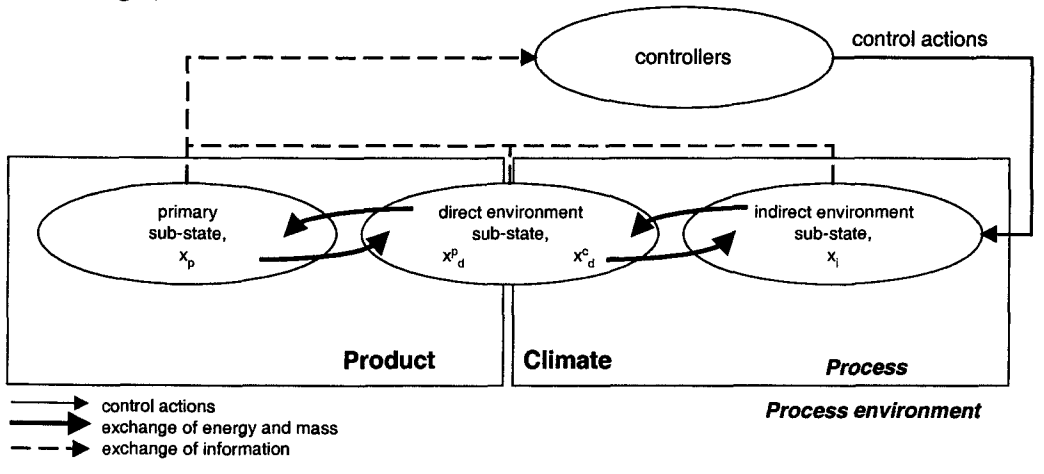

Figure 2: Relations between model components

This observation is characteristic in operations that involve agro-material. In Table 1 time scales are presented that are representative for transportation of agro-materials. The differences

between the time scales of the sub-states enable the development of a decoupled control structure.

Table 1: time scales in transport of agro-materials

time scales sub-states	transport
product	hours/days
direct environment	hours
indirect environment	Seconds/minutes
hardware controllers	Seconds

Thus, in this section a classification of the whole system into three sub-states is made. An example of the proposed classification in three hierarchically coupled sub-states as developed here is in potato storage where the sugar content is the primary state variable. The temperatures of the potatoes and the air directly surrounding the product belong to the direct environment. The direct environment consists of a non-quality product component (e.g. product temperature) and a climate component (e.g. air temperature). The temperatures of the air in the air channel and air room belong to the indirect environment.

Primary sub-state

The primary state variables are subject to reactions that take place inside the product. These reactions cause changes in the state variables and, therefore, in the quality attributes. The product model describes the dynamics of the primary state variables, x_p. It can be shown that the product model is defined by

$$dx_p/dt = K\,r, \qquad (1)$$

where the vector r is a vector valued function of the primary state variables and the matrix of functions K consists of the reaction constants that may depend on the direct environment states

$$r = r(x_p),$$
$$K = K(x_d). \qquad (2)$$

For example, the rate of the reactions, that take place inside the product, depend on product temperature. More details on modelling the product quality attributes are given in Verdijck (2001). The main assumption in Equation (2) is that the state variables in the direct environment are not limiting for the reactions inside the product.

Direct environment sub-state

The direct environment consists of a product component, x^p_d, and a climate component, x^c_d. Both can be constructed from the conservation laws for mass and energy. These balances result in ordinary differential equations for the temperature and mass concentrations of the different components. Examples of state variables in the product component are temperature and total mass. Product temperature influences reaction rates in the product and product mass is important in considering undesired weight-loss of the product. Weight-loss can not only decrease product quality, but may also be important for the financial yield of the product after transport. The dynamics of the state variables of the product component can be written as

$$d\,x^p_d/dt = f^p_d(x_p, x_d). \qquad (3)$$

These state variables are not controlled directly, but only through the manipulation of the climate component. Furthermore, they are not subject to outside disturbances, that is, these disturbances only affect the product component indirectly.
The dynamics of the state variables of the climate part, such as temperature and oxygen concentration of the air, can be written as

$$d\,x^c_d/dt = f^c_d(x_p, x_d, x_i). \qquad (4)$$

In case an interaction between x^p_d and x^c_d can be considered infinitely fast, an algebraic relation is added to the system description that reduces the dimension of this sub-state. Such a relation can be written as

$$0 = f\_c(x^p_d , x^c_d). \qquad (5)$$

In the proposed model approach only lumped state variables are considered. In case gradients inside the product or its environment are too important to be neglected, a spatial distribution could be considered. This step results in separate lumped (sub-)systems that together approximate the gradients and still fit in the proposed sequential model structure.
The non-linearities in this model component are located in state dependent model coefficients, e.g. temperature dependencies of heat transfer coefficients.

Indirect environment sub-state
The state variables in the indirect environment may be controlled directly and their dynamics can be written as

$$d\,x_i/dt = f_i(x^c_d, x_i, u, v_{md}, v_{ud}), \qquad (6)$$

where u represents control actions, and the measured and unmeasured disturbances are represented by v_{md} and v_{ud} respectively. The indirect environment in these processes has relatively fast dynamics. This is caused by the relatively low thermal mass in this part of the process. In container transport this indirect environment is the headspace.
The model may have non-linear terms in the control inputs. This occurs as e.g. both flow rate and incoming temperature of this flow act as controlled input. This would lead to a non-affine system (non-linear in the control input) which requires special care in choosing the control algorithms, as is mentioned in Mutha (1991).

Model structure
Equation (1) through (6) have been written in the presented form in order to show the (sequential) interaction between the sub-states and their effect upon product quality. The system can be described as a sequence of interacting sub-systems.

The complete state space model is summarised by

$$dx_p/dt = K\,r, \qquad (7)$$
$$dx_d/dt = f_d(x_p, x_d, x_i),$$
$$x_d = [x^p_d \;\; x^c_d]^T,$$
$$dx_i/dt = f_i(x^c_d, x_i, u, v_{md}, v_{ud}),$$
$$0 = f_c(x^p_d, x^c_d),$$
$$r = r(x_p),$$
$$K = K(x_d),$$

with the output relations

$$y = f_m(x), \qquad (8)$$
$$x = [x_p \;\; x_d \; x_i]^T,$$
$$z = f_r(y),$$
$$Q = f_q(y,z), \qquad (9)$$

where z represents the unmeasured process outputs to be reconstructed from the available measurements that are represented by y. The function $f_m(x)$ is the so-called measurement equation and the function $f_r(y)$ represents a reconstruction filter. As product quality, Q, often is a complex function of process outputs, both measured and reconstructed, an additional quality equation $f_q(y,z)$ is added to the model structure.

Control structure selection

Improving process control involves:
- the formulation of the control objective,
- building the necessary models,
- selection of the control structure,
- design of the selected controllers,
- validation of the control system and
- implementation of the controller.

The selection of a control structure is an important step, although this step is often not given much attention. It determines the inputs and outputs of the control components, the objectives of the different control components and the control performance. In this section a control structure will be proposed for the class of operations that is discussed in this paper. The control structure is applicable in an industrial environment, as will be shown in this document.

The control structure is not a trivial choice for the type of processes, discussed in this paper, as there are different time scales, uncertain information and practical constraints in the design procedure. A non-optimal control structure results in a non-optimal control design and, therefore, in non-optimal operation of the controller and the process. The selection of a control structure can be seen as an optimisation problem where the objective is to determine or select the control structure with low complexity without loss of performance. This involves the aspect of time scales that may occur in the process and the separation of time scales, if possible, and the optimal use of available information while considering the uncertainty of this information. Also, to achieve the desired process performance the system must be in the span of the controller. For the industrial application it is important to guarantee a certain degree of robustness and reliability, as the processes operate with a large variance in the product. These aspects will be discussed in this section.

Control structure

In selecting a control structure in climate controlled processing of agro-material, all aspects must be considered that are mentioned earlier in this section. In Figure 3 the general control structure is illustrated with a control component for each sub-state of the process model from the previous section. In short, the indirect environment is controlled by the local controllers. The direct environment and the primary state variables are controlled by short-term controller(s). The short-term controller(s) calculate the setpoints u_s for the lower level control components. The long-term controller performs an economical optimisation resulting in reference trajectories, u_l^{ref} (desired trajectories x_p^* and x_d^*), and settings for variables that are not controlled on the short-term level, u_l^{set}, the so-called partial control,

$$u_l = [u_l^{ref} \; u_l^{set}]^T. \qquad (10)$$

Examples of the different controlled variables will be discussed in more detail in the case studies. In the container case,
u_l^{ref} represents the product respiration trajectory, u_l^{set} e.g. the relative air humidity, and u_s the temperature and oxygen concentration in the container.

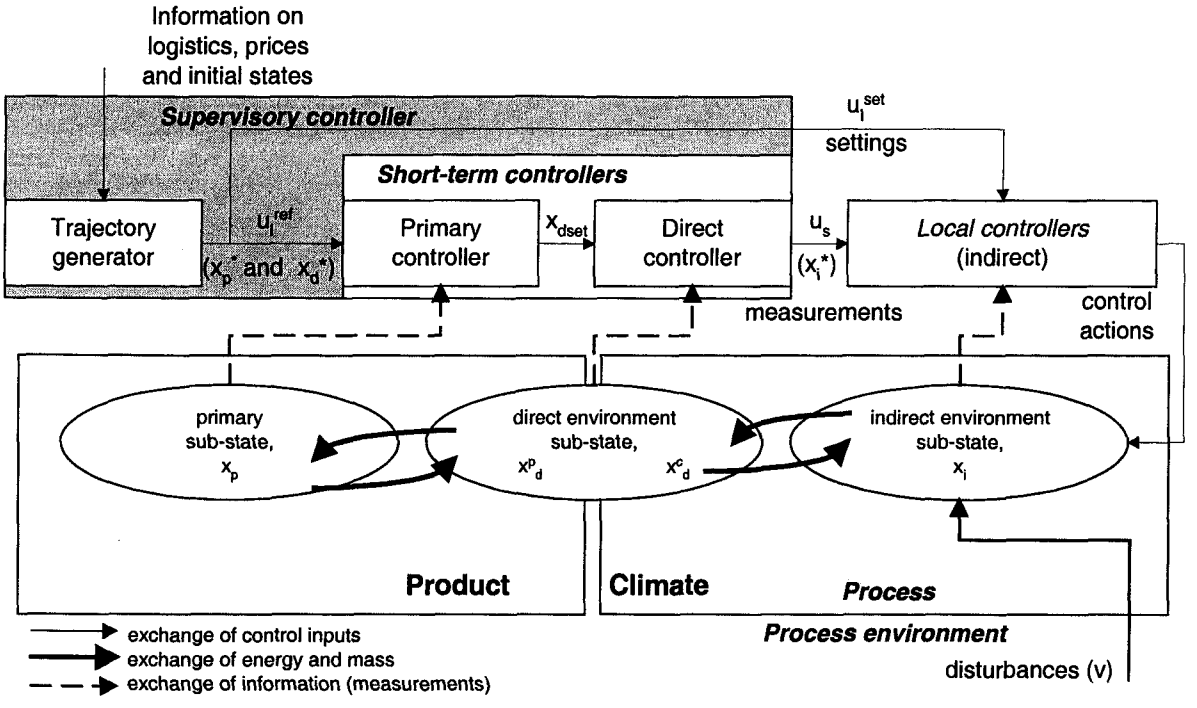

Figure 3: General control structure

In the following sections motivation and details for this control structure will be discussed. In the case studies it will be shown that in case the direct and indirect environment are strongly interrelated separate control components are not motivated, and only one short-term controller for the primary and direct environment state variables will remain.

Practical constraints

Often in an industrial environment, practical constraints are imposed on the control structure. One such constraint is that the model-based (supervisory) controllers may not control directly the process quantities of interest, but only by means of the settings of the local controllers. The advantage of this approach is that, in case of control system failure, the operator can return to the existing low level subsystems. Of course, the drawback is that the local control dynamics often can not be changed and must be taken into consideration in the development of the supervisory controllers. In the class of operations that is discussed in this paper, it is assumed that it is necessary to cope with this practical restriction. In the case studies presented in this paper this constraint will be illustrated.

In industrial practice there will be operating constraints for the controller. Constraints result from local controller performance possibilities, the product, outside weather and the process capabilities. These have to be included in the control problem of the supervisory control components.

Decoupling of time scales

Decoupling reduces controller complexity and improves understanding and insight in the controller and the process by the end-users. Decoupling is possible if there is a significant difference between the time scales in the process as illustrated in Table 1. On a supervisory control level the fast dynamics in the process can often be ignored by assuming a pseudo-steady state, while studying slow dynamic behaviour. This is a valid approximation in the presence of slowly fluctuating inputs. In this approximation the time for the fast dynamics to settle in the pseudo-steady state is ignored and the different time scales are decoupled. It should be noted that, in presence of fast fluctuating inputs, this could give rise to non-optimal control performance, as discussed in van Henten (1994) in the optimal control of greenhouse operation based upon singular perturbation theory.

The decoupling of dynamics, as done here, is supported by practical considerations for the class of operations in this research. These are that desired changes in the state variables by the controlled inputs are constrained to relatively slowly changing values to prevent product stress and that external disturbances only slowly affect the environment of the product. In transport and storage processes the expected disturbances often are the outside weather conditions that may change rather fast. However, due to insulation fast outside disturbances only affect the inside conditions with slow dynamics. Also in drying operations disturbances of outside conditions often are relatively small due to the factory building where the operation is located. The main disturbance in this process is the product flow, which often has slow dynamics. This motivates the choice for the decoupled control structure. The fast dynamics of the indirect environment are dealt with on the local control level. The relatively slow dynamics of the direct environment and the product are dealt with on the supervisory control level.

Availability of information

As presented before, on the supervisory control level there are sub-controllers for the different sub-states. These are the short-term controllers. Furthermore, there is a long-term controller or trajectory generator.

The different control components require process and product information. Together with the effect of the candidate inputs, the availability of this information determines which variables are controlled in each control component. There are essentially two types of problems regarding the availability of information in processing agro-material. The first type of problems is that necessary information is not always available or is rather uncertain. E.g., exact information on the outside weather conditions is only available at the actual time, predictions are available for five days at most and only averages over several years are available for long-term objectives. The second type of problems is that the influences of the different system inputs on product quality are not known with equal accuracy and that there often are more outputs than inputs of the system.

The first type of problems are solved by the separation in long-term and short-term control components. Information on weather averages over several years is used by the long-term controller to determine the trajectories for the process state. Weather predictions could be used in the short-term controllers to anticipate on this process input. The second type of problems are solved by the use of some of the long-term controller outputs directly as setpoints for the local controllers, and some as reference trajectories for the short-term controller. The reference trajectories, u_l^{set}, are used to control the main outputs exactly. Other process outputs, that outnumber the remaining inputs, are set directly by the long-term controller, u_l^{ref}. Of course, these outputs can only be kept within certain domains. Such a separation of controllable inputs could be evaluated in terms of partial control, see Kothare (1998). The choice whether or not the selected inputs should be controlled at all and by which controller is difficult to quantify. For uncertain systems robust analysis may answer this question, see e.g. Braatz (1996). However, in the processes that are discussed in this paper, often more information is available then only unmodelled dynamics. The model structure is often known. The selection of the controlled inputs for the controller components on the supervisory level is determined by the effect a candidate input has on the output y. A candidate input is controlled by the short-term controller if its effect on the output is sufficiently large. The effect of a candidate input can be calculated with

$$d\,u_0/d\,y_0 \;*\; d\,y\,/\,d\,u|_{u0,p0}, \qquad (11)$$

resulting in a i*j-matrix, with i the number of process outputs, j the number of inputs, and where u_0 and p_0 represent the operating conditions and nominal expected model parameters. The inputs with the larger effect are controlled by the short-term controller, in u_s. Otherwise they are controlled by the long-term controller, in u_l^{set}, or stay fixed. This will be illustrated when the application is discussed.

Limitations of the control structure

The control structure that is presented in this paper assumes slowly changing control inputs and disturbances. If this assumption is not met decoupling the sub-states could be inappropriate depending on the effect of the input on the system.

In general model-based control performance strongly depends on the quality of the models and that is also true for the processing of agro-material. Especially choosing or determining the model structure and the state variables of interest should be given enough attention. An inappropriate model structure would minimise the control performance. In case there is an appropriate model structure parameters in the model may be unknown, uncertain, or changing in time. This requires the use of a type of estimator, either on-line or off-line. This should improve the control performance as will be shown in the case study on potato storage.

Application to container transport

Climate controlled container transport of agro-material is a common way to get products at their desired location. During this transport the product quality changes due to time and transport conditions like temperature, relative humidity and concentrations of oxygen, carbondioxide and ethylene.

Model

Product quality is defined by respiration and bacterial/microbial activity. In this case study respiration is modelled with an algebraic relation as function of the oxygen concentration in the direct environment sub-state. The bacterial/microbial concentration acts as primary sub-state. The direct environment sub-state consists of product temperature, x_d^p, and moisture content as product component, and the air temperature, x_d^c, and humidity, and concentrations of oxygen and carbondioxide as climate component. A compartment model is built consisting of three parts to represent the spatial distribution that is caused by the inhomogeneous air flow inside the container. The indirect environment sub-state consists of e.g. the air conditions in the T-bar floor, x_i, and the head space. The differential equations for the substates are shown in Equation (12). For the direct and indirect environment only the equations for temperature are shown as those for the moisture content, O_2 and CO_2 would be similar. The model shown here is used for a time scale analysis. In the simulation studies a nonlinear model is used.

$$d\,x_p^m / dt = k_1(x_d)\, x_p^m \qquad (12)$$
$$d\,x_d^p / dt = 1/M_p\ Cp_p \cdot [R+U\,A\,(x_d^c - x_d^p)]$$
$$d\,x_d^c / dt = 1/M_{\_a}\ Cp_a * [rho_a\ F\ Cp_a\ (x_i - x_d^c) + U\,A\,(x_d^p x_d^c)],$$
$$d\,x_i / dt = 1/M_{T\text{-}bar}\ Cp_{T\text{-}bar} * rho_a\ F\ Cp_a\ (u - x_i)],$$

where conduction and evaporation is neglected. In Table 2 the eigenvalues, time constants and eigenvectors for this case study are shown.

Table 2: Characteristic values

sub-states	Description	eigenvalue	time constant (s)	Eigenvector
primary	Bacterial	10^{-6}-10^{-9}	$10^{\wedge 6}$-$10^{\wedge 9}$	[1*$10^{\wedge -8}$) 0 00]
Direct environment	Product and air in packaging	-1.508*10^{-5}	10^4	[-6.64*10^{-9} 0.7466 0.6653 0]
Indirect environment	T-bar	-0.00338	100	[0 -0.00989 0.231 0.973]

Control structure selection

Currently, transport is controlled by local controllers that try to stay as close as possible to the fixed setpoints that are given at the beginning of transportation. Product quality is not directly incorporated in the controller. To minimise quality decline, usually high rates of ventilation with outside air and/or circulation of internal air are used. This leads to unnecessary high cost, and to a

high evaporation rate and weight-loss. Therefore, a new control structure is developed that is illustrated in Figure 4.

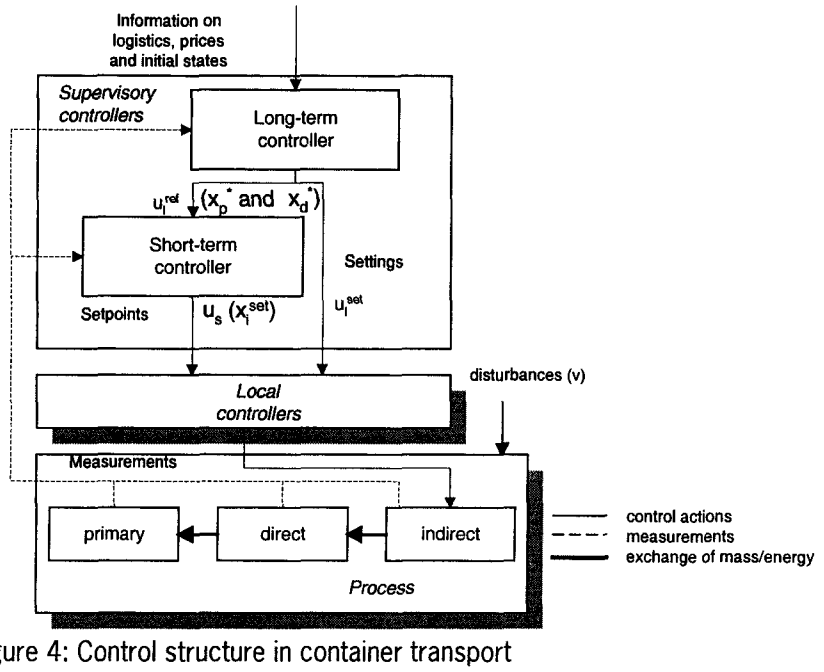

Figure 4: Control structure in container transport

In the control structure selection the incorporation of the local controllers was a practical constraint. A time scale decomposition is made that results in a long-term controller that calculates optimal and realisable reference trajectories, u_i^{ref} (x_p^* and x_d^*), and settings u_i^{set}, and a short-term controller. The short-term controller controls the primary state variables and calculates the desired indirect environment settings, u_s (x_i^*). This is motivated by the eigenvectors in Table 2 as the eigenvectors are related mainly to the state variables of the corresponding environment. The local controllers control the indirect environment state variables. Product temperature follows the direct surrounding air temperature closely, as other variables have less effect (low disturbance effects due to insulation). This can also be seen from the eigenvectors in Table 2.

Equation (11) is used to select the control variables for the short-term and long-term controller in u_s and u_i^{set} respectively. Results with this equation for the effect of the candidate inputs temperature, oxygen, carbondioxide and relative humidity on product respiration are shown in Table 3.

Table 3: Effect of candidate inputs on respiration

effect	$d u_0/dy_0 \cdot d y/ d u\}|_{u\,0.0\,0}$
oxygen	10^{-2}
carbondioxide	10^{-4}
temperature	10^{-3}
relative humidity	-

This resulted in the control inputs temperature and oxygen concentration for the short-term controller, as they are measurable and have the highest effect on the product quality. To limit the usage of energy resources not only the desired average temperature should be set, but also the allowed temperature differences in the container. The control variables relative humidity and CO_2 concentration are in u_i^{set} as they have less influence on the primary state variables and are used to restrict evaporation, condensation, and several product diseases within domains.

The control components have the same objectives as in the potato storage case presented before. Only, the time intervals for the predictive controller were one hour and the controller has multi-inputs and multi-outputs.

Results and perspectives

In the selected control structure, product quality is directly incorporated in the controller and this enables container settings that are more appropriate for the product that is transported. In Figures 5-8 simulation results with the new controller are shown and compared with the current controller. All reference trajectories are constant i.e. that the controller aims at keeping all process outputs at the corresponding operating point. Temperatures are shown for the three parts in the compartment model that correspond with a minimum air flow, a maximum air flow and nominal air flow for the bulk load (Figures 5 and 6). As can be expected product temperature with a high flow rate follows most closely the setpoint that is generated from the predictive controller. The manipulated variables, around the operating point, that are calculated by the new controller are shown in Figure 6. The flow in this figure is normalised with the maximum flow (flow in current practice) and has an order of magnitude of 1 $m^3 s^{-1}$.

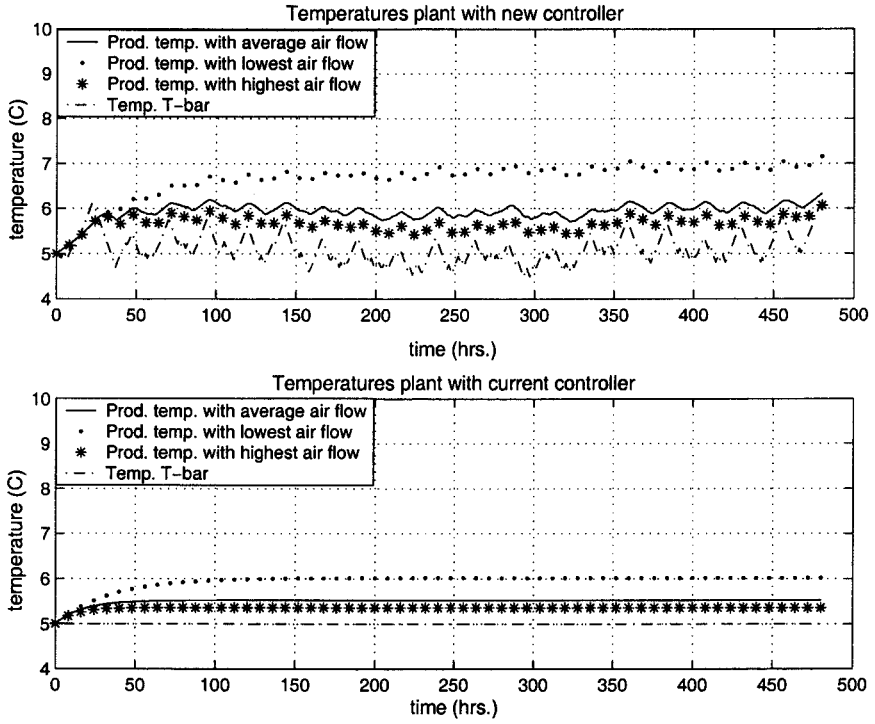

Figure 5: Temperatures in load and setpoint in container transport

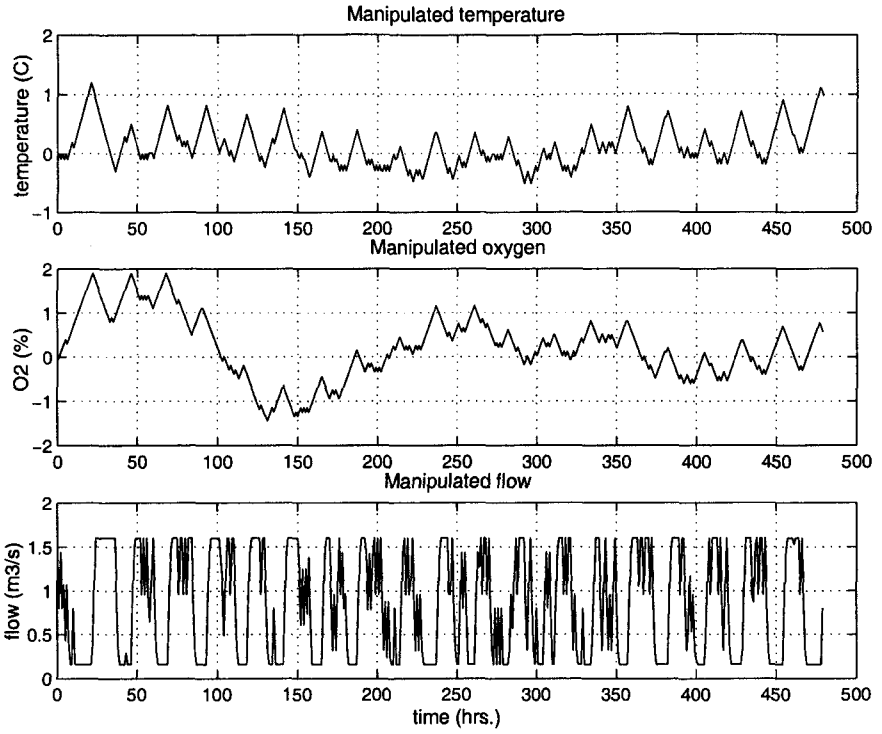

Figure 6: Manipulated variables in container transport

In Figure 7 temperature differences between the parts in the compartment model are illustrated and in Figure 8 the energy usage is shown. A significant reduction in energy consumption may be achieved.

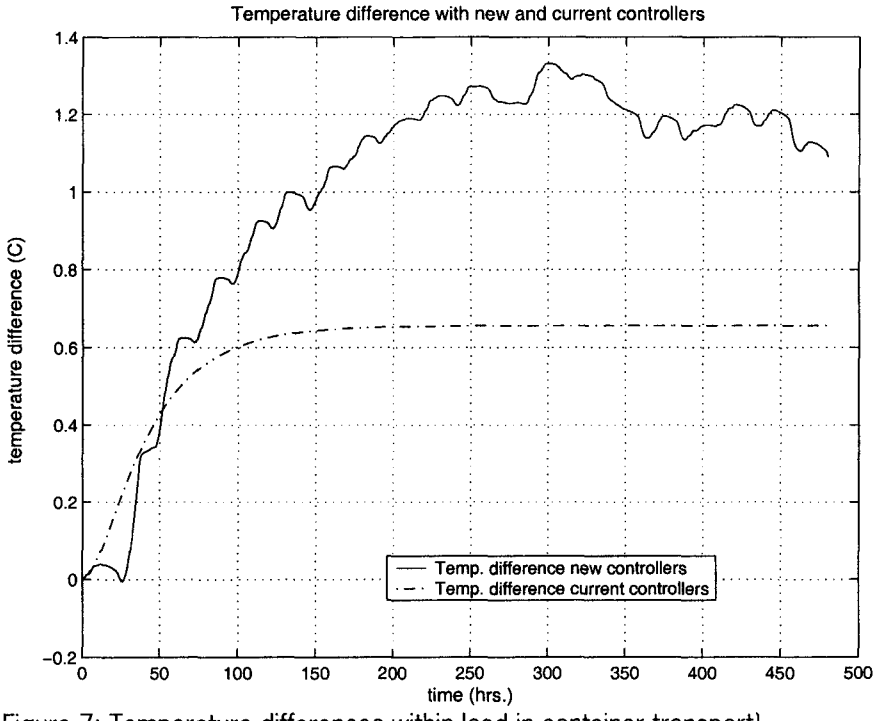

Figure 7: Temperature differences within load in container transport)

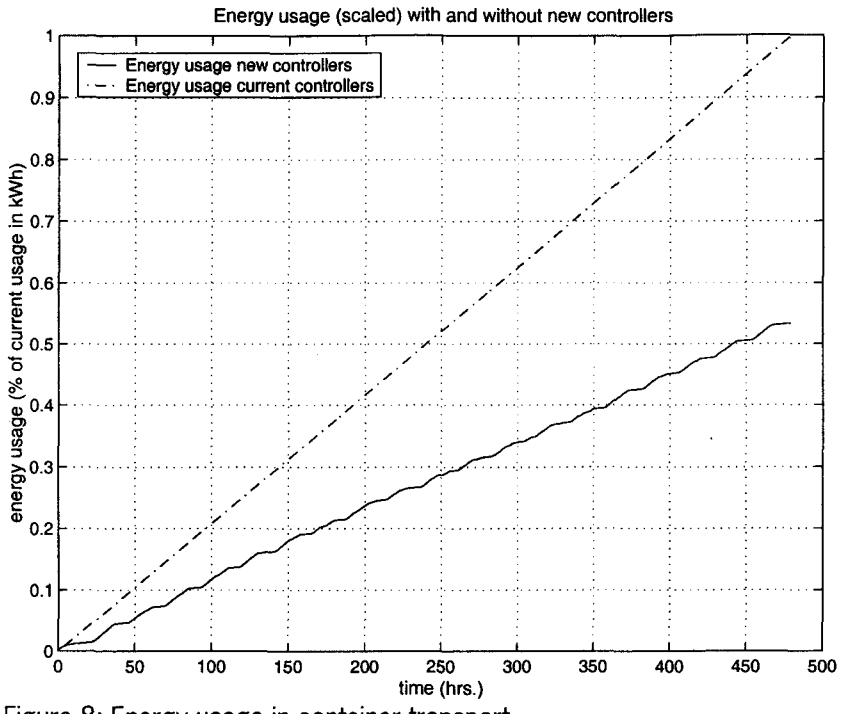

Figure 8: Energy usage in container transport

The control structure will reduce quality loss as this is directly controlled and decrease energy usage by reducing over-circulation and -ventilation. This will decrease weight-loss from the product through evaporation. The cost one has to pay for these results are higher temperature gradients in the container load. However, limited temperature differences are allowed as long as they do not affect product quality too much. Again, the explicit inclusion of the quality model in the controller structure makes it possible to realise savings that otherwise would not have been exploited.

Conclusions and further research

In this paper a modelling and control structure is presented for the class of climate controlled operations that process agro-material. This class is characterised by the presence of different time scales (as most post-harvest processes), and inputs -both disturbance as well as control inputs- that only drive the slow dynamics of the process.

The modelling distinguishes between primary state variables, direct and indirect environment. This leads not only to more insight in the process, but also to localised information that is useful for time scale decomposition. Time scale decomposition allows for (goal-based) controllers with improved economic performance.

The presented control structure is mainly characterised by the decoupling of the different time-scales that are involved in the process, resulting in a separation of the control structure into long-term, short-term and local controllers. Furthermore, the subject of partial control is handled. The control structure is applied in industrial case studies that show the applicability and benefits in an industrial environment. To improve the processing of agro-material in this class of processes the control structure directly incorporates (dynamic) product behaviour. Because of this direct control it is possible to operate these processes closer at the operation limits, leading to improved process performance with respect to both quality and cost.

The ideas and structures discussed in this paper could be useful in other classes of operations that process agro-material. The next step for the processes considered in this paper will be the further improvement of control algorithms for the different controller components dedicated to the characteristics of the class of operations that is considered. These algorithms should be sufficiently generic to enable their use in the whole class of processes, thereby significantly reducing development cost of model-based (supervisory) controllers that are dedicated to the product and its quality.

Notation

epsilon	product-air ratio	
rho	density	[kg m^{-3}]
A	exchange area	[m^2]
Cp	specific heat	[J kg^{-1}]
F	air flow	[m^3 s^{-1}]
H	time horizon	[s]
J	objective function	
K	system matrix	
M	total product mass	[kg]
P	product price	[dfl. kg^{-1}]
Q	quality attribute	
R	respiration	[J kg^{-1} s^{-1}]
U	heat exchange coefficient	[J kg^{-1} m^{-2}]
W	weighing factor	
f	function	
k	yield-coefficient	[s^{-1}]
r	reaction components	
t	time	[s]
u	input	
v	disturbance	
x	process state	
y	measurable outputs	
z	non-measurable outputs of interest	

Superscripts:

*	reference trajectory
a	assisting
c	climate
i	number of process outputs
j	number of inputs
p	product
ref	reference value
set	setpoint

Subscripts:

0	nominal value
T-bar	T-bar in container
A	air
d	direct environment state variable
c	climate
f	final processing time
h	hardware controller
I	indirect environment state variable
l	long-term
m	measurement
max	maximum value
md	measured disturbance
min	minimum value
p	primary state variable
q	quality
r	reconstruction from measurements
s	short-term
set	setpoint
ud	unmeasured disturbance
x	processing state

Achanta (1996)
Achanta, S., Okos, M. 1996
Predicting the quality of dehydrated foods and biopolymers - research needs and opportunities.
Drying Technology, 14 (6), 1329-1368.

Braatz (1996)
Braatz, R., Lee, J., Morari, M. (1996)
Screening plant designs and control structures for uncertain systems.
Computers and Chemical Engineering, 20 (4), 463-468.

Galara (1999)
Galara,D., Hennebicq, J. (1999)
Process control engineering trends.
Annual Reviews in Control, 23, 1-11.

Kothare (1998)
Kothare, M., Shinnar, R., Rinard, I., Morari, M. (1998)
On defining the partial control problem: Concepts and examples.
American Control Conference 1998.

Mutha (1997)
Mutha, R., Cluett, W., Penlidis, A. (1997).
Nonlinear model-based predictive control of control nonaffine systems.
Automatica, 33 (5), 907-913.

van Henten (1994)
van Henten, E. (1994)
Greenhouse Climate Management: An Optimal Control Approach.
PhD thesis, Wageningen Agricultural University.

Verdijck (2001)
Verdijck, G., Sillekens, J., Preisig, H. (2001)
A model structure for product quality in processing agro-materials for process control purposes.
Journal of Food Engineering, 51 (2), 151-161.

Appendices task 2

MODEL PREDICTIONS OF CONDITIONS IN A CA-REEFER CONTAINER

R.G.M. van der Sman and M. Sanders Agrotechnological Research Institute ATO
S. Duraisamy and P.G. Jolly, Carrier Transicold

1. Introduction

In the CEET research project we are developing novel ways to control the climate conditions inside a refrigerated sea-container (reefer), possibly equipped with a Controlled Atmosphere (CA) unit. The objective of this new control method is to minimise energy consumption, while retaining a certain (minimal) level of product quality. The control algorithm achieves this objective by making model predictions during shipment. The predictions are based on in-transit measurements of climatic conditions, and available physical models on the energy consumption, climatic conditions, and the product physiology. In order to reach the objective the controller will dynamically change the set points of the container.

In this chapter we will summarise the modelling approach used in this project, and show the predictive power of these models by comparing it with data obtained by validation experiments. With further simulation for a transport with apples we will give an indication of the impact on energy consumption and product quality of the novel control method. Details on the models are not given in this summary, but are given in an separate accompanying report.

2. Model-Predictive Control

A schematic diagram visualising the concept of the Model-Predictive Control is shown in figure 1. Based on predictions of future energy consumption and product quality change, the controller dynamically adjusts the set points of the cooling unit of the refrigerated container. The models take the control actions as input, and predict subsequently the climatic conditions of supply air, the air flowing around the pallets with packaged produce, the conditions of the air inside the package, the product quality change, and also the energy consumption of the cooling unit.

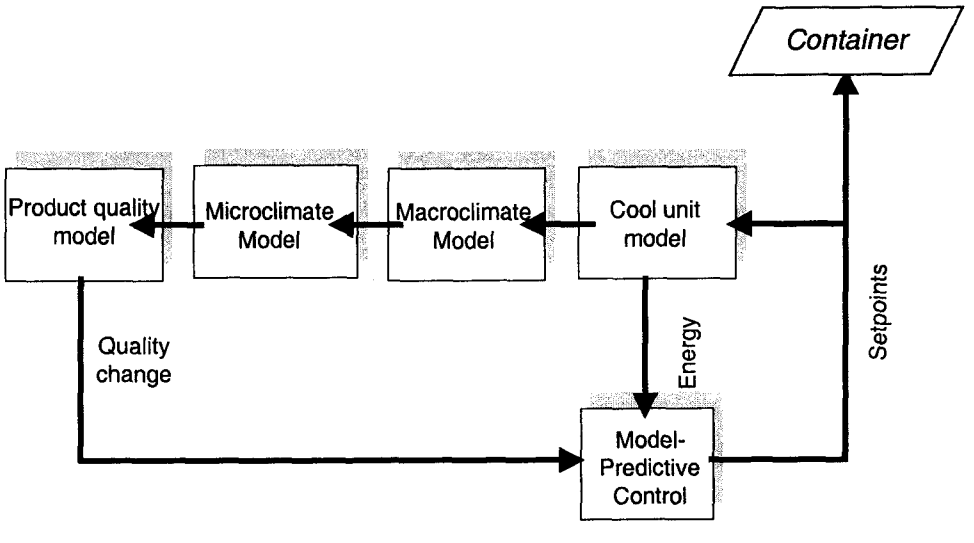

Figure 1. **Schematic diagram of Model-Predictive Controller driving the set points of a refrigerated container. Controller accepts input on energy consumption and product quality change from models.**

3. Cooling unit model

Given the set points this model computes the energy consumption, and also the conditions of the supply air, i.e. its temperature, humidity, and respiratory gas concentrations. Following Jolly et al. (2000), we have built a detailed model of the cooling unit, with modelled components shown in figure 2a. In co-operation with Carrier Transicold we have built a network model of the steady state heat flows, which are shown in figure 2b.

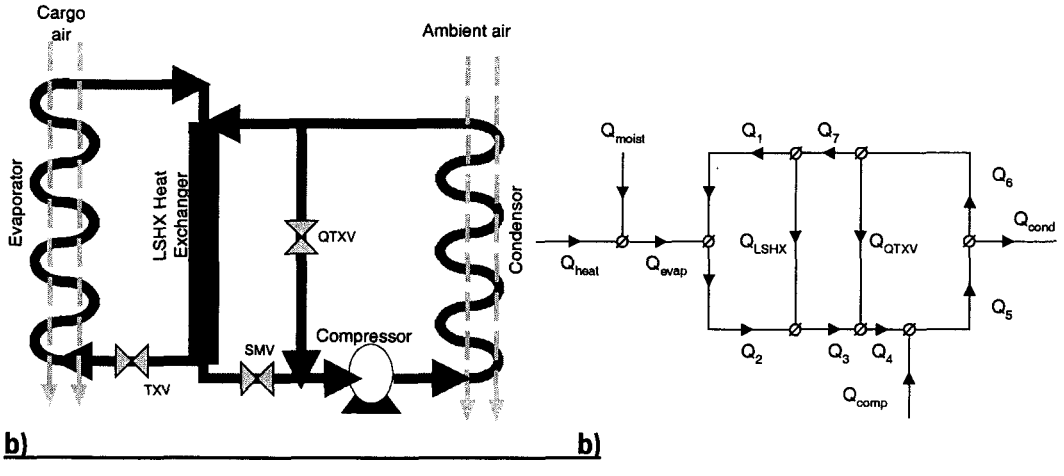

Figure 2**a) Schematic diagram of components in the model of the refrigeration unit, and b) Network diagram of heat flows in model of refrigeration unit. (Q)TXV are thermostatic expansion valves, and SMV modulates the refrigerant flow.**

This detailed model is part of a larger network model, encompassing other components in the cooling unit, namely the evaporator fan, the heaters, the fresh air intake, and the Controlled Atmosphere unit. The heat flow network representation of the model is depicted in figure 3, where it is shown that it is coupled to the climate models by the heat flow of the supply and return air. Next to the heat flows, a similar network model is used for the flow of water vapour, O_2, CO_2, and N_2. Due to the slow dynamics of the control of respiratory gases, the model also includes the logic for this control. A more detailed description of the cool unit model, you will find in the special report on modelling.

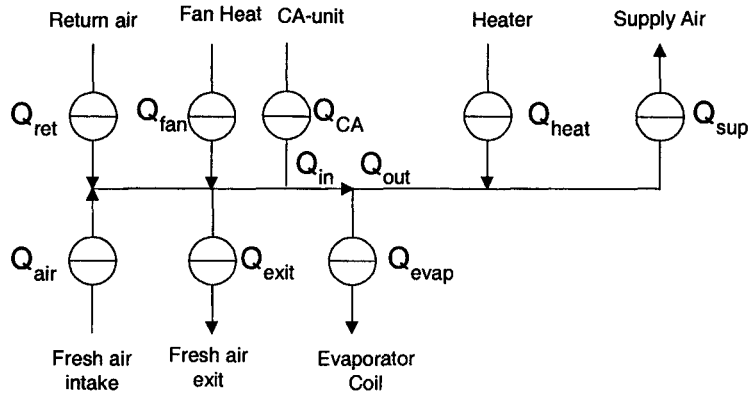

Figure 3. Network model of heat flows inside the cooling unit, with Q_{evap} given by the model depicted in figure 2.

We have tested the prediction of energy consumption of this model by comparing it to experimental data obtained at ATO and at the lab of Carrier Transicold. First, we have compared the model with data from a cooling experiment with the container. Using manufacturers data we have found that they do not match. The numerical estimates are much too low. This mismatch is

due to the fact that in our model we have not incorporated the action of Condenser Pressure Control (CPC) (because it is a dynamic effect, which is difficult to include in the static refrigerant circuit model). We correct for that using a different compressor model, $\gamma_1 = 1.7 * 1.234$, $\gamma_2 = 1.7 * 0.258$.

As shown in figure 4, the model has reasonable accuracy. The tests at Carrier Transicold are according industry standard, performed at specific temperatures given in Fahrenheit. Hence, the test conditions are given in those units in figure 4b.

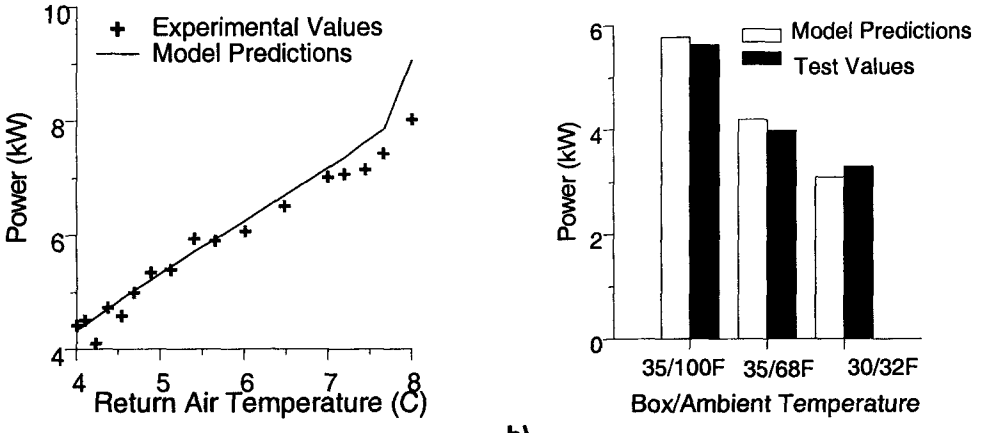

Figure 4. Comparison of results from the energy model with a) experimental data from our lab, and b) standard test data from the manufacturer.

4. Climate model

As a function of the conditions of the supply air, the climate model predicts the change in product temperature, humidity and gas conditions in the packaging. The heat flow network is shown in figure 5. Similar models have been built for the mass flows of water vapour and the respiratory gases. The model for the respiratory gas conditions is somewhat simpler, because experiments have shown that there are no gradients in gas concentrations inside the container. The mass flow models are coupled to the heat flow model, due to the heat produced by respiration (P_{resp}) and extracted by evaporation (P_{evap}).

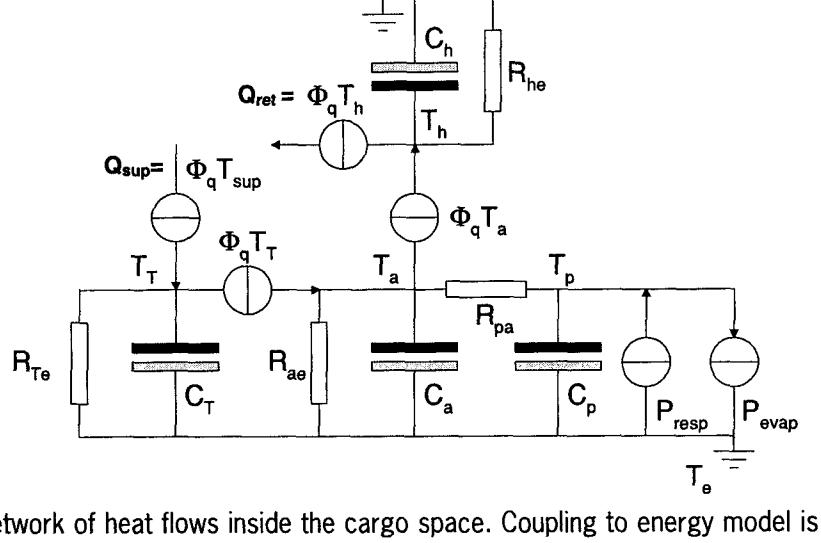

Figure 5. Network of heat flows inside the cargo space. Coupling to energy model is by Q_{sup} and Q_{ret}. Heat current sources are driven by the airflow forced by the evaporator fan, with $\Phi_q = \rho_a c_{p,a} \Phi_v$, and Φ_v the volumetric flow rate of the fan.

For the production/consumption of the respiratory gases we take a simple respiration model given by Peppelenbos (1996). The aerobic respiration follows a Michaelis-Menten kinetic

without inhibition by CO_2, and fermentative CO_2 production does have inhibition by O_2. The model is valid only for low CO_2 levels, a condition valid for refrigerated container transport.

A more detailed description of the climate model, you will find also in the special report.

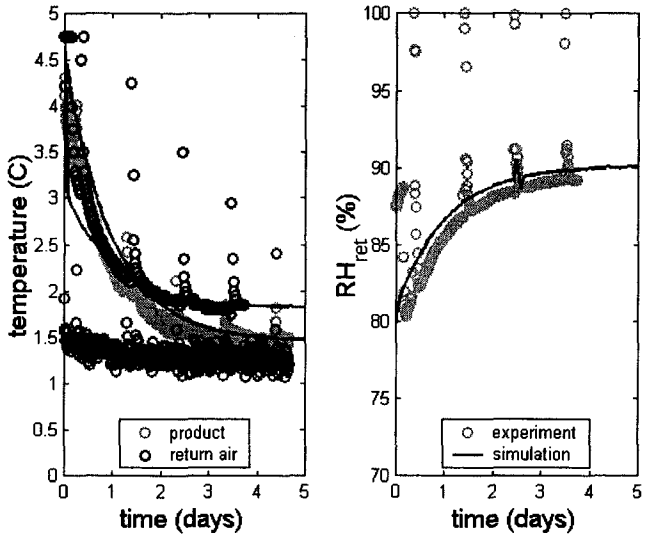

Figure 6. Comparison of climate model with lab experiment of cooling 15 tons of apples from 5°C to 1°C, packed in open trays. Shown are the average product temperature, temperature and relative humidity of return air.

The output of the climate model is fed to the cooling unit model, and the product quality model. We have tested the heat flow network model by comparing it to cooling experiments with a container loaded with 15 tons of apples. From the results in shown figure 6 follows that we can predict quite accurately the average product temperature, which is an important parameter for the product quality. Furthermore, we have tested the mass flow network model for the respiratory gases with CA-experiments on the same container with apples. From the results in figure 7 follows that we are able to predict accurately the change in oxygen.

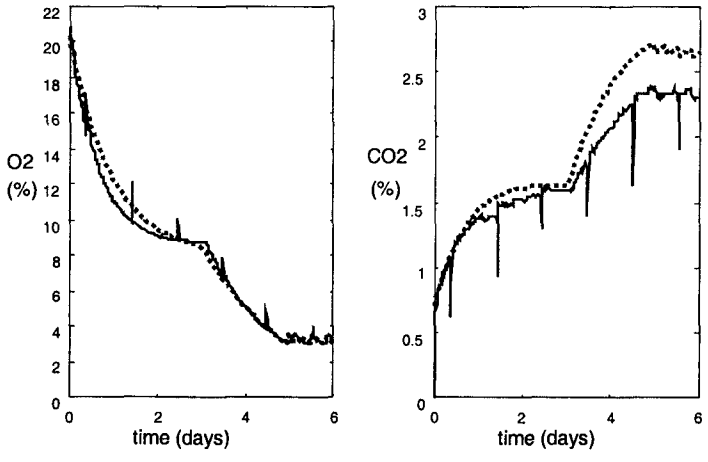

Figure 7. **Comparison of results from the model (dashed line) and CA-experiment (solid line).**

However, the prediction of CO_2 is a bit off for low oxygen levels, which is probably due to inaccuracy in the parameters for anaerobic respiration. For the purpose of this project this inaccuracy is not very significant, as the product quality is more influenced by temperature, moisture loss, and oxygen consumption (see below). The aim of this paper is to show the potential of the reduction of energy consumption with model predictive control, and hence the improvement of the accuracy of the CO_2 production will be dealt with in the follow-up research project.

At this stage the climate model only predicts the average climate conditions inside the container. As observed in experiments performed at ATO there is some slight temperature variation between front and backside of the cargo space. In the models to be developed in the follow-up project we like to extend the model with this temperature variation inside the container. In order to do this prediction of the air distribution inside the container and the airflow through the packages have to be known. The latter models have been developed (van der Sman,2002) (Vollebregt,2001), but the former model is currently still under development. A preprint of the study by van der Sman (2002) and a summary of the report by Vollebregt has been included in the special report.

5. Product quality change model

Coupling of product temperature, and oxygen consumption to product quality. For apples, which we use in simulations below, the most important quality parameter is firmness. We modelled the firmness of apples by extending the model postulated by Tijskens et al. (1997, 1998). A description of this model you will find in a subsequent chapter. This model has been validated against experimental data obtained with Elstar apples.

In the quality change model we state that firmness of apples, its most important quality aspect, is related to the decay of they cell walls – which are made of pectins. During ripening pectin is broken down by the action of so-called pectolytic enzymes. The production of these enzymes is triggered by the ripening hormone ethylene. The production of ethylene is regulated by temperature, respiratory gases, and by ethylene itself by autocatalysis.

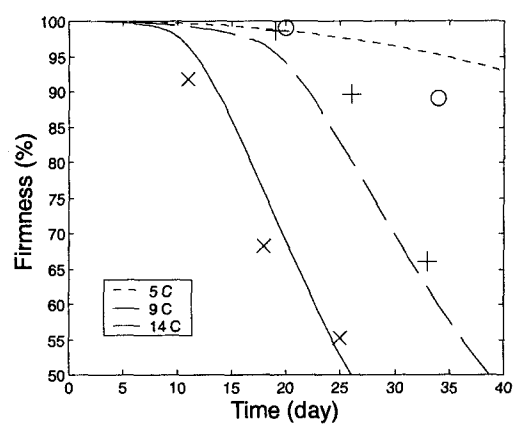

Figure 8. Firmness of Elstar apples stored at atmospheric conditions and various temperatures. Symbols indicate experimental values, and the lines indicate the values predicted with the product quality change model.

We have compared the product quality change model with experiments performed on Elstar apples, which are stored under different temperatures and CA-conditions. In figure 8 and 9 the model predictions are compared with experimental values. We have obtained reasonable agreement with experiment.

As shown in figure 8 both the model and experiments indicate that firmness shows an initial slow decay rate, and subsequently a fast decay rate. The change in decay rate is linked to the autocatalytic production of ethylene – which must be avoided in practice. As also found by Hertog et al. (2001), the initial slow rate of decay is proportional to the metabolic rate, which can be derived from the respiration model employed in the climate model.

Hence, by monitoring the respiratory rate, and linking it to the firmness of apples we can monitor the main quality aspect of apples. We envision that in the final CEET-concept ethylene sensors – being developed in this project - can be used, and hence the occurrence of the fast ripening can be detected and subsequent actions can be taken by the control algorithm (such as extensive ventilation, low temperatures or high carbon dioxide levels).

For other product it is expected that product quality change models can be linked to the respiratory rate (Tijskens and Polderdijk, 1996) (Hertog et al.,2001).

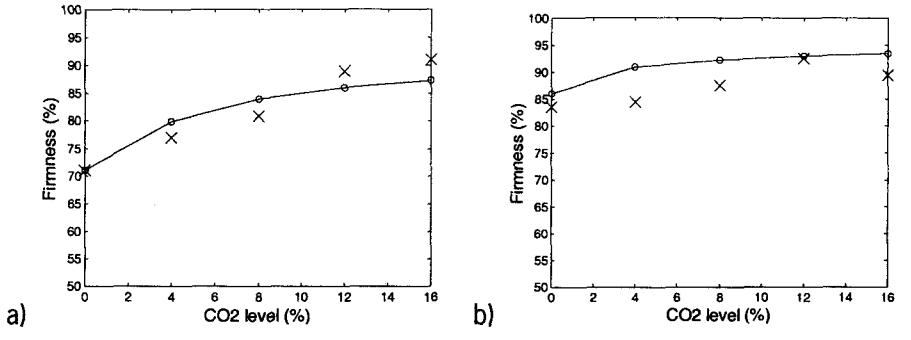

Figure 9. Firmness of Elstar apples after 21 days of storage at 18°C, and a) 21% O_2 and b) 3% O_2 and various CO_2 levels.
Symbols indicate experimental values, and the lines indicate model predictions.
Table I Ambient conditions during transport from New Zealand to Rotterdam

Days of travel	Temperature	RH
16	20	85
24	21	95
28	13	85
32	6	85

6. Energy reduction

After having validated that the various models have sufficient accuracy, with respect to our project goals, we test the total concept by coupling all models and compute the energy consumption for different scenarios. We apply the model calculation to a 32-day transport of 15 tons of apples from New Zealand to Rotterdam, the main port of Western Europe. The ambient temperature and humidity we take equal to the month-averaged values from the period January to March, which are shown in Table I.
We assume that the MPC control algorithm can change the following set points:

- supply air temperature
- gas conditions (O_2)
- fresh air intake
- air circulation rate

The CA-system of the container operates with a nitrogen membrane system, where the control of CO_2 is indirect. Hence, only the O_2 is taken as a set point. Initial product temperature is 7°C, and its set point is 4°C. Under standard conditions, we take fresh air intake is 75 m^3/h, and air circulation is 1 m^3/s.

In figure 10 and 11 we show the results of the simulations using different control algorithms. The graphs indicate 1) the energy consumption, 2) change in firmness, 3) product temperature, 4) gas conditions, 5) moisture loss from product, and 6) R.H. of the air surrounding the product. Moisture loss and R.H. of air around product are also indicative for the product quality. If moisture loss is more than 5%, the peel of apples shrivels, and is unacceptable for sale. If R.H. is 100% condensation occurs, which promotes mould growth.

For the simulation the change of set points is generated by simple rules. In the latter stage of the project the scenarios will be generated an actual MPC Controller. First we have performed calculations for two practical scenarios: 1) transport with constant temperature set point, without CA, and 2) transport with constant temperature, but now with CA. Subsequently, we have calculated two scenarios which allow variations in product temperature and/or gas conditions. These results are shown in figure 10 and 11.

The average power consumption in the various scenarios described above, is listed in Table II. One can observe from the results in figure 10 and 11 that short time variations in product temperature and gas conditions does not have much influence on quality parameters as firmness, weight loss, and risk of condensation (leading to spoilage). This finding has been confirmed by experiments performed at ATO by Boogaard et al. (2001).

But allowing temperature variation means that energy consuming compressors in cooling unit and CA system can be periodically be shut down, leading to significant energy reduction (See Table II).

Table II Energy consumption according to various control algorithms

Control Algorithm	Average Consumed Power (kW)
Standard Temperature Control – No CA	4.6
Standard Temperature Control with CA	7.6
Cooling unit compressor cycling , No CA	1.8
Standard Temperature Control, CA cycling	6.1

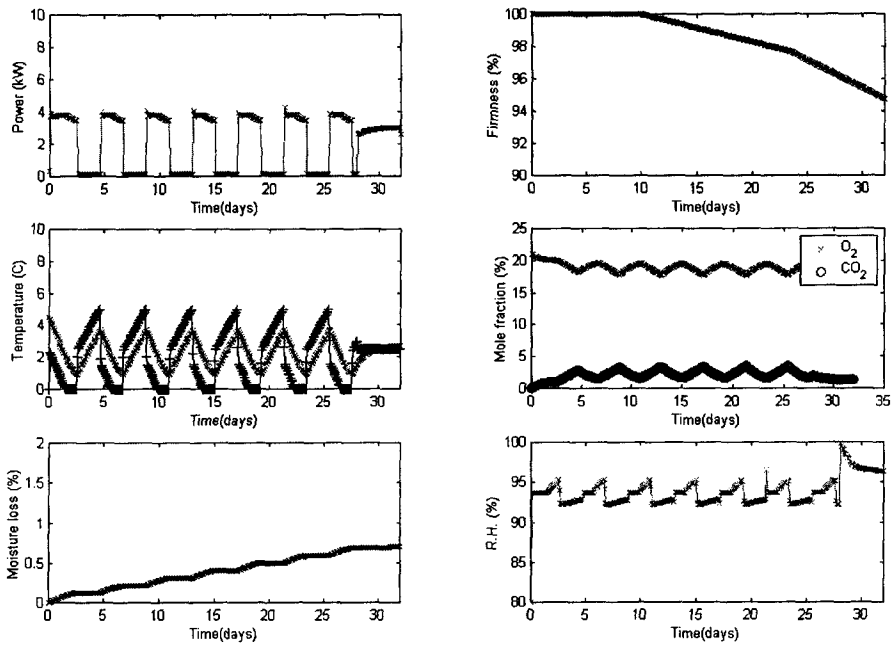

Figure 10 Simulation with control where compressor is cycled on and off, and furthermore Temperature set point and fresh air intake are changed dynamically. CA-system is off and air circulation is 0.5 m^3/s.

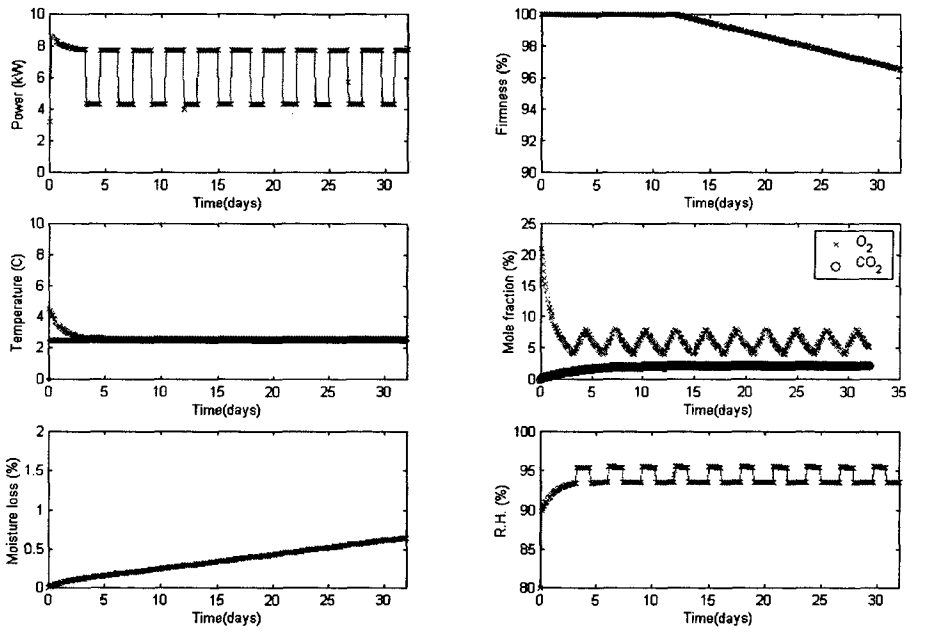

Figure 11. Constant temperature set point (4°C), but with variable O_2 – set point and fresh air intake control. Average O_2 set point is taken 6%. CO_2 is at about 2%. Air circulation is 0.5 m^3/s.

7. Conclusions

We have shown that by means of a new control algorithm, which dynamically changes set points, significant energy reduction in refrigerated container transport of perishables can be obtained without unacceptable loss of product quality. In the coming period we continue the research by coupling the model to a MPC-controller. Furthermore, we think our approach has potentials for incorporation of post-harvest treatments during transport, such as delayed storage (for prevention of chilling injury) or fruit ripening.

8. Further research

Crucial to the final success of the new method for energy reduction by dynamically changing set points is that no condensation occurs on the packed product. This aspect has not yet been investigated fully. Condensation may limit the amount of cycling of the cool unit. Hence, interaction between fluctuation of the supply air temperature and condensation has to be investigated. In container experiments using open trays as packaging for the product, we have observed that condensation has occurred very locally, namely mainly in the top layer of the pallets. For a reliable prediction of condensation, a more detailed description of the macro- and micro-climate inside the cargo space is needed.

The model describing the energy consumption of the cool unit, assumes that no ice frost occurs on the evaporator coil. During transport of produce requiring low temperatures, such as apples, this is not a valid assumption. Frost formation is known to have a significant impact on the cooling efficiency of the cool unit. Hence, for optimal operation of the supervisory control algorithm this effect has to be incorporated in the cool unit model.

During several container experiments we have observed a temperature gradient between front and backside of the cargo space. This is due to a quite non-uniform distribution of the airflow in the cargo-space. Preliminary calculations have shown that the airflow mainly flows between the first rows of pallets. We imagine better airflow distribution can be obtained by a 'false ceiling' in the headspace of the container. By extension and improvement of the preliminary model on the airflow distribution we can obtain a good design of this 'false ceiling'. Other benefits can be obtained by this false ceiling. By directing the airflow in the headspace directly above the pallets, to flow from

front to back, also the risk of condensation can be reduced significantly, because now this airflow will not be cooled, and therefore will not give condensation. Furthermore, redirection of the airflow will mean that during cycling of the cool unit, temperature fluctuations in the return air will be less pronounced than in the system nowadays. Hence, this also may lead some extra energy reduction.

In several container experiments we have observed a very significant effect of the type of packaging. The amount of time needed to cool the packed product is considerably less for open trays than that for more closed boxes, as used in the last container experiment. Hence, in open trays the product will experience much more the temperature fluctuations in the supply air during cool unit cycling. Hence, the effect of packaging has to be taken into account in the control algorithm. More research (model and experimental study) is needed on the humidity conditions in the packaging, as a function of packaging design and external conditions as airflow velocity, temperature and relative humidity. This research is an extension of the work by Vollebregt (2001).

Special designed boxes (measuring 30 x 40 x 15 cm) for container transport have been developed at ATO in other research projects, such as a modified humidity packaging for bell peppers, and modified atmosphere packaging for broccoli. These new packaging designs have a large impact on the product quality compared to existing packaging designs. We view that optimizing the packaging design will proof another way to reduce energy consumption.

The product quality change model needs to be validated using subsequent experiments. Also, similar models will be developed for other produce such as tomatoes, bell peppers etc. The focus of these models will be the link with respiration of the produce. If this link can be established, monitoring quality during transport can give an indication of the quality change of the product. Hence, in further research we will cooperate closely with the people in the project working on the experiments on respiration.

References

- Boogaard H.A.G.M., et al., 2001. *Acta Hort.*, proceedings CA2001, Rotterdam, in press.
- Jolly P.G., et al. 2000. Simulation and measurement on the full-load performance of a refrigeration system in a shipping container. *Int. J. Refr.* **23**(2): 112-126.
- Hertog, M.L.A.T.M., Nicholson, S.E., and Banks N.H. (2001). The effect of modified atmospheres on the rate of firmness change in 'Braeburn' apples. *Postharvest Bio. Techn.* **23**: 175-184.
- Peppelenbos, H.W. 1996. The use of gas exchange characteristic to optimize CA storage and MA packaging of fruits and vegetables. *Ph.D. Thesis* Univ. Wageningen, the Netherlands.
- van der Sman, R.G.M. 2002. Prediction of airflow through a vented box by the Darcy-Forchheimer equation. *J. Food Eng.*, in press.
- Tijskens L.M.M. and Polderdijk J.J. (1996). A generic model for keeping quality of vegetable produce during storage and distribution. *Agric. Syst.* 51: 431-452.
- Tijskens L.W. et al. 1997. Modelling the firmness of 'Elstar' apples during storage and transport. *Acta Hort.* **485:** 363-.
- Tijskens L.M.M. et.al. (1998) Kinetics of polygalacturonase activity and firmness of peaches during storage. *J. Food Eng.* **35**: 111-126.
- Verdijck, G.J.C., Lukasse, L.J.S., and Sillekens J.J.M. 2000. Aspects of Control Structure Selection in Post-Harvest Processes. *Proc. Agri-Control 2000*, Wageningen, the Netherlands.
- Vollebregt H.M. 2001. Modelling the effect of cross-flow on the climate in transport containers for perishable goods. *Final report of the post-graduate program* Mathematics for Industry, Stan Ackermans Institute, Eindhoven University of Technology

List of publications related to the research of the modeling work in this project

- R.G.M. van der Sman, and H.S. Yun, Modelling air flow in vented box packed with produce. *Refr. Sci. Techn.* Proc. Improving Postharvest Techn. Fruits, Vegetables and Ornamentals. Murcia, Spain: 866-871. (2001).
- Lukasse, L., R.G.M. van der Sman, et.al. Reefer containers, status quo and new developments. *Koude & Luchtbehandeling* 94(6):22-27 (2001).
- R.G.M. van der Sman, G.J.C. Verdijck. Model predictions and control of conditions in a CA-reefer container. *Acta Horticulturea* Proc. CA2001, Rotterdam, the Netherlands, in press (2002).
- R.G.M. van der Sman. Prediction of airflow through a vented box by the Darcy-Forchheimer equation. *J. Food Eng.*, in press (2002).
- H.M. Vollebregt. Modelling the effect of cross-flow on the climate in transport containers for perishable goods. *Final report of the post-graduate program* Mathematics for Industry, Stan Ackermans Institute, Eindhoven University of Technology (2001).

Refrigerant circuit model

R.G.M. van der Sman[1], P.G. Jolly[2], S. Duraisamy[2], K. Chuang[2]
[1]Agrotechnological Research Institute (ATO),
Wageningen University and Research, the Netherlands
[2]Carrier Transicold, Syracuse N.Y., U.S.A.

1. Introduction

For the model-predictive control, one needs to predict the energy consumption of the refrigerant circuit. Furthermore, one needs to predict the climate conditions of the airflow, leaving the evaporator coil. In this document we describe the model predicting these quantities.

In the model we will consider two situations:
- full load
- partial load

At full load the refrigerant circuit is not able to cool the air down to the temperature setpoint, because the cooling capacity is at its maximum value (it is fully loaded). If the temperature setpoint is meet, the cooling capacity is matched to the cooling demand (hence the cooling unit is partially loaded). Below we will describe the working of the refrigerant circuit in both situations. We will start with the more complex situation of partial loading of the cooling unit.

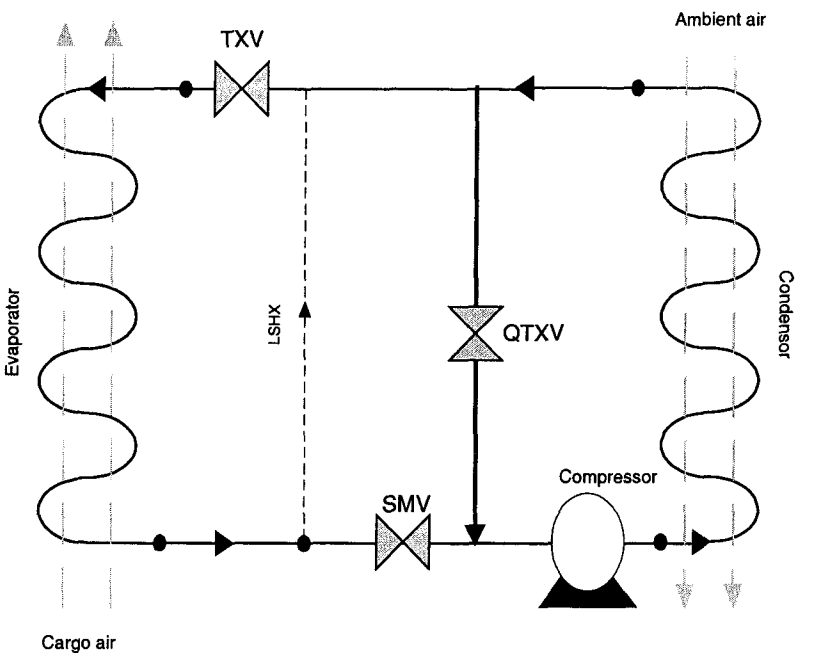

Figure 1.1 Refrigerant circuit with relevant components for the partial load case.

In figure 1.1 we have depicted the refrigerant circuit with relevant components for the case of partial load. We have distinguished the following components:
- Evaporator coil
- Compressor
- Condenser coil
- Thermostatic expansion valve (TXV)
- Liquid Suction-line Heat Exchanger (LSHX)
- Suction Modulation Valve (SMV)
- Quench line (QTXV)

The evaporator coil exchanges heat between the cargo air and the refrigerant flow. The heat is abosrbed by the evaporation of the refrigerant. The condenser coil exchanges heat between refrigerant flow and the ambient air. The heat is released by condensation of the refrigerant. In order to acquire a condensation temperature lower than the ambient temperature, the air is rised to high pressure by the compressor. This is the only component of the refrigerant circuit consuming electrical power. An evaporation temperature of the refrigerant lower than the setpoint requires low pressure in the evaporator coil. The pressure drop between condensor and evaporator is achieved by the TXV.

The cooling capacity is controlled by the SMV, which regulates the amount of refrigerant flow by inducing an extra pressure drop in the refrigerant circuit. We have incorporated two extra components, LSHX and QTXV, which induce some extra performance and security of the system. The LSHX transfers some heat from the liquid line (entering the evaporator coil) to the suction line (entering the compressor). The quench-line transfers hot refrigerant from the liquid line to the suction line, thereby preventing liquid refrigerant (leaving the evaporator) from entering the compressor.

At full load the refrigerant flow is at its maximum (the SMV is fully open), and the refrigerant flow through the quench is negligible. In the full load model, we do not consider these components. Figure 1.2 shows the refrigerant circuit considered for the full load case.

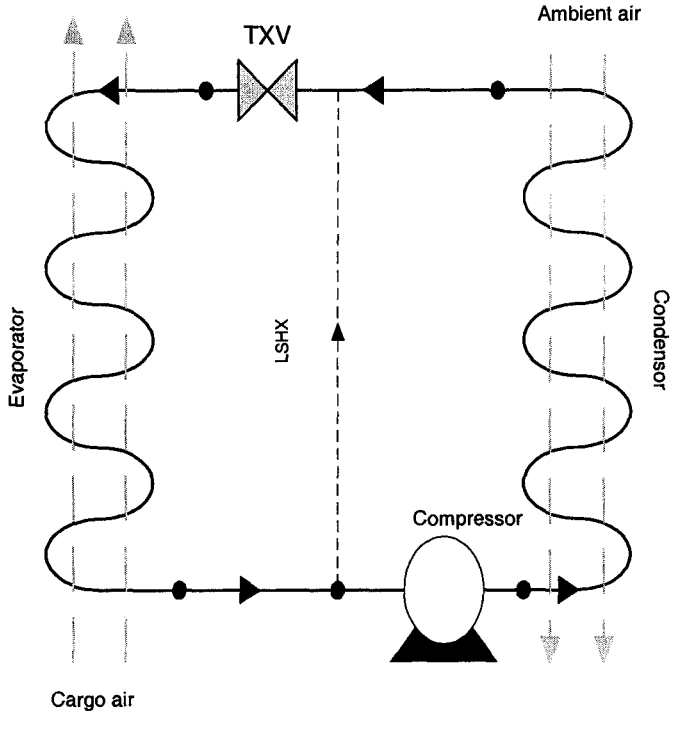

Figure 1.2 Refrigerant circuit with relevant components for the full load case.

For both models we will state heat and mass balances. These balance equations will be augmented with constitutive equations describing the operations of the various components. The balance equations of both models will be described in section 2. The component models, stating the constitutive equations, are described in section 3. Thermodynamic properties of refrigerant and air, which are needed for our models are described in section 4. The method of solution of these models we will describe in section 5. The model is validated against a detailed model from the manufacturer of the cooling unit. These results will be presented in section 6.

2. Heat balance equations

2.1 List of symbols

Symbols

$c_{p,a}$	specific heat of air	[J/kg.K]
h	specific enthalpy	[J/kg]
p	pressure	[Pa]
v	velocity	[m/s]
x_q	quality of refrigerant	[-]
y	mass fraction	[-]
A	area	[m^2]
ΔH	heat of vaporatization	[J/kg]
I	electrical current	[A]
M	molar weight	[kg/mol]
P	power	[J]
Q	heat flow	[J/s]
R	gas constant	[J/mol.K]
S	surface face area	[m^2]
T	temperature	[K]
α	heat transfer coefficient	[$W/m^2.K$]
β_a	thermal expansion coefficient of air [$kg/m^3.K$]	
ϕ	mass flow	[kg/s]
ρ	mass density of air	[kg/m^3]
Φ	volumetric flow rate	[m^3/s]

Subscripts

a	airflow
amb	ambient
coil	evaporator coil surface
comp	compressor
cond	condenser
evap	evaporation
hx	heat exchange
moist	condensed moisture
sat	saturated
sh	superheated
shc	superheat at compressor suction line
shv	superheated vapour
suct	suction
w	water removed by coil
z	zero celsius
C	condenser
E	evaporator
L	quench-line
LS	liquid-suction heat exchanger
R	refrigerant

2.2 Heat flowsheet partial load model

The heat flows in the partial load model and their connections are shown in the network diagram of figure 2.1. By applying the theorem of Kirchhoff (at each knot of the network the sum of heat flows is zero), we can state the list of heat balance equations governing the system.

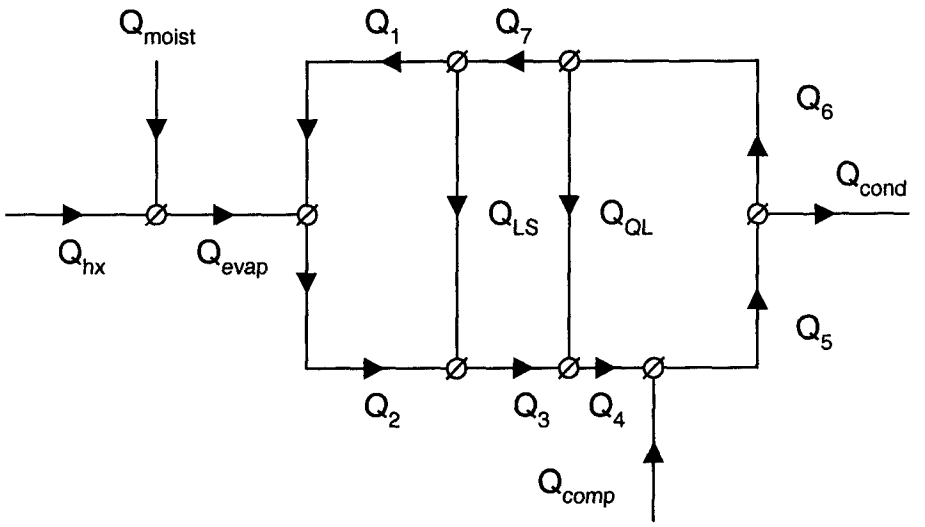

Figure 2.1 The heat flows in the refrigerant circuit in the case of partial load.

The governing heat balance equations are given by:

$$Q_1 = Q_7 - Q_{LS} \quad (2.1.1)$$
$$Q_2 = Q_1 + Q_{evap} \quad (2.1.2)$$
$$Q_3 = Q_2 + Q_{LS} \quad (2.1.3)$$
$$Q_4 = Q_3 + Q_{QL} \quad (2.1.4)$$
$$Q_5 = Q_4 + Q_{comp} \quad (2.1.5)$$
$$Q_6 = Q_5 - Q_{cond} \quad (2.1.6)$$
$$Q_7 = Q_6 - Q_{QL} \quad (2.1.7)$$
$$Q_{hx} = Q_{evap} - Q_{moist} \quad (2.1.8)$$

These equations are augmented with the following constitutive equations, which are described in detail in the component models in the next section.

$$Q_{evap}=Q_{evap}(\phi_{R,E}, T_{a,in}, \phi_a, y_{in}, T_{evap}) \quad (2.2.1)$$
$$Q_{LS} = Q_{LS}(T_{cond}-\Delta T_{sub}, T_{evap}+\Delta T_{sh}) \quad (2.2.2)$$
$$Q_{comp}=Q_{comp}(T_{suct}, T_{cond}, \phi_{R,C}) \quad (2.2.3)$$
$$Q_{cond}=Q_{cond}(T_{cond}, T_{amb}) \quad (2.2.4)$$
$$\phi_{R,C}=\phi_{R,C}(T_{cond}, T_{suct}) \quad (2.2.5)$$
$$Q_{QL}=Q_{QL}(\phi_{R,L}, T_{cond}-\Delta T_{sub}) \quad (2.2.6)$$
$$Q_{hx} = Q_{hx}(T_{a,in}, T_{a,out}, \phi_a) \quad (2.2.7)$$
$$Q_{moist}= Q_{moist}(\phi_{R,E}, T_{evap}, T_{a,in}, y_{in}) \quad (2.2.8)$$

The refrigerant mass flows are related:

$$\phi_{R,C}=\phi_{R,E} + \phi_{R,L} \quad (2.2.9)$$

We assume the following variables are specified:

$$T_{a,in}, \phi_a, y_{in}, \Delta T_{sub}, \Delta T_{sh}, T_{amb}, T_{a,out}, \Delta T_{shc}$$

Here ΔT_{sub}, ΔT_{sh}, ΔT_{shc} are design parameters, and represent the amount of subcooling or superheating of the refrigerant. The manufacturers takes the following values: ΔT_{sub}=4°C, ΔT_{sh}=2°C, ΔT_{shc}=25°C.

The set of heat balance equations are solved for the following variables: $Q_1..Q_7$. However, it is more practical to relate some heat flows to refrigerant mass flow rates, specific enthalpies and temperatures. In our model we have reformulated the heat flows as follows:

$$Q_1 = \phi_{R,E}\, h_{E,in} \quad (2.3.1)$$
$$Q_2 = \phi_{R,E}\, h_{vap}(T_{evap,}+\Delta T_{sh}, p_{R,sat}(T_{evap})) \quad (2.3.2)$$
$$Q_3 = \phi_{R,E}\, h_{shv}(T_3,\ p_{R,sat}(T_{evap})) \quad (2.3.3)$$
$$Q_4 = \phi_{R,C}\, h_{shv}(T_{suct},\ p_{R,sat}(T_{suct}-\Delta T_{shc})) \quad (2.3.4)$$
$$Q_5 = \phi_{R,C}\, h_{dis} \quad (2.3.5)$$
$$Q_6 = \phi_{R,C}\, h_{liq}(T_{cond}-\Delta T_{sub},\ p_{R,sat}(T_{cond})) \quad (2.3.6)$$
$$Q_7 = \phi_{R,E}\, h_{liq}(T_{cond}-\Delta T_{sub},\ p_{R,sat}(T_{cond})) \quad (2.3.7)$$

Here h_{vap}, and h_{liq} represent the specific enthalpy of vapour and liquid at saturation. The function h_{shv} represents the specific enthalpy of superheat vapour. Remember that the enthalpy of a gas is a function of both temperature and pressure.

By our reformulation of the heat flows, we obtain another set of unknown variables for which the model will be solved:

$$\phi_{R,E},\ T_{evap},\ T_{cond},\ T_{suct},\ h_{E,in},\ h_{dis},\ T_3$$

2.3 Heat flowsheet full load model

The heat flows in the full load model and their connections are shown in the network diagram of figure

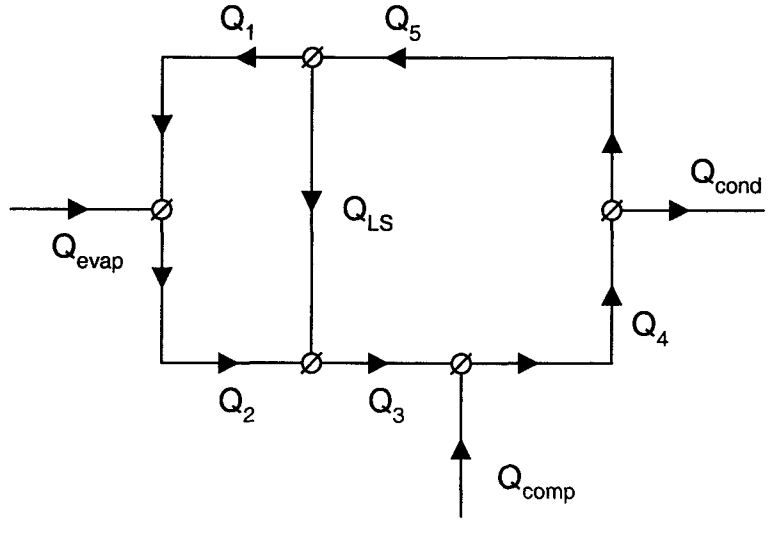

Figure 2.2 The heat flows in the refrigerant circuit in the case of full load.

By applying the theorem of Kirchhoff we obtain the list of heat balance equations:

$$Q_1 = Q_5 - Q_{LS} \quad (2.4.1)$$
$$Q_2 = Q_1 + Q_{evap} \quad (2.4.2)$$
$$Q_3 = Q_2 + Q_{LS} \quad (2.4.3)$$
$$Q_4 = Q_3 + Q_{comp} \quad (2.4.4)$$
$$Q_5 = Q_4 - Q_{cond} \quad (2.4.5)$$

The constitutive equations are given by:

$$Q_{evap}=Q_{evap}(\phi_R, T_{a,in}, \phi_a, y_{in}, T_{evap}) \quad (2.5.1)$$
$$Q_{LS} = Q_{LS}(T_{cond}-\Delta T_{sub}, T_{evap}+\Delta T_{sh}) \quad (2.5.2)$$
$$Q_{comp}=Q_{comp}(T_{evap}, T_{cond}, \phi_R) \quad (2.5.3)$$
$$Q_{cond}=Q_{cond}(T_{cond}, T_{amb}) \quad (2.5.4)$$
$$\phi_R=\phi_R(T_{evap}, T_{cond}) \quad (2.5.5)$$

Here T_{amb}, $T_{a,in}$, ϕ_a, and $y_{a,in}$ are specified by the conditions of the air entering the coil, the ambient air and the flow rate of the evaporator fan. ΔT_{sub} and ΔT_{sh} are design parameters of the circuit, and are also specified.

The system is solved for the heat flows $Q_{1\text{-}5}$, for which we use the following reformulations:

$$Q_1 = \phi_R\, h_{E,in} \quad (2.6.1)$$
$$Q_2 = \phi_R\, h_{vap}(T_{evap}+\Delta T_{sh}) \quad (2.6.2)$$
$$Q_3 = \phi_R\, h_{suct} \quad (2.6.3)$$
$$Q_4 = \phi_R\, h_{dis} \quad (2.6.4)$$
$$Q_5 = \phi_R\, h_{liq}(T_{cond}-\Delta T_{sub}) \quad (2.6.5)$$

This transforms the set of unknowns to the following set:

$$h_{E,in},\ T_{evap},\ h_{suct},\ h_{dis},\ T_{cond}$$

3. Component models

3.1 Evaporator model

In many models one assume a log-mean temperature model for the evaporator. However, we have experienced that the numerical solver has difficulties to convergence by the usage of such a model. A better approach is to divide the evaporator in control volumes, for which microbalances for heat and mass are stated, as such in figure 3.1. Below we will describe such a model.

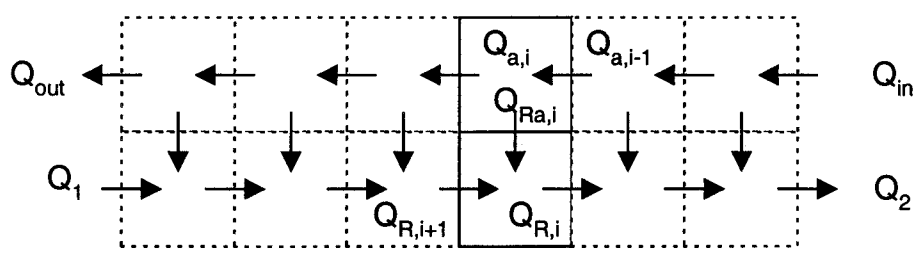

Figure 3.1 Heat microbalances in the evaporator coil, divided in 6 control volumes.

From the figure follows the heat microbalance for control volume *i*:

$$Q_{a,i-1} = Q_{Ra,i} + Q_{a,i}$$
$$Q_{R,i} = Q_{Ra,i} + Q_{R,i+1} \quad (3.1.1)$$

The mass microbalance for control volume *i* reads:

$$\phi_{v,i-1} = \phi_{w,i} + \phi_{v,i} \quad (3.1.2)$$

Note that $\phi_{w,i}$ is the rate of moisture condensation on section of the evaporator coil. The moisture is assumed to drip off the coil. Hence, this is a sink term for the mass microbalance.

The set of equations are closed by various constitutive relations. The rate of moisture condensation is given by:

$$\begin{aligned} &\phi_{w,i} = \beta_{air} A_{ext,i} (c_{a,i} - c_{sat,i}), \qquad \text{if } (c_{a,i} > c_{sat,i}) \text{ otherwise } \phi_{w,i}=0 \\ &c_{sat,i} = c_{sat,i} (T_{coil,i}) \\ &\phi_{v,i} = y_i \phi_a \\ &c_{a,i} = y_i \rho_a(T_{a,i}) \end{aligned} \tag{3.1.3}$$

Here $T_{coil,i}$ is the coil surface temperature in control volume *i*, which will be determined by the heat microbalance. The density of the air varies the temperature $T_{a,i}$.

For the various heat fluxes the following relations hold:

$$\begin{aligned} &Q_{a,i} = \phi_a h_{a,i} \\ &Q_{R,i} = \phi_R h_{R,I} \end{aligned} \tag{3.1.4}$$

With the enthalpies defined as:

$$\begin{aligned} &h_{a,i} = c_{p,a} (T_{a,i} - T_{ref}) + \Delta H_w y_i \\ &h_{R,i} = x_i h_{vap}(T_{evap}) + (1-x_i) h_{liq}(T_{evap}) \end{aligned} \tag{3.1.5}$$

For a given T_{evap}, the quality of the refrigerant x_i in the control can be computed. Consequently, by the definition of the enthalpy the refrigerant temperature can be computed.

The transferred heat from coil surface to the refrigerant is given by:

$$Q_{Ra,i} = \alpha_{coil} A_{int,i} (T_{coil,i} - T_{R,i}) \tag{3.1.6}$$

The transferred heat from air to is given by:

$$Q_{Ra,i} = \alpha_{air} A_{ext,i} (T_{a,i} - T_{coil,i}) + \phi_{w,i} \Delta H_w - \phi_{w,i} c_{p,w} (T_{coil,i} - T_{ref}) \tag{3.1.7}$$

Here $A_{ext,i}$ is the (external) surface area of the coil in the control volume, and hence $\Sigma_i A_{int,i}=A_{int}$, and $\Sigma_i A_{ext,i}=A_{ext}$. With $T_{ref}=0°C$. The air velocity is obtained for the air mass flow, and the cross section area of the evaporator coil S_{coil}:

$$v_{air} = \phi_a / \rho_a(T_{a,in}).S_{coil} \tag{3.1.8}$$

The mass transfer coefficient β_{air} is calculated using the fact that the Lewis number for air is nearly 1.

$$Le = 1 = (\alpha_{air}/\rho_a.c_{p,a}) / \beta_{air} \tag{3.1.9}$$

3.2 Heat transfer coefficients at air and refrigerant side

We assume the heat transfer coefficients to be linear dependent on the air velocity, following a well-known correlation for airflow over a flat wall (ASHRAE):

$$\alpha_{air} = \alpha_{air,0} + \alpha_{air,1} v_{air} \tag{3.2.1}$$

Fitting manufacturers data we have found that $\alpha_{air,0}$ = 17 W/m^2.K , and $\alpha_{air,1}$=29 J/m^3.K. However, we have found a better fit of our evaporator model (compared to the detailed model of the manufacturer) for other values: $\alpha_{air,0}$ = 0 W/m^2.K , and $\alpha_{air,1}$= 25 J/m^3.K.

For the heat transfer on the refrigerant side, we follow the usual theory, which state that the heat transfer coefficient clearly depends on the quality of the refrigerant. Hence, distinction must be made between superheated zone and two-phase zone.

In the superheated zone, the heat transfer coefficient α_{sh} is given by the Dittus-Boelter correlation (Jolly et.al.,2000)

$$Nu_{sh} = \alpha_{sh}\, d_{tube} / \lambda_{vap} = 0.023\, Re^{0.8}\, Pr^{0.4} \qquad (3.2.2)$$

We expect little variation in the physical properties of the refrigerant vapour with temperature.

For the two-phase zone a correlation with the Martinelli number X_{tt} is widely used (Wang,1991):

$$\alpha_{2ph}/\alpha_{liq} = 3 / X_{tt}^{0.66} \qquad \text{if } (x<0.8) \qquad (3.2.3)$$

The numerical coefficient show some variation in literature, and maybe best estimated from experiments.

The Martinelli number is given by:

$$X_{tt} = [(1-x)/x]^{0.9}\, (\rho_{R,vap}/\rho_{R,liq})^{0.5}\, (\mu_{R,liq}/\mu_{R,vap})^{0.1} \qquad (3.2.4)$$

α_{liq} is the heat transfer coefficient for the pure liquid, which also follows the Dittus-Boelter, but now with the properties of the refrigerant liquid:

$$Nu_{liq} = \alpha_{liq}\, d_{tube} / \lambda_{liq} = 0.023\, Re^{0.8}\, Pr^{0.4} \qquad (3.2.5)$$

If ($x>x_d$ = 0.8) the liquid is in the dry-out regime, for which a quadratic interpolation between α_{2ph} and α_{sh} is applied:

$$\alpha_{do} = \alpha_{2ph} - [(x-x_d)/(1-x_d)]^2\, (\alpha_{2ph} - \alpha_{sh}) \qquad (3.2.6)$$

In the evaporator the temperature of the refrigerant does not change much, hence the ratios of the density and viscosity of vapour and liquid does not change much.

Other relevant parameters for liquid van vapour phase of the R134a refrigerant are given in the Table below, which are taken from NIST data (RefProp).

Parameter	Liquid	Vapour
λ (W/m.K)	0.094	0.012
μ (μPa.s)	285.7	10.9
ρ (kg/m^3)	1294	14.23
C_p (kJ/kg.K)	1.320	0.828

For the calculation of the heat transfer from air to refrigerant flows, the dimensions of the coil have to be known. Data of the manifacturer state that refrigerant tube diameter = d_{tube}=9.2 mm, internal area of the tubes: A_{int}=4.5 m^2, external surface area of the fins A_{ext} = 50.5 m^2. Face area of the coil is S_{coil}= 0.65 m^2. Heat resistance of metal fins and tube: h_{metal} = 631 W/m^2.K, which is negligible compared to the heat transfer by air or refrigerant.

3.3 Condenser model

This model computes the amount of released heat by the condenser. As a first approximation we assume that the transferred heat is proportional with the temperature difference between air and refrigerant:

$$Q_{cond} = UA_C \, (T_{cond} - T_{amb}) \qquad (3.3.1)$$

We have tested this hypothesis with data obtained form a detailed model of the manufacturer. Here we have varied the ambient temperature (between 0 and 20°C) and the condensation temperature. By using linear regression we estimated that UA_C = 1048 W/K. Comparison between our simple model, given by Eq.(3.3.1) and the detailed manufacturers model is shown in figure 3.3.1.

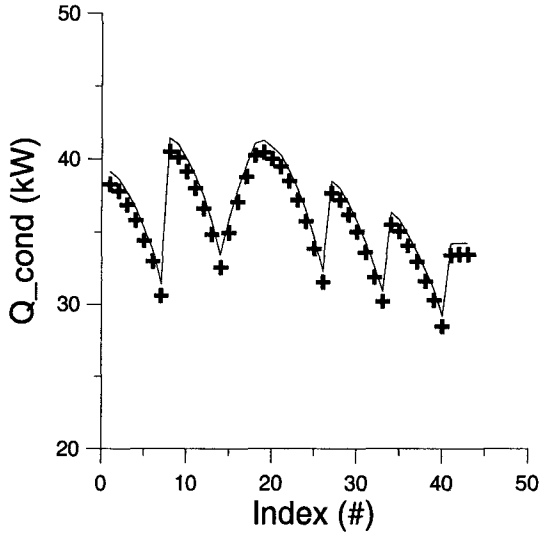

Figure 3.3.1 Comparison of model prediction (symbols) and manufacturers data (lines).

For the general case, Eq.(3.3.1) would probably be invalid, but for our application of (mainly) sea transport of persihables, thus limiting the range of T_{amb} and T_{cond}, we think Eq.(3.3.1) is a good first approximation.

3.4 Compressor model

This submodel predicts the consumed electrical power by the compressor, the amount of heat dissipated by the compressor in the refrigerant circuit, and the amount of refrigerant displaced by the compressor.

From manufacturers information one can state that the electrical power consumed by the compressor can be divided in a constant power needed to overcome the friction P_{fric} (which is only proportional with the compressor speed) and a power for the mechanical compression P_{work}:

$$P_{comp} = P_{fric} + P_{work} \qquad (3.4.1)$$

For P_{work} one can use the following correlation:

$$P_{work} = p_{suct} . \Phi_R \, (\gamma_1 + \gamma_2 \, r_p) \qquad (3.4.2)$$

Here p_{suct} is the pressure at the suction line of the compressor, Φ_R is the volumetric displacement of the refrigerant, and r_p is the pressure ratio between discharge and suction pressure $r_p = p_{dis}/p_{suct}$.

Regression analysis of manufacturers data (at 50 Hz) shows:

$$P_{fric} = 600\ W,\ \gamma_1 = 1.234,\ \gamma_2 = 0.258$$

The results of the regression analysis for Eq.(3.4.2) is shown in figure 3.4.1 Here we have plotted the rescaled power: $P' = P_{work} / p_{suct}.\Phi_R$ versus the pressure ratio r_p.

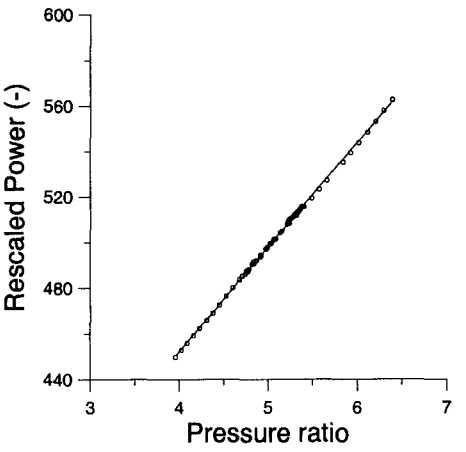

Figure 3.4.1 Rescaled power for mechanical work (corrected for friction) versus pressure ratio

Analysis of 60Hz data shows that both P_{fric} and P_{work} are proportional with the compressor speed, which is proportional with the applied mains frequency. Hence previous results have to be rescaled with the ratio in frequency. (For 60 Hz the ratio is 6/5).

According to the manufacturers model, one can state that the volumetric displacement Φ_R is linear with the pressure ratio $r_p = p_{dis}/p_{suct}$. Regression analysis of the simulation data of the manufacturers data state that (see also figure 3.4.2):

$$\Phi_R = 0.01638 - 0.00068\ r_p \quad (3.4.3)$$

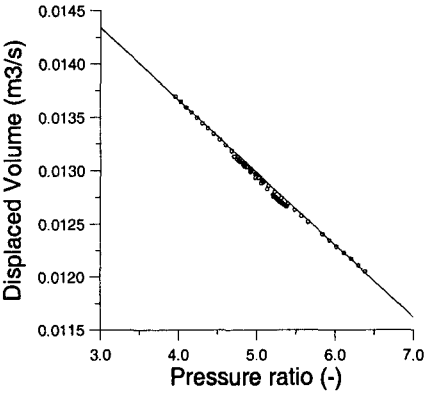

Figure 3.4.2 Volumetric displacement of compressor versus the pressure ratio

The suction and discharge pressures are equal to the saturation pressures of the refrigerant at the evaporation temperature T_{evap} and the condensation temperature T_{cond} respectively. The expressions for these relations are listed in section 4.

The mass flow rate of the refrigerant is linear with the volumetric displacement and the mass density at the suction temperature T_{suct}. The mass density can be computed by assuming the

refrigerant gas to be an ideal gas (which hold for temperatures well below the critical temperature T_{crit}≈100°C). Hence, we have

$$\phi_R = \rho_R(T_{suct})\, \Phi_R \qquad (3.4.4)$$

The expression for the mass density is given in section 4. Below in figure 3.4.3 we compare the data computed with Eq.(3.4.4) with the data from the manufacturers model.

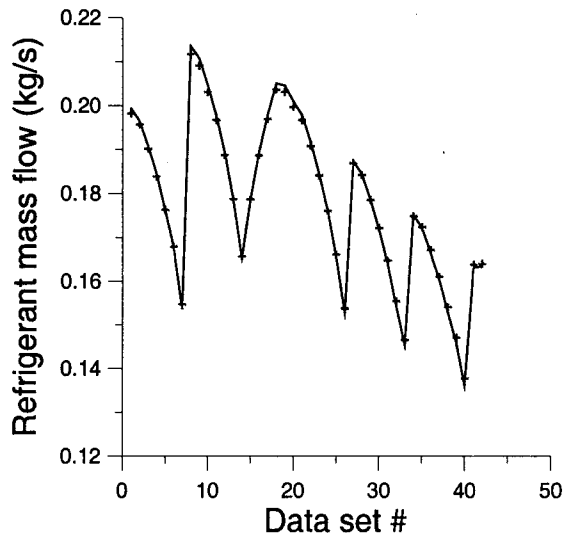

Figure 3.4.3 Manufacturers data versus prediction by Eq.(3.4.4).

The major fraction of the heat generated by the compressor is absorbed by the refrigerant, Q_{comp}. From the manufacturers data we relate the electrical power P_{comp} to the change in enthalpy of the refrigerant, see figure 3.4.4. From regression analysis we obtain:

$$Q_{comp} = 0.805\, P_{comp} \qquad (3.4.5)$$

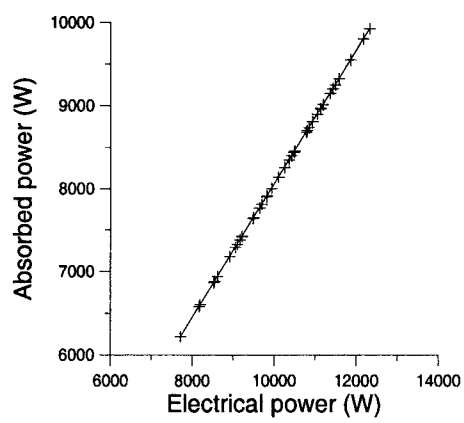

Figure 3.4.4 Heat from the compressor absorbed by the refrigerant versus the consumed electrical power.

3.5 Heat exchanger

There is a heat exchanger line between the liquid and suction line (LSHX). This submodel gives a constitutive relation for the heat transferred between suction and liquid line. The heat exchanger is a simple counter flow shell-and-tube heat exchanger, as drawn schematically in figure 3.5.1.

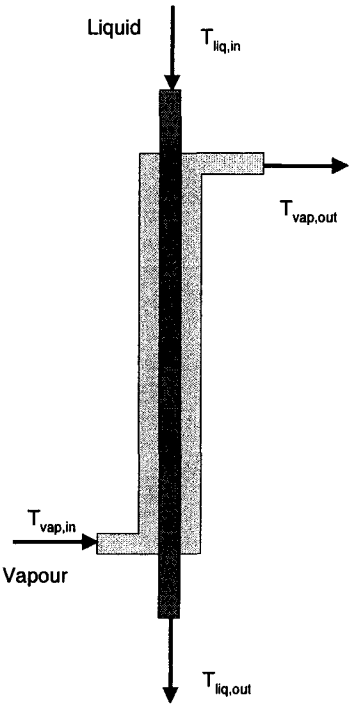

Figure 3.5.1 Shell and tube LSHX heat exchanger

The inlet temperatures of vapour and liquid are given by:

$$T_{liq,in} = T_{cond} - \Delta T_{sub}$$
$$T_{vap,in} = T_{evap} + \Delta T_{sh} \qquad (3.5.1)$$

We assume that the transfer heat is proportional to the temperature difference between liquid and vapour, and that the heat transfer coefficient is dependent on these temperatures and the mass flow rate:

$$Q_{LS} = UA_{LS}(T_{liq,in}, T_{vap,in}, \phi_R)\,(\,T_{liq,in} - T_{vap,in}\,) \qquad (3.5.2)$$

By regression of manufacturers data, see figure 3.5.2, we have found:

$$UA_{LS} = 2.68 + 0.438\,T_{evap} - 0.144\,T_{cond} + 346\,\phi_R \qquad (3.5.2)$$

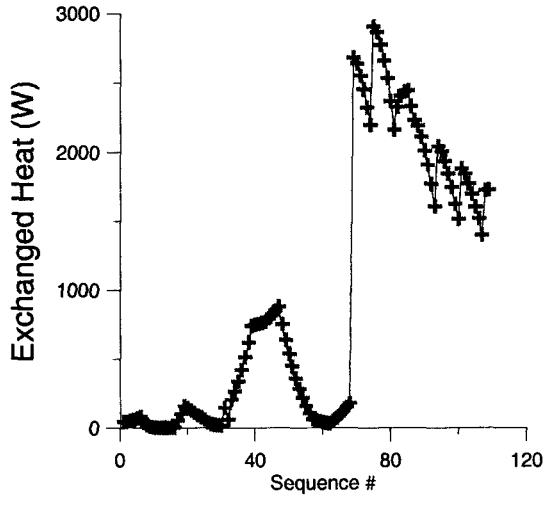

Figure 3.5.2 Exhanged heat according to manufacturers model (symbols) and Eq.(3.5.2).

3.6 Suction Modulation Valve

This valve induces an extra pressure loss in the suction line, and thereby reducing the volumetric displacement of the refrigerant (as stated by Eq.(3.4.3)). The resulting pressure p_{suct} can be identified by the saturation temperature T_{suct} of the gas at that pressure:

$$p_{suct} = p_{R,sat}(T_{suct}) \qquad (3.6.1)$$

For the partial load case we can use T_{suct} as a variable for matching the flow rate to the required cooling demand $Q_{hx}+Q_{moist}$.

3.7 Quench line

The quench line draws a portion of the subcooled liquid ($\phi_{R,QL}$), leaving the condensor, and expands it to vapour at the suction pressure p_{suct} and injects it into the gas flow entering the compressor, therby ensuring a superheat of ΔT_{shc}=25°C. The heat flowing through the quench line is given by:

$$Q_{QL} = \phi_{R,QL}\, h_{liq}(T_{cond}-\Delta T_{sub}) \qquad (3.7.1)$$

4. Thermal properties of fluids

4.1 Refrigerant vapour properties

Enthalpies for saturated vapour and liquid
In general the enthalpy of the refrigerant is a complex function of the temperature and the pressure. At saturation the temperature and pressure are related (see below). Hence, the enthalpies for saturated liquid and vapour can be given as a function of their saturation temperature. We have approximated it with a quadratic function of temperature in the range between –10 and +85°C. For the vapour phase the enthaply (in kJ/kg) is equal to:

$$h_{vap}(T) = h_{vap}(T_z) + 0.625\,(T - T_z) - 0.00250\,(T - T_z)^2 \quad [kJ/kg.K] \qquad (4.1.1)$$

and the liquid phase:

$$h_{liq}(T) = h_{liq}(T_z) + 1.316\,(T - T_z) + 0.00283\,(T - T_z)^2 \quad [kJ/kg.K] \qquad (4.1.2)$$

with T_z = 273.15 K = 0°C. Note, $\Delta H_z = h_{vap}(T_z) - h_{liq}(T_z)$ = 201 kJ/kg. In figure 4.1 we have depicted the change of enthalpy of both phases with temperature. Near the critical point (about 100°C) the enthalpy of both phases becomes about equal.

The heat of vaporisation of the refrigerant is about by substracting (4.1.1) from (4.1.2):

$$\Delta H_R(T) = \Delta H_z - 0.69\,(T - T_z) - 0.0063\,(T - T_z)^2 \qquad (4.1.3)$$

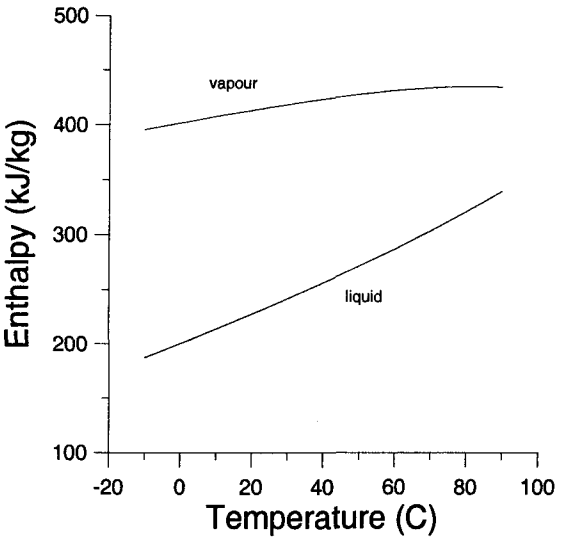

Figure 4.1 Change of specific enthalpy with temperature for refrigerant R134a.

Enthalpy of superheated vapour

For the superheated vapour entering the compressor, one needs an expression relating the enthalpy to the temperature and pressure. Because the amount of superheat at the suction line of the compressor is constant (ΔT_{shc}=25°C), and the temperature is well below the critical temperature (T_{suct} < 10°C), we approximate the enthalpy h_{shv} as the saturated vapour enthalpy ($h_{vap}(T_{suct})$) at saturation temperature T_{suct} added with an additional term which is proportional to the temperature ($T_{suct}+\Delta T_{shc}$):

$$h_{shv}(T_{suct}) = h_{vap}(T_{suct}) + 16.65 + 0.07\,(T_{suct} + \Delta T_{shc}) \qquad (4.1.4)$$

The validity of this approximation is shown in figure 4.2, where the manufacturers data is compared to values according to Eq.(4.1.4).

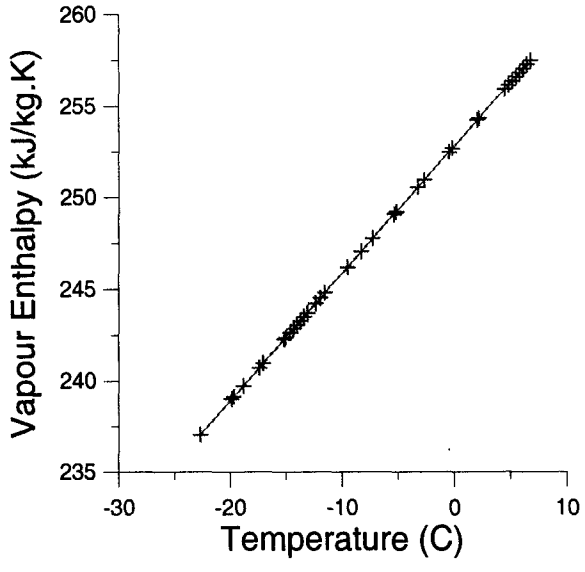

Figure 4.1.4 Prediction of vapour enthalpy entering the compressor, with 25°C superheat.

Saturated vapour pressures

The saturated vapour pressure $p_{sat,R}$ of the refrigerant is related to temperature T_R (in Kelvin) by the Clausius-Clayperon relation:

$$p_{sat}(T_R) = p_{R,0} \exp (- M_R \Delta H_R(T_R) / R.T_R) = p_{R,0} \exp (- \zeta_R \Delta H_R(T_R) / T_R) \quad (4.1.5)$$

From the manufacturers data follows that:

$$p_{R,0} = e^{10.42} \text{ kPa}$$
$$\zeta_R = 6.54 \text{ K.kg/kJ}$$

The relation between the vapour pressure and the temperature of the refrigerant is shown in figure 4.1.5, together with the regression line, as follows from the Clausius-Clapeyron relation Eq.(4.1.5).

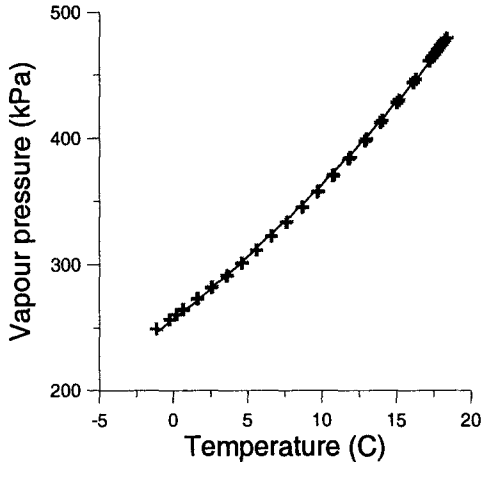

Figure 4.1.5 Saturated vapour pressure of R134a refrigerant versus temperature, according to NIST tables (line) and Clausius-Clapeyron (symbols).

Liquid mass density

Density of refrigerant liquid as a function of temperature T_{evap}, between -10°C and 30°C:

$$\rho_{R,liq}(T_{evap}) = \rho_{R,liq}(T_z) - \beta_{R,liq} (T_{evap} - T_z) \quad (4.1.6)$$

From the NIST-Tables we have $\rho_{R,liq}(T_z)$=1293 kg/m^3, and $\beta_{R,liq}$=3.428 kg/m^3.K.

Vapour mass density

The mass density of refrigerant vapour (well below the critical temperature) follows the ideal gas law:

$$\rho_{R,vap}(T,T_{sat}) = p_{R,sat}(T_{sat})\, M_R / R.T \quad (4.1.7)$$

Here the pressure follows Eq.(4.1.5), with the saturation temperature T_{sat}. From regression of the manufacturers data follows that the molar mass M_R=109.1 g/mol, which is comparable with the molar mass of the pure refrigerant R134a, which is M_R=102.3 g/mol. The difference can be accounted for by the oil added to the refrigerant.

Specific heat of liquid

The specific heat of liquid refrigerant we assume to be linear with temperature:

$$c_{pR,liq}(T_{evap}) = c_{pR,liq}(T_z) + \gamma_{c,liq} (T_{evap} - T_z) \quad (4.1.8)$$

With linear regression applied to the NIST Tables we find $c_{pR,liq}(T_z)$=1.345 kJ/kg.K, and $\gamma_{c,liq}$=0.0031 kJ/kg.K^2.

Specific heat of vapour

The specific heat of refrigerant vapour in equilibrium with liquid at T_{evap} we also assume to be linear with temperature. From the NIST Tables we have for T_{evap} between -10^{0}C and 30^{0}C:

$$c_{pR,vap}(T_{evap}) = c_{pR,vap}(T_z) + \gamma_{c,vap} (T_{evap} - T_z) \quad (4.1.9)$$

With $c_{pR,vap}(T_z)$=0.90 kJ/kg.K, and $\gamma_{c,vap}$=0.0050 kJ/kg.K^2.

4.2 Air properties

Saturated vapour pressure

The saturated water vapour pressure also follows the relation of Clausius-Clapeyron:

$$p_{sat}(T) = p_{w,0} \exp (- \Delta H_w M_w / R.T) \quad (4.2.1)$$

Here the heat of vaporisation is ΔH_w = 2.476 MJ/kg, the molar weight water is M_w = 18 10^{-3} kg/mol, and $p_{w,0}$ = 2.057 10^{11} Pa.

Mass density

The air density changes linear with temperature in the range of 0 to 30^{0}C:

$$\rho_a = \rho_{a,0} - \beta_a (T - T_z) \quad (4.2.2)$$

with $\rho_{a,0}$ = 1.29 kg/m^3 and β_a = 0.0044 kg/m^3.K.

Enthalpy

In the range of –10 to +30^{0}C the specific heat of air is about constant: $c_{p,a}$ = 1.006 kJ/kg.K. Hence, the specific enthalpy of moist air is linear with temperature and with mass fraction of water vapour y_w.

$$h_a(T) = h_a(T_z) + [(1 - y_w) c_{p,a} + y_w (c_{p,w}+\Delta H_w)] (T - T_z) \quad (4.2.3)$$

Here $c_{p,a}$ = 1 kJ/kg.K is the heat capacity of dry air, and $c_{p,w}$ = 2 kJ/kg.K is the heat capacity of water vapour.

5. Solution methods

5.1 Evaporator model

We assume the following know variables:

- The air temperature entering the coil: $T_{a,in}$
- The humidity of the air entering the coil: y_{in}
- The mass flow rates: ϕ_a, ϕ_R
- Evaporation temperature: T_{evap}
- The amount of superheating: ΔT_{sh}

Hence, the heat flows Q_{in}, Q_2 and the mass flow $\phi_{v,in}$ at the air intake side of the evaporator are known. In the first control volume, we assume the temperatures to equal to $T_{a,1} = T_{a,in}$ and $T_{R,1}=T_{evap}+\Delta T_{sh}$. Via an iterative solution of the microbalances for each control volume, starting at the air inlet side, we will solve the model for the following variables:

- The air temperature leaving the coil: $T_{a,out}$
- The humidity of air leaving the coil: y_{out}
- The amount of removed moisture: $\phi_w = \Sigma_i \phi_{w,i}$
- The amount of removed heat: $Q_{evap} = \Sigma_i Q_{Ra,i}$

At each iteration step we solve the microbalances given in section 3.1. The heat microbalance is iteratively solved for the surface temperature by the bisection method, which is chosen for its robustness. After calculating the transferred heat and mass, $Q_{Ra,i}$ and $\phi_{w,i}$, we calculate heat and mass flows entering or leaving the next control volume, $Q_{R,i+1}$, $Q_{a,i+1}$, and $\phi_{v,i+1}$. Using these flows and the constitutive relations, we calculate the refrigerant temperature, air temperature and air humidity in the next control volume.

Finally we end up with the control volume at the refrigerant inlet side. The heat and mass flow leaving the coil gives us the temperature and humidity of the air. By summation of the transferred heat and moisture at each control volume, we calculate Q_{evap} and ϕ_w.

We have tested the evaporator model against data of the manufacturers, build for the case of full loading of the evaporator coil. In our model we have divided the evaporator in 6 control volumes. By using the relations for the heat and mass transfer coefficients as stated in section 3.2, we obtained good results, as shown in figures 5.1 and 5.2. For figure 5.1 we used data from the manufacturers model for a full loaded refrigeration unit.

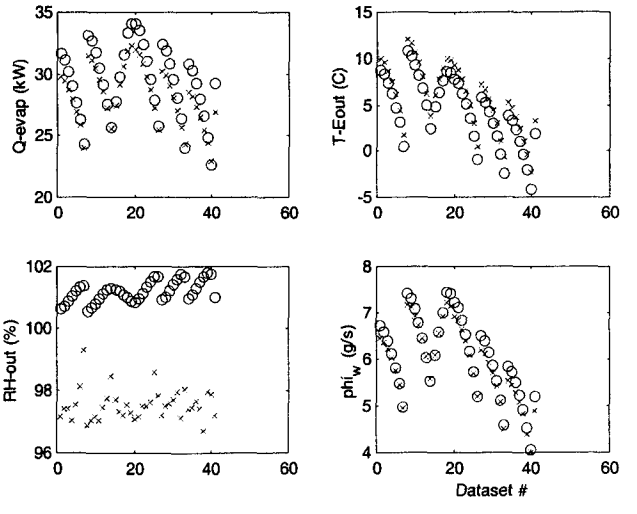

Figure 5.1 Comparison control volume evaporator model with manufacturers model for the full load case.

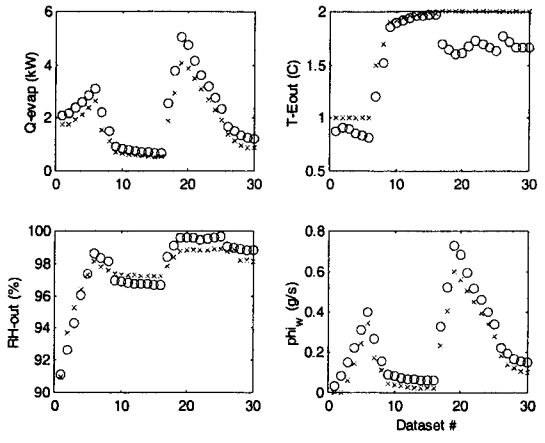

Figure 5.2 Comparison control volume evaporator model with manufacturers model for the partial load case.

The control volume model gives very reasonable predictions of the air temperature leaving the evaporator coil (indicated by T-Eout in the figures), the amount of moisture removed (phi_w), and the amount of heat absorbed by the refrigerant (Q_{evap}). The last quantity is an input for the solution of the heat balances, as stated in section 2. The conditions of the air leaving the coil will be an output required for the climate model, describing the climate conditions of air and product inside the cargo space.

5.2 Heat balances for the partial and fully load case

The heat balances as stated in section 2, for both the partial and the full load case, are simultaneously solved by the Newton-Rhapson procedure. As initial guess we take the average value of the variables as calculated by the manufacturers model (i.e. the dataset we will test our model against). Results are shown in figures 5.3 and 5.4.

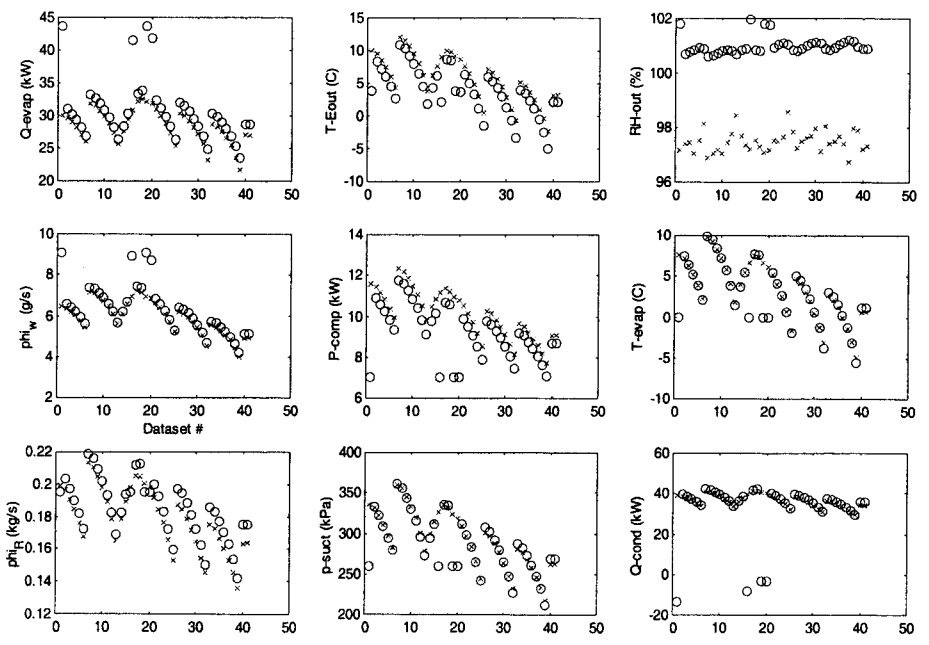

Figure 5.3. Comparision of manufacturers model (crosses) and our model (circles) for a full load case. For 4 data points we obtained no convergency.

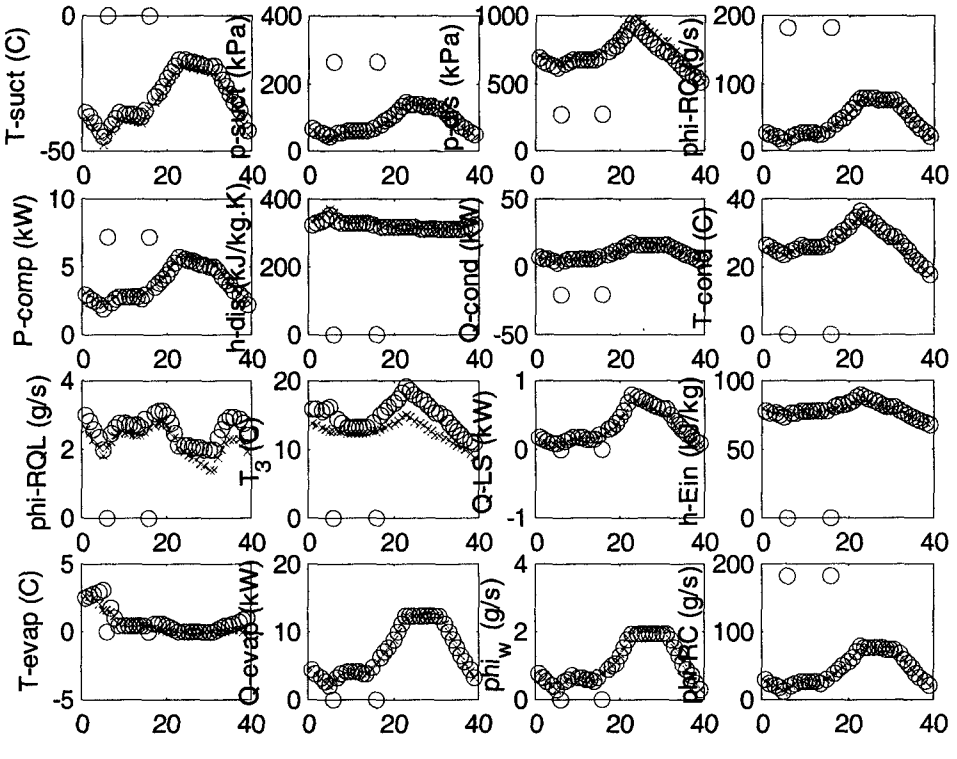

Figure 5.4. Comparision of manufacturers model (crosses) and our model (circles) for a partial load case. For 2 data points we obtained no convergency.

The range of input variables for the partial load case are shown in figure 5.5.

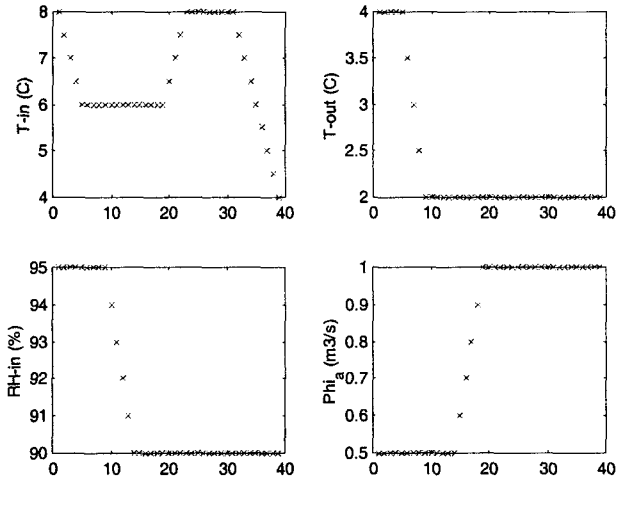

These figures show that our model gives reasonable prediction of various variables of the manufacturers data. For several isolated cases the Newton-Rhapson solver did not converge. This is probably due to the little robustness of the solver. If robustness remains a problem one can apply more robust solvers like the Broyden method, but which is more complicated from a computational point of view.

References

- ASHRAE, Handbook - Fundamentals. 1985.
- P.G. Jolly, et.al. Simulation and measurement on the full-load performance of a refrigeration system in a shipping container. *Int. J. Refr.* **23**: 112-126 (2000).
- H. Hasse et.al. Top-down model for dynamic simulation of cold-storage plants. *Int. J. Refr.* **19**(1): 10-18. (1996).
- C.T. Kiranoudis, N.C. Markatos. Design of tray tunnels for food deep chilling. *J. Food Eng.* **40**: 35-46. (1999).

Model of the Climate Conditions in a Refrigerated Container

R.G.M. van der Sman
Agrotechnological Research Institute (ATO-DLO)
Wageningen, the Netherlands

1. Introduction

In the CEET research project we are developing a model-based supervisory control algorithm, which dynamically adjusts the settings of a refrigerated container for optimal energy consumption and maintenance of product quality. A part of this algorithm is a model describing the climate conditions inside the refrigerated container. This document reports on this model.

2. Model description

The dynamics in the climate conditions (temperature and humidity) are described in terms of energy and mass balances. For the model we take the following assumptions:

- The load of packed products can be modelled as a single heat capacity

2.1 Heat balances

In figure 2.1 we have depicted the heat balance using an electrical analogy. The capacitors represent heat capacities (which store energy). Between the capacitors heat flows conducted by heat resistances. The return air and supply air of the cool unit and the heat of respiration and transpiration are modelled as sources and sinks.

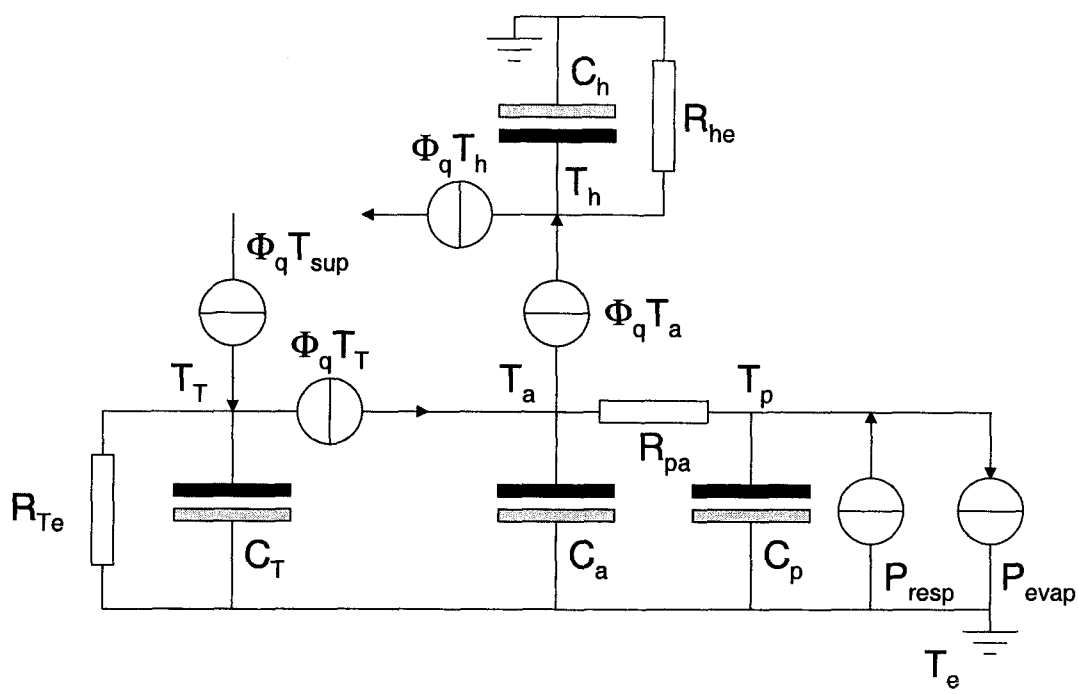

Figure 2.1 Heat balance for the stowage space of a refrigerated container.

For the heat balance we distinguish the following heat capacitors:

- C_p the produce packed on pallets with boxes (includes packaging)
- C_a the air in between the pallets
- C_h the air in the headspace above the pallets
- C_T the T-bar floor.

The supply air enters the T-bar floor, and then flows in between the pallets, and returns via the headspace to the cool unit. The airflow convects heat, which is indicated with the current sources.

(Conductive) heat exchange with the environment is modelled with the heat resistances R_{Te}, R_{ae} and R_{he}. Heat exchange between the airflow between the pallets and the produce is also assumed to be mainly by conduction, as modelled by the heat resistance R_{pa}. The produce produces heat by respiration, and looses heat by evaporation. These processes are modelled by heat current sources. Below you will find how respiration and evaporation is modelled.

From figure 2.1 follows the total heat balance:

$$\begin{aligned} C_T\, d_t T_T &= + \Phi_q (T_{sup} - T_T) - (T_T - T_e) / R_{Te} \\ C_a\, d_t T_a &= + \Phi_q (T_T - T_a) + (T_p - T_a) / R_{pa} \\ C_p\, d_t T_p &= - (T_p - T_a) / R_{pa} + P_{resp} - P_{evap} \\ C_h\, d_t T_h &= + \Phi_q (T_a - T_h) - (T_h - T_e) / R_{he} \end{aligned} \qquad (2.1)$$

Here we have abbreviated $\rho_a\, c_{p,a}\, \Phi_V = \Phi_q$.

2.2 Properties of container

The volume of the stowage space is V_c = 11.6 x 2.28 x 2.50 = 66 m^3. The height of the headspace above the product load = 0.08 m. Hence, the volume of the head space is 2.11 m^3. The maximum pay-load is 25.7 ton. Hence, the products listed in Table I will reach this maximum limit.

The thermal insulation is made of foamed poly-urethaan, with a thermal conductivity of 0.021 W/m.K. The thickness of the floor-insulation is 95 mm, of the front and side-walls 67 mm, the door 80 mm, and of the roof 95 mm. Its density is 38 kg/m^3, and its weight is 375 kg.

The T-bar floor is made of alumnium, it has a thickness of 4 mm, its height= 63.8 mm, its width=30 mm and the number of T-bars=35. Hence, the mass of the T-bar floor = 700 kg.

The roof is lined with 0.8 mm thick alumnium, and the walls are lined with stainless steel plates with 0.7 mm thickness. Hence, the mass of the roof lining is 57 kg, and the mass of the wall lining is 383 kg. The heat capacity of alumnium and stainless steel are respectively 0.88 kJ/kg.K and 0.46 kJ/kg.K. The heat capacity of the liners will be incorporated in the heat capacity of the head space. In the model we will also abosrb the heat capacity of the packaging into the heat capacity of the head space.

The weight of the exterior steel is set equal to the tare weight (4740 kg) minus the weight of inner linings, the T-bar floor and insulation. Hence, its weight is equal to 3250 kg and its heat capacity is equal to C_T=2860 kJ/K.

The volumetric flow rate, Φ, is typically 20 to 80 times the empty volume of the stowage space (V_c) per hour. Hence Φ = 0.4 to 1.6 m^3/s. The airflow through the product load is from bottom to top. The superficial airflow velocity in the load is then typically: u = 1.5 to 6 cm/s.

2.3 *Heat resistances*

Product-air interface

The heat resistance of product to air, R_{pa}, is equal to:

$$R_{pa} = 1 / h_{pa,eff} A_{pa}, \qquad (2.2)$$

Here A_{pa} is the surface area for packaging, which is equal to 1650 m^2. The effective heat transfer coefficient $h_{pa,eff}$ is dependent on the type of packaging, and therefore it will be estimated.

T-bar floor-ambient interface

This resistance is mainly due to the insulation of the bottom, and is given by:

$$R_{Te} = 1 / (\lambda_{PU}/d_{PU}).A_{Te} \quad (2.3)$$

Here λ_{PU}=0.021 W/m.K the thermal conductivity of polyurethaan foam, d_{PU}=90mm the thickness of the bottom insulation, and A_{Te}=26 m^2 the surface area of the floor. Hence, R_{Te} = 0.17 K/W.

Head space-ambient interface

The heat flow through the side walls, we will absorb in the heat flow from the headspace to the ambient. Hence, the heat resistance is then due to the insulation of the roof and the side walls, and is given by:

$$R_{he} = 1 / \Sigma_i (\lambda_{PU,i}/d_{PU,i}) A_{ce,I} + R_{rad} \quad (2.4)$$

Here λ_{PU}=0.021 W/m.K the thermal conductivity of polyurethaan foam, $d_{PU,i}$ the thickness of the insulation components, and $A_{ce,i}$ surface area of the roof and the side walls. R_{rad} is the contribution due to black body radiation.

Black body radiation (between exterior and sky) is given by P_{sky}, which can be linearized for small temperature differences:

$$P_{sky} = 4 A_{top} \sigma \varepsilon_e \theta_0^3 (T_e - T_0) \quad (2.5)$$

Here σ=5.7 10^{-8} W/m^2.K^4 is the Stefan-Boltzmann constant, θ_e is the absolute temperature of the exterior, θ_0 is the absolute temperature of the sky (ambient), ε_e=0.95 is the emissity of the exterior. A_{top}=26 m^2 is the surface area of the roof. The radiation is assumed to be absorbed only by the roof. This can be modelled as a heat resistance:

$$R_{rad} = 1 / 4 A_{top} \sigma \varepsilon_e \theta_0^3 \quad (2.6)$$

3 Mass balance

The mass balance are depicted in figure 3.1:

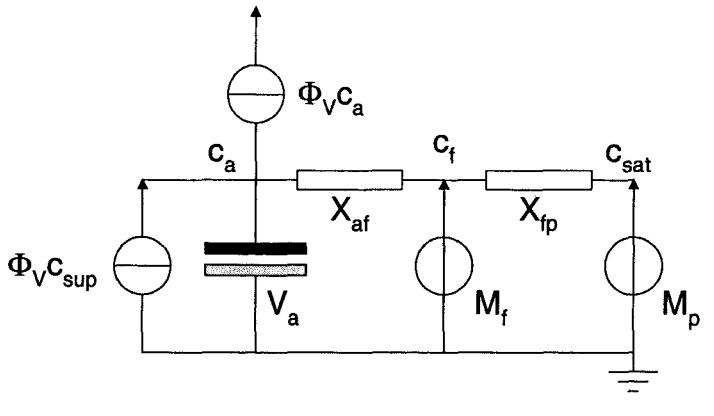

Figure 3.1 Mass balance for water vapour in the stowage space.

Here there are three elements which can contain water, either as vapour or as liquid. They are:

- V_a the total air inside the cargo space
- M_f a film of condensed moisture on the product
- M_p the moisture contained in the product

The mass balance, taking condensation into account, is given by:

$$
\begin{aligned}
& V_a \, d_t \, c_a = \Phi_V (c_{sup} - c_a) + (c_{sat} - c_a) / X_{pa} \\
& X_{pa} = X_{af} + X_{fp} && \text{if } M_f <= 0 \text{ and } c_a < c_{sat}(T_p) \\
& X_{pa} = X_{af} && \text{if } M_f > 0 \text{ or } c_a > c_{sat}(T_p) \\
& d_t \, M_f = (c_{sat} - c_a) / X_{af} && \text{if } M_f > 0 \text{ or } c_a > c_{sat}(T_p) \\
& d_t \, M_p = (c_{sat} - c_a) / X_{pa} && \text{if } M_f <= 0 \text{ and } c_a < c_{sat}(T_p)
\end{aligned}
\qquad (3.1)
$$

c_a is the water vapour concentration of water vapour in the air of the cargo space, having a volume of V_a. M_f and M_p are the amounts of moisture contained in the condensed film and the produce. The change in c_a is driven by the convection of vapour by the airflow in the cargospace and the mass exchange with the produce or condensed film. The airflow enters the cargo space with concentration c_{sup} with airflow rate Φ_V. The mass exchange is proportional with the mass transfer resistance X_{pa} and the so called water vapour deficit (c_{sat}-c_a), with c_{sat} the saturated water vapour concentration at the product temperature T_p.

The mass exchange resistances are given by

$$
\begin{aligned}
& X_{af} = 1 / \beta_f . A_p \\
& X_{fp} = 1 / \beta_{eff} . A_p
\end{aligned}
\qquad (3.2)
$$

Mass transfer coefficient β_f is estimated using the relation that $Sh=\beta_f . d_p / D_w = 2$ for stagnant air. (Here d_p is the diameter of the produce, D_w is the diffusivity of water vapour in air). A_p is the total surface area of the produce. The mass transfer coefficient β_{eff} depends on the skin resistance of the produce and also on the type of packaging. This parameter will be estimated using experimental data.

The heat absorbed by evaporation is linked to the rate of evaporation and the latent heat of evaporation ($\Delta\varepsilon_{evap}$)

$$P_{evap} = \Delta\varepsilon_{evap} (c_{sat} - c_a) / X_{pa} \qquad (3.3)$$

4. Gas exchange model

4.1 Introduction

The refrigerated container may be equipped with a Controlled-Atmosphere (CA) unit, for which also a model is developed. The CA-unit controls the gas conditions inside the container. It will keep the container at low oxygen and carbon dioxide levels, which slow down the respiration of the product, and consequently the decay in the quality. The unit operates by injecting air with high nitrogen levels in the container. The container investigated can inject the nitrogen at two purity levels, which also differ in flow rate. To keep the CO_2 level within bound, the CA-unit can also inject actively fresh air into the container.

Under normal CA-operation the fresh air intake take is shutdown. By the injection of nitrogen the pressure will rise inside the container. Through (inevitable) leaks in the container some air will flow from the container to the environment.

4.2 Mass balances

The dynamics in the gas conditions (oxygen, carbon dioxide and nitrogen) are described in terms of mass balances. For the model we take the following assumptions:

- There are no gradients in the gas concentrations inside the container, i.e. the container is well mixed.
- There is no fresh air intake.
- The (volumetric) flow rate of air, which leaks out of the container, is always equal to flow rate of the air injected by the CA-unit.

These assumptions have been checked experimentally. By analysing air samples from various locations inside the container, we have noticed no significant differences in gas conditions. Also we have monitored the pressure difference between container and environment. These measurements show that the container is pressurised within minutes. Hence, for long time scales the last assumption is valid.

The mass balances for the gasses are given by:

$$\begin{aligned} V_a\, d_t\, n_{o2} &= -J_{resp,o2} + J_{unit}(x_{O2,unit} - x_{O2}) \\ V_a\, d_t\, n_{co2} &= +J_{resp,co2} - J_{unit}\, x_{CO2} \\ V_a\, d_t\, n_{N2} &= +J_{unit}(x_{N2,unit} - x_{N2}) \end{aligned} \qquad (4.1)$$

Here n_i are the molar concentrations of a gas, J are the molar fluxes, and x_i are molar fractions. The unit injects gas at a rate of J_{unit} into the container, composed of nitrogen and oxygen with fractions $x_{O2,unit}$ and $x_{N2,unit}$. The respiration of the product consumes oxygen at the rate of $J_{resp,o2}$, and produces carbon dioxide at the rate $J_{resp,co2}$. These rates are obtained from the respiration model given below. The leakage out of the container is modelled by the terms $J_{unit}\, x_i$, with *i* indicating the gas component of the air.

The CA-unit can operate on two levels, each characterised by a flow rate and a nitrogen level, as listed in Table I below. These values are obtained by analysis of experiments.

Table I Flow rates and nitrogen levels of gas injected by CA-unit

Level	O_2 concentration	Flow rate (m^3/h)
ambient	21%	6.7
high	9.0%	2.2
low	0.5%	0.7

For the respiration model we take the respiration model of Peppelenbos (1996). The oxidative respiration is described by Michaelis-Menten kinetics with non-competitive inhibition of CO_2:

$$J_{resp,O2} = m_p\, J_{resp,O2,max} \cdot x_{O2} / [K_{m,O2} + x_{O2}] \cdot [1 + K_{m,CO2} / x_{CO2}] \qquad (4.2)$$

Here m_p is the mass of the product.

The production of CO_2 is due to oxidation and fermentation:

$$J_{resp,CO2} = J_{resp,CO2,ox} + J_{resp,CO2,f} \qquad (4.3)$$

Using the definition of the respiratory quotient (RQ_{ox}), the oxidative flux given by

$$J_{resp,CO2,ox} = RQ_{ox}\, J_{resp,O2} \qquad (4.4)$$

and the fermentative flux given by competitive Michaelis-Menten kinetics:

$$J_{resp,CO2,f} = m_p J_{resp,CO2,f,max} / [1 + x_{O2}/K_{m,O2,f}] \quad (4.5)$$

The respiration is temperature dependent, which follows the usual Arrhenius relation:

$$J_{O2,max} = J_{O2,max,ref} \exp (- \Delta\varepsilon_{ox} / R (\theta_p - \theta_{ref}))$$

$$J_{CO2,f,max} = J_{CO2,max,f,ref} \exp (- \Delta\varepsilon_f / R (\theta_p - \theta_{ref})) \quad (4.6)$$

The activation energy is quite independent of the product (the rule of van 't Hoff). $\Delta\varepsilon_{ox}$ = 53 kJ/mol. The temperatures θ_p are given in Kelvins. R is the gas constant.

The heat of respiration is linked to the production of CO_2. Mind that oxydation and fermentation have different release of energy, as expressed in the different amount of ATP that is released per mole CO_2. The heat of respiration is given by:

$$P_{resp} = q_{ox} J_{resp,CO2,ox} + q_f J_{resp,CO2,f} \quad (4.7)$$

Here q_{ox} = 447 kJ/(mole CO2) and q_f is 63.5 kJ/(mole CO2). Their ratio is about 7:1, which is about the ratio in the production of ATP (6:1).

4.3. **Control logic model**

The control logic can switch the CA-unit to various states, as shown in figure 4.1. Considering large time scales, the membrane can either generate continuous flows (at ambient, high or low purities) or cycle between various purities. The control logic is shown schemetically in figure 4.1.

From pressure decay measurements, and the decay rate of gas concentrations, as shown in figure 4.2, we have estimated the fluxes from the CA-unit using the following assumptions: 1) the flow rate of air leaking out of the container is to the pressure difference (Darcy's law), and 2) the rate of leakage to be equal to the flow rate of the membrane. Flow rate from the CA-unit are given in the Table IV below.

Table IV Flow rates of gas with different purities emitted from the CA-unit

Nitrogen Purity	Flow rate (m^3/h)
Ambient	6.3
Low	2.1
High	0.7

References

Peppelenbos H.W. "The use of gas exchange characteristics to optimise CA storage and MA packaging of fruits and vegatables" *Ph.D. thesis*, University of Wageningen, 1996.

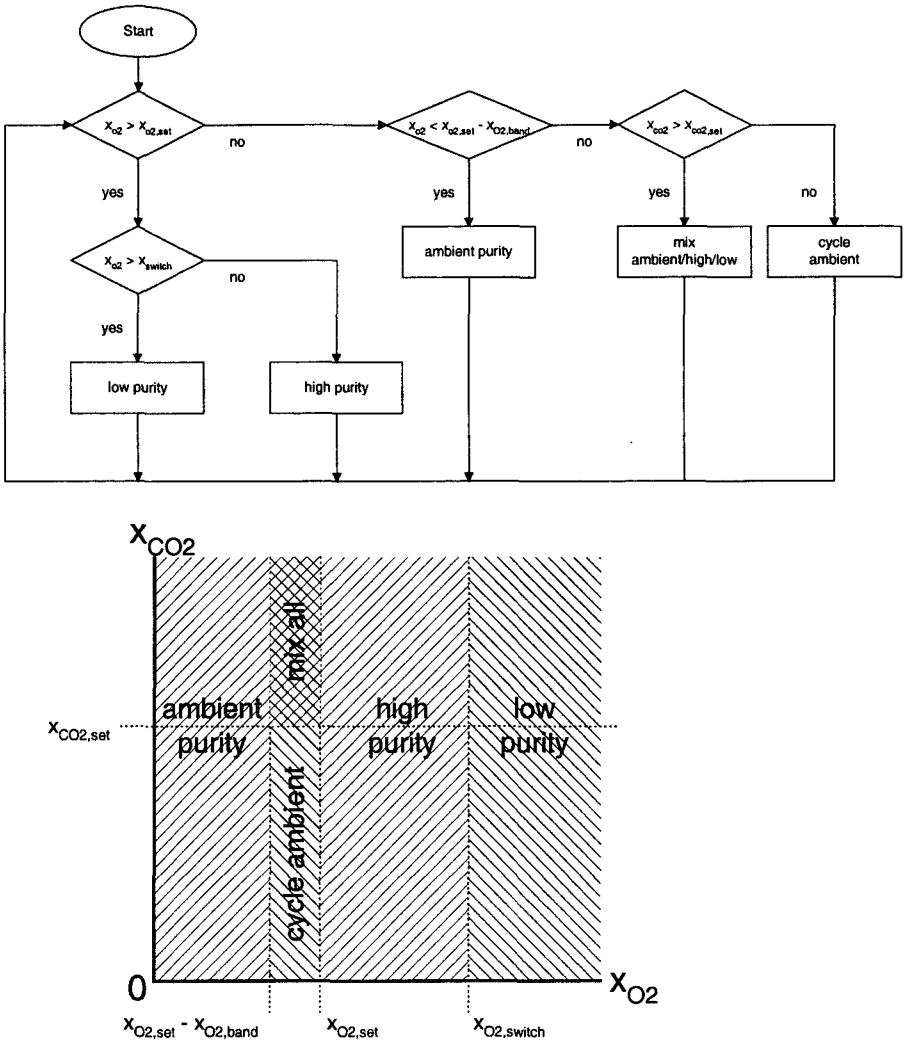

Figure 4.1 Control logic of the CA unit.

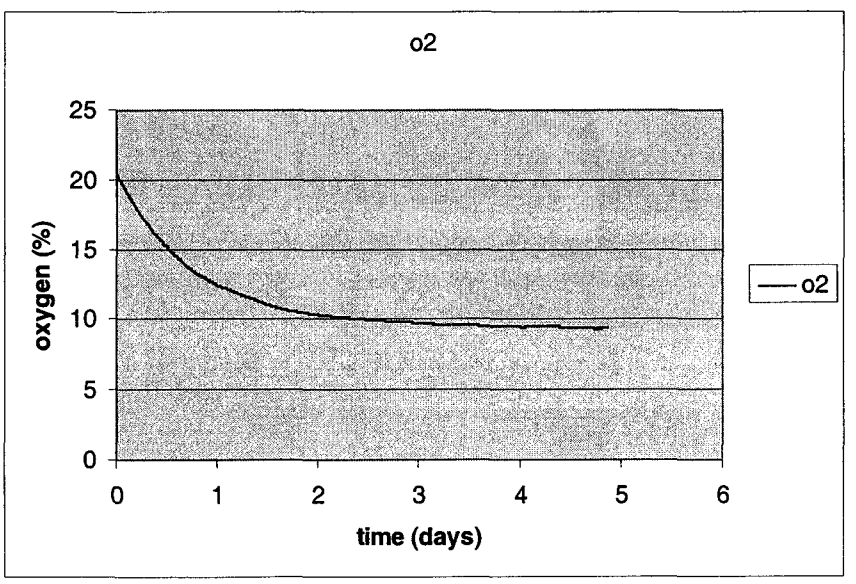

Figure 4.2 Decay of oxygen during pull down using low purity nitrogen emitted from the CA-unit.

Prediction of firmness of apples

R.G.M. van der Sman, M. Sanders
Agrotechnological Research Institute

1. Introduction

In this paper we present a model for the description of the firmness of apples. As for most fruits firmness is for apple one of the important quality aspects. For keeping and transporting apples while maintaining a minimum level of quality and keeping energy consumption at an acceptable level, it is desirable to known how environmental factors like temperature and gas conditions impart the firmness of apples. (Van der Sman and Verdijck, 2001).

Apple belong to a large class of fruits, the so-called climacteric fruits, which all show similar biochemical behaviour in the ripening process, during which loss of firmness occurs. Hence, for the development of the model we assume that most models and hypotheses, which hold for other climacteric fruits – especially those also belonging to the rose family like pears and peaches - can also be applied to apple.

It is commonly known that loss of firmness during ripening of climacteric fruits is due to alterations in the cell wall and middle lamella structure (Seymour and Gross,1996), (Brownleader et.al.,1999) (Wakabashyi,2000). In climacteric fruits the main effect during ripening is the solubilization of cell wall pectin, involving the action of the polygalacturonase (PG) enzyme (Brownleader et.al.,1999) (Ketsa and Daengkanit, 1999) (Wakabashyi,2000). The loss of firmness can not be totally explained by the action of PG. This is shown in some fruits like tomatoes, where the action of other hemicellulytic enzymes is responsible for 10-25% of the total loss of firmness (Brownleader et.al.,1999), (Wakabayashi,2000). In apples PG is present, but at much lower levels as compared to tomato, and is active in latter stages of ripening. (Wu et al, 1993) (Siddiqui et al,1996).

Furthermore, it is probable that the action of PME is required prior to the action of PG (Brownleader et.al.,1999) (Wakabashyi,2000). However, in riping fruit PME activity is not of importance (Brummell and Harpster, 2001). For other storage disorders like wooliness in fruits like peaches and nectarines, it is an important aspect. It is known that wooliness (a kind of chilling injury) is due to an imbalance between PG and PME (Zhou et.al.,2000). It is likely that mealiness in apples is due to similar processes. Hence, it is worthwhile to take the aspects of PME in to account in more detailed models, to be developed in the future.

Henceforth, in our model we assume that the loss of firmness in apples in primarily due to the action of some softening inducing enzyme (Enz), which (partly) models the action of PG. We assume that the action of Enz for a large part follows an existing model for peaches (Tijskens et.al.,1998). Tijskens et.al. have postulated that formation of PG is regulated by a pre-cursor (or activator Act), which they did not specify.

By the usage of the ethylene inhibitor 1-MCP, it is shown that the softening of apples is regulated by ethylene (Fan et al.,1999) (Watkins, 2000), as is assumed for many other climacteric fruits (Sitrit and Bennet,1998) (Brownleader et.al.,1999). The studies by Hertog et al.(2001) and Johnston et al.(2001) give a good qualitative indication of this regulation. In the pre-climacteric stage the ripening is slow, and is proportional with the metabolic rate. During the onset of the climacteric rise of ethylene, the ripening is accelerated if the ethylene crosses some threshold. The level of ethylene does not influence the rate of the loss of firmness (Johnston et.al.,2001). Hence, we assume the activator (Act) for the action of softening inducing enzyme Enz to be regulated by ethylene.

Currently, there is no knowledge of the regulation of the activator Act by ethylene. In our model we do not intend to model the details of the complex biochemical processes. But, we model the action of ethylene and the activator by more simple kinetics. Because the climacteric rise of

ethylene is an autocatalytic process (Mathooko,1996), the regulation of the activator can be viewed as a non-linear process far from equilibrium. These kinds of processes are known to show universal behaviour, which is largely independent of the biochemical details (Meinhardt,1995). Hence, they can be described with kinetics, which can be much simpler than the real thing. Our hypothesis is that the kinetics of the autocatalytic production of ethylene and the subsequent regulation of the activator Act, can be described by an activator-depleted substrate scheme (Meinhardt,1995). This scheme usually decribes the behaviour of excitable media. The observations of Artes et.al.(1998), who have shown that short intermittent warming of tomatoes can excite several times a small ethylene peak, support the idea of climacteric fruit being excitable media.

In our model we also describe the action of oxygen and carbon-dioxide on the regulation of the activator. We assume it follows the same dependency on O_2 and CO_2 as the ethylene biosynthesis.

Below we will describe our model in two parts. The first part describes the kinetics of the softening inducing enzyme Enz and its effect on firmness. The second part describes the kinetics of the activator-depleted substrate scheme.

2. *Model description*

Kinetics of softening inducing enzyme and firmness loss

This part of our model largely follows the model of Tijskens et.al.(1998), describing the firmness loss of peaches. They state firmness loss in peaches is mainly due by the solubilization of pectin (Pe) by the action of PG. The rate of solubilization (d_tPe) is assumed to be proportial to the loss of firmness (d_tF), which can be can be described by the following equation (Tijskens et.al.,1998):

$$d_t Pe = d_t F = - k_{Enz} Pe\ Enz \qquad (1)$$

The amount of the softening inducing enzyme Enz changes in time by 1) the formation of Enz, and 2) the denaturation of Enz. Here again we follow the kinetics for PG in the model of Tijskens (1998). The formation of Enz thought to be proportional to the activator Act, which is regulated by ethylene (C_2H_4), as described in the next section. Hence, the kinetics of the enzyme Enz we describe as follows:

$$d_t Enz = k_f Act - k_d Enz \qquad (2)$$

In the model of Tijskens et al.(1998), which holds for peaches, k_{Enz} and k_f, are assumed to be temperature dependent, and that they follow and Arrhenius function. However, some apple cultivar show little temperature dependency on the rate of softening (Johnston et al.,2001).

Kinetics of the activator

The combined effect of the autocatalytic production of ethylene and the regulation of the activator by ethylene is described by an activator-depleted substrate scheme. (Meinhardt, 1995). In this scheme the autocatalytic production of the activator (Act) is limited by depletion of its substrate (Sub), which is produced at a lower rate. This limiting growth of the substrate will halt the production of the activator, and can take it into decline or keep it at a certain level. When applied to the activator Act of the softening inducing Enzyme, the substrate Sub can be identified as the substrate of ethylene, AdoMet. It is known that the rate limiting step in ethylene biosynthesis is the conversion of AdoMet to ACC by ACC-synthase (Brownleader et.al.,1999). Details on the kinetics of the ethylene biosynthesis can be found in (Mathooko,1996).

In standard activator-depleted substrate schemes the peak in activator production can be very sharp, which is not often observed in the production of ethylene. The sharpness of the peak can be reduced by introducing saturation of the autocatalysis of the activator (Meinhardt,1995).

For describing ripening in apple fruit under CA-conditions we have to augment the scheme of (Meinhardt,1995) with the action of oxygen and carbon dioxide. Oxygen is a second substrate for the production of ethylene, as it is needed for the oxidation of ACC (Mathooko,1996). Furthermore carbon dioxide is an inhibitor of the synthesis of ACC by ACC-synthase (Mathooko,1996). We describe the action of the respiratory gases on the production of the autocatalytic production of the activator similar to the model van de Wild et.al.(1999), who describe the action of these gases on the ethylene production in pears.

Softening also occurs in the pre-climacteric apples (Hertog et al., 2001) (Johnston et al.,2001). In pre-climacteric fruits ethylene is produced at a low rate by a non-autocatalytic process, called System-I (Mathooko,1996). We assume through this non-autocatalytic production of ethylene there is also a small production of the activator Act, using the same substrate Sub. For this non-autocatalytic production of the activator Act we assume simple first order kinetics, which is not regulated by respiratory gasses.

For the formation of the substrate of ethylene, Adomet, ATP is required (McKeon, 1995). Hence, we assume that the production of the substrate Sub is proportional with the metabolic rate, or in other words the respiration rate. We view in this way the effect of respiratory gasses on softening of apples stored under controlled atmosphere (CA) conditions can be modelled. In absence of the autocatalytic production of the activator, our model is very similar to the model proposed by Hertog et al. (2001), describing the softening of Braeburn apples under CA-conditions.

The last element in our model is the removal of ethylene from the interior of the fruit by diffusion. In storage the environment of the apples is normally ventilated, and thereby removing the ethylene diffusing out of the fruit. This diffusion process is modelled effectively as a decay of the activator. The action of exogenous ethylene (Exo) can be taking into account easily in this model. The diffusion is proportional to the concentration difference between endogenous and exogenous ethylene.

Hence, the activator-depleted substrate scheme for the production of the activator Act is given by:

$$d_t\,Act = + S_{autocat} - S_{diffusion} + S_{system,I} \quad (3)$$

$$d_t\,Sub = - S_{autocat} - S_{system,I} + S_{prod} \quad (4)$$

$$S_{autocat} = k_{au}.Sub.O_2.Act^2/(1 + k_{as}.Act^2)/[(1 + K_{me,co2}\,CO_2).(K_{me,02} + O_2)] \quad (5)$$

$$S_{system,I} = k_I.Sub \quad (6)$$

$$S_{diffusion} = k_{diff}.(Act - Exo) \quad (7)$$

$$S_{prod} = k_{prod}.[(O_2/(1 + CO_2/K_{mo,CO2}).(1 + K_{mo,02}\,O_2) + \eta/(1 + O_2/K_{mf,02})] \quad (8)$$

For the levels of the various compounds (Act, Sub, Enz, Pe) we use dimensionless numbers. The level of Sub and Pe is normalized to their initial value.
Here, k_{au} is the reaction rate for the autocatalytic production, which is assumed to temperature dependent, following an Arrhenius relation. k_{as} is a measure of the saturation of the autocatalysis. The inhibition of the production of the activator by CO_2 is modelled by uncompetitive inhibition, following (de Wild et al.,1999). $K_{me,CO2}$ and $K_{me,O2}$ are Michaelis-Menten constants related to the inhibition of ethylene production by O_2 and CO_2. k_I is the production rate of the activator by the ethylene system I. Note that we assume that the production of the activator by system I does not depend on the level of respiratory gases. k_{diff} is the removal rate of the activator (i.e. ethylene), which is assumed to diffuse to the ambient, which has a concentration of Exo. k_{prod} is the

production rate of the substrate. The production of the substrate is assumed to be governed by the rate of the production of ATP as produced by respiration. Hence, the effects of respiratory gases on the production of substrates follows the respiration model of Peppelenbos (1996), using the uncompetitive inhibition of O_2 and CO_2. η is the ratio of ATP production between aerobic and anaerobic respiration, which is $\eta=1/7$. $K_{mo,CO2}$, $K_{mo,O2}$ and $K_{ma,O2}$ are Michaelis-Menten constants related to respiration.

We assume only k_{au}, k_{prod} and k_l to be temperature dependent, and that it follows an Arrhenius relation with activation energy E_a. We assume these reaction rates have the same activation energy, and it is equal to that of respiration.

The validity of the activator-depleted substrate scheme is tested by modelling internal ethylene concentration of Golden Delicious, as measured by Song and Bangerth (1996). Measured ethylene production of apples after harvest for 45 days at 20°C. We assume that ethylene release from product is proportional with the internal ethylene production (due to a high internal diffusion resistance). Hence we can compare our model with these results, which show remarkable similar behaviour.

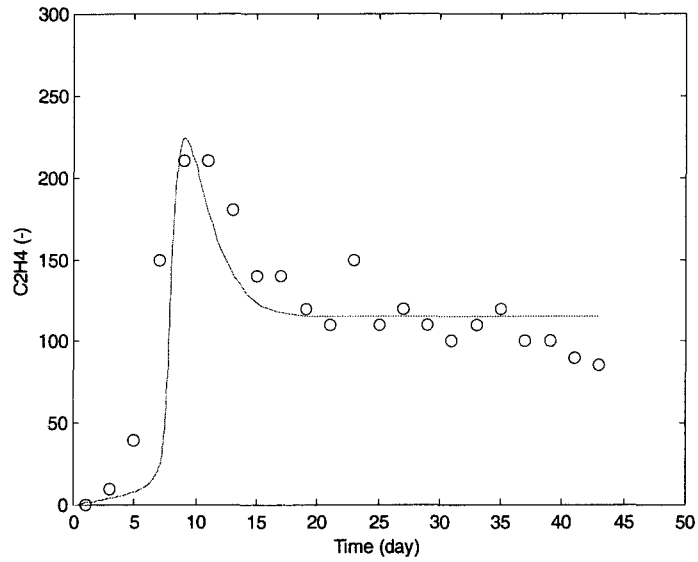

Figure 1. Ethylene release of Golden Delicious according to experiment (symbols) by Song and Bangerth (1996) and model prediction of internal ethylene concentration (sold line), rescaled to fit the units used by Song and Bangerth. Parameters k_{au}= 1.06 (day^{-1}), k_{as} = 3, k_{prod}= 1.85 (day^{-1}), and k_l=0.01 (day^{-1}). We have used dimensionless values for the levels of Act and Sub. Initial level used are Sub(t=0)=1, and Act(t=0)=0.

The activator/depleted-substrate scheme is very versatile, it can capture also the ethylene production of fast ripening tropical fruits like durians (Ketsa and Daengkanit, 1999). In figure 2 we have reproduced the data presented by Ketsa and Daengkanit (1999), and show our model predictions. In most fast ripening fruits a sharp peak in ethylene concentration is observed, as is also shown in figure 2. This sharp peak is due to a high reaction rates k_{au} and k_l and compared to the production rate of the substrate.

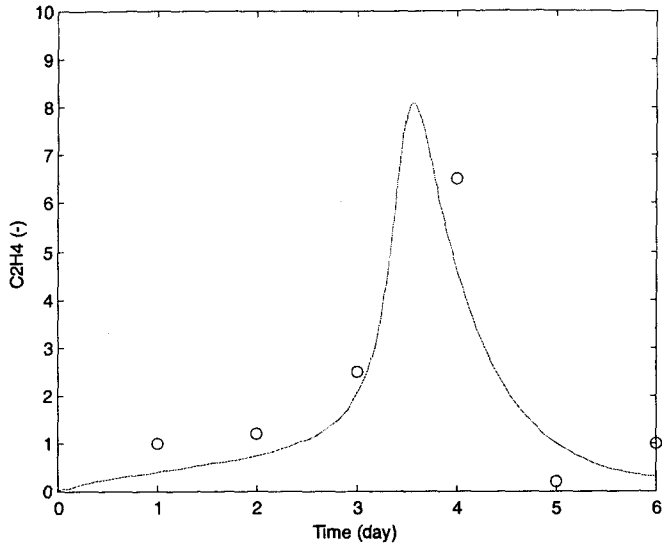

Figure 2. Ethylene release of Durians according to experiment (symbols) by Ketsa and Daengkanit (1999) and model prediction of internal ethylene concentration (sold line), rescaled to fit the units used by Ketsa and Daengkanit. Parameters k_{au}= 12 (day^{-1}), k_{as} = 0, k_{prod}= 0.30 (day^{-1}), and k_i=0.077 (day^{-1}). We have used dimensionless values for the levels of Act and Sub. Initial level used are Sub(t=0)=1, and Act(t=0)=0.

3. Application to Elstar apples

We apply the model to predict the change in firmness of Elstar apples. In the first set of experiments apples are stored for about 30 days in atmospheric and standard CA-conditions, at several temperatures. At intervals of about 1 week, firmness and ethylene gas exchange is measured. The experiments are performed with 4 different batches either short after harvest, or after CA-storage. The experimental results are shown in figure 3. Here we observe that softening also occurs at an initially slow rate, and a subsequent fast rate. The transition between slow and fast softening rate depends on temperature. In all four batches the times the transition occurs are very comparable for apples stored at equal temperatures. However, the transition is not quite correlated with the time the peak in the climacteric rise of ethylene occurs. As suggested by Johnston et al.(2001), the transition occurs at early stages of the climacteric rise of ethylene, which then triggers the production of the activator. Henceforth, the change of ethylene concentration in latter stages of the climacteric rise is probably not a good measure for the time of transition.

Elstar apples from the same batches are also stored under CA-conditions (1.2 kPa O_2 and 2.5 kPa CO_2). For a period of 30 days the firmness and ethylene release are monitored. The experiments have shown that firmness remained at the initial level, and the climacteric rise of ethylene was absent. Henceforth, the apples stored under CA-conditions remained in the slow softening regime. These results indicate that the transition between slow and fast softening rate is regulated by the climacteric production of ethylene.

With our model we will focus only on the prediction of the change of firmness of the apples stored under atmospheric conditions at different temperatures. The autocatalytic rise of the activator Act, we try to link with the transition between slow and fast softening. A valuable data set showing clear transitions in softening rates is from the batch of October 2001. The transitions occurs at 10, 20 and 30 days for apples stored at respectively 14, 9 and 5°C. In the other experiments the transitions occurred at comparable times. Hence, the October 2001 data set will be used for the validation of the model.

Another dataset used to validate our model is shown in figure 4. At two levels of oxygen, 21% and 3%, and 18°C apples are stored at various CO_2 levels. After 21 days of storage the loss of

firmness (relatively to the initial firmness) is measured. Figure 4 shows that carbon dioxide has a strong inhibition on the loss of firmness. At low CO_2 one sees significant effect on the O_2 level. Both effects have been incorporated in the model.

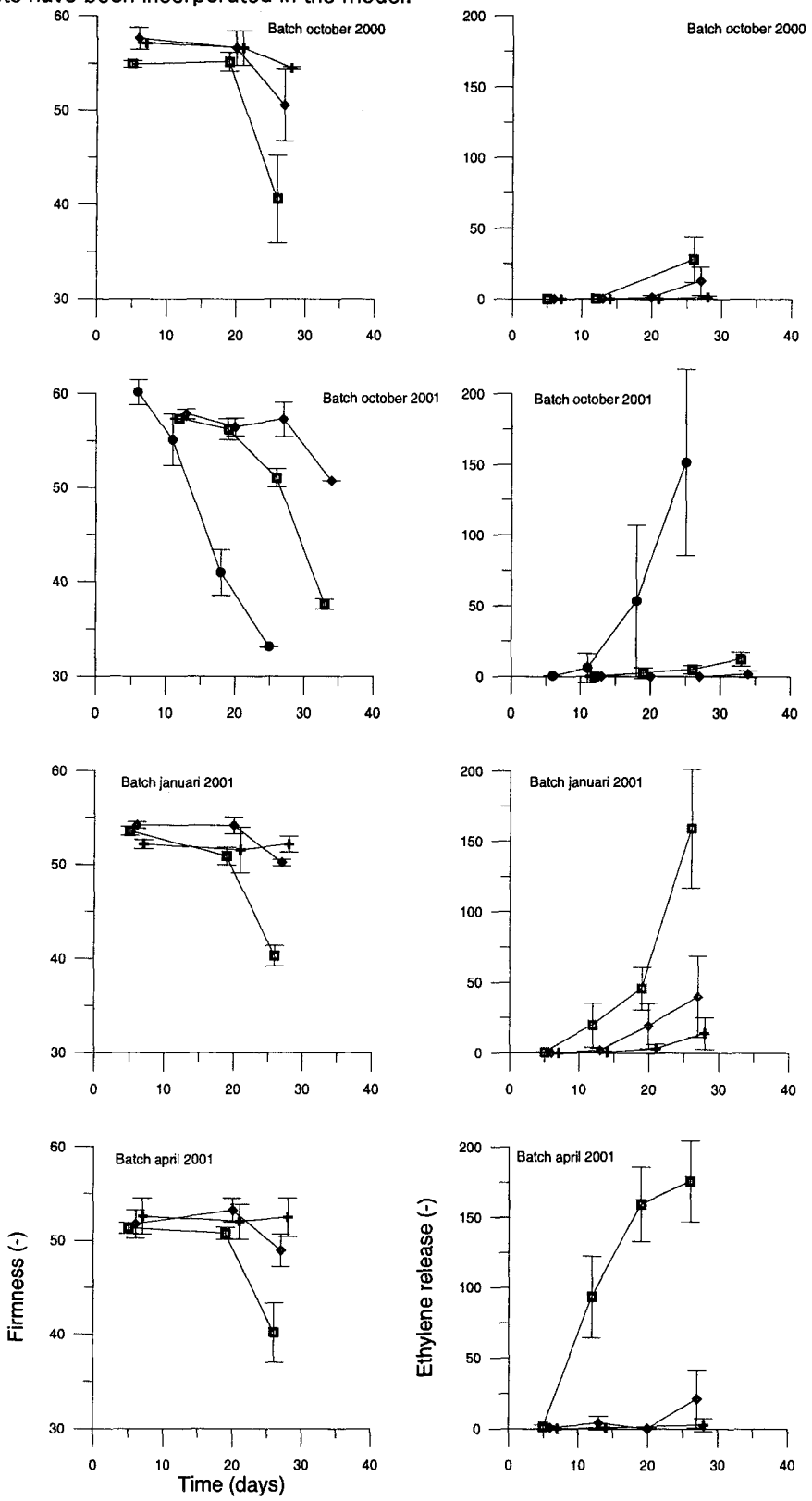

Figure 3. Firmness and ethylene gas exchange of Elstar apples stored under atmospheric conditions at various temperatures. (Cross=2^{0}C, Diamonds=5^{0}C, Squares=9^{0}C, and circles=14^{0}C). Data are given for 4 different batches.

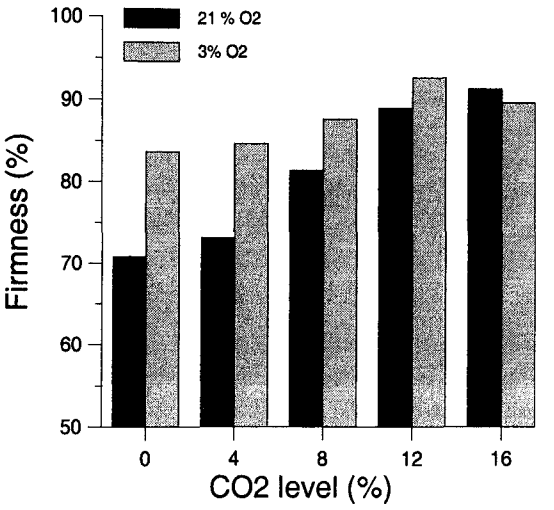

Figure 4. Firmness after 21 days of storage at 18°C and 21% or 3% O_2, and various levels of CO_2, expressed relatively to the initial firmness. Initial firmness is 6.4 kg/cm^2.

As much as possible, parameter values will be estimated from literature values. The value of the activation energy for Elstar apples, E_a/R=6380 K, is taken Hertog et al. (1998). k_{diff} is estimated from the diffusion resistance of the skin of apples for oxygen, which is said to be comparable to that of ethylene (Banks,1985). For Elstar apples the diffusion resistance is estimated to be 780 s/mm. The Elstar apples have a diameter of approximately 6 cm. Hence, the removal rate of ethylene by diffusion is about k_{diff}=2.0 day^{-1}. The decay rate of the softening enzyme Enz, k_d, is estimated from data in the study of Zhou et al.(2000b), where it is said that PG activity decays in 9 days from 100% to 10% at 0°C. Hence, we estimate that k_d=0.25 day^{-1}. Values for parameter related to respiration are taken from the data given for Elstar apples by Peppelenbos (1996): $K_{mo,CO2}$ = 91 kPa, $K_{mo,O2}$ = 4.6 kPa, $K_{mf,O2}$ = 0.2 kPa.

As initial values for the various compounds we take the following values (in dimensionless units) Act=0, Sub=1, Enz=0, and Pe=1. Using these initial conditions and the above-mentioned estimates of some reaction rates, we have fitted the model to the experimental as shown in figures 3 and 4.

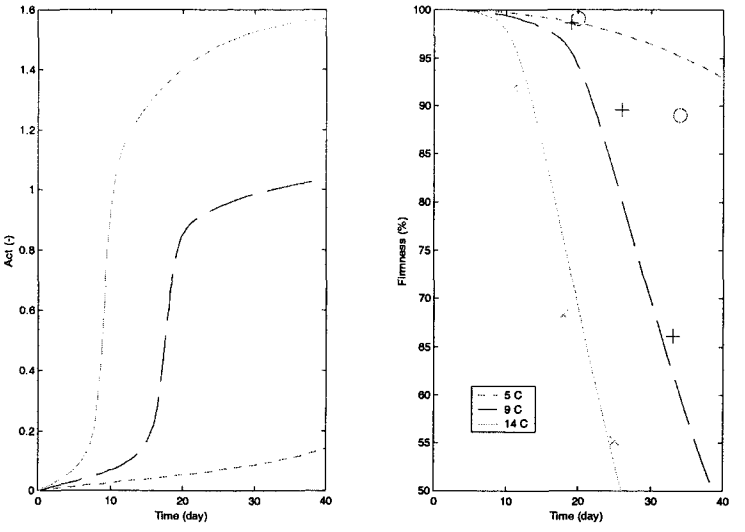

Figure 5. Model predictions of the level of the activator, and the loss of firmness of Elstar apples stored under different temperatures (solid line = 14°C, dashed line = 9°C, and dotted line = 5°C). Firmness is expressed relative to the initial firmness. Parameter values are listed in the text below. Symbols relate to experimental values of firmness as measured in the batch of October 2001 (see figure 3).

For simplicity we have choosen $k_f=k_{Enz}$ and $K_{mo,O2} = K_{me,O2}$. We have estimated their values from data points set from figure 4 with high CO_2, where apples have stayed pre-climacteric, the firmness decays about 10% over 21 days. Fitting to all data points shows that good agreement with experiments is obtained by the following choice of parameters: $k_{as}=5.0$, $k_{prod} = k_{prod,0} \exp(-E_a/RT)$ with $k_{prod,0}=3.2 \exp(+E_a/RT_{ref})$ (day^{-1}), $T_{ref}=14°C=287K$, $k_{au}=k_{prod}/8$ (day^{-1}), $k_l=k_{prod}/400$, $k_f = k_{Enz} = 0.1 day^{-1}$, $K_{me,CO2} = 12$ kPa. The predictions using these parameter values and the experimental data are presented together in figures 5 to 7.

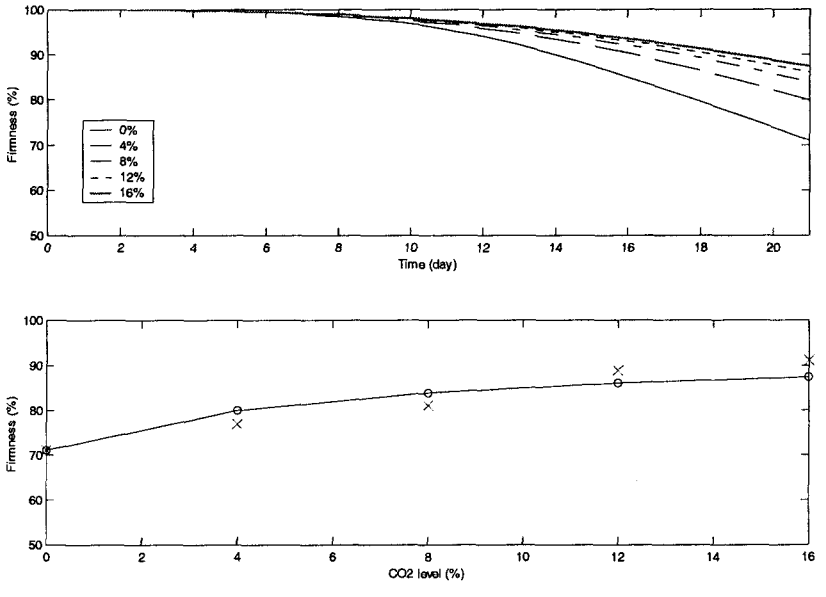

Figure 6. Model versus experimental data (crosses). Firmness after 21 days of storage at 18°C and 21% O_2, and various levels of CO_2, expressed relatively to the initial firmness. Level of CO_2 used are indicated in the legend.

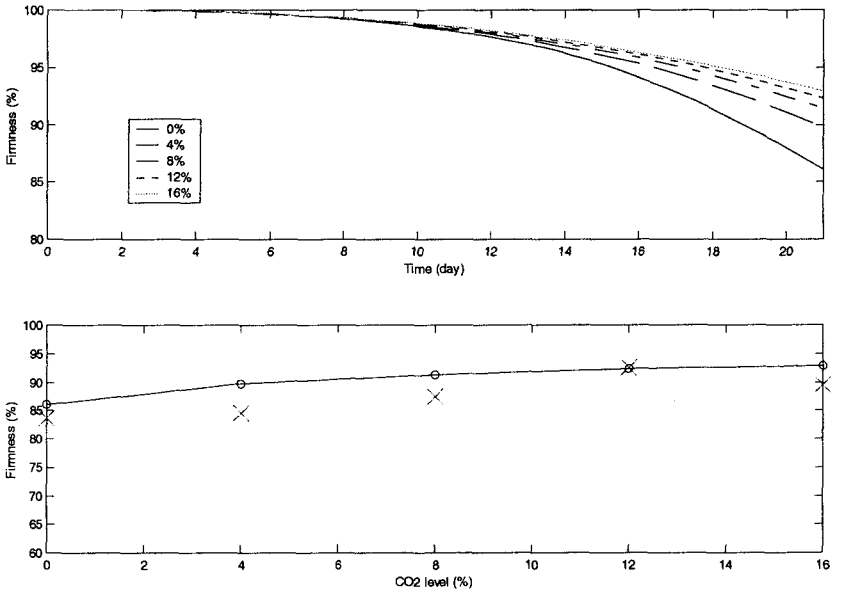

Figure 7. Model versus experimental data (crosses). Firmness after 21 days of storage at 18°C and 3% O_2, and various levels of CO_2, expressed relatively to the initial firmness. Level of CO_2 used are indicated in the legend.

4 Conclusions

We have presented a model for the prediction of the loss of firmness of (Elstar) apples and have compared the predictions with experimental data. The model is based on (universal) kinetics of biochemical reactions, following the approach of Tijskens and coworkers (1996,1997,1998). After fitting a few parameters the model predictions have shown good agreement with experiments.

As postulated by Hertog et al. (2001), and also shown by our experiments, firmness of apples has an initial slow decay rate, and subsequently a fast decay rate. The change in decay rate is linked to the autocatalytic production of ethylene (or climacteric rise). The climacteric rise is strongly influenced by 1) temperature, 2) carbon dioxide, and 3) oxygen (to a lesser extend). The initial slow rate of decay is proportional to the metabolic rate, which can be derived from respiration models as studied by Peppelenbos (1996). All these qualitative aspects are reproduced by our model, and compare well with experiments.

References

Artes F. et.al. (1998). Physiological responses of tomato fruit to cyclic intermittent temperature regimes. *Postharvest Bio. Techn.* **14**: 283-296.

Banks N.H. (1985). Estimating skin resistance to gas diffusion in apples and potatoes. *J. Exp. Bot.* **36**:1842-1850.

Brownleader M.D. et.al. (1999). Molecular aspects of cell wall modifications during fruit ripening. *Crit. Rev. Food Sci. Nutr.* **39**(2):149-164.

Brummel D.A., and Harpster M.H. (2001). Cell wall metabolism in fruit softening and quality and its manipulations in transgenic plants. *Plant Mol. Bio.* **47:** 311-340.

Dadzie B.K., Banks N.H., Cleland D.J., and Hewett E.W. (1996). Changes in respiration and ethylene production of apples in response to internal and external oxygen partial pressures. *Postharvest Bio. Techn.* **9**(3): 297-309.

Fan X., Blankenship S.M., and Mattheis J.P. 1-MCP inhibits apple ripening. *J. Am. Soc. Hort. Sci.* **124**(6):690-695.

Feng et.al. (2000). Control of ethylene responses in avocado fruit with 1-MCP. *Postharvest. Bio. Techn.* **20**:143-150.

Gorny J.R. and Kader A.A. (1996a). CA-suppression of ACS and ACO in Golden Delicious apples during long-term cold storage. *J. Amer. Soc. Hort. Sci.* **121**(4): 751-755.

Gorny J.R. and Kader A.A. (1996b). Regulation of ethylene biosynthesis in climacteric apple fruit by elevated CO_2 and reduced O_2 atmospheres. *Postharvest Bio. Techn.* **9**: 311-323.

Hertog M.L.A.T.M., Peppelenbos H.W., Evelo R.G., et al. (1998). A dynamic and generic model of gas exchange of respiring produce: the effects of oxygen, carbon dioxide and temperature. *Postharvest Bio. Techn.* **14**(3): 335-349.

Hertog, M.L.A.T.M., Nicholson, S.E., and Banks N.H. (2001). The effect of modified atmospheres on the rate of firmness change in 'Braeburn' apples. *Postharvest Bio. Techn.* **23**: 175-184.

Johnston, J.W., Hewett E.W., Hertog, M.L.A.T.M, and Harker F.R. (2001). Temperature induces differential softening resopnses in apple cultivars. *Postharvest Bio. Techn.* **23**: 185-196.

Ketsa S. and Daengkanit T. (1999). Firmness and activities of enzymes in ripening durian harvested at different stages of maturity. *Scientia Hort.* **80:** 181-188.

Lurie S. (1998). Review: Postharvest heat treatments. *Postharvest Bio. Techn.* **14**: 257-269.

Mathooko F.M. (1996). Review: Regulation of ethylene biosynthesis in higher plants by carbon dioxide. *Postharvest Bio. Techn.* **7**: 1-26.

Meinhardt. H. (1995) The algoritmic beauty of sea shells. *Springer Verlag, Berlin.*

McKeon T.A. (1995). Fernandez-Maculet J.C. and Yang S.F. Biosynthesis and metabolism of ethylene. *Plant Hormones: Physiology, Biochemistry and Molecular Biology.* Kluwer, Dordrecht, the Netherlands.

Peppelenbos H.W. (1996). The use of gas exchange characterictics to optimize CA storage and MA packaging of fruits and vegetables. *Ph. D. Thesis.* University of Wageningen, the Netherlands.

Seymour G.B. Gross K.C. (1996). Cell wall disassembly and fruit softerning. *Postharvest News Inform.* **7**, 45N-52N.

Siddiqui S. et.al. (1996). Controlled atmosphere storage of apples: cell wall composition and fruit softening. *J. Hort. Sci.* **71**:613-620.

Sitrit Y. and Bennet A.B. (1998). Regulation of Tomato Fruit PG mRNA accumulation by ethylene: a re-examination. *Plant. Physiol.* **116**: 1145-1150.

Sman, van der R.G.M., and Verdijck G.J.C. (2002). Model predictions and control of conditions in a CA-reefer container. *Acta Horticulturea.* Proc. CA2001, Rotterdam, the Netherlands. *In press.*

Song J. and Bangerth F. (1996). The effect of harvest date on aroma from Golden Delicious and relationship to respiration and ethylene production. *Postharvest Bio. Techn.* **8**:259-269.

Stow J. and Genge P. (2000). Keeping quality of 'Gala'apples. *J. Hort. Sci. Biotechn.* **75**(4): 393-399.

Tan T. and F. Bangerth (2000). Regulation of ethylene, ACC, MACC, ACO at various stages of maturity of apple fruit and the effect of exogenous ethylene treatment. *Gartenbauwissenschaft* **65**(3): 121-128.

Tijskens L.M.M. and Polderdijk J.J. (1996). A generic model for keeping quality of vegetable produce during storage and distribution. *Agric. Syst.* 51: 431-452.

Tijskens L.W. et al. (1997) Modelling the firmness of 'Elstar' apples during storage and transport. *Acta Hort.* **485:** 363-.

Tijskens L.M.M. et.al. (1998) Kinetics of polygalacturonase activity and firmness of peaches during storage. *J. Food Eng.* **35**: 111-126.

Wakabayashi K. (2000) Changes in Cell Wall Polysaccharides During Fruit Ripening. *J. Plant Res.* **113:** 231-237.

Watkins C.B. et.al. (2000). Responses of apples to 1-MCP under air and CA-conditions. *Postharvest Bio. Techn.* **19**: 17-32.

Wild H. de, Woltering E., and Peppelenbos H. (1999). Carbon dioxide and 1-MCP inhibit ethylene production and respiration of pear fruit by different mechanisms. *J. Exp. Bot.* **50**: 837-844.

Wu Q.D., Szakacsdobozi M., Hemmat H., and Hrazdina G. (1993). Endo-PG in apples and its expression during fruit ripening. *Plant Physiology* **102**(1): 219-225.

Zhou H.W. et.al. (2000). Delayed storage and controlled atmosphere storage of nectarines: two strategies to prevent wooliness. *Postharvest Bio. Techn.* **18**: 133-141.

Zhou H.W., Ben-Arie R., and S. Lurie. (2000b). Pectin esteratse, polyglacturonse and gel formation in peach pection fractions. *Phytochemistry* **55**: 191-195.

Electrical and Thermal Energy Model of a Refrigerated Container

R.G.M. van der Sman[1], P.G. Jolly[2], S. Duraisamy[2], K. Chuang[2]
[1]Agrotechnological Research Institute (ATO),
Wageningen University and Research, the Netherlands
[2]Carrier Transicold, Syracuse N.Y., U.S.A.

1. Introduction

In the CEET research project we are developing a model-based supervisory control algorithm, which dynamically adjusts the settings of a refrigerated container for optimal energy consumption and maintenance of product quality. A part of this model concerns the prediction of the energy consumption (energy model) and how the reefer unit reconditions the return air into the supply air, which flows back into the stowage space (controller model). First we have considered the temperature and humidity control. The sub models concerning the CA unit will be presented in a subsequent paper.

The controller model is based on heat and mass balances, from which one can derive the conditions of the supply air. The reefer unit can operate in different states, in which airflow is cooled or heated etc. For each state of the unit, different energy and mass balances hold. How the unit switches between states is determined by the control logic, which is also part of the controller model. Using the data from the energy and mass balances, and the state of reefer unit, the energy model predicts the energy consumption. The interaction between the different sub models and other models (i.e. the stowage space model, describing the behaviour of the packed product.) is illustrated in figure 1.1

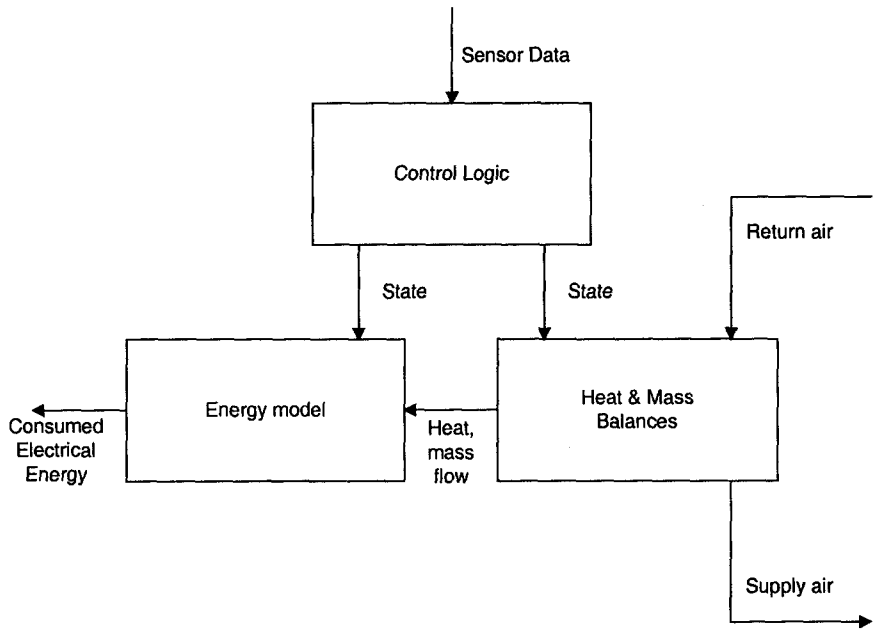

Figure 1.1 The interaction between sub models in the Energy/Controller model.

From the heat and mass balances the required heat and mass flows from the reefer unit to the refrigerated air are calculated. For the calculation the state of the controller must be known, and is given by the control logic. Using the required heat and mass flows, and the state of the controller, the energy model calculates the actual electrical energy drawn by the reefer unit.

Below in the following chapters we will describe the details of the individual sub models, as indicated in figure 1.1. In the final chapter some preliminary analysis of experiments with the model are presented.

List of symbols

Symbols

c	concentration	[kg/m^3]
$c_{p,a}$	specific heat of air	[J/kg.K]
p	pressure	[Pa]
r	heat of evaporation	[J/kg]
v	velocity	[m/s]
x	relative humidity	[-]
A	area	[m^2]
COP	coefficient of performance	[-]
ΔH	heat of vaporatization	[J/kg]
I	electrical current	[A]
M	molar weight	[kg/mol]
P	power	[J]
Q	heat flow	[J/s]
R	gas constant	[J/mol.K]
T	temperature	[K]
V	voltage	[V]
W	mechanical power	[W]
α	heat transfer coefficient	[W/m^2.K]
β	mass transfer coefficient	[m/s]
ϕ	mass flow	[kg/s]
η	efficiency	[-]
ρ_a	mass density of air	[kg/m^3]
Φ_V	volumetric flow rate	[m^3/s]

Subscripts

air	fresh air intake
C	condensor
cfan	condensor fan
comp	compressor
cond	condensed moisture on evaporator coil
evap	evaporator
exit	fresh air outlet
fan	evaporator fan
in	air entering the evaporator coil
out	air leaving the evaporator coil
R	refrigerant
ret	return air
sat	saturated
sup	supply air
set	set point
w	water
C	compressor
E	evaporator
R	refrigerant

2. Heat and mass balances

Following the top-down approach of Hasse et.al. (1996), we will describe below heat and mass balances of the reefer unit. As input for the model we have the set points and the state of the reefer unit. The model generates the following output: the conditions of the supply air and the heat and mass flows required for this conditioning. We assume the dynamics of the reefer is fast with respect to the changes in the conditions of the return air. Hence, the heat and mass balances can be expressed as algebraic equation. Note that this assumption does not hold for frosting conditions (with ice formation on the evaporator coil). So, the balances below assumes no frosting on the coil.

2.1 Mass balance for humidity

The condensed water on the evaporator coil, is assumed that it is removed from the container instantly. Hence, the mass balance is an algebraic equation. In figure 2.1 the occurring mass flows are depicted. Note the position of the fresh air exit, which is between the fan deck and the evaporator coil.

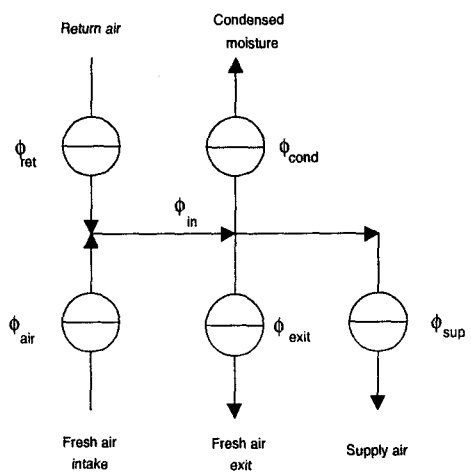

Figure 2.1. The (humidity) mass flows in the cool-unit.

The corresponding mass balances are given by:

$$\phi_{ret} + \phi_{air} = \phi_{in} \qquad (2.1.1)$$

$$\phi_{out} - \phi_{in} = \phi_{cond} + \phi_{exit} \qquad (2.1.2)$$

The complementary constitutive equations are given by:

$$\phi_{ret} = \Phi_{fan}\, C_{ret}$$

$$\phi_{air} = \Phi_{air}\, C_{air}$$

$$\phi_{in} = (\Phi_{fan} + \Phi_{air})\, C_{in} \qquad (2.1.3)$$

$$\phi_{sup} = \Phi_{fan}\, C_{out}$$

$$\phi_{exit} = \Phi_{air}\, C_{in}$$

Solution method

The set of mass balances can be solved by successive substitution. With Eq.(2.1.1) we can calculate c_{in}, and subsequently with Eq.(2.1.2) we solve c_{out}, which is the quantity we like to know (as it is the input for the climate model).
Setpoints of the reefer are expressed in relative humidity. Below we state how relative humidity is related to water vapour concentration and temperature. The relative humidity x is defined as the ratio of the water vapour pressure p_w and the saturated vapour pressure p_{sat}. Using the ideal gas law, one can also equate the relative humidity to the ratio of the water vapour concentration c_w [kg/m^3] and the saturated water vapour concentration c_{sat}:

$$x = p_w / p_{sat} = c_w / c_{sat} \qquad (2.1.4)$$

The saturated vapour pressure $p_{sat}(T)$ is temperature dependent and follows from the Clausius-Clapeyron relation:

$$p_{sat} = p_0 \exp (- \Delta H_w M_w / R T) \qquad (2.1.5)$$

With T the temperature in Kelvin, p_0=2 10^{11} Pa, ΔH_w the latent heat of evaporisation, M_w the molar weight of water, and R the gas constant. Using the ideal gas law one relates the water concentration to the water vapour pressure:

$$c_w = p_w M_w / R.T \qquad (2.1.6)$$

2.2 Heat balance

In figure 2.2 we have depicted the occurring heat flows. The corresponding heat balances are given by:

$$Q_{in} = Q_{ret} + Q_{air} + Q_{fan} - Q_{exit} \qquad (2.2.1)$$

$$Q_{evap} = Q_{out} - Q_{in} \qquad (2.2.2)$$

$$Q_{sup} = Q_{out} + Q_{heat} \qquad (2.2.3)$$

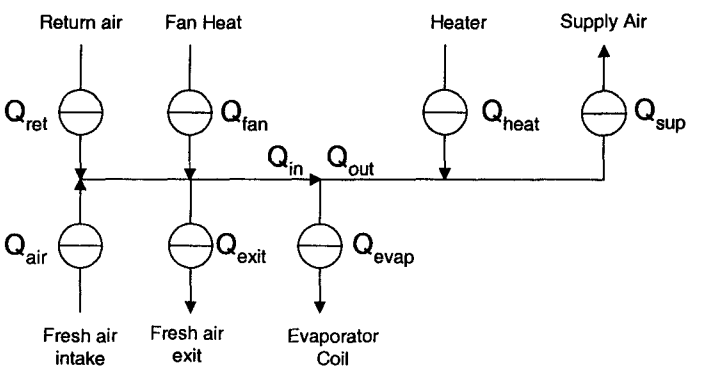

Figure 2.2. Heat flows in the cool-unit

The heat balances are complemented with the following constitutive equations:

$$Q_{ret} = \Phi_{fan} \rho_a c_{p,a} T_{ret}$$

$$Q_{sup} = \Phi_{fan} \rho_a c_{p,a} T_{sup}$$

$$Q_{air} = \Phi_{air} \rho_a c_{p,a} T_{amb}$$

$$Q_{exit} = \Phi_{air}\, \rho_a\, c_{p,a}\, T_{in} \qquad (2.2.4)$$

$$Q_{in} = \Phi_{fan}\, \rho_a\, c_{p,a}\, T_{in}$$

$$Q_{out} = \Phi_{fan}\, \rho_a\, c_{p,a}\, T_{out}$$

$$Q_{evap} = Q_{evap}(\phi_{cond}, T_{out}, T_{in}, T_{amb}, c_{in}, c_{out}, \Phi_{fan})$$

$$Q_{fan} = Q_{fan}(\Phi_{fan})$$

Q_{heat} is a controlled variable, used for controlling the relative humidity of the return air. Its maximal value is given in the next section. Q_{evap} follows from the refrigeration circuit model, described in another document. Q_{fan} is a function of the volumetric flow rate of the fan (Φ_{fan}), which is described in the next section.

Solution method

We have to distinguish three control regimes:

a) Temperature is not within range, and is above setpoint
b) Temperature is not within range, and is below setpoint
c) Temperature is in range, RH is not controlled or RH is below setpoint
d) Temperature is in range, RH is controlled and is above setpoint

For each regime we have to use another setting of unknown variables in the refrigeration circuit model (RCM).

In regime a) T_{out} is above at setpoint, and the cool unit is on and is at maximum cooling capacity. T_{out} is estimated by the RCM. Hence, we solve the system as follows:

1) Calculation of T_{in} by means of Eq.(2.2.1)
2) Calculation of T_{out} by means of Eq.(2.2.2), which is solved by the RCM.

If the temperature is not in range, the heater is off. Hence $Q_{sup}=Q_{out}$.

In regime b) T_{out} is below setpoint and the cooling unit is switched off, and the heater is set to maximum. Hence, we solve the system as follows:

1) Calculation of T_{in} by means of Eq.(2.2.1)
2) Equate $T_{out}=T_{in}$
3) Calculation of T_{sup} by means of Eq.(2.2.3)

In regime c) T_{out} is at setpoint, and the cool unit runs at partial cooling capacity, and the heater is switched off. c_{out} is estimated by the RCM, and passed on to the mass balance equations. Hence, we solve the system as follows:

1) Calculation of T_{in} by means of Eq.(2.2.1), and is input for the RCM.
2) Equate $T_{sup}=T_{out}=T_{set}$

In regime d) T_{sup} is at setpoint, and the cool unit runs at partial cooling capacity. c_{out} is estimated by the RCM, and passed on to the mass balance equations. Hence, we solve the system as follows:

1) Calculation of T_{in} by means of Eq.(2.2.1), and is input for the RCM.
2) Compute required amount of removed moisture $\phi_w = \Phi_{fan}\,(\,c_{in} - c_{set}\,)$
3) Calculation of T_{out} by means of RCM, with constraint that $\phi_w = \Phi_{fan}\,(\,c_{in} - c_{set}\,)$
4) Compute required amount of heating $Q_{heat} = \Phi_{fan}\, \rho_a\, c_{p,a}\,(\,T_{set} - T_{out}\,)$
5) If Q_{heat} is smaller than $Q_{heat,max}$ then equate $T_{sup}=T_{set}$, and $c_{out}=c_{set}$, otherwise
6) Calculate T_{out} from constraint $Q_{heat,max} = \Phi_{fan}\, \rho_a\, c_{p,a}\,(\,T_{set} - T_{out}\,)$
7) Compute c_{out} by RCM with T_{out} given by previous step.

3. Thermal and Electric Energy model of components

There electricity consuming parts in the refrigeration unit are:
- The compressor
- The evaporator fans
- The heaters
- The condensor fan

Hence the total electrical energy is given by:

$$P_{tot} = P_{comp} + P_{fan} + P_{cfan} + Q_{heat} \quad (3.1)$$

The electrical energy consumption of the compressor is given by the RCM, and is discussed in another document. Because the compressor is an 3-phase AC motor, it changes the power factor (cos (ϕ)) of the electrical energy supply and thereby influences the power consumption of heaters and fans. Below we will discuss the change of the power factor as a function of P_{comp}.

The thermal energy of the evaporator fans, and of the electrical heaters is dissipated and are accounted for in the heat balances in section 2.2. Below we will describe the electrical and thermal energy consumed and dissipated by these models. Furthermore, we will describe the electrical energy consumption of the condensor fans.

3.1 Power factor

Due to the use of inductive motors, there will be a phase shift between voltage and current, which must be taken into account in the calculations of the consumed power. For example, the power consumption of a three-phase motor is given by:

$$P_{tot} = \cos(\phi)\,(V_l/\sqrt{3})\;\Sigma_i\, I_i \quad (3.2)$$

Here V_l is the line-to-line voltage ($V_l \approx 380$ V), I_i the line currents of the 3 phases and cos(ϕ) is the power factor, with ϕ the phase shift between voltage and current.

The power factor changes with the load. If a three-phase motor is fully loaded the power factor is equal to one. If several motors are operating, each contribute to the phase shift. But, in the refrigeration unit the power factor is mainly determined by the compressor motor (which has the largest power consumption). The change of the power factor as a function of P_{comp} as shown in figure 3.1, which is a graph obtained from the manufacturer.

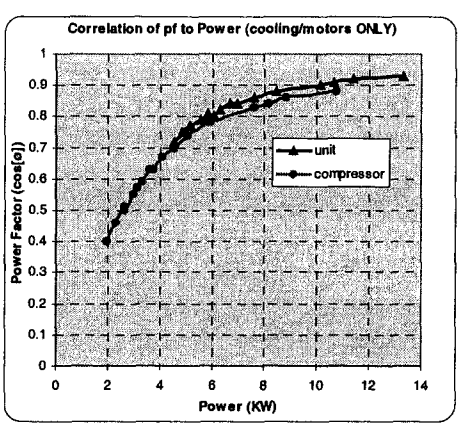

Figure 3.1. Power factor cos(ϕ) as a function of the apparent consumed compressor power P_{comp}.

An analytical approximation to the curves in figure 3.1 is:

$$\cos(\phi) = 1 - \exp\left(P_{comp} / P_{tau} \right) \quad (3.3)$$

with P_{tau} = 4.0 kW.

Mind however, if the compressor is cycled off (during heating, are in holding mode with only evaporator fan running) the fan motors are fully loaded, and the power factor can be taken equal to $\cos(\phi)=1$.

3.2 Electrical Heaters

The power of the heaters is constant, but can be cycled during heating and active dehumidification. During defrost the dissipated heat is constant. In our energy model we take the time-averaged amount of dissipated heat Q_{heat}, which is a continuous variable in the range $0 < Q_{heat} < Q_{heat,max}$, with

$$Q_{heat,max} = \cos(\phi)\, P_{heat,0} \quad (3.4)$$

Here $P_{heat,0}$ is the maximum generated heat (at $\cos(\phi)=1$), which is equal to 2 kW at 50 Hz, and 3.8 kW at 60 Hz.

3.3 Evaporator fans

In general the electrical power drawn by the evaporator fan motors is dependent on the airflow resistance of the system. In the case of palletised cargo this resistance is almost independent of the airflow resistance of the load. However, below we will describe the general case.

The mechanical power delivered by the fan is equal to:

$$W_{fan} = \Delta p_{fan}\, \Phi_V \quad (3.2.1)$$

Which pressure drop and flow rate the fan creates, depends on the fan characteristic curve and the airflow resistance of the unit. The fan curve is normally expressed as a second order polynomial in flow rate Φ_V, which is a monotone decreasing function:

$$\Delta p_{fan} = \gamma_0 + \gamma_1\, \Phi_V + \gamma_2\, \Phi_V^2 \quad (3.2.2)$$

The pressure drop due to the airflow resistance is given by:

$$\Delta p_{fan} = 1/2\, \rho_a\, C_D\, \Phi_V^2 \quad (3.2.3)$$

The fan curve and the airflow resistance are established experimentally. For a cargo consisting of palletised goods, the airflow resistance is independent of the resistance of the cargo, and is mainly determined by the containerbox. Hence, for these types of cargo we can use the manufacturers data.

The fan can operate at low and high fan speeds. The power consumption at full load and the volumetric flow rates at high and low fan speeds are given in Table III.1. (Denoted as $P_{fan,max}$)

Table III.1 Power consumption and flow rate of evaporator fan, in container box without cargo.

Frequency (Hz)	Low fan speed Power (kW)	Flow rate (m^3/s)	High fan speed Power (kW)	Flow rate (m^3/s)
50	0.16	0.5	1.0	1.0
60	0.5	0.6	1.8	1.2

If the compressor is in operation, the power factor is smaller than one. Hence, the fan power consumption is:

$$P_{fan} = \cos(\phi)\, P_{fan,max} = 1/\eta_{fan}\, W_{fan} \qquad (3.2.4)$$

Due to the shift in the power factor, the mechanical work done by the fan decreases, and consequently also the volumetric flow rate, as indicated by Eq.(3.1.1) and (3.1.3), which state that the power is proportional with Φ_v^3. For standard fans the efficiency is about $\eta_{fan} = 0.25$.

The (motor input) power drawn by the fans P_{fan} that is not converted into mechanical power W_{fan}, is dissipated in the airflow. The dissipated power Q_{fan} is:

$$Q_{fan} = (1 - \eta_{fan})\, P_{fan} \qquad (3.2.5)$$

Due to the power factor, the RCM and the fan model are coupled. Hence, they have to be solved simultaneously. This can be done by incorporation of the fan model in the RCM, or solve the system by the bisection method.

3.3 Condensor fan

The control logic cycles the condensor fan on and off. In our energy model we take the time averaged power consumption of the condensor fan. As a first approximation we take that the condensor fan is cycled on for a fixed fraction of time: f_{cfan}. This fraction will be determined by experiment. We expect this fraction to be a function of the heat load of the evaporator coil Q_{evap}, and the ambient temperature T_0.

At full load, the power consumption is $P_{cfan,max}$ = 550W at 60Hz, and 320W at 50 Hz. The condensor fan operates only if the refrigeration unit cools, and hence the compressor determines the power factor.

The time-averaged power consumption of the condensor fan is:

$$P_{cfan} = f_{cfan}(Q_{evap}, T_{amb}) \cos(\phi)\, P_{cfan,max} \qquad (3.3.1).$$

JFOE 2657
DISK / 28/12/01

ARTICLE IN PRESS

No. of pages: 9
DTD 4.2.0/ SPS

ELSEVIER

Journal of Food Engineering xxx (2001) xxx–xxx

JOURNAL OF FOOD ENGINEERING

www.elsevier.com/locate/jfoodeng

Prediction of airflow through a vented box by the Darcy–Forchheimer equation

R.G.M. van der Sman *

Agrotechnological Research Institute (ATO), P.O. Box 17, 6700 AA Wageningen, Netherlands

Abstract

A model is presented describing the airflow through a vented box packed with horticultural produce. The model is based on the Darcy–Forchheimer–Brinkman theory of flow through confined porous media. Though questions are raised on the applicability of this theory for the description of high airflow in vented boxes, we show that the model can reproduce experimental data on pressure drop over vented boxes quite accurately. Moreover, we confirm the hypothesis of a power law relationship between the pressure drop and the vent hole ratio of the box. Given the good comparison with experimental data, one can conclude that the model describes the airflow inside the box reasonably well, and when coupled to convection–diffusion models describing heat and water vapour transport, it can be used to improve designs of vented packages of horticultural produce. © 2001 Published by Elsevier Science Ltd.

Keywords: Package design; Numerical model; Porous media; Darcy–Forchheimer

1. Introduction

For the quality conservation of packaged horticultural products the control of the exchange of heat, moisture and gases with the environment is of great importance. For the enhancement of these exchange processes, packaging systems are frequently provided with vent holes, which allow air to flow in and out of the package (Chau, Gaffney, Baird, & Church, 1983; Talbot, 1988; Tanner, 1998; van der Sman, Evelo, Wilkinson, & van Doorn, 1996; van der Sman, 1999).

The vent hole design of most packaging systems is based on a rule of thumb, which is more arbitrary than scientific (Talbot, 1988). One of the methods to determine the optimal vent hole design is to conduct experimental evaluations (Chau et al., 1983; Haas, Felsenstein, Shitzer, & Manor, 1976; Wang & Tunpun, 1969; Yun, Cho, & Park, 1996). However, these experimental studies are expensive and scarce, as they involve much time and labour. A more feasible approach is to develop a numerical model describing the physical processes in the vented packaging system and verify the numerical results with a limited number of experiments. Talbot (1988) was one of the first conducting such an approach, although the model developed showed to be not very successful in predicting the airflow through the packaging system correctly. Yet, subsequent studies (Tanner, 1998; van der Sman, 1999, 1998), aided by the increase of computing power, have been successful in designing packages with vent holes using a model-based approach.

These latter studies only involve low airflow velocities driven by natural convection. In the model of van der Sman (1999), the packed produce is assumed to behave like a porous medium in the Darcy regime, with the airflow velocity proportional to the pressure gradient. The porous medium approach is a common assumption for the description of airflow through granular foodstuffs like grains (Bakker-Arkema, Patterson, & Bickert, 1969). However, in some food applications such as precooling and storage in a cold store, air velocities inside the packaging will be higher and will not be linear with the local pressure gradient. Inertial terms, which are quadratic in the flow rate, should be included already at (particle) Reynolds number $Re_p > 1$. Traditionally, this flow regime in confined porous media is described by the Darcy–Forchheimer–Brinkman (DFB) equation (Vafai & Tien, 1980). For packed beds of spheres parameters of the DFB equation can be derived from the geometrical properties of the packed bed using the Ergun relation (Ergun, 1952). In this paper we investigate whether the DFB model is applicable for packages filled with large

* Fax: +31-317-475347.
E-mail address: r.g.m.vandersman@ato.wag-ur.nl (R.G.M. van der Sman).

0260-8774/02/$ - see front matter © 2001 Published by Elsevier Science Ltd.
PII: S0260-8774(01)00241-2

food products (such as fruits and vegetables), which are vented with high velocity airflow.

Before using this model for our type of applications, two serious questions have to be resolved:

1. Is the Darcy–Forchheimer equation applicable for packed beds of large (spherical) food products? The point is that the airflow in the packed bed can be in the (post-Forchheimer) turbulent regime, with $Re_p > 300$, where the Darcy–Forchheimer description is questionable (Antohe & Lage, 1997; Lage, Antohe, & Nield, 1997; Pakrash, Turan, Li, Mahoney, & Thorpe, 2001).
2. Does the porous medium description apply in the region of the vent hole? Here, one can expect steep velocity gradients at spatial scales comparable to or smaller than the products diameter (Wang & Tunpun, 1969). In this regime one questions the validity of the porous medium approach (Whitaker, 1999).

After explaining the Darcy–Forchheimer theory in Section 2, we investigate the first above-stated question in Section 3. To solve this question we use experimental data on pressure drop–velocity correlations for bulks of packed potatoes (Irvine, Jayas, & Mazza, 1993) and oranges (Chau et al., 1983). Subsequently in Section 4, we test the Darcy–Forchheimer description for vented packagings filled with spherical food stuff by comparing it with experimental data for tomatoes and mandarins (Yun et al., 1996).

2. Theory

A commonly used assumption in models for packed beds of agricultural produce is that the packed bed can be considered as a porous medium (Bakker-Arkema et al., 1969). For small airflows the airflow rate is proportional to the applied pressure drop, which is the statement of the well-known Darcy's law. At higher flow rates, at particle Reynolds number $Re_p > 1$, the airflow is described by the Darcy–Forchheimer equation, which includes a quadratic term. For flow through a confined packed bed, such as a vented packaging, the Darcy–Forchheimer equation is extended with the Brinkman term, which is required for the description of the boundary layer at the solid/porous-media interface (Vafai & Tien, 1980)

$$-\nabla p = \frac{\mu}{\kappa}\vec{u} + \beta\rho u\vec{u} - \mu_{\text{eff}}\nabla^2\vec{u}, \tag{1}$$

which is complemented with the continuity equation

$$\nabla \cdot \vec{u} = 0. \tag{2}$$

Here p is the pressure, μ is the dynamic viscosity of air, κ is the permeability of the porous medium, u is the airflow velocity, ρ is the density of air, β is the Forchheimer constant, and μ_{eff} is the effective dynamic viscosity in the boundary layer at the solid/porous-media interface. It can be assumed that $\mu_{\text{eff}} \approx \mu$ (Vafai & Tien, 1980).

The effect of the Brinkman term is that it will give rise to a small boundary layer, where the velocity reduces to zero exactly at the solid wall. On the scale of the vented box, the velocity profile is nearly uniform. Omitting this term from Eq. (1) will result in numerical solution of the velocity profiles showing bumps near the wall, which is not physical, but a numerical artefact (Vafai & Tien, 1980). On the global scale the Brinkman term does not have a significant influence on the pressure drop over the packed bed, and will follow the global Darcy–Forchheimer equation. Consequently, the coefficients in Eq. (1) can be computed for near spherical products, using the Ergun relations (Ergun, 1952)

$$\frac{1}{\kappa} = \frac{K_1(1-\varepsilon)^2}{d_{\text{eff}}^2\varepsilon^3} \quad \text{and} \quad \beta = \frac{K_2(1-\varepsilon)}{d_{\text{eff}}\varepsilon^3}. \tag{3}$$

Here d_{eff} is the effective product diameter, and is calculated by $d_{\text{eff}} = 6V/A$, with V the volume of the product, and A the surface area. The porosity of the packed bed is denoted as ε. For spherical products the constants have the following values $K_1 = 180$, and $K_2 = 1.8$ (MacDonald et al., 1979). For packed beds with objects having other shapes or rough surfaces the parameters K_1 and K_2 can have other values (Comiti & Renaud, 1989). Here A should be taken as the 'wetted' surface area of the packed object. For objects having only point contacts such as spherical products, the 'wetted' surface area is equal to the surface area of a single product.

The first term in Eq. (1) originates from Darcy's law ($-\nabla p = \mu/\kappa u$) which holds in the range of small airflow velocities, indicated by the particle Reynolds number $Re_p < 1$. Here the particle Reynolds number is defined as $Re_p = \rho u d_{\text{eff}}/\mu$. Some studies have questioned the validity of the Darcy–Forchheimer equation for the turbulent regime, indicated by $Re_p > 300$ (Antohe & Lage, 1997; Lage et al., 1997; Tobis, 2001; Pakrash et al., 2001). The experimental study of Lage et al. (1997) suggests that in the turbulent (post-Forchheimer) regime the pressure drop correlates with a cubic polynomial in the fluid velocity. The nature of porous media flow in the turbulent post-Forchheimer regime is at this moment still a controversial issue as indicated by the very recent studies of Pakrash et al. (2001) and Tobis (2001). The main difficulty for resolving this question is the almost inaccessibility of porous media for a detailed flow measurement.

Using the values for the air kinematic viscosity $\mu/\rho = 13 \times 10^{-6}$ m^2/s, and a typical product diameter of $d_{\text{eff}} = 0.05$ m, one can expect this turbulent regime to occur at velocities $u > 0.08$ m/s which typically hold for the applications concerned, namely pre-cooling and storage in a cold store. Hence, the validity of the Darcy–Forchheimer equation has to be checked for packed

beds with large produce. This will be investigated below, by analysing experimental data obtained from bulk packed beds of larger produce such as potatoes and oranges.

Another question concerning Eq. (1) arises when applying it to vented packaging, where it is questionable whether one of the underlying assumptions of Eq. (1) holds. These assumptions are given by Whitaker (1999), where he derives Eq. (1) from the Navier–Stokes equation from first principles using the volume-averaging method. This method is commonly accepted as the theoretical basis for the porous medium description of packed beds. One of the main assumptions of this theory is that the spatial scale of the airflow velocity is larger than the diameter of the granular material (i.e. the vegetable or fruit in our case). This assumption does not hold in the region of small vent holes (having typically a diameter of 2 cm), where one can expect steep gradients in the airflow velocity (Wang & Tunpun, 1969). This last question concerning the validity of DFB model near holes of vented boxes will be investigated by comparing a numerical solution of Eq. (1) to experimental data for confined packed beds of fruits (tomato and mandarins), having a vent hole in the front and back faces of the confinement.

3. Airflow through bulk of produce

In order to test the validity of the Darcy–Forchheimer equation, and particularly the Ergun equation for packed beds of large agricultural produce, information must be available on structural parameters such as the porosity and the particle diameter. This information is seldom given in studies concerning airflow through beds of vegetables and fruits. To our knowledge, the only studies, which do give the information on the structural parameters, are by Irvine et al. (1993) and Chau et al. (1983). Hence, with these data sets we test whether the Ergun equation can be applied to packed beds of potatoes and oranges.

3.1. Potatoes

In the study by Irvine et al. (1993) the pressure drop–velocity correlations are determined experimentally for bulks of potatoes. Experiments are performed on bulks of cleaned potatoes of several cultivars. In the experiments the airflow velocities range from 0.05 to 0.5 m/s. The average diameter of the potatoes used in this study is $d = 65$ mm. Hence, the particle Reynolds number is in the range of about $160 < Re < 1600$, which is for a great part within the range of turbulent flow. The potatoes are contained in a cubical bin with sides of 1.00 m, which allows either horizontal or vertical airflow.

Using the data of the dimensions of the potato and the bulk density ρ_b as given by Irvine et al. (1993), we have calculated the effective diameter and the porosity. For this calculation the potato is assumed to have an ellipsoidal shape. Volume and surface area are calculated using the algebraic software package Maple™. Given the value for the mass density of potatoes $\rho_p = 1090$ kg/m^3 (Beukema, 1980) the porosity can be calculated using the expression $\varepsilon = 1 - \rho_b/\rho_p$. Using the values for the effective diameter and the porosity we estimate the constants K_1 and K_2 by fitting the Ergun equation to the pressure drop data from Irvine et al. (1993).

In Table 1 the estimated values of K_1 and K_2 are listed for several potato cultivars and flow directions. The dimensions of the ellipsoidal potatoes are given in Table 1 by the parameters d_1, d_2 and d_3, from which the effective potato diameter d_{eff} is computed. Furthermore, Table 1 lists the computed values of the porosity and its standard error $\Delta\varepsilon$, obtained from the standard deviation of the bulk density as determined by Irvine et al. (1993). In the last column the error of the fit is given, which is calculated by Error $= \sum_v |\hat{p}_n - p_n|/p_n$, with $\hat{p}_n$ the estimated value of the pressure drop using the Ergun equation, and p_n the experimental data from Irvine et al. (1993).

As shown in Table 1 four experimental data sets follow to a good approximation the Ergun equation for smooth spheres ($K_1 = 180$, $K_2 \approx 1.8$), with fit errors of

Table 1
Parameters determining the airflow resistance of bulk piled potatoes[a]

Cultivar	d_1 (mm)	d_2 (mm)	D_3 (mm)	d_{eff}[b] (mm)	ε[b]	$\Delta\varepsilon$[b]	Flow direction	K_1[c]	K_2[c]	Error (%)[d]
Nordchip	84	65	54	65	0.360	0.005	Vertical	180	1.8	5.2
Nordchip					0.375	0.009	Horizontal	180	1.8	5.0
Russet	114	57	47	61	0.383	0.012	Vertical	180	1.9	6.6
Russet					0.370	0.016	Horizontal	180	1.3	3.3
Yukon G.	109	80	58	76	0.367	0.011	Vertical	180	1.8	6.1
Yukon G.					0.376	0.012	Horizontal	180	1.5	6.2

[a] Experimental data obtained by Irvine et al. (1993).
[b] Values computed by the author from structural parameter values given by Irvine et al. (1993).
[c] Parameter values used by the author to fit Ergun equation to experimental data.
[d] Error estimate, as defined in the text, expressing the difference between the Ergun fit by the author and the experimental data given.

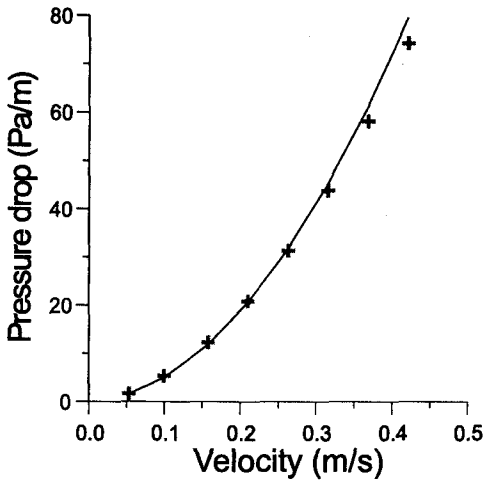

Fig. 1. Comparison of experimental data (symbols) of pressure drop over a bulk pile of potatoes, as obtained by Irvine et al. (1993), and the Ergun equation (solid line), as fitted by the author using structural parameter values as measured by Irvine et al.

about or less than 6%. An example of the good fit between the experimental data and the Ergun equation is shown in Fig. 1.

For the two experiments with Russet and Yukon G. potatoes, where the (horizontal) airflow is along the main axis of the potato, the value of the K_2 coefficient is smaller than the value for a bed of spheres. These lower values can be explained by the difference in form of the potato cultivars. Ellipsoidal objects, aligned with the flow, experience lesser drag than spherical objects. Consequently, the K_2 factor, accounting for the form drag, shows a lower value.

The calculated values of the porosity, as shown in Table 1, are all in the small range $0.36 \leqslant \varepsilon \leqslant 0.38$, which are quite comparable to the theoretical values of the porosity for a random packed bed of spheres $0.36 \leqslant \varepsilon \leqslant 0.41$ (Dullien, 1979).

3.2. Oranges

Another valuable data set is obtained by Chau et al. (1983), who have studied the pressure drop–velocity correlation in bulks of oranges, which have a nearly spherical shape. Oranges are packed in a rectangular bin with a cross-section of 55 cm × 55 cm, and a variable height of 30–50 cm. Experiments are performed for four sizes of product diameters (6–8 cm) and four stacking patterns. The porosity is measured for each bed of oranges. The superficial velocity is in the range 0.10–1.00 m/s, such that the particle Reynolds number is in the range $300 < Re < 4000$. Also here the Reynolds number is in the turbulent range.

Using the measured values of the product diameter and the porosity, Chau et al. (1983) have fitted the Ergun equation to his experimental data. The set of estimated coefficients K_1 and K_2 has shown not to be independent of product diameter, porosity and stacking pattern, which is in contradiction with the Ergun equation of packed beds of spheres. Observing the large variation in the measured values of the porosity (as reproduced in Table 2), the inconsistency of the experimental data and the Ergun equation might be explained by uncertainty of the values of the porosity induced by the relatively small confinement of the packed bed with oranges. Small confinements are known to give deviations from the Ergun relations (Eisfeld & Schnitzlein, 2001).

Another way to test the validity of the Ergun equation is to assume $K_1 = 180$, and $K_2 = 1.8$, and subsequently calculate the apparent porosity ε_{fit}, and compare it to the measured value given by Chau et al. (1983). In Table 2 the apparent porosities ε_{fit} are given for 12 combinations of stacking pattern and product diameter, next to the values from Chau et al. (1983). The goodness of fit of the Ergun equation is determined by summing the relative errors: Error $= \sum_v |\hat{p}_n - p_n|/p_n$, with again $\hat{p}_n$ the fitted pressure drop values and p_n the experimental data.

The reasonable small values of the fit errors as shown in Table 1 indicate that the Ergun equation can be fitted to the pressure drop data of packed oranges, if one re-estimates the porosity of the packed bed with oranges. When observing the set of re-estimated porosities ε_{fit}, one sees that the values for the oranges with the diameters 6.73 and 7.35 mm are about equal to the values as measured by Chau et al. One may conclude that in any case the Ergun equation holds for the smaller oranges.

Table 2
Re-estimation of porosity from data of pressure drop over bed of oranges[a]

Stacking pattern	d (mm)[b]	$\varepsilon_{\text{bulk}}$[c]	ε_{fit}[d]	Error (%)[e]
Random	8.31	.460	.440	2.6
	8.1	.503	.450	0.6
	7.35	.439	.440	5.2
	6.73	.422	.425	5.2
Square staggered	8.31	.451	.380	5.0
	8.1	.435	.390	2.5
	7.35	.405	.377	6.4
	6.73	.377	.363	6.0
Hexagonal staggered	8.31	.384	.338	3.6
	8.1	.409	.353	2.3
	7.35	.367	.372	4.6
	6.73	.339	.347	4.9

[a] Experimental data obtained by Chau et al. (1983).
[b] Product diameter as given by Chau et al. (1983).
[c] Porosity of the packed beds as given by Chau et al. (1983).
[d] Porosity of packed bed as obtained by the author by fitting the Ergun equation to experimental data and using $K_1 = 180$, and $K_2 = 1.8$.
[e] Error estimate, as defined in the text, expressing the difference between the Ergun fit by the author and the experimental data given by Chau et al. (1983).

For the larger diameters the deviation of the data from Ergun equation may be explained by the small ratio of the dimensions of the cross-section of confinement of the packed bed (55 cm × 55 cm) and the fruits diameter. Consequently, the experimental data do not represent the behaviour of a bulk packed bed, but rather a confined packed bed, which has significant channelling of airflow along the sides of the box (Vafai & Tien, 1980).

3.3. Discussion

In the literature questions are raised concerning the validity of the Darcy–Forchheimer equation for porous media in the turbulent regime (Antohe & Lage, 1997). The turbulent regime also holds for packed beds of large horticultural produce. However, above we have found that several data sets from studies performed with bulk packed beds of potatoes and oranges do follow the Darcy–Forchheimer and also the Ergun equation for packed beds of spheres. An explanation for these seemingly contradicting findings is that turbulence has little effect on the macroscopic pressure drop in porous media (Liu & Masliyah, 1996).

Deviations of the Ergun equation can be expected for small confinements (if compared to the products diameter) and for non-spherical products. Having resolved the first question concerning our model as raised in the introduction, we can proceed with analysis of the validity of the model for vented packages.

4. Airflow through vented packages

4.1. Numerical model

The DFB model, as expressed by Eqs. (1) and (2), is solved numerically in three dimensions (3-D) with the finite element solver FIDAP (FIDAP, 1993). For the numerical scheme we have used trilinear isoparametric elements with eight nodes. The grid is made more dense near the walls of the package and near the vent holes, as shown in Fig. 2(b). Near the edges of inlets and outlets a nearly singular point in the pressure field and the velocity field is expected (Sun, Arnaud, & Fohr, 1992). Hence, at these points a very fine mesh is needed for an accurate resolution of the pressure and velocity fields. The finite element equations are solved iteratively by a conjugate gradient solver. The pressure field is discretised explicitly using a discontinuous pressure approximation.

The boundary conditions at the vent holes are prescribed as constant pressures across the complete area of the in- and outlet vent holes. The pressure at the outlet is defined as zero, and the pressure at the inlet is defined as Δp_{tot}. Furthermore, the fluid velocity components per-

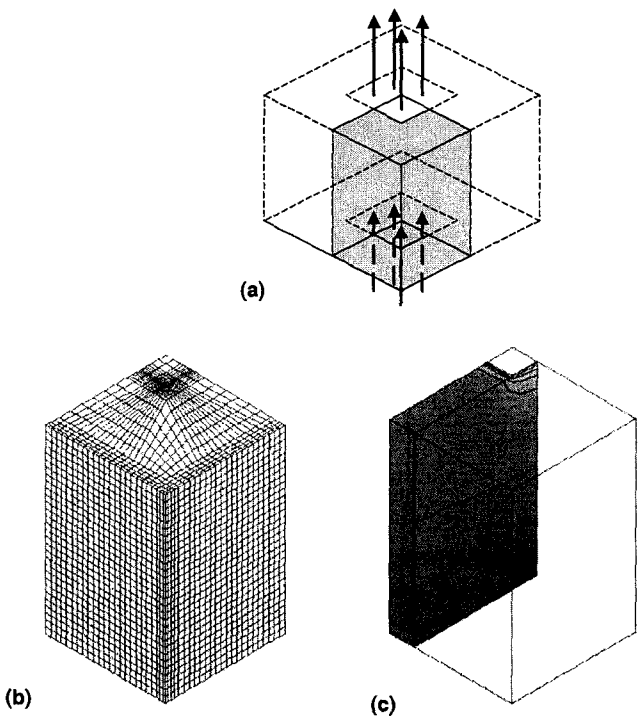

Fig. 2. (a) Example of mesh used in FEM model of a vented box with horticultural produce. (b) Typical simulation results of the distribution of pressure field in the vented box. Contour lines are spaced at a 10 Pa interval.

pendicular to the main flow direction are prescribed to be equal to zero at the inlet and outlet vent holes. The porous medium in the box is assumed to be homogeneous.

This set of boundary conditions will give rise to a certain amount of airflow through the box. The flow rate is determined by calculating the average velocity in the cross-section in the middle of the box, perpendicular to the main flow direction. This calculation of average velocity is performed by using a feature of the numerical package FIDAP.

In Fig. 2(c) we show the results of an exemplary numerical simulation. Here is shown a contour plot of the pressure in a plane, parallel to the main flow direction, and cutting through the vent holes. Almost all contour lines are concentrated near the vent holes, indicating steep gradients in the pressure near the vent holes. These steep gradients result also in steep gradients in the airflow velocity. This is in compliance with the expectations of Wang and Tunpun (1969).

Because the main pressure loss occurs near the vent holes, possible variation of the porosity near the walls of the box will not have much influence on the total pressure drop. However, this variation might affect the local heat and mass transfer, which is important in the application of packaging horticultural produce. This theme will be considered in a subsequent study.

4.2. Experimental validation

The experimental data, against which the numerical model is tested, are obtained from Yun, Cho, and Park (1995, 1996). In their study the total pressure drop versus the average flow rate is determined for packaged produce with the vent hole ratio in the range 2.5–20%. The vent hole ratio (O) is defined as the area of the vent hole divided by the total surface area of the face of the box the vent hole is placed: $O = A_{\text{hole}}/A_{\text{face}}$. The products used are mandarins (with an average diameter of 4.9 cm and a porosity of 0.29) and tomatoes (with an average diameter of 6.4 cm and a porosity of 0.44). A staggered stacking pattern is used. The products were placed in a square enclosure (with a cross-section 40 cm by 40 cm) having at the front and the back two steel plates, spaced $\Delta l = 30$ cm apart. Each plate has one rectangular vent hole at its centre, with a vent hole ratio of $O = 2.5\%$, 5%, 10% or 20%. The average airflow velocity ranged from 0.1 to 1 m/s.

By analysing their experimental data Yun et al. (1996) have hypothesised that the total pressure drop Δp_{tot} over the system of packed produces and plates with vent holes can be described as

$$\Delta p_{\text{tot}} = \Delta p_{\text{holes}} + \Delta p_{\text{bulk}} O^{-1.5}. \quad (4)$$

Yun et al. have defined Δp_{hole} as the pressure drop over the empty package, and Δp_{bulk} as the pressure drop over the bulk of produce. It is important to note that Δp_{bulk} is to be measured if the plates with vent holes are removed, or in other words if the vent hole ratio is $O = 100\%$. In the case of $O = 100\%$ we have that $\Delta p_{\text{holes}} = 0$, and consequently it follows from Eq. (4) that $\Delta p_{\text{tot}} = \Delta p_{\text{bulk}}$, which is exactly the definition of Δp_{bulk}. In the range of parameters of their experiment Yun et al. (1996) have shown by measurements that the pressure drop over the empty box Δp_{holes}, is negligible compared to the total pressure drop Δp_{tot}.

The pressure drop over the bulk of produce Δp_{bulk} is measured using the same experimental setup, only now without the front plates (i.e. $O = 100\%$). Because the tomatoes and mandarins are nearly spherical, it should be expected that Δp_{bulk} follows the Ergun relations, Eq. (3). However, the experimental data by Yun et al. (1996) have shown *not* to follow Eq. (3). As above, a possible cause is the airflow channels along the walls of the package, where the porosity is known to be considerably higher than in the centre of the packed bed (Vafai & Tien, 1980; Talbot, 1988). This effect is especially evident in cases with low ratio of particle diameter d_p and the hydraulic diameter D_h of the confinement of the packed bed (Eisfeld & Schnitzlein, 2001). For the experimental setup of Yun et al., this ratio is equal to $d_p/D_h = 6.25$, which can give lower pressure drops (about 10%) when compared to the pressure drop for bulk packed beds (Eisfeld & Schnitzlein, 2001). However, the pressure drop over confined packed beds can be described with a modified Ergun equation (Eisfeld & Schnitzlein, 2001).

Given the above considerations, we have to estimate the parameters β and κ from the experimental data, rather than from the Ergun relations. Moreover, we have to estimate them from the data from experiments with a vented box. In these vent hole regions almost all pressure losses occur, as shown in Fig. 2(c). Hence, we need to estimate the pressure drop over the bulk with the same porosity as in the vent hole region.

The experimental data by Yun et al. (1996) have shown that Δp_{tot} is only quadratic with the average velocity u. Hence, there is no significant effect of the linear term of Eq. (1), and consequently only the parameter β of the quadratic term has to be estimated. The parameter κ has to be set to a sufficiently large number such that the linear term in Eq. (1) is negligible compared to the quadratic term. Preliminary simulations, in which we have set the values of parameters β and κ equal to those given by the Ergun relation and we have varied the vent hole ratio O, show that Δp_{tot} scales with $O^{-1.5}$, as stated in Eq. (4). Given the negligible contribution of Δp_{holes} on the total pressure drop in the flow regimes considered, we can state that $\Delta p_{\text{tot}} \approx \Delta p_{\text{bulk}} O^{-1.5}$. Hence, the parameter β can be estimated from the experimental data obtained for a vented box.

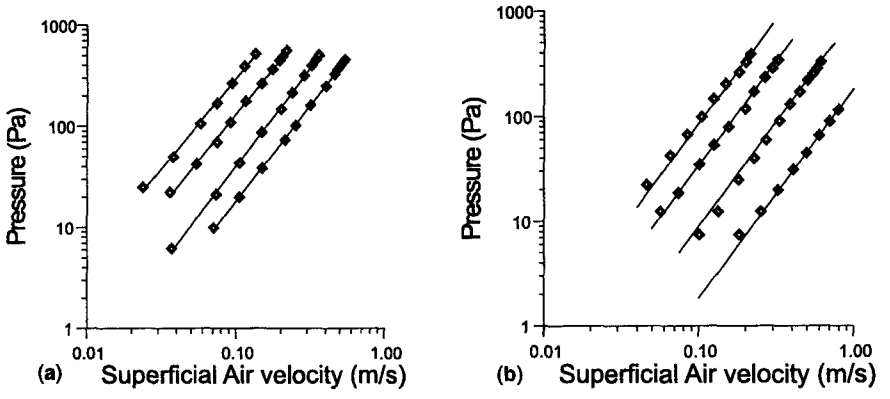

Fig. 3. Reprint of experimental data obtained by Yun et al. (1997), describing the pressure drop versus the superficial air velocity for a vented box with (a) mandarins and (b) tomatoes. Each curve corresponds with different vent hole ratios, which were 2.5%, 5%, 10%, and 20% (curves from top to bottom). The solid lines are results of regression using the assumption that the pressure drop scales with the velocity squared.

4.3. Mandarins

Using experimental data for the pressure drop over a vented box with a vent hole ratio of 5%, we estimated that Δp_{bulk} for mandarins follows the correlation $\Delta p_{\text{bulk}}/\Delta l = 1283u^2$. From this result we have computed the Forchheimer parameter β of Eq. (1), and used it in our following numerical simulations.

In these numerical simulations we have varied the vent hole ratio (25%, 15%, 5%, and 2.5%) and the total pressure drop ($\Delta p_{\text{tot}} = 40, \ldots, 200$ Pa). From the simulation results the average velocity (u) in the box is computed. As can be expected from Eqs. (1 and 4) we have found that in the flow regimes considered the total pressure drop over the vented box is quadratic with the average velocity: $\Delta p_{\text{tot}} = Ku^2$, with K being considered as a kind of pressure loss coefficient. From the numerical results we have determined the friction coefficient for each vented box configuration (varying in vent hole ratio), by applying linear regression between Δp_{tot} and u^2. In Fig. 3(a) the estimated coefficient K is plotted against the vent hole ratio (O). One can observe from this figure that the total pressure drop indeed scales as $O^{-1.5}$, as hypothesised by Yun et al. (1996).

4.4. Tomatoes

The same procedure, as above, is now applied to the data concerning tomatoes. From linear regression of experimental data of the pressure drop over a vented box with 5% vent hole ratio, we have found $\Delta p_{\text{bulk}}/\Delta l = 222u^2$. Subsequently, with this new value of β, we have estimated the friction coefficient for boxes packed with tomatoes and varying vent hole ratio. The results of these numerical simulations are shown in Fig. 3(b). This figure shows that the numerical results for packed tomatoes also follow Eq. (4).

4.5. Scaling with bulk pressure drop

Another test for the numerical model is whether it can predict that the total pressure drop Δp_{tot} over a

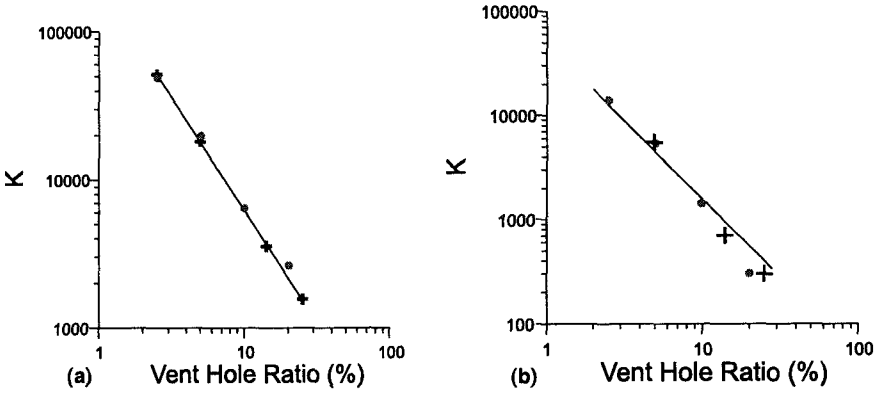

Fig. 4. Loss coefficient K of a vented package with mandarins (a) or tomatoes (b) versus the vent hole ratio (O). The crosses are numerical results, and the bullets are values derived from experimental data by Yun et al. (1997). The solid line is fitted according to the hypothesis Eq. (4), which states that coefficient K scales with $O^{-1.5}$.

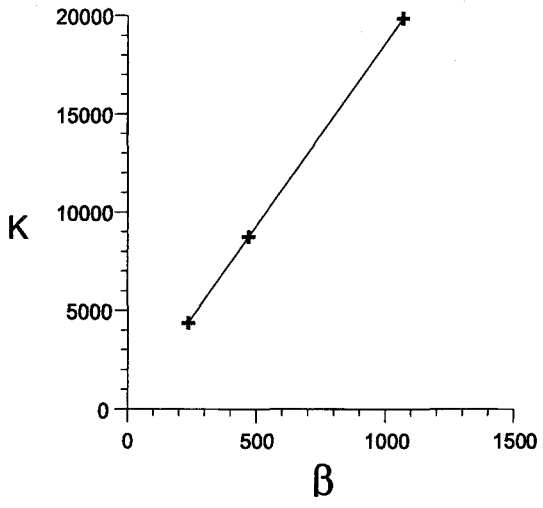

Fig. 5. The loss coefficient K of a vented box packed with horticultural produce and a vent hole ratio of 5%, versus the Forchheimer coefficient β of the packed bed of produce.

vented box filled with produce scales linear with Δp_{bulk}. Therefore, simulations are performed for various values of the parameter (β) of the Forchheimer term in Eq. (1), and keeping the vent hole ratio constant. In Fig. 4 β is plotted versus the friction coefficient K for a package with a vent hole ratio of 5%. From these results one can conclude that the total pressure drop Δp_{tot} is indeed linear with the bulk pressure drop Δp_{bulk} (see Fig. 5).

4.6. Discussion

In this section we have shown that the numerical solution of the DFB model, Eqs. (1) and (2), is in agreement with experimental data obtained by Yun et al. (1996). Moreover, the numerical model confirms the hypothesis stated by Yun et al. that there is a power law between the total pressure drop over the box and the vent hole ratio: $\Delta p_{tot} \sim O^{-1.5}$, and that it scales linear with the Forchheimer parameter β (for the flow regimes considered).

When comparing the experimental data (Yun et al., 1996) for the pressure drop over the bulk of oranges or tomatoes with the Ergun relations, we have found that the data do not agree. As in the case of the study of Chau et al. (1983), Yun et al. (1996) have used a small confinement of the packed bed if compared to the products diameter. Hence, channelling of airflow along the walls of the confinement can be expected (Vafai & Tien, 1980), leading to deviation of the behaviour of bulk product (Eisfeld & Schnitzlein, 2001).

5. Conclusions

By comparing with experimental data it is shown that the DFB model is able to predict the pressure drop over bulks of large horticultural produce and over vented boxes packed with produce. This result is remarkable because in the literature questions have been raised about the validity of the model in our type of applications.

One question concerns the fact that in our type of applications the flow is in the turbulent regime, and consequently the DFB model does not capture the full description of the flows (Antohe & Lage, 1997). However, it is said that turbulence has little effect on total pressure drop in porous media (Liu & Masliyah, 1996), and hence the model can give good predictions of the total pressure drop over the vented box. Whitaker (1999) assumes the porous medium approach not to hold in regions with steep gradients (at scales comparable to the produce diameter). Our results seem to indicate that the porous medium approach can also describe these regimes. This point is worth to be investigated further on a fundamental level.

Given the good comparison with the experimental data we expect that the model gives reasonable prediction of the airflow in vented boxes on large time and spatial scales. These are the scales of interest when designing vent holes of packages for horticultural produce. By coupling the airflow model to convection–diffusion models (van der Sman, 1999, 1998), one can describe the change of temperature and humidity inside the boxes in response to the outside conditions occurring in the distribution chains. Consequently, model-based design of vent holes in packages of horticultural produce is possible in both low and high airflow velocity regimes.

Further research will be directed at refinement of the airflow model, incorporating the effect of channelling along the walls of the vented box. Also, we will investigate the effect of channelling through a small headspace in between the packed bed of produce and the lid of the vented box, as experimentally investigated by Vignault, Goyette, and da Silva (1999).

6. Uncited reference

van der Sman (1997).

Acknowledgements

We would like to thank H.S. Yun for rendering his data sets on pressure drop over vented boxes packed with mandarins and tomatoes. Furthermore we acknowledge the financial support of this research from

the EET program of the Dutch department of Economic Affairs.

References

Antohe, B. V., & Lage, J. L. (1997). A general two-equation macroscopic turbulence model for incompressible flow in porous media. *International Journal of Heat and Mass Transfer, 20*(13), 3013–3024.

Bakker-Arkema, F. W., Patterson, R. J., & Bickert, W. G. (1969). Static pressure-airflow relationships in packed beds of granular biological materials such as cherry pits. *Transactions of the American Society for Metals, 12*, 134–137.

Beukema, K. J. (1980). *Heat and mass transfer during cooling and storage of agricultural products as influenced by natural convection.* Agric. Res. Rep. 897. Ph.D. Thesis. Agric. Univ., Wageningen.

Chau, K. V., Gaffney, J. J., Baird, C. D., & Church, G. A. (1983). Resistance to airflow of oranges in bulk and in cartons. *ASAE Paper*, 83–6007.

Comiti, J., & Renaud, M. (1989). New model for determining mean structure parameters of fixed beds. *Chemical Engineering Science, 44*(7), 1539–1545.

Dullien, F. A. L. (1979). *Porous media: Fluid transport and pore structure.* New York: Academic Press.

Eisfeld, B., & Schnitzlein, K. (2001). The influence of confining walls on the pressure drop in packed beds. *Chemical Engineering Science, 56*, 4321–4329.

Ergun, S. (1952). Fluid flow through packed columns. *Chemical Engineering Progress, 48*(2), 89.

FIDAP (1993). Theory Manual v7.0. *Fluid Dynamics International*, Evaston, Ill.

Haas, E., Felsenstein, G., Shitzer, A., & Manor, G. (1976). Factors affecting resistance to airflow through packed fresh fruit. *ASHRAE Transactions, 82*(2), 548–554.

Irvine, D. A., Jayas, D. S., & Mazza, G. (1993). Resistance to airflow through clean and soiled potatoes. *Transactions of the American Society for Metals, 36*(5), 1405–1410.

Lage, J. L., Antohe, B. V., & Nield, D. A. (1997). Two types of nonlinear pressure-drop versus flow-rate relation observed for saturated porous media. *Journal of Fluids Engineering, 199*, 700–706.

Liu, S. J., & Masliyah, J. H. (1996). Single fluid flow in porous media. *Chemical Engineering and Communication, 150*, 653–732.

MacDonald, I. F. et al. (1979). Flow through porous media-Ergun equation revisited. *Industrial Engineering Chemistry and Fundamentals, 18*, 199–208.

Pakrash, M., Turan, O. F., Li, Y., Mahoney, J., & Thorpe, G. R. (2001). Impinging round jet studies in a cylindrical enclosure with and without a porous layer: Part I – Flow visualisations and simulations. *Chemical Engineering Science, 56*, 3855–3878.

Sun, L., Arnaud, G., & Fohr, J. P. (1992). Heat and moisture transfer between ducts in an industrial cerial dryer. In A. S. Mujumdar (Ed.), *Drying'92* (pp. 1399–1407). Amsterdam: Elsevier.

Talbot, M. T. (1988). An approach to better design of pressure-cooled produce containers. *Proceedings of the Florida State Horticultural Society, 101*, 165–175.

Tanner, D. (1998). *Mathematical modelling for design of horticultural packaging.* Ph.D. Thesis. Massey Univ., Palmerston, New Zealand.

Tobis, J. (2001). Turbulent resistance of complex bed structures. *Chemical Engineering and Communication, 184*, 71–88.

Vafai, K., & Tien, C. (1980). Boundary and intertial effects of convective mass transfer in porous media. *International Journal of Heat and Mass Transfer, 25*(8), 1183–1190.

Vignault, C., Goyette, B., & da Silva, A. (1999). Design of plastic container to maximize air flow through fruits and vegetables. *ASAE Paper*, 99–6108.

van der Sman, R. G. M., Evelo, R. G., Wilkinson, E. C., & van Doorn, W. G. (1996). Quality loss in packed rose flowers due to *Botrytis cinerea* infection as related to temperature regimes and packaging design. *Postharvest Biology and Technology, 7*, 341–350.

van der Sman, R. G. M. (1997). Lattice-Boltzmann scheme for natural convection in porous media. *International Journal of Modern Physics C, 8*(4), 879–888.

van der Sman, R. G. M. (1999). Solving the vent hole design problem for seed potato packages with the Lattice Boltzmann scheme. *International Journal of Comparative Fluid Dynamics, 11*(3–4), 237–248.

Wang, J. K., & Tunpun, K. (1969). Forced-air precooling of tomatoes in cartons. *Transactions of the American Society for Metals, 12*, 804–805.

Whitaker, S. (1999). *The method of volume averaging.* Dordrecht: Kluwer Academic Publishers.

Yun, H. S., Cho, Y. K., & Park, K. K. (1995). Resistance to airflow through packed fruits and vegetables in vented box. *Journal of the Korean Society of Agricultural Machinery, 20*(4), 351–359 (in Korean).

Yun, H. S., Cho, Y. K., & Park, K. K. (1996). Resistance to airflow of fruits in bulk and in a carton. In *Proceedings of ICAME'96, Korea.*